

AD-A147 626

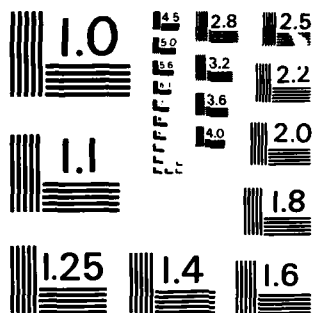
PROCEEDINGS OF THE WORKSHOP ON NONDESTRUCTIVE  
EVALUATION (NDE) OF TITANIUM. (U) NAVAL RESEARCH LAB  
WASHINGTON DC N K BATRA ET AL. JUL 84

1/4

UNCLASSIFIED

F/G 11/6

NL



MICROCOPY RESOLUTION TEST CHART  
NATIONAL BUREAU OF STANDARDS-1963-A

2

OFFICE OF NAVAL RESEARCH  
ARLINGTON, VA 22217



**Proceedings of the Second  
Workshop on Nondestructive Evaluation (NDE)  
of Titanium Alloys**

**HELD**

2-4 February 1982  
Naval Research Laboratory  
Underwater Sound Reference Detachment  
Orlando, Florida

**EDITED BY**

N. K. Batra and H. H. Chaskelis

*Naval Research Laboratory  
Washington, DC*

O. P. Arora

*Office of Naval Research*

**ADMINISTERED BY**

*Office of Naval Research*

July 1984

Approved for public release; distribution unlimited.

DTIC  
ELECTRONIC  
OCT 23 1984  
A

AD-A147 626

DTIC FILE COPY

84 10 1 130

NOV 29 1984

A

(SOURCE): Orlando, Florida.  
Naval Research Laboratory, Washington, DC.

THE COMPONENT PART IS PROVIDED HERE TO ALLOW USERS ACCESS TO INDIVIDUALLY AUTHORED SECTIONS OF PROCEEDINGS, ANNALS, SYMPOSIA, ETC. HOWEVER, THE COMPONENT SHOULD BE CONSIDERED WITHIN THE CONTEXT OF THE OVERALL COMPILATION REPORT AND NOT AS A STAND-ALONE TECHNICAL REPORT.

AD#:	TITLE:
AD-P004 121	NDE of Oxygen Contaminated Titanium Alloys and Weldments.
AD-P004 122	Effects of Oxygen on the Microstructure and Properties of Titanium 6211 Alloys.
AD-P004 123	Nonlinear Ultrasonic Characterization of Oxygen Impurities in Titanium.
AD-P004 124	Effects of Oxygen-Contamination-Induced Microstructural Changes on the Reverberation of Ultrasound in Ti-6211 Alloys.
AD-P004 125	Acoustical Characterization of Ti-6211 Weldments and Oxygen Contamination Ti-6211 Plate.
AD-P004 126	Ultrasonic Evaluation of Titanium Contamination with Correlation Techniques.
AD-P004 127	Photoacoustic Microscopy of Oxygen Contaminated Titanium Alloys.
AD-P004 128	High Resolution Acoustic Microstructural Characterization of Titanium with Interstitial Contamination.
AD-P004 129	Feasibility Study to Demonstrate Detection of Low Levels of Oxygen Contaminant in Titanium Using Eddy Current and Ultrasonic NDE Techniques.
AD-P004 130	Evaluation of Interstitial Gas Contamination in Titanium Alloys Using Induced Magnetic Field Analysis.
AD-P004 131	Electromagnetic NDE of Interstitial Contamination in Titanium Alloy Weldments.
AD-P004 132	Evaluation Thermoelectric Method for Determination in Interstitial Gases in Titanium.
AD-P004 133	Measurement of Oxygen Contamination in Titanium Alloy Ingots by Fast Neutron Activation Analysis.
AD-P004 134	Neutron Activation Analysis of Titanium with Oxygen Contamination.
AD-P004 135	Non-Destructive Evaluation of Titanium Alloys: (ESCA, ISS, and SIMS EXAMINATION) of Titanium Alloy Solid Surfaces.

UNPROCESSED AT GOVERNMENT EXPENSE



REPORT DOCUMENTATION PAGE					
1a REPORT SECURITY CLASSIFICATION <b>UNCLASSIFIED</b>			1b RESTRICTIVE MARKINGS		
2a SECURITY CLASSIFICATION AUTHORITY			3 DISTRIBUTION / AVAILABILITY OF REPORT  Approved for public release; distribution unlimited		
2b DECLASSIFICATION / DOWNGRADING SCHEDULE					
4 PERFORMING ORGANIZATION REPORT NUMBER(S)			5 MONITORING ORGANIZATION REPORT NUMBER(S)		
6a NAME OF PERFORMING ORGANIZATION  Naval Research Laboratory		6b OFFICE SYMBOL (If applicable) 5834	7a NAME OF MONITORING ORGANIZATION  Office of Naval Research		
6c ADDRESS (City, State, and ZIP Code)  Washington, DC 20375			7b ADDRESS (City, State, and ZIP Code)  Arlington, VA 22217		
8a NAME OF FUNDING / SPONSORING ORGANIZATION  Office of Naval Research		8b OFFICE SYMBOL (If applicable)	9 PROCUREMENT INSTRUMENT IDENTIFICATION NUMBER		
8c ADDRESS (City, State, and ZIP Code)  Arlington, VA 22217			10 SOURCE OF FUNDING NUMBERS		
			PROGRAM ELEMENT NO 66153W	PROJECT NO	TASK NO 022-02-02
			RR		WORK UNIT ACCESSION NO. 58-1504-04
11 TITLE (Include Security Classification)  Proceedings of the Second Workshop on Nondestructive Evaluation (NDE) of Titanium Alloys					
12 PERSONAL AUTHOR(S) Batra, N. K., Chaskelis, H. H. and Arora, O. P.					
13a TYPE OF REPORT Proceedings		13b TIME COVERED FROM TO		14 DATE OF REPORT (Year, Month, Day) 1984 July	
15 PAGE COUNT 316					
16 SUPPLEMENTARY NOTATION					
17 COSATI CODES			18 SUBJECT TERMS (Continue on reverse if necessary and identify by block number)		
FIELD	GROUP	SUB-GROUP	Nondestructive evaluation (NDE) Neutron activation		
			Eddy-currents Titanium		
			Ultrasonics		
19 ABSTRACT (Continue on reverse if necessary and identify by block number)  <i>(No distribution evaluation)</i>  Various NDE techniques based on acoustical, electromagnetic and nuclear physics principles were investigated to evaluate quantitatively the oxygen contamination levels (varying from 0.075% to 0.290% by wt.) in NRL supplied titanium plate samples. These edited proceedings present the results of these investigations (which were also presented at The Second Workshop).					
20 DISTRIBUTION AVAILABILITY OF ABSTRACT <input type="checkbox"/> UNCLASSIFIED UNLIMITED <input checked="" type="checkbox"/> SAME AS RPT <input type="checkbox"/> DTIC USERS			21 ABSTRACT SECURITY CLASSIFICATION <b>UNCLASSIFIED</b>		
22a NAME OF RESPONSIBLE INDIVIDUAL O. P. Arora			22b TELEPHONE (Include Area Code) 202 696-4402		22c OFFICE SYMBOL ONR

## PREFACE

A second workshop on NDE of Titanium Alloys was held on February 2-4, 1982. The workshop was attended by approximately fifty professionals representing various industries, universities, research organizations and government agencies. The workshop opened with remarks from Dr. B.A. MacDonald, ONR and Mr. J.L. Cavallaro, DTNSRDC, on the scope of the program ranging from fundamental studies to engineering applications of NDE for Naval structures. This workshop explored the scientific basis for quantitative determination of oxygen contamination. Special NDE techniques involving ultrasonics, and neutron activation analysis have been subsequently pursued to determine the oxygen contamination in titanium alloys.

These Proceedings consist of edited manuscripts from most of the papers presented at the workshop. The Proceedings deal with the specific problem of determining oxygen contamination in titanium, in contrast to the First Proceedings which covered some of the state-of-the-art NDE techniques applicable to titanium alloys.

We wish to thank the participants and authors for their input during the workshop. Special appreciation is given to Drs. B.A. MacDonald, H.H. Vanderveldt, and O.P. Arora for their continued interest and interaction in this area. Special thanks to Dr. Joseph E. Blue and Mr. Elmo Thomas of the Underwater Sound Reference Detachment for their hospitality in hosting this workshop.

N. K. Batra  
H. H. Chaskells

iii

Distribution For	
GRA&I	<input checked="checked" type="checkbox"/>
TAB	<input type="checkbox"/>
Unpublished	<input type="checkbox"/>
Classification	
Distribution/	
Availability Codes	
Dist	Avail and/or
AI	Special

## List of Sections

Preface .....	iii
---------------	-----

### PART A GENERAL

NDE of Oxygen Contaminated Titanium Alloys and Weldments ..... H.H. Chaskelis and N.K. Batra	3
Effects of Oxygen on the Microstructure and Properties of Titanium 6211 Alloys ..... M.A. Imam, B.B. Rath, A.C. Ehrlich, and D.J. Gillespie	9

### PART B ACOUSTICAL TECHNIQUES

Nonlinear Ultrasonic Characterization of Oxygen Impurities in Titanium ..... Harry I. Ringermacher and Richard S. Williams	35
Effects of Oxygen-Contamination-Induced Microstructural Changes on the Reverberation of Ultrasound in Ti-6211 Alloys ..... George J. Gruber and Gary J. Hendrix	49
Acoustical Characterization of Ti-6211 Weldments and Oxygen Contamination Ti-6211 Plate ..... Sanford R. Buxbaum and Robert E. Green, Jr.	71
Ultrasonic Evaluation of Titanium Contamination with Correlation Techniques ..... E.S. Furgason, B.B. Lee and G.O. Deputy	97
Photoacoustic Microscopy of Oxygen Contaminated Titanium Alloys ..... R.L. Thomas and L.D. Favro	113
High Resolution Acoustic Microstructural Characterization of Titanium with Interstitial Contamination ..... Alan M. Greenburg, Donald E. Yuhas and Michael G. Oravec	125

### PART C ELECTROMAGNETIC TECHNIQUES

Feasibility Study to Demonstrate Detection of Low Levels of Oxygen Contaminant in Titanium Using Eddy Current and Ultrasonic NDE Techniques ..... Susan N. Vernon, John M. Jamieson and Anthony M. Mucciardi	145
Evaluation of Interstitial Gas Contamination in Titanium Alloys Using Induced Magnetic Field Analysis ..... Kenji J. Krzywosz	173

Electromagnetic NDE of Interstitial Contamination in Titanium Alloy Weldments .....	193
Robert M. Rose	

Evaluation Thermoelectric Method for Determination in Interstitial Gases in Titanium .....	215
Harry J. Marks and Francis G. Karchnak	

#### PART D NUCLEAR TECHNIQUES

Measurement of Oxygen Contamination in Titanium Alloy Ingots by Fast Neutron Activation Analysis .....	245
Adel Abusamra	

Neutron Activation Analysis of Titanium with Oxygen Contamination .....	265
I.L. Morgan	

Non-Destructive Evaluation of Titanium Alloys: (ESCA, ISS, and SIMS EXAMINATION) of Titanium Alloy Solid Surfaces .....	283
Gheorghe D. Mateescu and Yoh-Han Pao	

#### PART E LIST OF ATTENDEES

Attendees at Titanium Workshop .....	307
--------------------------------------	-----

**PART A**  
**GENERAL**

## SECTION 1

# NDE OF OXYGEN CONTAMINATED TITANIUM ALLOYS AND WELDMENTS

H.H. Chaskelis and N.K. Batra  
*Structural Integrity Branch*  
*Naval Research Laboratory*  
*Washington, D.C. 20375*

## ABSTRACT

This paper provides an overview of progress made on the NDE of homogeneously contaminated Ti-6211 alloys. It discusses the future work that is needed to address the practical NDE problems which may arise in these alloys and their welds. Problem areas include inhomogeneity in the distribution of oxygen; the presence of their contaminants such as  $\text{Co}_2$ ,  $\text{N}_2$ ,  $\text{H}_2$ , etc.; critical flaw size relative to the grain size; and variations in the microstructure due to causes other than oxygen contamination.

AD-P004 121

## A. INTRODUCTION

Titanium alloys possess high strength to weight ratios and are corrosion resistant. Accordingly, they are viewed favorably for primary load-bearing structural applications. However, titanium alloys and their weldments are susceptible to gas contamination, particularly oxygen. Titanium alloys are normally fabricated and welded under protective inert gas atmosphere; nevertheless, minute quantities of oxygen can dissolve in the weldments. This dissolved oxygen may reside at interstitial sites or may form oxides. (The exact form of oxygen contamination is a subject of later discussion in this report.) The microstructure, grain size and distribution of phases in titanium alloys vary according to the fabrication technique. Oxygen contamination can affect the microstructure and the alpha phase is strengthened by dissolved oxygen. Oxygen contamination of alloys and weldments causes embrittlement and can induce transverse cracking. Clearly this can degrade the performance of titanium structures and may even lead to premature failure. In order to minimize these potential problems, it is critical to be able to measure quantitatively the oxygen contamination level in titanium alloys by nondestructive evaluation (NDE).

The objective of this research is to identify the potential problems in the NDE of titanium weldments and forgings and to develop viable approaches leading to the formulation of practical NDE inspection techniques. Upon the successful laboratory demonstration of several NDE techniques capable of measuring oxygen contamination, a reliable, efficient, and cost-effective NDE technique will be selected that can be developed into a portable system for "in-situ" NDE inspection of titanium structures.

## B. POTENTIAL NDE TECHNIQUES

In this program most of the available NDE techniques which can be used to quantitatively determine oxygen levels have been considered. These techniques are based on the principles of acoustics, electromagnetic theory and nuclear physics. In order to demonstrate the applicability of NDE techniques in detection of oxygen contamination, several titanium plates were fabricated with varying levels of oxygen. Table 1 shows the concentrations of oxygen by weight in these plates. The exact chemical compositions of these plates is listed in Section 2.

Table 1 — Oxygen Levels in Fabricated Titanium Plates

Specimen	Oxygen Content (wt%)
A	0.075
B	0.136
C	0.194
D	0.238
E	0.290

Plates of sizes approximately 5" x 5" x 1" were cut, coded, and supplied to various contractors. Oxygen detection was performed by NDE specialists on the samples. Edited versions of their reports are included in the subsequent chapters of these proceedings. No attempt has been made to assess the significance or overall rationale behind each of the NDE techniques. Except for neutron activation analysis which measured the oxygen content directly and gave absolute values of the levels of contamination, most of the NDE techniques presented in these proceedings detected changes in a physical material parameter affected by the oxygen contamination.

Oxygen has profound effect on the microstructure of these alloys. Microstructural changes, however, can be negated by post heat treatment; therefore, one needs to know the complete history of the specimen. Oxygen refines the prior beta grains; this results from an increase in the beta transus temperature as well as a decrease in the beta grain kinetics. The transformed microstructure does not

significantly change within the oxygen contamination range studied by Imam et al. (Section 2). This study indicates that the crystallographic texture of the beta annealed alloy remains essentially unaltered, while increasing oxygen significantly hardens the alloy.

The NDE techniques evaluated for their potential for measurement of oxygen contamination level are as follow:

*(i) Acoustic Techniques*

The microstructure of titanium alloys is affected by the oxygen contamination. This change in the microstructure manifests itself by changes in the elastic moduli and grain size. The moduli affect the ultrasonic wave propagation speed whereas the grain size affects the attenuation of the propagating ultrasonic wave. The oxygen contamination level can be measured quantitatively from ultrasonic techniques by measuring attenuation and velocity, provided one has a prior knowledge of these quantities in the uncontaminated base material. Sections 3 to 9 present the basic ultrasonic techniques for such measurements. For contaminated Ti alloys, the amplitude of the second harmonic of a high power ultrasonic wave propagating through the material deviates from the perfect square law behavior. This deviation has been correlated by Ringermacher et al. to the oxygen impurity content (Section 3). Gruber et al. correlated the time specific amplitude of spatially averaged ultrasonic reverberation decay envelopes in these contaminated samples with the oxygen content (Section 4). Bauxbaum and Green measured the longitudinal velocity and attenuation of ultrasound as a function of contamination (Section 5).

There is always a scatter in the physically measured values of attenuation and velocity. Combined effects of the degree of roughness of surface, lack of parallelism, variation in the coupling of ultrasound into the sample, and inhomogeneity in the material properties of the base material as a function of spatial coordinates can lead to uncertainty in the measured values of attenuation and velocity. In the most desirable ultrasonic technique, the contribution of these sources of error (noise) must not exceed the contribution due to the maximum tolerable oxygen contamination levels. This may require novel signal processing techniques. Furgason et al. used a digital correlation flaw detection system to obtain signal-to-noise ratio enhancement (Section 6). By studying the frequency dependence of ultrasonic attenuation in samples with different surface roughness and oxygen contamination, they could decipher the effect of contamination on the attenuation. They showed that the slope of the attenuation vs. frequency is dependent on the oxygen contamination level. There are several other state-of-the-art ultrasonic signal processing techniques which may prove useful in measuring low levels of the oxygen contamination; however, these techniques have not been applied specifically to the problem at hand and discussion of these techniques is excluded from these proceedings.

In Sections 7 and 8 several state-of-the-art acoustic imaging techniques are discussed. Thomas and Favro used Scanned Photo Acoustic Microscopy (SPAM) to study the effect of contamination (Section 7). This novel technique, though very useful for quick analysis, requires surface preparation and is capable of detecting qualitatively only the near-surface contamination. Greenberg et al. have discussed the application of Scanning Laser Acoustic Microscopy (SLAM) to the contamination problem (Section 8). At present these imaging techniques are qualitative only.

Vernon, et al., assumed that oxygen contamination could cause dispersion in the longitudinal velocity (Section 9). They found that  $v_L/v_S$  (ratio of longitudinal/shear velocities) varies as a function of  $O_2$  content. However, it is not clear whether this variation is due to both  $v_L$  and  $v_S$ , or just of  $v_S$  due to texture variation.

All the ultrasonic techniques that have been used in this study require calibration of the physical quantities measured. Most of the acoustic measurements required surface preparation suitable for ultrasonic studies.



### (ii) Electromagnetic Techniques

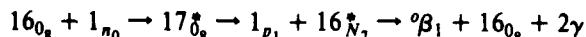
There was an attempt in this program to detect the changes in the material properties using eddy current techniques. Any detectable change in the electrical conductivity due to oxygen contamination makes the eddy current techniques applicable. Factors measurable by eddy current techniques include: alloying, heat treatment, hardness, depth of case and near-surface defects; consequently, the effects of the oxygen may be masked by these conditions. Preliminary eddy current evaluation of oxygen contaminated samples by Vernon et al. were inconclusive and need further systematic work (Section 9).

Even after the removal of the brittle surface layer ( $\alpha$ -case) formed by penetration of  $O_2$ , it is found that there are measurable conductivity changes in the bulk material. Krzywosz et al. used an improved version of conventional eddy current techniques to study  $O_2$  contamination. Instead of measuring the minute changes in the impedance of the eddy current probe, they monitored directly the RF magnetic reaction field by using a Hall sensor coaxial with an excitation probe. They performed this procedure at various excitation frequencies (0.3 kHz to 100 kHz) and observed that the magnetic reaction field, in general, decreased as a function of contamination (Section 10).

Rose measured the resistivity of oxygen-contaminated samples using a 4-point probe (Section 11). Unfortunately, the change in the resistivity is very small. Since this could be due to microstructural changes from causes other than oxygen, we feel this technique is not a viable candidate for oxygen contamination measurement. The possibility of using thermoelectric effects to study the oxygen concentration was ruled out due to inconsistent variation in the chemical composition of the base alloy (Section 12). Such compositional variations tend to mask the effect of the  $O_2$  on thermal e.m.f.

### (iii) Nuclear Techniques

Quantitative measurements of oxygen by fast neutron activation analysis have been carried out independently by Abusamra (Section 13) and Morgan (Section 14). When the contaminated titanium samples are irradiated by a flux of  $10^8 - 10^{11}$  neutrons/cm<sup>2</sup>/sec and of energy  $\sim 14$  MeV from a neutron generator, the  $O_2$  in the Ti goes through the following reaction:



The half life of  $^{16}N_7^*$  is  $\sim 7.35$  sec, decaying via  $\beta$ -decay to  $^{16}O_8$  and the emitted  $\gamma$ -rays of energies 7.14 MeV and 6.12 MeV are counted by a NaI crystal detector. The method is sensitive, fast, accurate and reliable and is capable of detecting a few parts per million of oxygen contamination. Though there is a general feeling that  $O_2$  contamination is interstitial, ESCA (Electron Spectroscopy for Chemical Analysis), ISS (Ion Scattering Spectroscopy) and SIMS (Secondary Ion Mass Spectroscopy) experiments of Mateescu et al. tend to imply that oxygen contamination is in the form of a metal oxide (Section 15). Further work in this direction by Mateescu using an ultrahigh vacuum system or the muonic X-ray experiment scheduled by Morgan may be able to determine, the nature of the oxygen contamination, i.e., whether it is atomic, molecular or bound.

## C. FUTURE WORK

As seen from the above research and through the details of the reports included in these proceedings, it is possible to measure oxygen contamination levels in Ti-6211 alloys by various ultrasonic, electromagnetic and nuclear methods. Each technique has its merits and limitations.

All of the data presented in these proceedings were on titanium samples containing homogeneous oxygen contamination levels throughout the volume. It is conceivable that in practical situations involving the fabrication and welding of such alloys, the dissolved  $O_2$  may be inhomogeneous. In such instances, the above techniques, at best, will be able to determine only the average concentration of  $O_2$ .

which may be misleading by providing values well below the critical tolerable level of contamination. Further studies should be considered which can measure the concentration profiles of contamination throughout the volume of the Ti-structure. Neutron activation analysis may be a solution to this problem.

Another problem which involves use of ultrasound and eddy currents relates to the microstructural variations caused by thermomechanical treatment of these alloys. In order to determine unequivocally the effects of oxygen on physically measured parameters by these techniques, a study is proposed which involves samples with the same thermomechanical history but varying oxygen contents. From a practical point of view a study of oxygen concentration vs. damage in these alloys is needed. This involves interfacing with fracture mechanics scientists and conducting tensile studies of contaminated Ti samples. Such a study would provide data on critical levels of oxygen contamination. The above NDE techniques must be improved to achieve the sensitivities and accuracies required to detect low levels of contamination.

Knowledge and NDE experience gained from the techniques discussed in these proceedings should enable us to extend measurement capabilities of contamination in Ti weldments. An area of concern from the NDE technology point of view is our experimental ability to measure quantitatively the minimum flaw size. NDE techniques must be able to detect and quantify flaws in these alloys below the critical size. The requirement for the maximum allowable flaw size must come from the fracture mechanics specialists. The NDE specialist must improve or devise new techniques capable of measuring such small flaws accurately. The critical flaw size relative to the grain size should be evaluated and the capabilities of NDE techniques should be improved (new signal processing techniques) where the signal/noise ratio due to these flaws is marginal.

The effects of other contaminants such as  $\text{CO}_2$ ,  $\text{H}_2$  and  $\text{N}_2$  on the material performance of titanium alloys may require attention. Depending upon their seriousness NDE techniques should be devised to detect these contaminants also. The variation in the microstructure (background noise from the NDE point of view) due to the variation in the fabrication process should be established to make the measurements more reliable.

SECTION 2  
**EFFECTS OF OXYGEN ON THE MICROSTRUCTURE AND PROPERTIES  
OF TITANIUM 6211 ALLOYS**

M. A. Inam, B. B. Rath, A. C. Ehrlich and D. J. Gillespie

*Physical Metallurgy Branch  
Naval Research Laboratory  
Washington, D.C. 20375*

**Abstract**

A systematic investigation has been conducted to evaluate the role of oxygen in modifying the microstructure and properties of Ti-6Al-2Cu-1Ta-1Mo alloy. Variation of oxygen 0.075 to 0.290 wt. percent was found to significantly reduce the prior-beta grain size without discernable changes in the transformed widmanstätten structure or crystallographic texture in the beta processed condition. Resulting from alpha stabilization effect, oxygen increases the beta transus temperature at an approximate rate of 13°C per 0.1 wt. percent increase in oxygen content. Oxygen, within the range of this investigation, solution strengthens the alloys by linearly increasing the overall hardness and tensile properties. Variation in oxygen was found to alter both low temperature resistivity and superconducting temperature. For example, the superconducting temperature is found to increase from 3.1K to 4K when oxygen concentration changes from 0.075 to 0.290 wt. percent.

AD-P004 122

## Introduction

Titanium alloys with widely varying chemistry and fabrication procedures have been developed with the purpose of optimizing specific property requirements for different structural applications. Properties such as fracture toughness and crack tolerant behavior have been emphasized in some cases at the expense of strength. Early investigations have shown that the interstitials such as oxygen, nitrogen, carbon and hydrogen have profound effects on almost all properties of titanium alloys (1,2). It is now established that the interstitial solute atoms in titanium occupy the octahedral void of HCP lattice resulting in tetragonal distortion (3), in dilute solutions remain randomly distributed as single atoms (4), depending on species and concentration increases Young's modulus (5,6), alters the nature of slip induced deformation from prismatic to pyramidal (7), introduces ordering in alpha phase (7,9) and promotes formation of alpha-2 phase ( $\text{Ti}_3\text{Al}$ ) (10,11), and promotes fracture by cleavage under suitable test condition and environment (12,13).

Although these solid solution strengthening effects of interstitials in titanium and titanium alloy have been recognized, the exact mechanism of strengthening is not understood. Conrad and coworkers (14), examining the normalized stress dependence of activation volume for the plastic flow of Ti-N, Ti-C and Ti-O alloys, have concluded that the solute atom clustering concept cannot be unequivocally identified as the mechanism for alloy strengthening. An alternate postulate to explain the strengthening effect of interstitials has been to relate ordering of the solute in the alpha-phase of the Ti-lattice (9). Short range ordering of oxygen atom over the entire range of its solubility, which is approximately 30 at.% at ambient temperatures (15), has been attributed to the observed property variations. Although a shift of the slip system from the prismatic to the pyramidal

may be rationalized on the basis of ordering, it is difficult to understand why such an ordering occurs in titanium when oxygen is present in very dilute concentrations. Furthermore, the effects of major alloy additives on either the solubility of oxygen or on its non-random distribution in the alpha-lattice is not known.

An investigation was undertaken to evaluate the oxygen effects in a near alpha titanium alloy (Ti-6Al-2Cb-1Mo-1Ta). Since this is a weldable alloy, an understanding of the role of oxygen on the alloy properties is essential in predicting load bearing characteristics of welded structures.

#### Experimental Procedure

Five Ti-6Al-2Cb-1Ta-1Mo alloys with varying oxygen contents, ranging between 0.075 to 0.290 wt.% (0.22 to 0.87 at.%), were prepared. Samples were prepared from these alloys in two batches. The first was examined in the as-received condition while the second was given an additional heat treatment at 1065°C for two hours and air cooled. The oxygen levels of the alloys have been identified, for this study, as A through E and are listed in Table I.

Table I

Composition of Ti-6211 in Wt. Percent  
(H<sub>2</sub> in ppm)

Element	A	B	C	D	E
Al	6.0	6.0	5.9	5.8	5.9
Cb	1.95	2.09	1.90	2.05	2.16
Mo	0.7	0.9	0.8	0.8	0.7
Ta	0.88	0.97	0.94	0.99	1.06
O	0.075	0.136	0.194	0.238	0.290
H(ppm)	40.0	49.0	42.0	61.0	54.0
N	0.010	0.006	0.005	0.006	0.008
C	0.02	0.02	0.02	0.02	0.03

Specimens of appropriate dimensions were prepared for optical microscopy, crystallographic texture, differential thermal analysis, macro and microhardness, and uniaxial tensile tests for flow stress evaluations. A set of specimens were prepared from the as-received batch for resistivity measurements. These sets of samples were 2 cm long with a cross-sectional area of 1 sq. mm. These were spark machined and polished to avoid deformation during sample preparation. Two current and two potential wires of Pt were spot welded on each of the five samples. The samples were mounted on a quartz cover slide and the test assembly was well heat sunk to a thermostatically controlled copper plate in the cryostat. Imbedded in this plate are a silicon diode and carbon glass temperature sensor which are used to determine the sample temperature.

Measurements were taken in the magnetic field (0 to ~10 Tesla) of a superconducting solenoid. A temperature controller, which uses a field independent capacitance sensor to sense the temperature, maintains the sample temperature to within 0.1K of the set point. Vaporized liquid helium gas and joule heating are used to cool or heat the samples.

Standard four probe techniques were used to measure the resistivity. A constant current source (stable to ~5 ppm) supplied the sample current (75 mA or less). A Keithly 181 nanovoltmeter was used to measure the sample potential. The output of the nanovoltmeter is converted to resistance and then recorded on the y-axis of an x-y recorder. Either the temperature or the magnetic field of the sample is recorded on the x-axis. A schematic diagram of the set-up is shown in Fig. 1.

The resistance is converted to resistivity by multiplying the resistance by the form factor,  $A/\ell$ , i.e.,  $\rho = RA/\ell$ , where  $R$  is the resistance,  $\ell$  is the distance between potential probes, and  $A$  is the cross-sectional area. The largest error in the resistivity is caused by the uncertainty in the measurement of the cross-sectional area. However, when the density of the material is known, the uncertainty can be reduced by using the relation  $A = W/(DL)$ , where  $D$  is the density,  $L$  is the length of the sample, and  $W$  is the weight of the sample. Also, when the density of each of the samples is the same (as is close to being true in the present study) additional precision is gained because the error in the cross-sectional area becomes

largely systematic between the alloys rather than random. For samples in this report we used a density of 4.48 g/cc in determining the cross-sectional area.

### Results and Discussion

The microstructures of the as-received and beta annealed specimens were examined at two magnifications. As-received microstructures of the five alloys are shown in Figures 2 and 3. The elongated prior beta grain consistent with hot working is evident in the micrographs (Fig. 2). All alloys show the formation of grain-boundary alpha decorating the prior beta grains independent of oxygen content although it is not clear if the prior beta grain size is affected by the oxygen content. The transformed microstructure is more clearly delineated at higher magnifications as shown in Fig. 3 whereas at the two high oxygen (0.238 and 0.290 % oxygen) levels the widmanstatten structure is typical of beta processed alloy. At lower oxygen content presence of equiaxed and elongated alpha phase suggests that these alloys were processed either at below the beta transus temperature or subjected to interruption during cooling from processing temperature. There does not appear any constant change in the alpha phase morphology which can be related to a variation in the oxygen content of the alloys. Alloy C in particular shows maximum departure from any observable variations that can be associated with oxygen content. It is concluded that the processing conditions such as hot rolling temperatures, reduction per pass, intermediate or final anneal and cooling rates were not kept constant during fabrication for all the five alloys prepared for this study.

In order to distinguish the effects of thermomechanical history from those due to oxygen on the resulting microstructure, all samples were subjected to a beta annealing schedule consisting of heating to 1065°C (1950°F) for two hours in vacuum followed by a moderate cooling rate in helium atmosphere. The resulting microstructure at low magnification is shown in Fig. 4. The influence of increasing oxygen content on a systematic decreasing beta grain size is clearly evident in these micrographs. This observation may be attributable to two distinct effects: (1) a change in beta transus temperatures increasing with oxygen content and (2) an increase in nucleation frequency accompanied with a reduced growth rate of the beta grains at annealing temperature associated with increasing oxygen content.

A systematic study of the grain growth kinetics above the beta transus temperature of each alloy is required to establish the relative contributions of the above mentioned variables. Oxygen does not appear to significantly alter the widmanstatten structure resulting from a constant cooling rate from the high temperature beta phase. The characteristics of grain boundary alpha size of the widmanstatten packet as well as the width and aspect ratio of alpha laths appear to be nearly the same for all oxygen concentrations as shown at higher magnifications in Fig. 5. Although micrograph 5E suggests that the average width of the alpha platelets is larger, consistent with the alpha stabilizing effects of oxygen, a systematic investigation is needed to quantitatively establish the role of oxygen on the morphology of the transformed products. The role of oxygen on the beta grain morphology and size is further illustrated in Fig. 6. At a magnification of 5X, the pronounced effect of oxygen on the size of equiaxed beta grain is evident. The beta grain size was evaluated using a quantitative metallographic method as shown in Fig. 7. The results suggest that the grain size is reduced by a factor of three when the oxygen content is increased from 0.075 to 0.290. The grain size is more sensitive to oxygen content in low levels up to about 0.2% oxygen beyond which further addition of oxygen does not significantly alter the beta grain size.

Crystallographic texture in these alloys were measured by evaluating the prismatic pole ( $10\bar{1}0$ ) distribution. The pole distributions were examined from x-ray reflection measurements over an  $80^\circ$  angular distribution. Results showed that all samples have a very weak transverse-basal texture and are nearly independent of oxygen content. There is a weak indication that the number of texture components decrease with increasing oxygen content. These observations are illustrated in two ( $10\bar{1}0$ ) pole figures for the lowest and highest oxygen levels in the alloy (see Fig. 8).

Since oxygen is known to be an alpha stabilizer in titanium, it would be expected that the beta transformation temperature would increase with increase in oxygen content. Several earlier studies have shown that an increase of oxygen content by 0.1% wt. in pure titanium increases the transformation temperature somewhere between  $13^\circ\text{C}$  and  $20^\circ\text{C}$  (16,17). Jaffee (17) and coworkers showed that titanium containing 4% Al is even more sensitive to the oxygen induced change in transformation temperature,



varying by as much as 29°C per 0.1 wt.% change in oxygen. The beta transus temperature in Ti-6211 was measured using a high temperature differential thermal analyzer. The temperature difference  $T$  between the sample with varying oxygen contents and the reference ( $\text{Al}_2\text{O}_3$ ) was examined as a function of temperature both in the heating and cooling cycles. The beta transus temperature were determined from the intersection of the forward-extrapolated baseline with the backward-extrapolated initial side of the peak. This temperature is referred to as the onset temperature. The change in onset temperature as a function of oxygen content is shown in Figure 9. The beta transus temperature increases in a linear manner with oxygen content at an approximate rate of 13°C per 0.1 wt.% oxygen. The sample 'C' exhibited an anomalous behavior with a significant deviation from the expected transus temperature, which may be attributed to a variation in the local variations in the oxygen content and/or the alloy chemistry. The observed behavior, consistent with those seen with pure titanium may be rationalized on the basis of a balancing effect between the alpha and beta stabilizing effect on the oxygen induced variation in the transformation temperature.

Micro and macrohardness of the Ti-6211 were determined using Vicker and Rockwell C hardness scale. Vicker hardness measurements were made with 100 gm load. Increasing hardness with oxygen content is shown in Figures 10 and 11. Both sets of measurements show a consistent linear increase in hardness with dissolved oxygen. Both sets of measurements made on the as-received and beta annealed alloys shows a linear increase in hardness within the range of oxygen content investigated. Beta annealing followed by air cool produces a finer widmanstatten structure which contributes to an increase in the hardness of the alloy, as is apparent from the figure. This is in good agreement with previously reported results (18). However, it is interesting to note that the rate of increase in microhardness with increasing oxygen content is significantly higher for alloy in the as-received condition than those subjected to subsequent beta anneal. This observation is consistent with Rockwell 'C' value of the alloys in both heat treatment conditions. Since the resulting hardness is strongly influenced by microstructural parameter such as phase size and morphology as well as by the solution hardening effects of oxygen, it is difficult to isolate the hardening effect of dissolved oxygen.

Tensile tests were performed at room temperature using the beta annealed specimens in sample configuration consistent with ASTM specifications. The yield stress,  $\sigma_y$ , ultimate tensile stress,  $\sigma_{uts}$ , and fracture stress,  $\sigma_f$ , as a function of oxygen content is shown in Figure 12. With the exception of an anomalous behavior seen in sample 'C' which has been consistently observed throughout the study, the strength related parameters linearly increase with oxygen content. The difference in the ultimate stress and fracture stress gradually decreasing with oxygen content is indicative of loss in ductility of Ti-6211 with higher dissolved oxygen.

Changes in the resistivity of titanium 6211 alloys both as a function of temperature and as a function of oxygen concentration were easily observed. The total change in resistivity after cooling the samples from 300K (room temperature) to 10K was a decrease of 17% for the sample with the lowest oxygen concentrations and a decrease of 13% for the sample with the highest oxygen concentration. The temperature coefficient of resistivity ( $\frac{1}{\rho} \frac{d\rho}{dT}$ ) varied from  $6.5 \times 10^{-4} K^{-1}$  for lowest oxygen concentrations to  $5.2 \times 10^{-4} K^{-1}$  for the highest. The sample to sample variation of the resistivity was 12% at 10K and less than 8% at room temperature. The room temperature variation is shown as a function of oxygen concentration in Fig. 13. The resistivity minimum (1%) seen in this figure was observed at all measured temperatures. These measurements were reproducible to better than 0.1% and the accuracy is estimated to be of the order of 0.1%.

The results of the transverse magnetoresistance measurements are shown in Fig. 14 and Fig. 15. The first of these two figures shows an example of change in resistivity with magnetic field for a sample at 10K. The total change in resistivity for all samples was very small - about 0.02%, and to within experimental accuracy, all samples yielded the same magnetoresistance (see Fig. 15). At higher temperatures the temperature stability of the cryostat was such that small temperature changes yielded resistivity changes which were greater than the total magnetoresistivity, thus making magnetoresistance measurements impractical except at the lowest temperatures.

The major surprise of the experiment was the observation of superconductivity in these alloys at relatively high transition temperatures and the fact that the transition temperature is strongly sample dependent. The superconducting transition for the various samples is shown in Fig. 16 and the dependence of this transition with oxygen content is shown in Fig. 17. (The transition temperature,  $T_c$ , is taken to be the temperature at which the resistance is 1/2 that at a temperature of 5K.) These results indicate that for alloys with oxygen concentration greater than 0.4 at.% it is possible to sensitively distinguish the oxygen concentration by measuring the superconducting transition.

The results of Fig. 13 which show an electrical resistivity minimum as a function of oxygen concentration are interesting in two respects. First, they show the resistivity to be a double valued function of oxygen concentration and thus resistivity measurements will be ambiguous for identifying levels of oxygen (at least at the lowest concentrations). More important, the fact that there is a resistivity minimum as a function of oxygen content implies a more complex reaction than simple dissolution. The variation of the resistivity with oxygen concentrations will be monotonic unless some secondary change, such as a change in the crystallographic morphology, accompanies the oxygen variation.

The small magnitude of the magnetoresistance is as expected. The mean free path of a conduction electron is very short in this alloy system relative to the radius of curvature of a moving electron in the applied magnetic fields and generally these short mean free path yield small magnetoresistance (19). The inability to distinguish the variation of this small magnetoresistance as a function of oxygen content is also not unreasonable since the addition of small amounts of oxygen will not produce large changes in the mean free path of the conduction electrons. However, the field dependence of the magnetoresistance is somewhat surprising. The saturation of the resistivity at high fields does not even qualitatively fit the usually observed straightforward theory for the magnetoresistance of alloys whose electron mean free paths are short compared to their radius of curvature (20).

Most surprising of all is the nature of the superconductivity in this system - in particular the strong dependence of the superconducting transition temperature upon the oxygen concentration. Anderson's theorem (21) for superconductivity in concentrated alloy systems shows that the superconducting transition temperature will be unaffected by non-magnetic impurities. Thus, it appears that for oxygen concentrations above 0.4 at.%, the oxygen acts not only as an impurity but also as a kind of catalyst which introduces significant changes in the morphology of the alloy system. It is these changes in turn which are easily detected by the change in the superconducting transition temperatures of the alloys.

### Conclusions

1. Oxygen has a profound effect on the microstructure and the resulting properties of Ti-6211 in the range of oxygen content varying between 0.075 to 0.290 wt.%. Dissolved oxygen refines the prior beta grains resulting from an increase in the beta transus temperature as well as a decrease in the beta grain growth kinetics. However, the transformed microstructure does not significantly change with oxygen within the range studied in this investigation.

2. While the crystallographic texture of the beta annealed alloy remains essentially unaltered, increasing oxygen significantly hardens the alloy as evidenced by a systematic increase in hardness and tensile parameters.

3. Variation in oxygen content alters both low temperature resistivity and superconducting temperature.

### References

1. R. I. Jaffee, Prog. Met. Phys. 7, 65 (1968).
2. H. Conrad, M. Doner and B. de Meester, Titanium Science and Technology, Plenum Press, New York, 969 (1973).
3. H. T. Clark, Jr., Trans. AIME, 185, 588 (1949).
4. B. Holmberg and T. Dagerhamn, Acta Chem. Scand., 15, 919 (1961).
5. A. D. McQuillan and M. K. McQuillan, Titanium Academic Press, New York (1956).

6. R. I. Jaffee, H. R. Ogden and D. J. Maykuth, Trans. AIME, 188, 1261 (1950).
7. A. T. Churchman, Proc. Royal Soc., A, London, 226, 216 (1954).
8. G. Welsch and W. Bunk, Met. Trans. 13A, 889 (1982).
9. S. Yamaguchi, Journal of Physical Society of Japan, 27, 155 (1969).
10. M. J. Blackburn and J. C. Williams, Trans. TMS-AIME, 239, 287 (1967).
11. M. A. Imam and B. B. Rath, unpublished result
12. D. A. Meyn and G. Sandoz, Trans. TMS-AIME, 245, 1253 (1969).
13. R. J. H. Wanhil, Acta Met. 21, 1253 (1973).
14. H. Conrad, Progress in Materials Science, Pergamon Press, 26, (1981).
15. M. Hansen, Constitution of Binary Alloy, McGraw Hill, Inc. (1958).
16. A. E. Jenkins and H. W. Worner, Journal of the Institute of Metals, 80, 157 (1951).
17. H. R. Ogden and R. I. Jaffee, TML Report No. 20, Battelle Memorial Institute, Columbus, Ohio, 12 (1955).
18. C. M. Gilmore and M. A. Imam, Titanium and Titanium Alloy, Plenum Press, New York, 1, 637 (1982).
19. F. J. Blatt, Solid State Physics, 4, 199 (1957).
20. *ibid*, 233
21. P. W. Anderson, J. Phys. Chem. Solids, 11, 26 (1959).

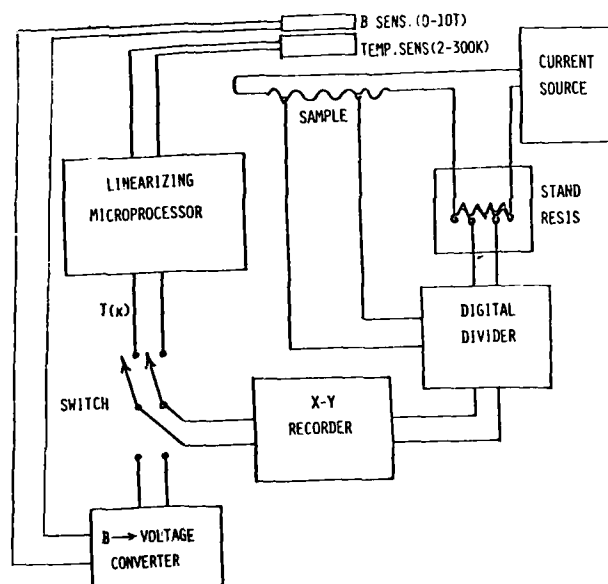
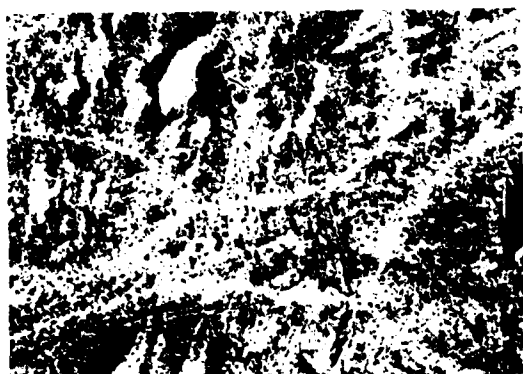


**Figure 1. Automatic Resistivity Measuring Apparatus**



.075 %O<sub>2</sub>



.136 %O<sub>2</sub>



.194 %O<sub>2</sub>



.238 %O<sub>2</sub>



.290 %O<sub>2</sub>

0.4 mm

Figure 2. Effect of Oxygen on the Microstructure  
of Ti-6211,  $\alpha$ - $\beta$  Processed (As Received )



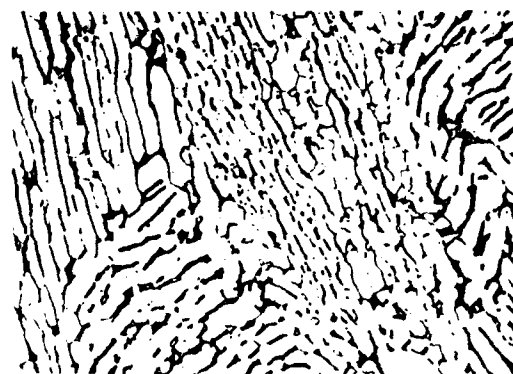
.075 %O<sub>2</sub>



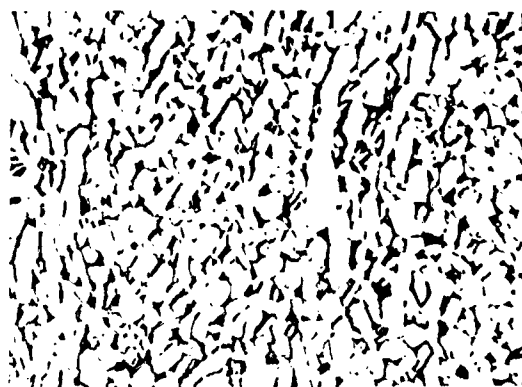
.136 %O<sub>2</sub>



.194 %O<sub>2</sub>



.238 %O<sub>2</sub>

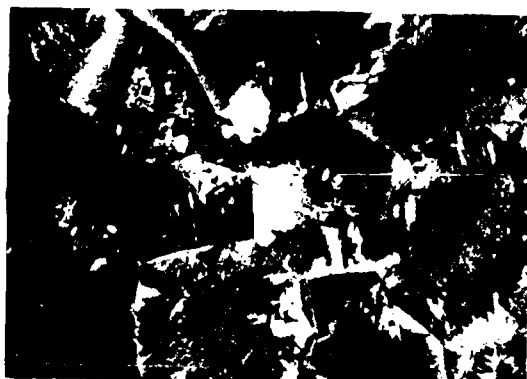


.290 %O<sub>2</sub>

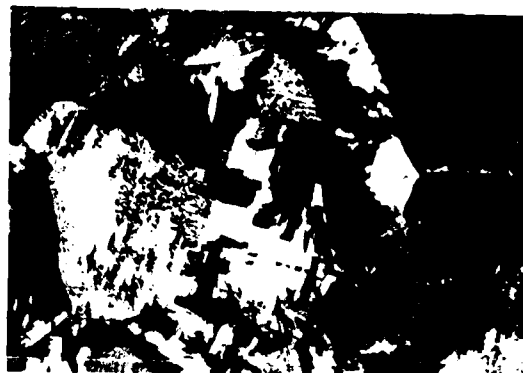
40 μm

Figure 3. Effect of Oxygen on the Microstructure of Ti-6211 ,  $\alpha$ - $\beta$  Processed (As Received)





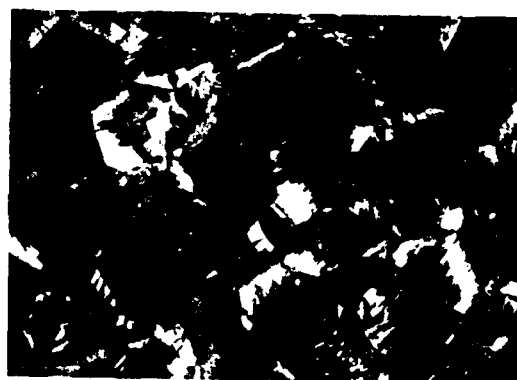
.075 %O<sub>2</sub>



.136 %O<sub>2</sub>



.194 %O<sub>2</sub>



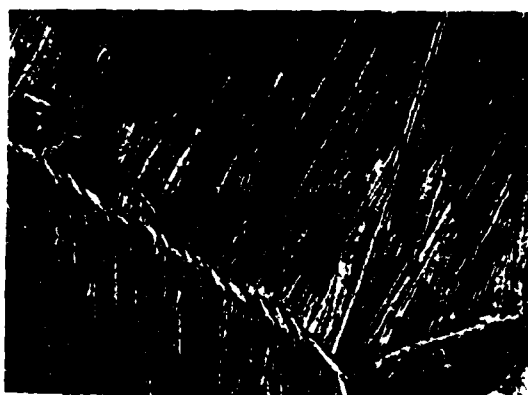
.238 %O<sub>2</sub>



.290 %O<sub>2</sub>

1.4 mm

Figure 4. Effect of Oxygen on the Microstructure  
of Ti-6211, Annealed - 1065 °C /2h/AC



.075%O<sub>2</sub>



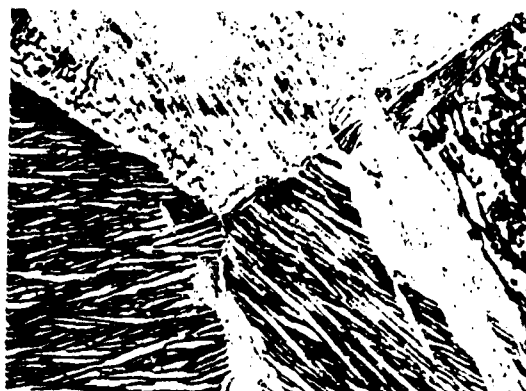
.136%O<sub>2</sub>



.194%O<sub>2</sub>



.238%O<sub>2</sub>



.290%O<sub>2</sub>

40 μm

Figure 5. Effect of Oxygen on the Microstructure  
of Ti-6211, Annealed - 1065 °C /2h/AC

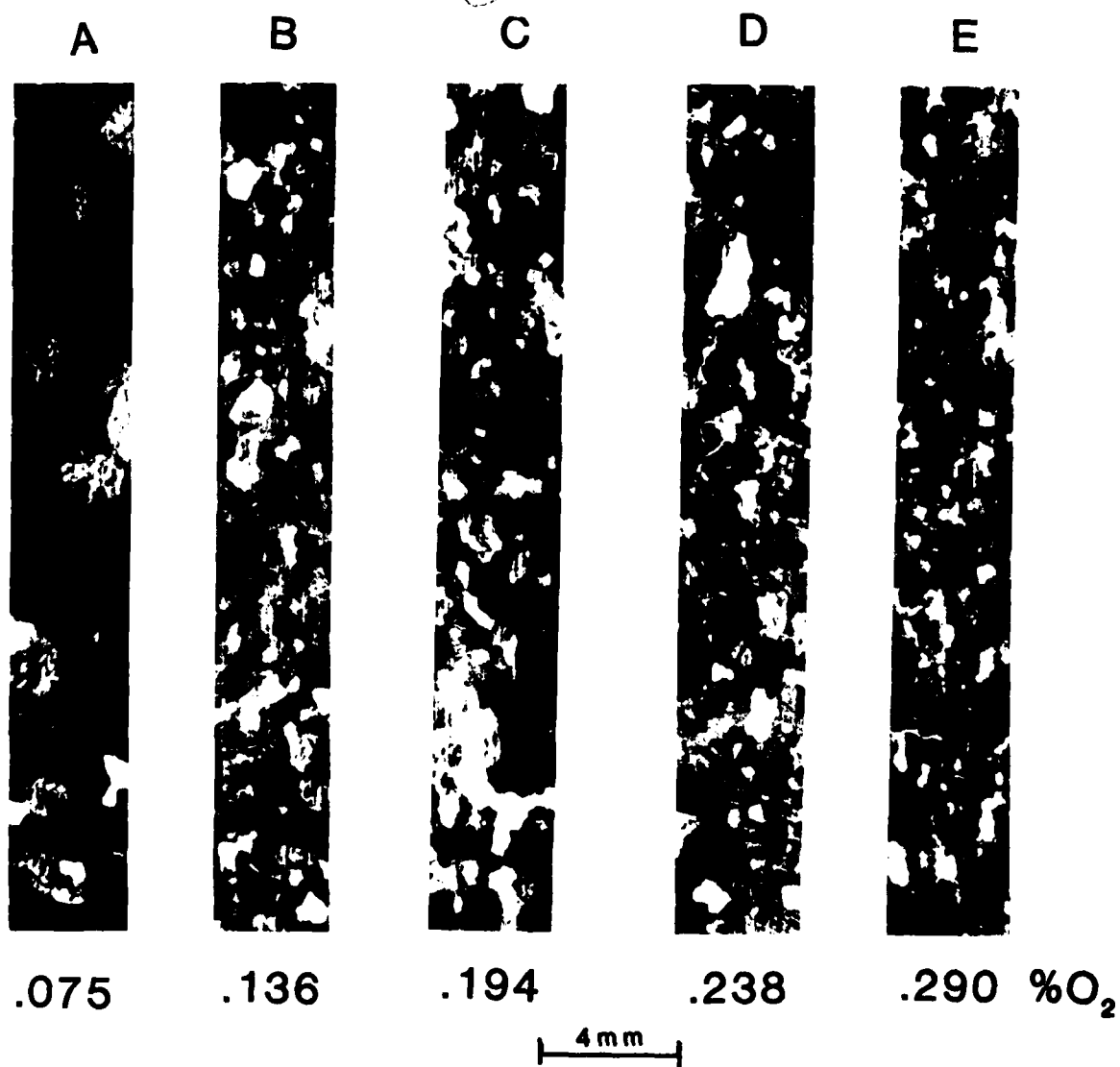
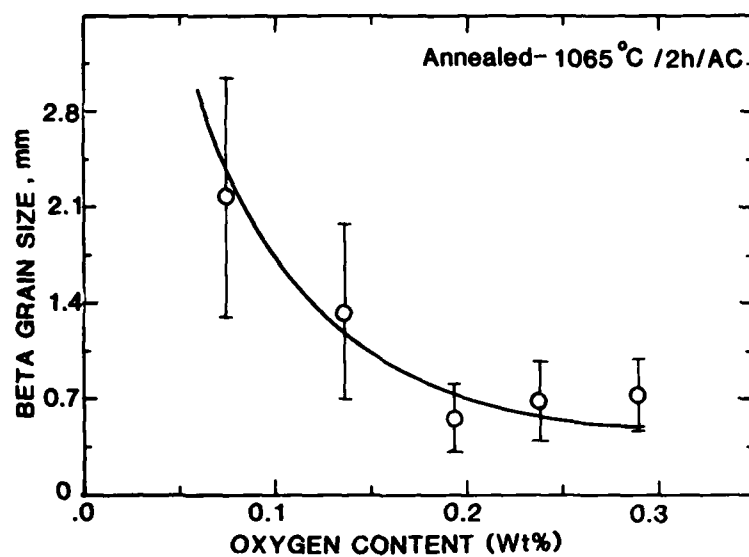
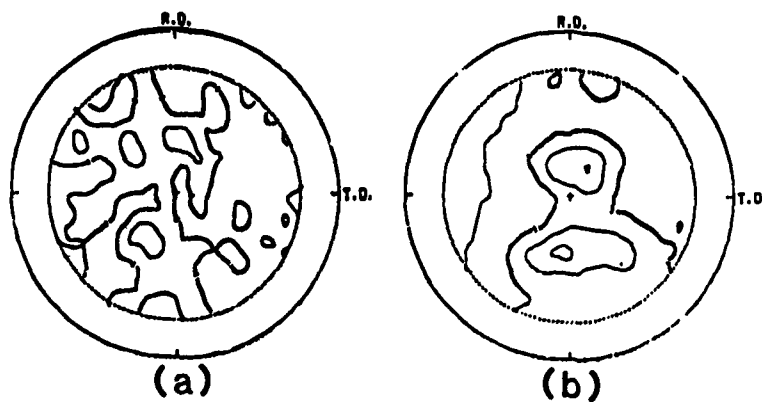


Figure 6. Effect of Oxygen on the prior-beta Grain Structure of Ti-6211  
Annealed - 1065°C/2h/AC



**Figure 7. Effect of Oxygen Content in Ti-6211 on Grain Size**



**Figure 8. (10 $\bar{1}$ 0) Pole Figure of Ti-6211 for (a) 0.075 wt % O<sub>2</sub>, (b) 0.290 wt.% O<sub>2</sub>**

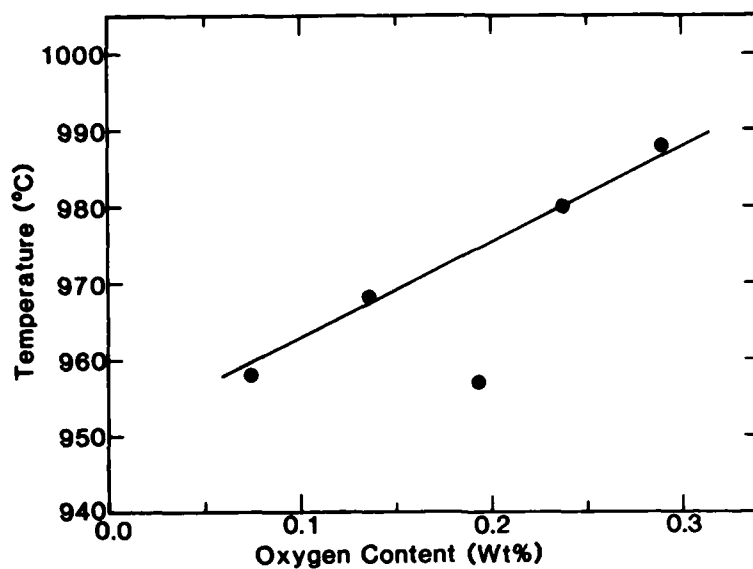


**Figure 9. Effect of Oxygen Content in Ti-6211  
Beta Transus Temperature**

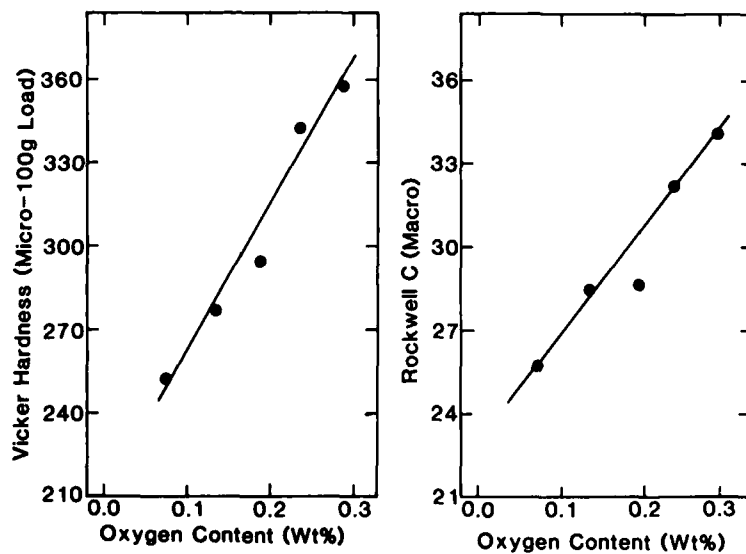


**Figure 10. Effect of Oxygen Content on Hardness  
in Ti-6211,  $\alpha$ - $\beta$  Processed (As Received)**

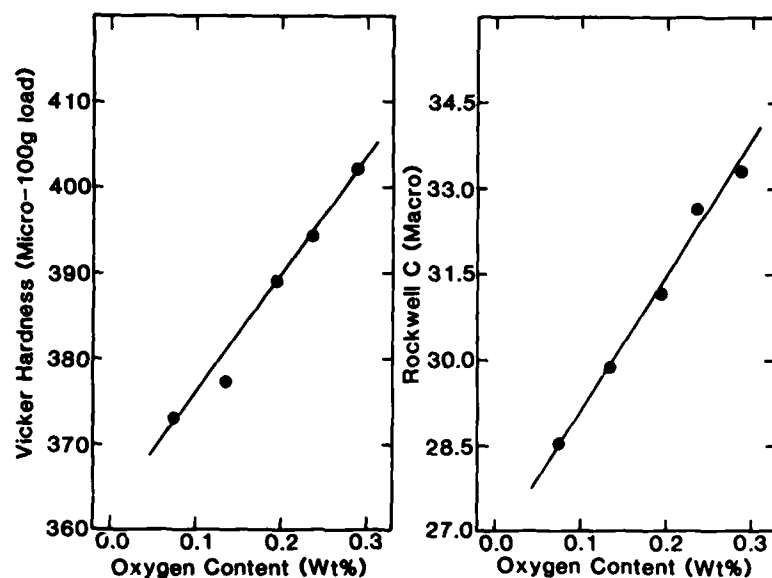


**Figure 11 Effect of Oxygen Content on Hardness in Ti-6211, Annealed-1065 C/2h/AC**

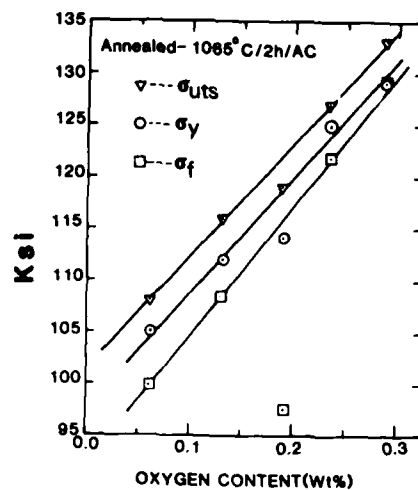


**Figure 12. Effect of Oxygen Content in Ti-6211 on Yield Stress ( $\sigma_y$ ), Ultimate Tensile Stress ( $\sigma_{UTS}$ ) and Fracture Stress ( $\sigma_f$ )**

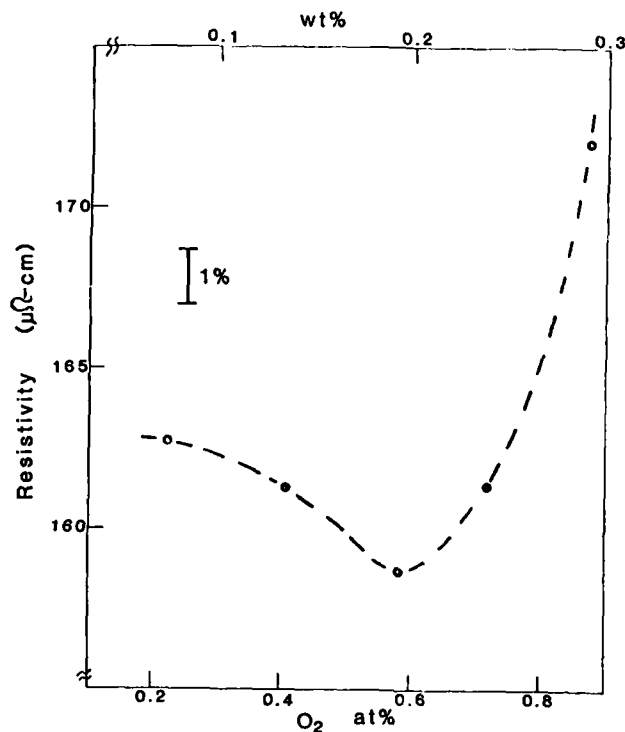


**Figure 13. Effect of Oxygen Content in Ti-6211 on Resistivity at Room Temperature**

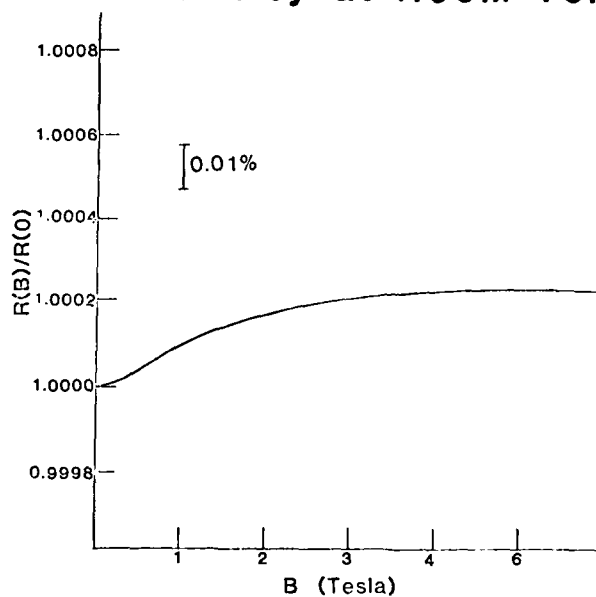


**Figure 14. Ratio of Magnetoresistance to Zero Field Resistance as a Function of Magnetic Field with 0.2 at.% O<sub>2</sub> at 10K**

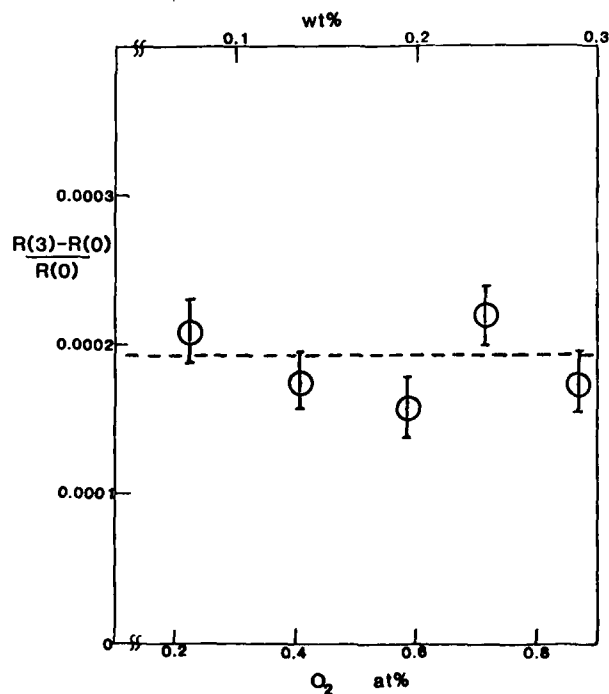


Figure 15. Effect of Oxygen Content on the Fractional Change in Resistance in Going from Zero Field to a Field of 3 Tesla

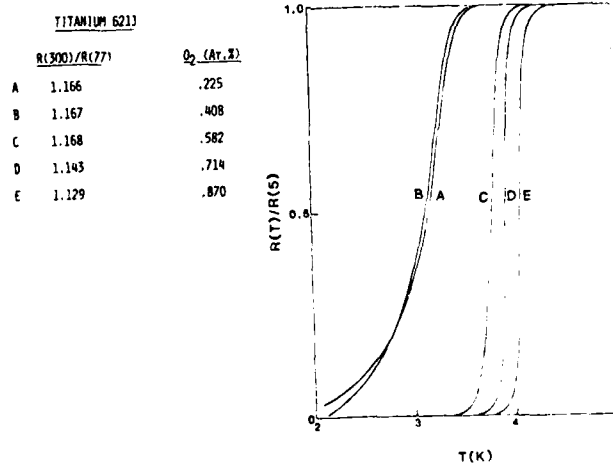
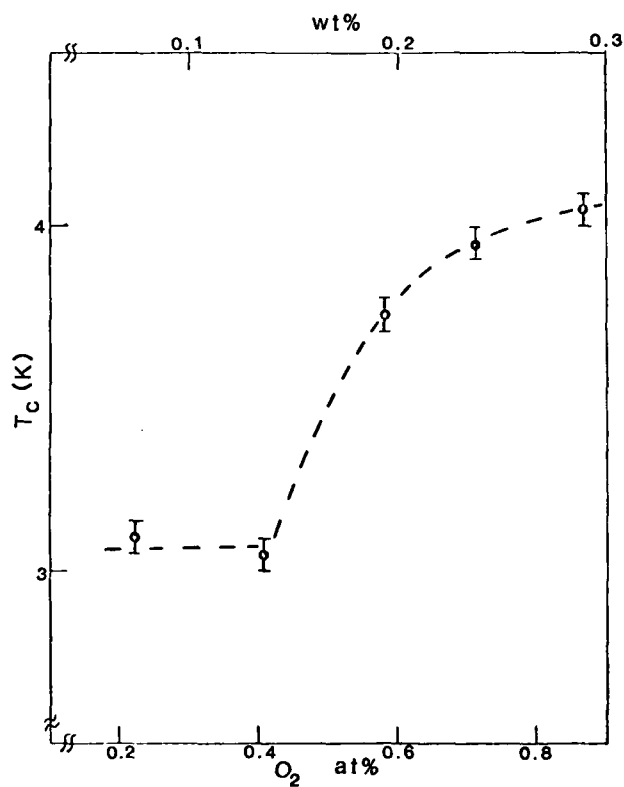


Figure 16. Ratio of Resistance at Temperature T to 5K as a Function of Oxygen Content





**Figure 17. The Superconducting Transition Temperature as a Function of Oxygen Content**

**PART B**  
**ACOUSTICAL TECHNIQUES**

**SECTION 3**  
**NONLINEAR ULTRASONIC CHARACTERIZATION OF**  
**OXYGEN IMPURITIES IN TITANIUM**

**Harry I. Ringermacher and Richard S. Williams**

*United Technologies Research Center*  
*East Hartford, CT 06108*

Titanium specimens containing oxygen impurities ranging from 0.1 to 0.5 percent by weight have been examined using nonlinear ultrasonic techniques. Second harmonic amplitude deviation from the expected square law behavior has been observed. This is consistent with theory relating dislocations and impurity content to ultrasonic second and third harmonic generation in materials. The results of these tests are presented and directions for future work outlined.

AD-P004 123

## INTRODUCTION

The presence of oxygen in titanium alloys is known to alter their material properties. Oxygen concentrations as low as 0.1 wt% dramatically increase the strength and hardness of these alloys (Ref. 1). At the same time, however, the alloy ductility is decreased (Ref. 2). These effects are particularly important at weld sites where oxygen embrittlement can pose a serious problem when contamination occurs. The level of contamination will determine the severity of embrittlement. It is, therefore, useful to seek a simple, nondestructive, field-worthy technique with high sensitivity to the presence of oxygen impurities in these alloys.

Ultrasonic techniques generally satisfy the above requirement. Hardness and internal friction must influence sound velocity and the attenuation - frequency spectra in these materials. At the very least, the presence of oxygen is expected to change the density and, hence, the sound velocity. In addition, oxygen should alter the elastic constants, although observation of this effect can be more complicated.

## THEORY

### Basis for Nonlinear Methods

For the present task, a novel nonlinear ultrasonic approach was chosen, since it is well known that the motion of dislocations in single crystals can be a source of second harmonic generation (Ref. 3). Hikata has shown (Ref. 4) that the presence of impurities can pin dislocation motion thereby altering both the second and third harmonic content. Grain size in a polycrystalline sample may also have an effect on harmonic generation. While this is essentially an unknown area, Jon, et al., (Ref. 5), have shown that 99.96 percent pure polycrystalline titanium demonstrates a strict square law second harmonic behavior, apparently arising from lattice anharmonicity.

The present nonlinear approach is based on the assumption that oxygen acts upon the dislocations either by pinning or by generating localized stresses and thereby alters the third harmonic content of the observed ultrasonic signal. If perfect square law behavior for second harmonic generation is assumed, then the presence of third harmonics, dependent on oxygen content, will appear as a deviation from square law behavior and vary monotonically as a function of the oxygen concentration in the titanium specimens.

### Basis for Linear Methods

For the sake of completeness, the titanium specimens were also characterized using linear ultrasonic techniques. In particular, velocity of sound and attenuation - frequency spectra were investigated. As discussed further, under Experimental Results, correlation between oxygen content and the attenuation - frequency spectrum was observed. However, it was not as well resolved as that observed with the nonlinear methods. Further, sound velocity data, within experimental accuracy showed no dependence on oxygen content.

## EXPERIMENTAL TECHNIQUES

### Specimens and Transducers

Five, rough surface, titanium plate specimens, with wt.% oxygen contents of 0.075 (specimen A), 0.136 (B), 0.194 (C), 0.238 (D), and 0.290 (E) were provided by the NRL for the present investigations. Prior to performance of the ultrasonic tests, the plates were machine ground flat with opposite parallel faces.

Lithium niobate ( $\text{LiNbO}_3$ ) transducers were used for all the nonlinear data collection. A 1.25 cm dia, 5 MHz,  $36^\circ$ -Y cut transducer was used as the transmitter for longitudinal waves. The receiver, bonded on the opposite side of the plate, was a 0.625 cm dia, 10 MHz transducer of the same variety. All the transducers were bonded with Nonaq grease and "wrung in". Contact to the transducers was made through fine wires spot-soldered on the ground side and center of the coaxial plating.

### Instrumentation

A block diagram of the ultrasonic system assembled for the nonlinear measurements is shown in Fig. 1. A Matec 515A gated RF amplifier provided 2  $\mu\text{s}$  pulses at up to 2 kW power to the  $\text{LiNbO}_3$  transducer. Alan 50HT82.5 high power attenuators on the input and output sides permitted precisely controlled attenuation changes for calibration control of the data. To ensure correct Alan attenuator calibration, 3 dB, 50 ohm feedthroughs, fixed attenuators were placed on both sides of the Alans so they were certain to look into 50 ohms in both directions. In this way, the attenuator switch combinations could be made to reproduce performance within 0.25 dB. The input pulse was sent through a 5 MHz lowpass filter to inhibit transmission of 10 MHz rf, and the received signal was passed through a 10 MHz high pass filter to eliminate the 5 MHz fundamental transmission signal while permitting passage of any second harmonic 10 MHz rf generated within the sample as a result of its nonlinear response. A Matec 251 tuned preamp further restricted the bandwidth. A Matec 605 broadband receiver was used for the final gain stage to a recording instrument.

All the linear ultrasonic data was taken on a similar Matec system (Fig. 2) that was microprocessor controlled to vary frequency over a programmed range, and accumulate and plot attenuation data.

### Procedures

It was important, in taking the nonlinear data, to ensure that the observed nonlinear behavior was not generated in the electronic equipment. To avoid this, the receiver amplifier was always operated at or near a fixed point on its response

FIG. 1

# ULTRASONIC SYSTEM FOR ANALYSIS OF MATERIAL NONLINEARITY

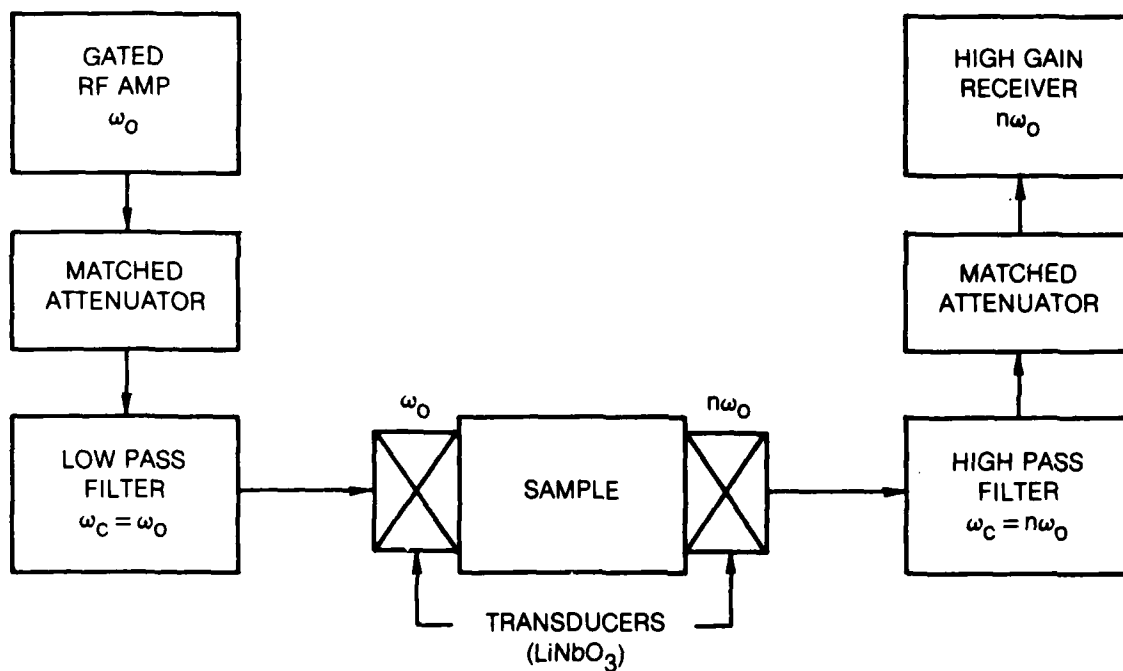
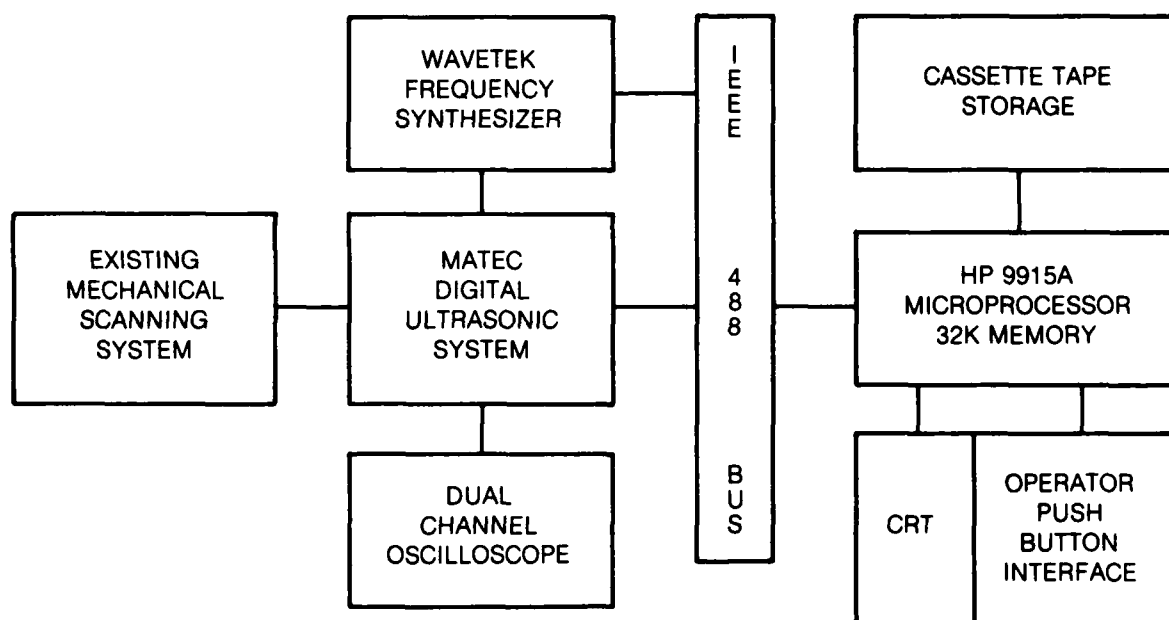


FIG. 2

# ULTRASONIC SYSTEM FOR AUTOMATED MEASUREMENT OF ATTENUATION





curve, for all input signal levels. It was assumed that the second harmonic amplitude  $A_2$  is precisely proportional to the square of the fundamental  $A_1$ :

$$A_2 = KA_1^{2.000} \quad (1)$$

Starting at the highest power level to the input transducer, for every 1.0 dB of attenuation inserted at the input side, 2.0 dB was withdrawn on the output side. This, in effect, fixed the exponent at 2.000. In this manner, a perfect square law response would show as a constant signal out independent of signal in. Matching the attenuators as just described, and using lithium niobate, which is known to have an extremely linear response at high power levels, further helped to ensure valid results. System linearity was constantly monitored with each new power level, and maintained to within 1.5 percent.

A single, arbitrary point on the surface of each specimen was used for taking the power data rather than averaging many points. The consistency of the resulting data suggests that this technique represents an absolute method of comparison between independent samples.

## EXPERIMENTAL RESULTS

### Nonlinear Method

Data was obtained over an input amplitude range of 16 dB with a maximum input voltage to the transducer of approximately 400 volts peak-to-peak. The input amplitude was decreased from its maximum value in 2.0 dB steps, while output attenuation was simultaneously removed in 4.0 dB steps. To first-order, the output amplitude remained constant, thus indicating an approximate square law output behavior with input amplitude change. Since the deviation was small, a statistical method that disregards the quantitative nature of the deviation within each sample data set was employed. An average output amplitude  $A_2$  was calculated for each sample using the power levels evaluated. The deviation of each amplitude level from the average output amplitude was taken to be a statistical representation of the deviation from perfect square law behavior and a mean square deviation,  $\Delta A_2$ , was calculated for each sample.

The mean square deviation was then translated into an exponent deviation,  $\Delta N$ , using:

$$\Delta N = N \frac{\Delta A_2}{A_2 \ln A_2}$$

Here we set  $N = 2.000$ .

The nonlinear data results are presented in Fig. 3, with the exponent deviation from perfect square-law behavior,  $\Delta N$ , plotted against oxygen concentration. As can be seen, excellent correlation exists between a linear increase in the exponent deviation and the oxygen contamination with the exception of sample B.

Experimental error in the data arises primarily from the  $\pm 0.25$  dB attenuator calibration error. Over a 16 dB input amplitude range, this amounts to an average error of 8 percent or less; i.e., within the circular regions plotted in Fig. 3.

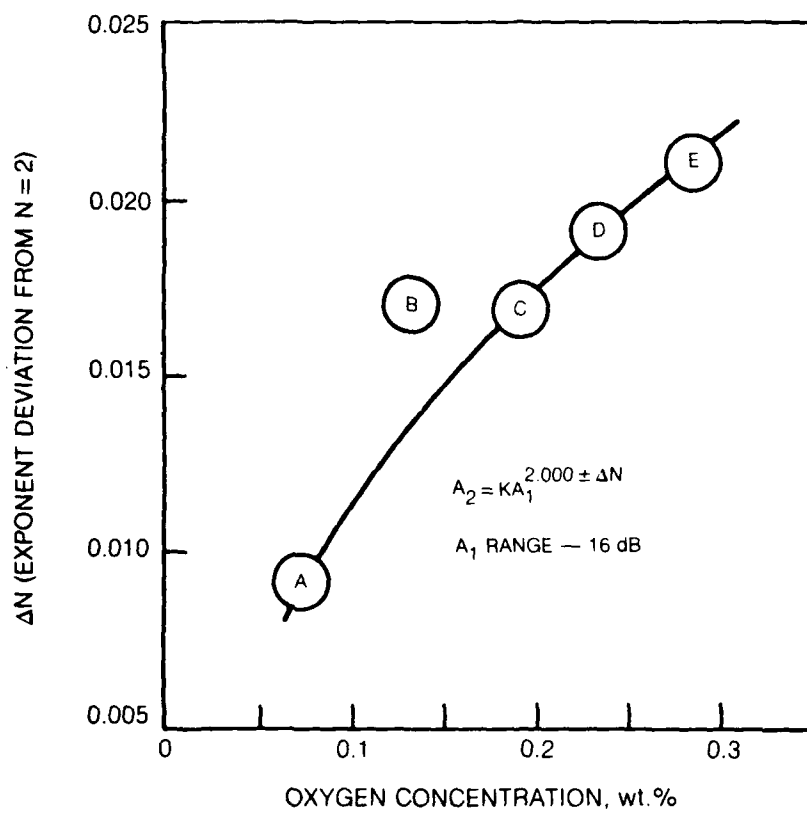
### Linear Methods

#### Velocity of Sound Measurements

Velocity of sound data was obtained on all five titanium specimens using direct pulse-echo transmission methods. Results are shown in Table I. There are essentially no differences in the measured velocities within the  $\pm 1$  percent experimental error. Hsu and Conrad has previously reported (Ref. 6) an increasing sound velocity with oxygen content in titanium which they attributed to changing density and elastic

FIG. 3

SQUARE LAW DEVIATION AS A FUNCTION OF OXYGEN CONCENTRATION



constants. However, their work involved specimens with oxygen contents up to 0.9 wt.%, while the present data extends only to 0.3 wt.%. The present velocity values agree with their low concentration values to within their data scatter.

TABLE I  
SUMMARY OF SPECIMEN PROPERTIES

<u>Specimen</u>	<u>Oxygen Content wt.%</u>	<u>Long Sound Velocity cm/sec</u>
A	0.075	$(6.13 \pm 0.06) \times 10^5$
B	0.136	$6.11 \pm 0.06$
C	0.194	$6.02 \pm 0.06$
D	0.238	$6.05 \pm 0.06$
E	0.290	$6.11 \pm 0.06$

#### Attenuation-Frequency Spectra

Attenuation data in polycrystalline specimens is generally quite susceptible to errors arising from variations in the grain structure. These can include phase cancellation effects, which predominate when the ultrasonic wavelength  $\lambda$  is comparable to grain dimension  $D$ , and diffusion effects arising when  $\lambda \ll D$ . The major contributors to attenuation in the present regime ( $\lambda \gg D$ ) arise from lattice hysteresis and Rayleigh scattering.

The five specimens were examined over a frequency range of 10-20 MHz, with the results presented in Fig. 4. The attenuation levels are seen to vary considerably in the five specimens over the entire frequency range. To suppress any frequency independent effects, the slope of attenuation versus frequency was evaluated and is presented in Fig. 5. Data above 20 MHz is not reliable due to poor signal-to-noise levels. Below 20 MHz, some correlation can be seen between the slope of attenuation and the oxygen content. The slope decreases with increasing oxygen concentration. A, B, and C are not well resolved, while D and E show increasingly significant slope changes with frequency.

FIG. 4

ATTENUATION AS A FUNCTION OF FREQUENCY FOR SAMPLES A-E

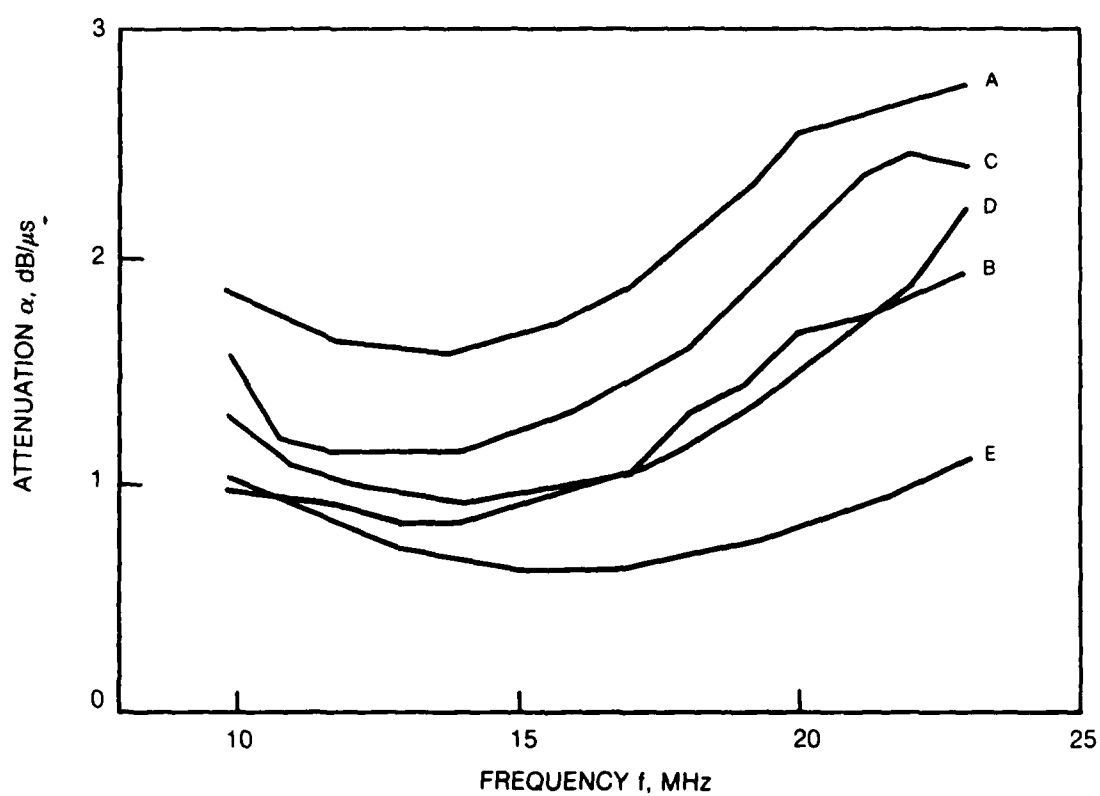
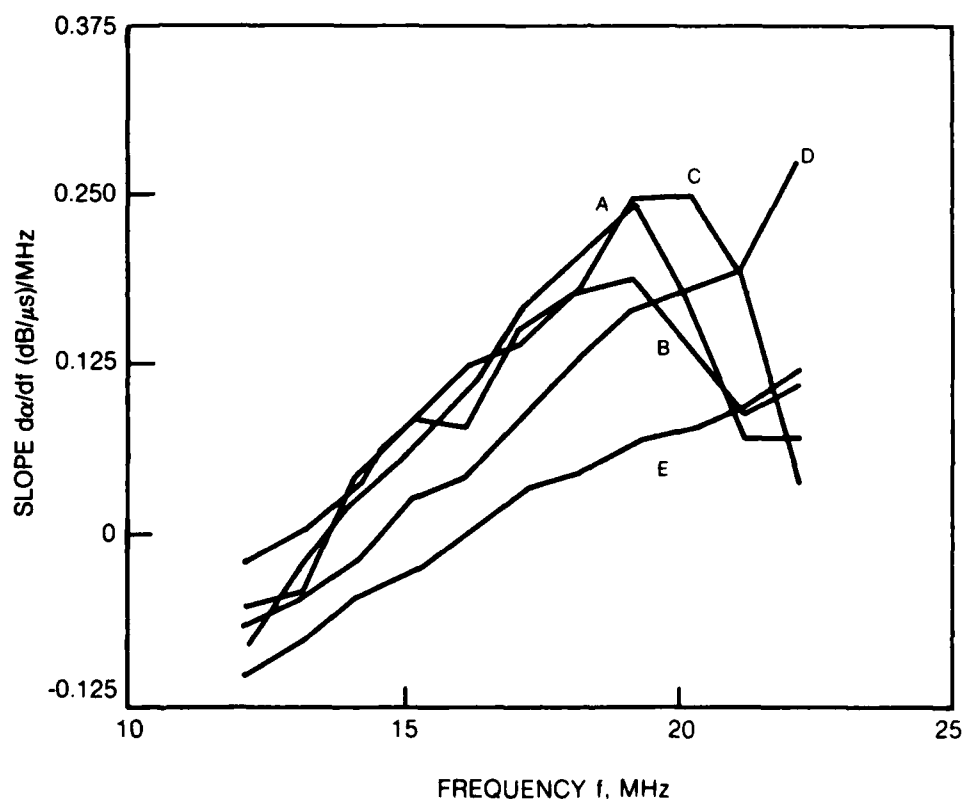


FIG. 5

**SLOPE OF ATTENUATION AS A FUNCTION OF FREQUENCY FOR SAMPLES A-E**



## CONCLUDING REMARKS

Linear techniques, although demonstrating some correlation, appear to be more sensitive to measurement artifact errors arising from material inhomogeneities and, hence, demand greater care in data measurement and interpretation.

Nonlinear ultrasonic techniques showed an excellent correlation between deviation from the ideal, perfect material, second harmonic amplitude square-law behavior and the oxygen impurity concentration.

Furthermore, the excellent correlation obtained using a randomly chosen point for the data on each specimen suggests this technique shows promise in giving results independent of the above-mentioned artifact errors.

#### REFERENCES

1. Sargent, G. A., and H. Conrad: On the Strengthening of Titanium by Oxygen. Scripta Metallurgica 6, 1099 (1972).
2. Gupta, D., and S. Weinig: The Dislocation-Oxygen Interaction in Alpha Titanium and its Effects on the Ductile-to-Brittle Transition. Trans. of the Metallurgical Soc. of AIME 215, 209 (1959).
3. Hikata, A., F. A. Sewell, Jr., and C. Elbaum: Generation of Ultrasonic Second and Third Harmonics due to Dislocations. II, Phys. Rev. 151, 442 (1966).
4. Hikata, A., and C. Elbaum: Generation of Ultrasonic Second and Third Harmonics Due to Dislocations. I, Phys. Rev. 144, 469 (1966).
5. Joh, M. C., W. P. Mason, and D. N. Beshers: Observation of Acoustic Harmonics Generated by Long Range Motion of Dislocations. J. App. Phys. 49, 5871 (1978).
6. Hsu, N. and H. Conrad: Ultrasonic Wave Velocity Measurements on Titanium-Oxygen Alloys. Scripta Metallurgica 5, 905 (1971).



SECTION 4  
**EFFECTS OF OXYGEN-CONTAMINATION-INDUCED  
MICROSTRUCTURAL CHANGES ON THE  
REVERBERATION OF ULTRASOUND IN Ti-6211 ALLOYS**

G. J. Gruber and G. J. Hendrix

*Southwest Research Institute  
San Antonio, Tx 78284*

← Titanium alloys of extra low oxygen levels are necessary for manned, deep-diving naval vessels because small amounts of dissolved oxygen markedly increase the brittleness of these alloys at low temperatures. The lack of reliable and an accurate nondestructive method for the determination of interstitial oxygen contamination of titanium forgings and weldments is a serious problem.

A pulse-echo ultrasonic technique was used to measure the decay of ultrasound in five Ti-6211 alloy plate specimens containing known concentrations of dissolved oxygen (from 0.075 to 0.290 percent by weight). Surface conditions of the immersed plates had no influence on the ultrasonic results obtained for the bulk of the test specimens. Both the time-specific amplitude and decay rate of the spatially averaged reverberation curves proved to be sensitive indicators of the microstructural variations among the test specimens. The correlation between the ultrasonic-reverberation and oxygen-contamination levels was found to be significant ( $p < 0.08$ ). The present study has confirmed that interstitial oxygen in Ti-6211 forgings and weldments can be monitored through its microstructure-mediated effect on the reverberation of a focusable interrogating ultrasonic beam.

↑

AD-P004 124

## I. INTRODUCTION AND SUMMARY

### A. Background

Small amounts of dissolved oxygen in Ti-6211 markedly increase the brittleness of these alloys at low temperatures. Interstitial oxygen contamination (IOC) must, therefore, be closely controlled in the finished products. To characterize these alloys, the following needs must be met (Table 1). Presently, the lack of a reliable and an accurate NDE technique for the quantitative assessment of IOC of Ti-6211 forgings and weldments is perceived as the most serious NDE problem.

TABLE I

<u>Field</u>	<u>Need</u>
Nondestructive Evaluation	(1) Quantify level of interstitial oxygen contamination in base and weld metals  (2) Detect small flaws in base and weld metals  (3) Estimate characteristics of detected flaws
Fracture Mechanics	(4) Establish critical interstitial oxygen contamination levels in relation to material properties  (5) Establish critical flaw size in relation to other flaw characteristics, stresses and material properties.

## B. Objective

The main objective of the reported work was to demonstrate the feasibility of the reverberation-decay-measurement technique (1) for the quantitative assessment of IOC-induced microstructural changes in the five contaminated plate specimens provided by the government.

## C. Accomplishments

The laboratory findings are as follow:

- (1) The reverberation-decay-measurement technique was implemented with standard ultrasonic transducers and equipment to yield a fast IOC-measurement system.
- (2) The spatial-averaging technique for the nondestructive determination of microstructural features was successfully extended from single-phase metals to two-phase metals (alpha-beta titanium alloys).
- (3) The statistical measures of the averaged reverberation decay curves proved to be sensitive indicators of the IOC-induced microstructural variations among the five test specimens.
- (4) The amplitude and slope of the reverberation curves were shown to vary systematically with the morphology of the alpha phase.
- (5) The microstructures were observed to change from a fine alpha structure to a dendritic alpha structure in the highly alpha-phase-stabilized, IOC-rich alloys. The differences in alpha particle spacing, aspect ratio of the primary alpha and acicular-alpha-to-globular-alpha ratio were notable.
- (6) The interaction of dissolved oxygen with the alpha phase (oxygen goes into the alpha phase and stabilizes it) was postulated as the mechanism for the observed changes in alpha-phase morphology with increasing IOC.

## D. Significance of Findings

The successful accomplishment of the program objective has the potential to:

- (1) Speed the development of field-qualified ultrasonic procedures and equipment for the acceptance of bulk plates as well as heavy weldments and weld repairs from the viewpoint of oxygen contamination.
- (2) Provide a working prototype that can be upgraded to a compact system applicable to weldments on the production lines.

## II. REVERBERATION-DECAY-MEASUREMENT TECHNIQUE

The salient analytical and experimental features of the applied statistical ultrasonic technique are presented in this section.

### A. Analytical Considerations

There is a well established body of literature concerning the ultrasonic evaluation of the microstructures of single- and multi-phase metals. The scattering of shear waves is particularly affected by the random grain and phase boundaries where discontinuities in the acoustic impedance occur. Grain sizes determined metallographically and by means of reverberation-decay measurements agree surprisingly well considering the simplicity of the mathematical model (1). These tests made the nondestructive measurements of IOC in the five plates a definite possibility. Provided that the samples contain sufficiently large oxygen concentrations for substantial microstructural changes to occur, it should be possible to obtain a significant correlation between alpha-phase morphology (particle spacing, aspect ratio, volume fraction, etc.) and reverberation-decay statistics. The main scattering centers in the plates are postulated to be the alpha-phase particles with different elastic modulus from that of the beta matrix.

In the pulse-echo mode, a fraction of the scattered energy returns to the transmitting probe that can be switched to the receiver of the ultrasonic instrument after a dead time. The amplitude of the *average* back-scattered waveform,  $A_s(x)$ , can be measured as a function of sound path  $x$  (or time of flight  $t$  where  $x = ct$  and  $c$  is the wave velocity). In the ~~Rayleigh-scattering~~ region (wavelength is at least 10 times larger than the mean grain or phase size), the intensity of the backscattered wave is proportional to  $C a^3 f^4$  where  $C$  is the volume concentration of the arbitrarily shaped scatterers,  $a$  is the mean size of the scatters and  $f$  is frequency. Figure 1 shows two exponentially decaying reverberation envelopes obtained at different frequencies for the same material (1). As expected, the higher the frequency, the faster the disappearance of the reverberation signals in the electronic noise. Figure 2 shows two reverberation envelopes obtained for different ASTM\* materials at the same frequency. As expected, the coarser the material, the faster the reverberation decay.

### B. Experimental Protocol

The mean size of the secondary phase in Ti-6211 alloys can be estimated by using relatively high frequencies so that significant multiple scattering is produced. To satisfy the condition for Rayleigh scattering ( $\lambda > 10a$  where  $\lambda$  is the wavelength) in the test plates characterized by secondary phase sizes  $a < 10 \mu\text{m}$ , the center frequency for the transducer was chosen to be less than 30 MHz. To enhance the ultrasonic energy returned to the pulse-echo probe by

\*ASTM = American Society for Testing of Materials.

the random phase boundaries, 10- and 20-MHz transducers transmitting moderately long shear-wave pulses were selected for the experimental program.

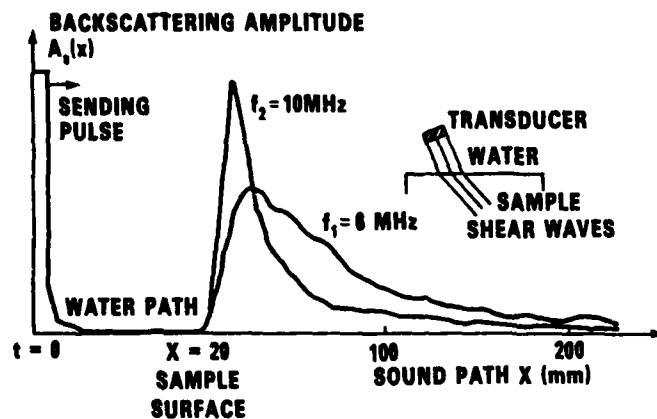


FIGURE 1. DECAY OF REVERBERATION ENVELOPES OBTAINED AT TWO FREQUENCIES (Adapted from Reference 1)

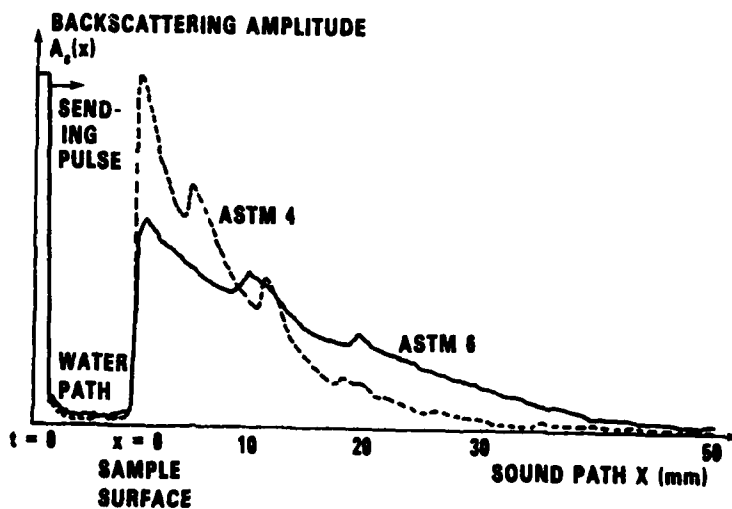


FIGURE 2. DECAY OF REVERBERATION ENVELOPES OBTAINED FOR TWO MATERIALS (Adapted from Reference 1)

Figure 3 shows the block diagram of the equipment used. The contaminated specimens were examined in a water tank. The angle of the transmitted shear wave ( $\beta$ ) could be varied by adjusting the angle of the incident longitudinal wave ( $\alpha$ ). Moderately damped probes tuned to 10 to 20 MHz, respectively, were used to produce 48-degree waves ( $\alpha = 20^\circ$ ) and 72-degree shear waves ( $\alpha = 27^\circ$ ). A Krautkraemer USIP 11 Ultrasonic Flaw Detector was used as the pulser-receiver instrument. Four radio-frequency (RF) waveforms received by a USIP 11 instrument from a contact probe located at adjacent positions 1-mm apart are shown in Figure 4, traces A) through D) (1). Note that a small movement of the probe on the specimen surface yields a statistically independent (entirely new) reverberation waveform,  $A_i(t)$ . Trace E) is the result of summing the four reverberation waveforms after they had been rectified. The addition of 256 rectified waveforms yields a rather smooth decaying envelope [Trace F)]. The amplitude of the spatially average wave forms is evaluated as a function of time of flight. Microstructural information is contained in both the time-specific amplitude ( $A_i, i = 1, 2$  or  $3$  corresponding to discrete times) and the slope of the measured reverberation envelopes (see also Figures 1 and 2). Thus, samples with different microstructures can be quickly evaluated under controlled experimental conditions.\*

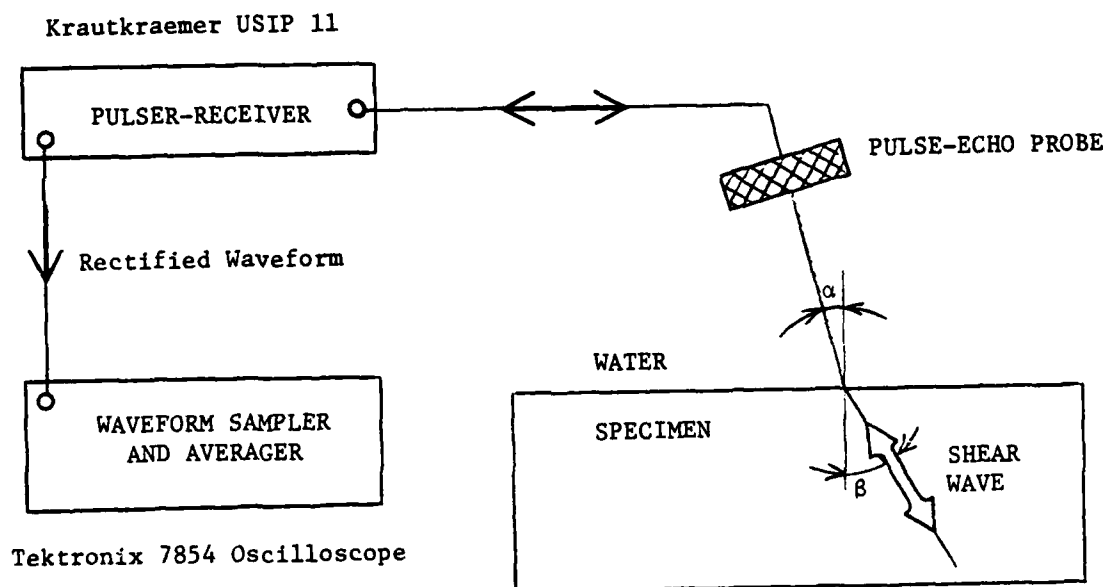


FIGURE 3. BLOCK DIAGRAM OF DATA ACQUISITION AND PROCESSING SYSTEM

\*The collection and processing of 256 waveforms for a specimen take less than 30 seconds.

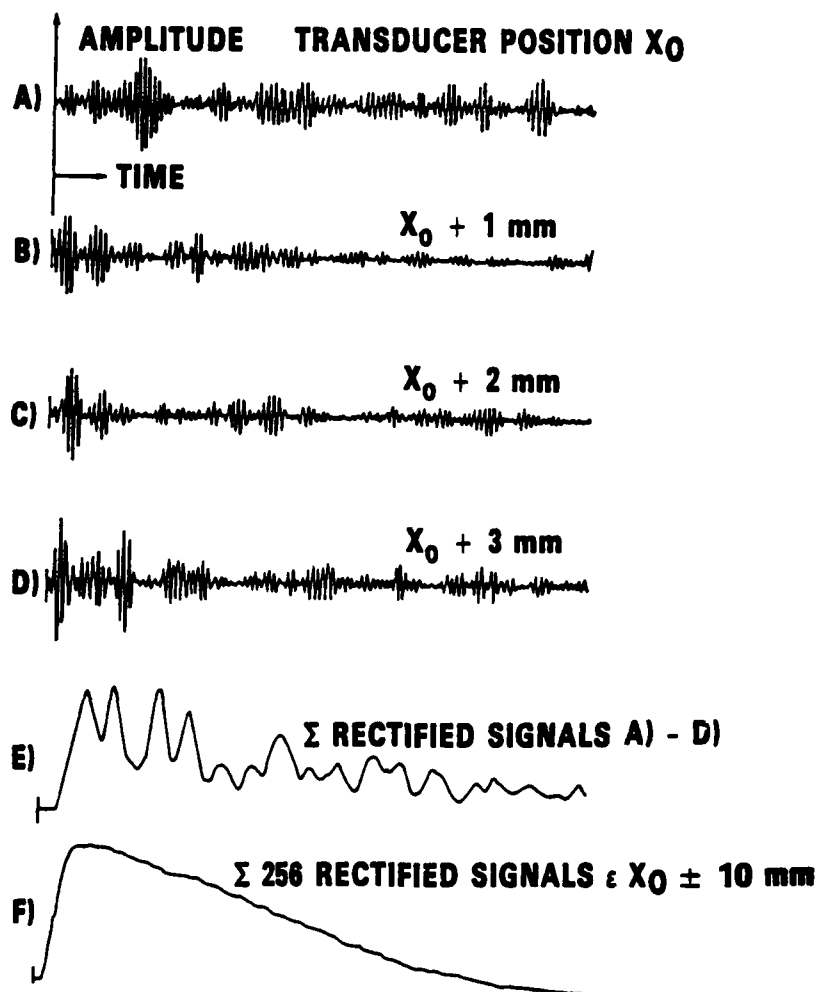


FIGURE 4. SMOOTHING OF REVERBERATION WAVEFORMS

### III. RESULTS

The results of metallographic and ultrasonic examinations of the five NRL plates, labelled A through E in increasing order of IOC, are presented in this section.

#### A. Metallographic Testing

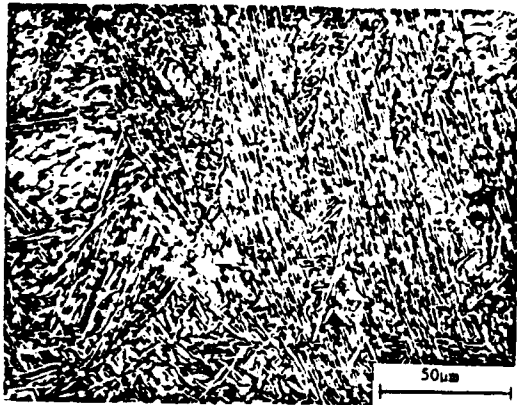
A portion of each specimen's surface was examined metallographically to yield microstructural features that might be correlatable with contamination and/or reverberation levels. The resulting X5000 photomicrographs are shown in Figure 5. The white areas represent the alpha phase in the beta matrix (dark lines). Delination between the alpha and beta phases is sharp. Within the large beta grains, the distribution of the reverberating alpha platelets is quite uniform. Significant differences in the width and aspect ratio of the alpha particles exist among the test specimens. Oxygen goes into the alpha phase and this phase is strengthened by the presence of dissolved oxygen. A tendency for the specimens to consist of more nearly equiaxed or spheroidized alpha particles with increasing IOC (i.e., in going from plate A to plate E) is clearly seen. The microstructure of plate A is characterized by the finest alpha particles. The mean width of the globular scattering centers contained in plate E is estimated to be 5  $\mu\text{m}$ .

#### B. Ultrasonic Testing

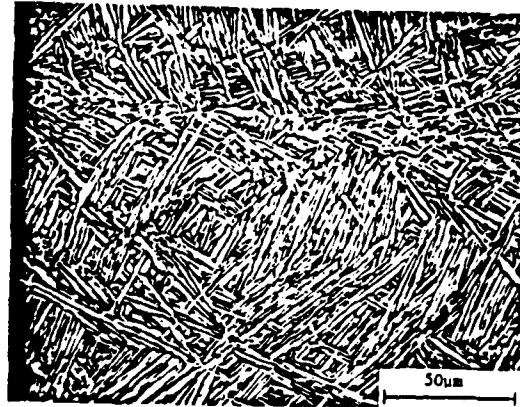
Two sets of reverberation envelopes are shown in Figures 6 and 7. The first set of reverberation decay curves was obtained with 48-degree shear waves ( $\alpha = 20^\circ$ ) and the second set was obtained with 72-degree shear waves ( $\alpha = 27^\circ$ ). Each curve was the result of averaging 1,000 statistically independent reverberation waveforms received from a restricted volume of each specimen (one measurement per plate). As expected, the time-specific amplitude data (enclosed in circles and squares in Figures 6 and 7) as well as the decay-rate data appear to contain IOC-information and/or microstructural information (see also Figure 5). Specific times in arbitrary units ("2" and "4" in Figure 6 and "5" and "9" in Figure 7) were selected for analysis of the reverberation level data. The results of time-specific amplitude measurements obtained with 48- and 72-degree shear waves are plotted as a function of IOC in Figures 8 and 9, respectively. Figure 10 contains data similar to those shown in Figure 8 except that the variations in time-specific reverberation levels within each specimen are also indicated by the one-standard-deviation error bars drawn around the averaged results of 8 scans per plate.

The data collected in Table 2 are for comparing the averaged and standard-error results of 12 scans obtained through the machined (smooth) surfaces with those obtained through the unmachined (rough) plate surfaces. As expected, surface quality does not influence the ultrasonic results obtained for the bulk of the specimen.

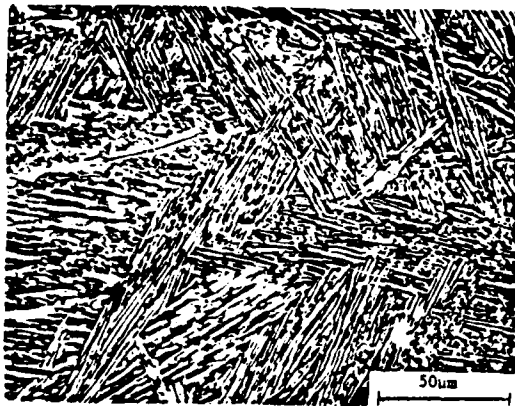




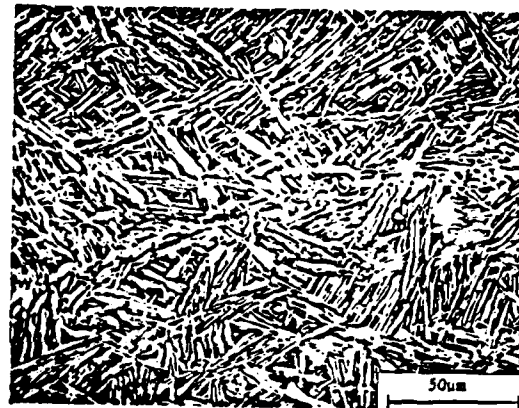
"A"



"B"



"C"



"D"

"E"

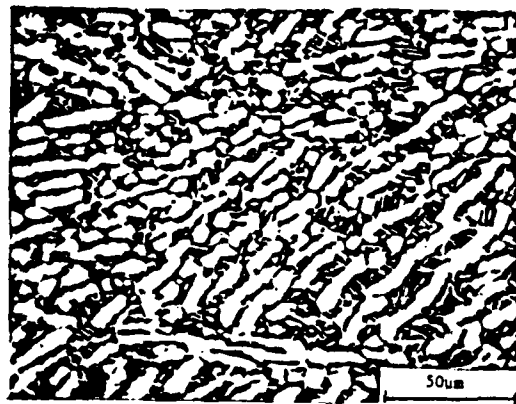


FIGURE 5. MICROSTRUCTURES OF THE TEST SPECIMENS

$$(\alpha = 20^\circ)$$

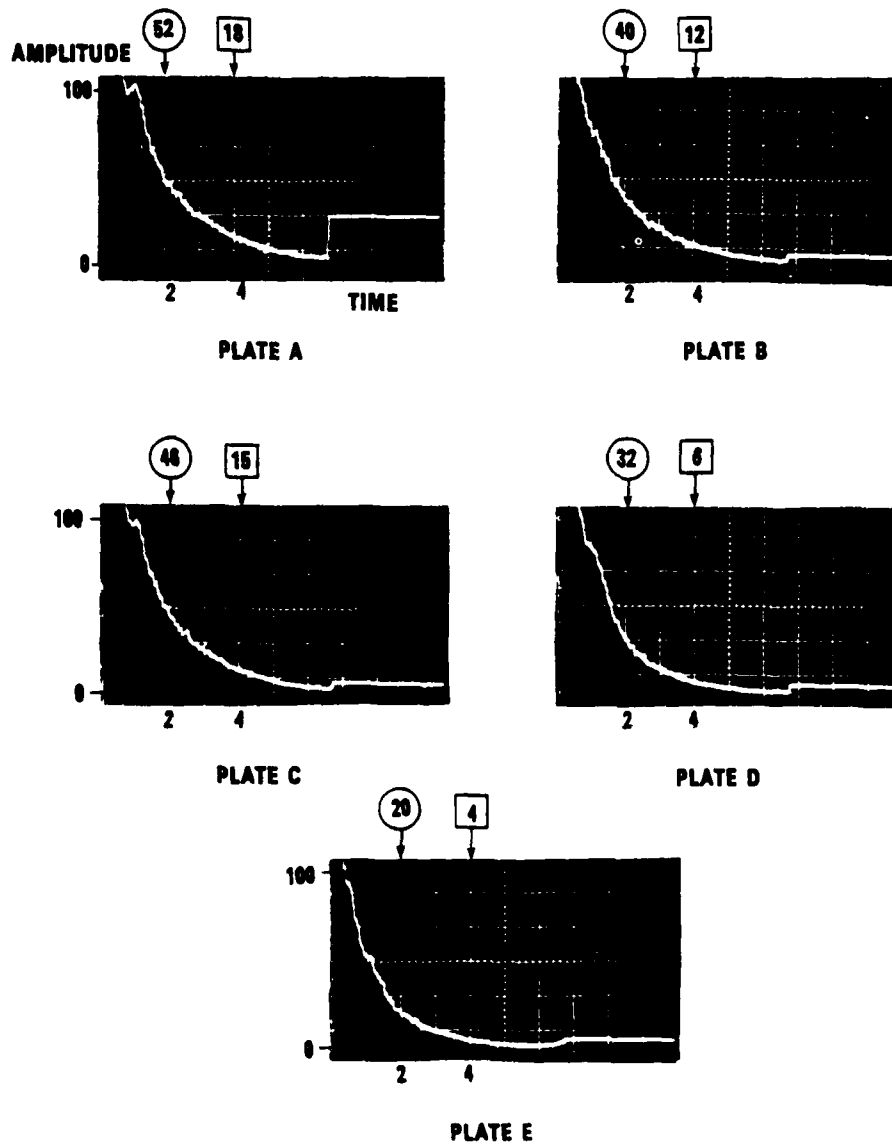


FIGURE 6. REVERBERATION DECAY ENVELOPES  
OBTAINED WITH 48-DEGREE SHEAR WAVES

$(\alpha = 27^\circ)$

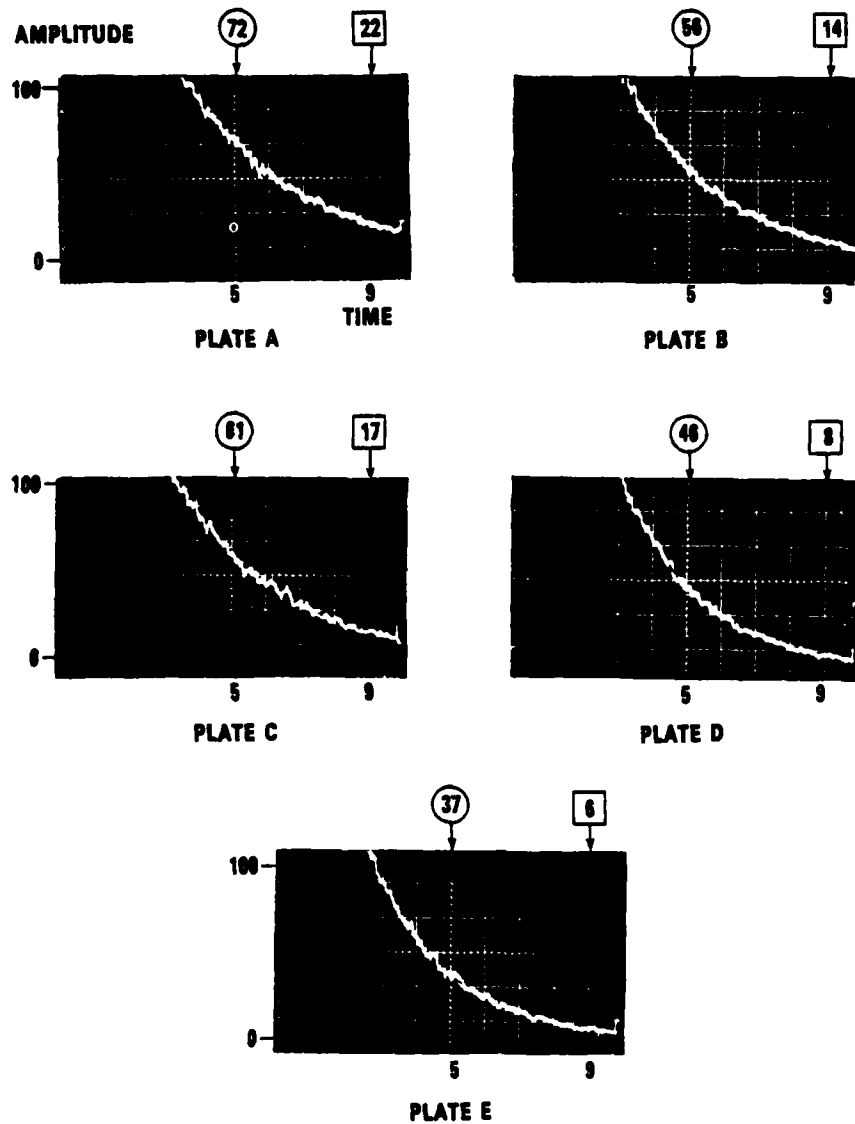


FIGURE 7. REVERBERATION DECAY ENVELOPES  
OBTAINED WITH 72-DEGREE SHEAR WAVES

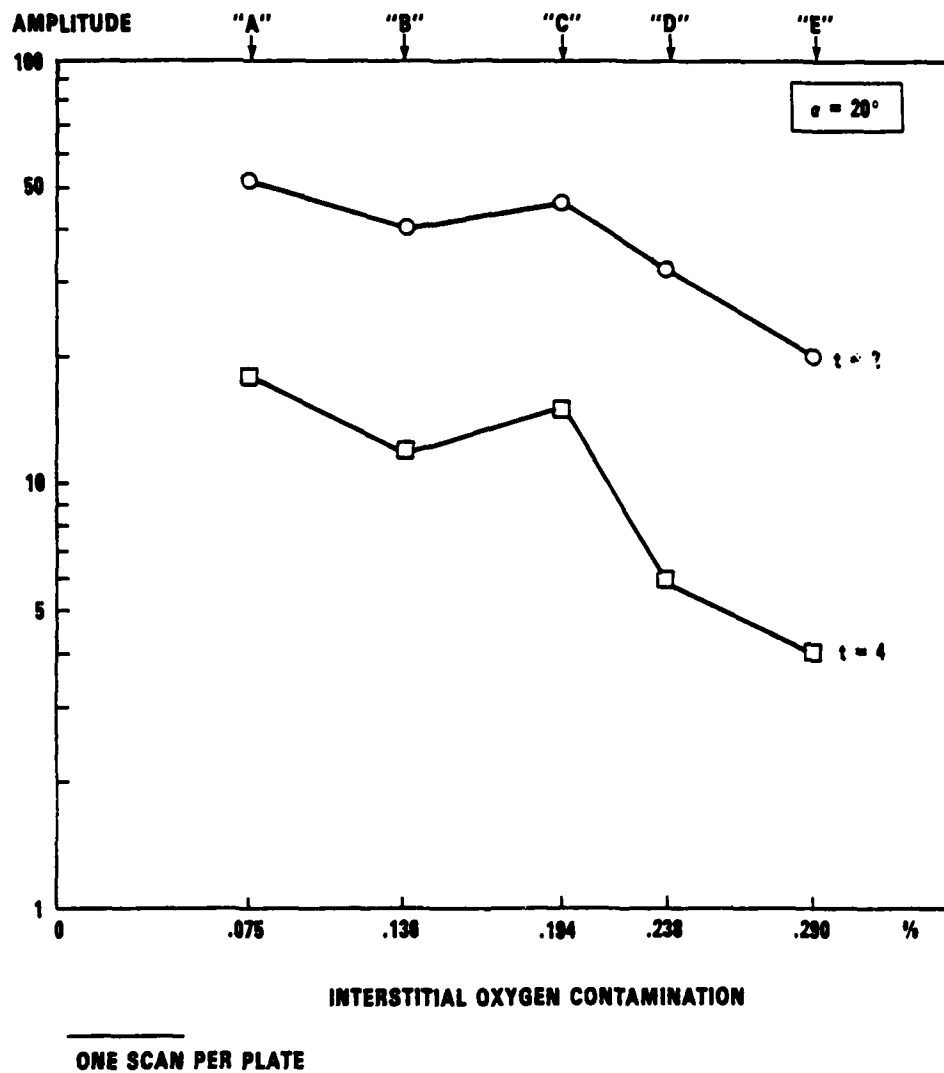
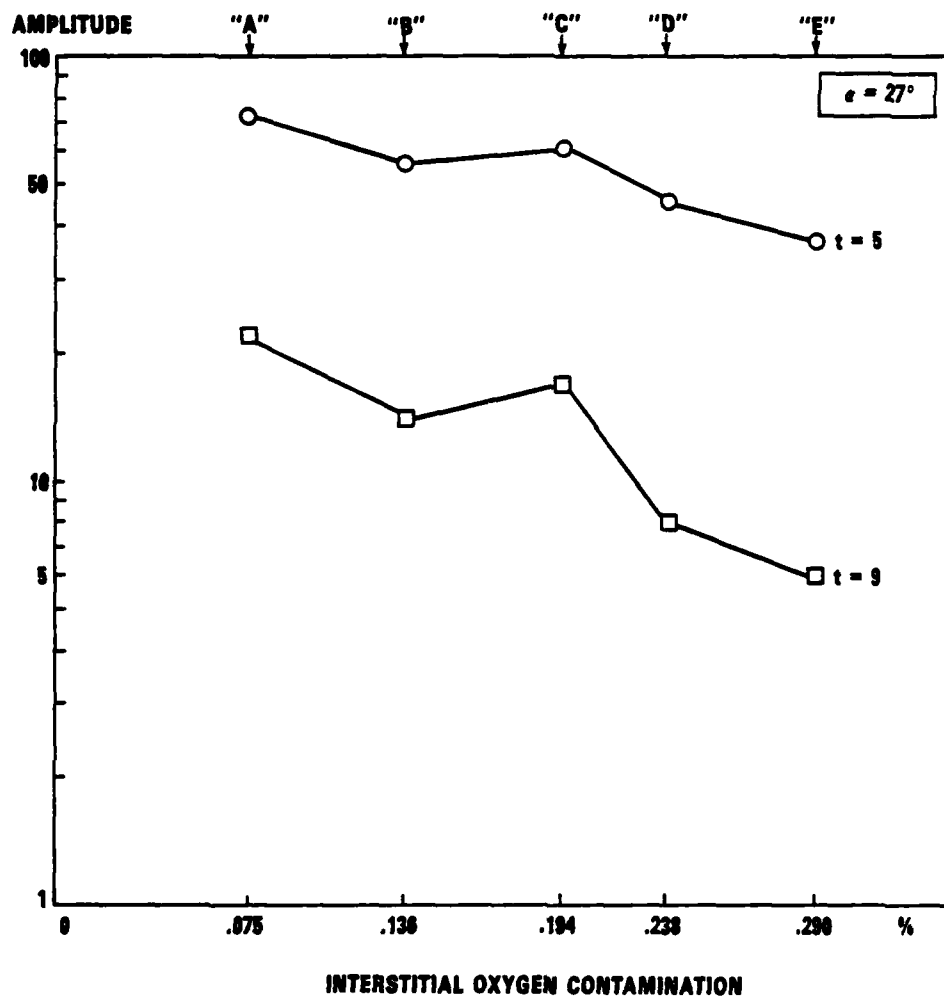
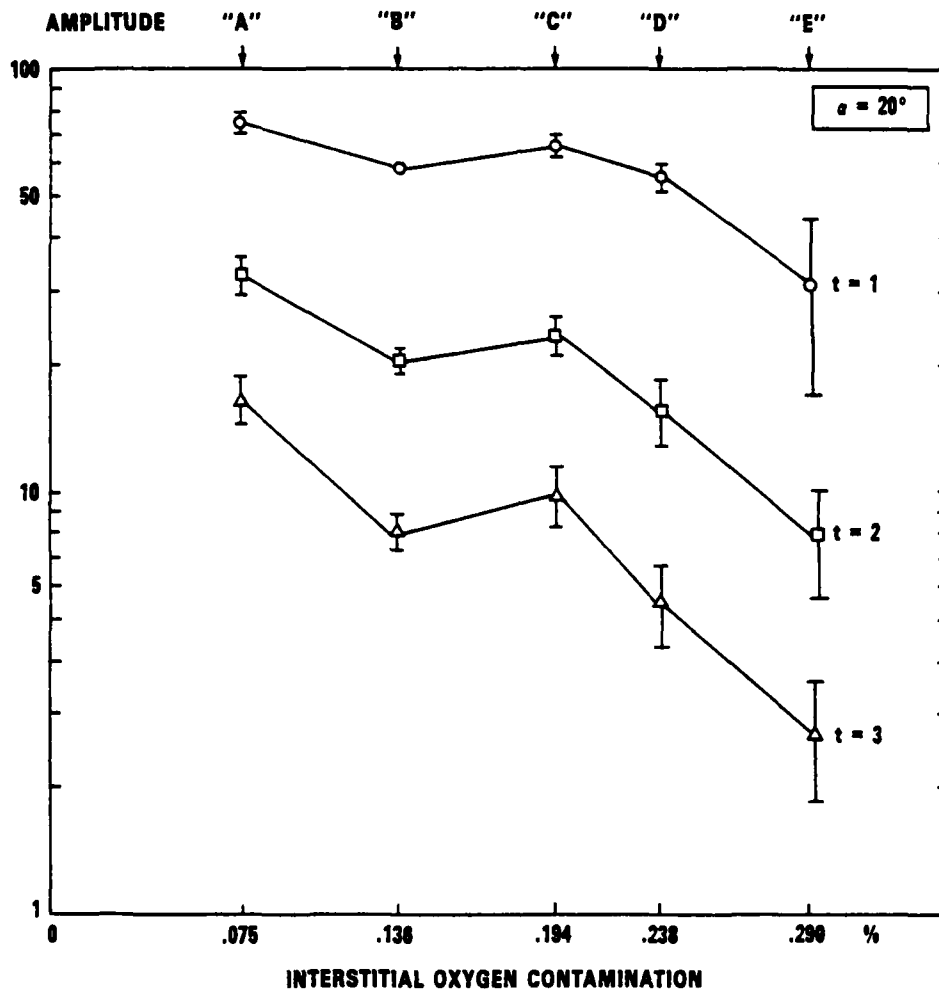


FIGURE 8. CORRELATION BETWEEN TIME-SPECIFIC REVERBERATION LEVELS OBTAINED WITH 48-DEGREE SHEAR WAVES AND INTERSTITIAL OXYGEN CONTAMINATION



ONE SCAN PER PLATE

FIGURE 9. CORRELATION BETWEEN TIME-SPECIFIC REVERBERATION LEVELS OBTAINED WITH 72-DEGREE SHEAR WAVES AND INTERSTITIAL OXYGEN CONTAMINATION



AVERAGE OF 8 SCANS PER PLATE

FIGURE 10. CORRELATION BETWEEN TIME-SPECIFIC REVERBERATION LEVELS OBTAINED WITH 48-DEGREE SHEAR WAVES AND INTERSTITIAL OXYGEN CONTAMINATION

TABLE 2. VARIATION OF REVERBERATION LEVEL  
WITH SURFACE ROUGHNESS

PLATE	AVERAGE/STD. ERROR		
	12 SCANS THROUGH MACHINED SURFACES	12 SCANS THROUGH UNMACHINED SURFACES	24 SCANS
A	436/34	426/31	431/32
B	568/27	569/29	568/27
C	528/30	510/39	518/35
D	625/35	620/29	623/31
E	781/68	763/89	772/78

The averaged and standard-error results of 24 scans per specimen, involving both plate sides, four beam orientations and three bordering plate volumes, are shown in Figure 11. The reverberation-decay statistic plotted on the vertical axis of Figure 11 is the area above the reverberation curve over a specific time interval (integrated reverberation level).

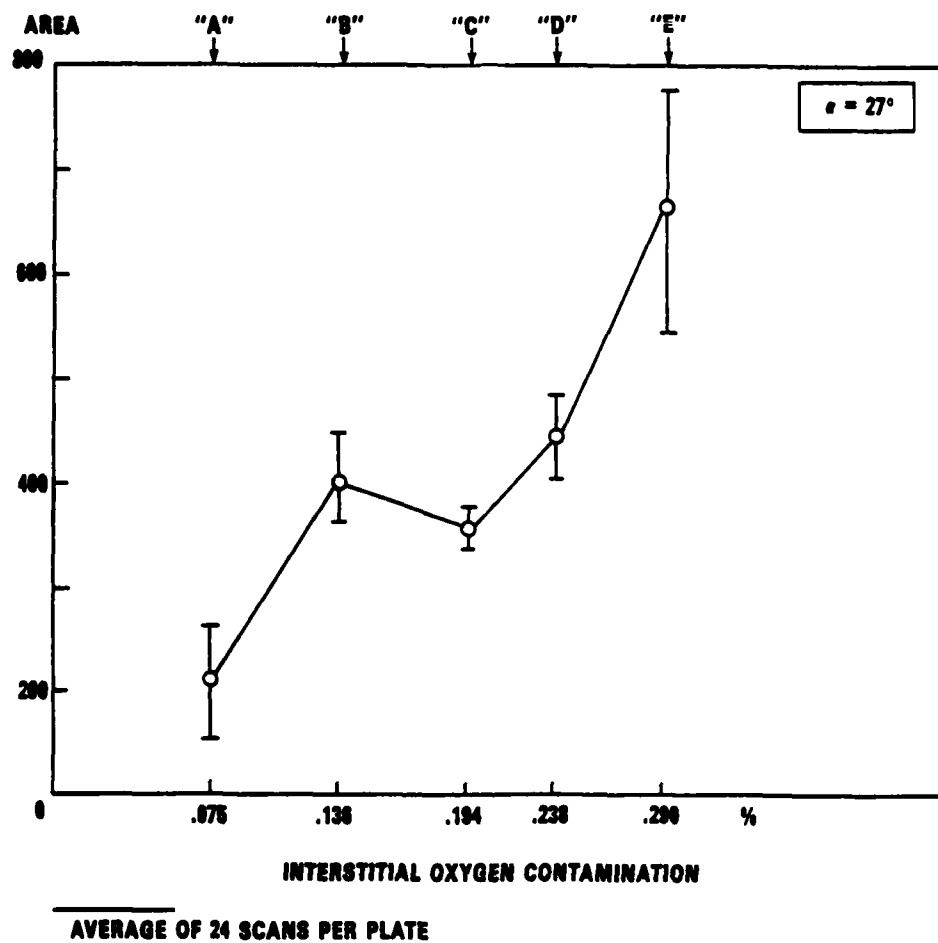


FIGURE 11. CORRELATION BETWEEN INTEGRATED REVERBERATION LEVEL (AREA ABOVE REVERBERATION DECAY ENVELOPE) OBTAINED WITH 72-DEGREE SHEAR WAVES AND INTERSTITIAL OXYGEN CONTAMINATION



#### IV. DISCUSSION

The uncovered interrelationships among the three sets of known or measured variables (oxygen contamination, reverberation level and alpha-phase morphology) are discussed in this section. It is reasoned that the relationships between alpha-phase morphology and reverberation level and between oxygen contamination and alpha-phase morphology are causal, but that between oxygen contamination and reverberation level is indirect (mediated by the IOC-induced microstructural changes).

##### A. Correlation of Alpha-Phase Morphology with Interstitial Oxygen Contamination

With one exception, due presumably to unknown or uncontrolled difference in thermomechanical histories, the thickness of the alpha platelets in the five plates increases with increasing IOC (see Figure 5). The exception is the reversal in the ranking of plates B and C when the five plates are ordered according to mean alpha phase size ("C" is closer to "A" than "B") rather than according to IOC. Any existing differences in thermomechanical processing must be considered in part responsible for the less than perfect rank/order correlation between secondary phase size and IOC. The microstructural findings are generally consistent with the known behavior of dissolved oxygen as an alpha stabilizer. Thus, IOC has a direct effect on the morphology of the alpha phase in Ti-6211 alloys.

The microstructure of plate E is unique in that the alpha particles have increased substantially in size and developed an extensive preferred orientation (texture).

##### B. Correlation of Reverberation-Decay Statistics with Alpha-Phase Morphology

Comparison of the metallurgical results (Figure 5) with the ultrasonic results (Figures 6 through 11) for the five contaminated plates indicates that several measures of the alpha-phase morphology vary systematically with the measured reverberation-decay statistics (time-specific amplitude, decay rate, integrated reverberation level, etc.). In both Figures 5 and 11, the ranking of plates B and C are reversed ("C" is closer to "A" than "B" from both the metallurgical and ultrasonic points of view). This finding is consistent with the hypothesis that, rather than the IOC, the morphology of the scattering alpha platelets has a direct effect on the reverberation of ultrasound in Ti-6211 alloys. The ultrasonic results are also consistent with the theory of Rayleigh scattering in that both wave-velocity and density changes at the phase boundaries affect the reverberation-decay statistics.

Substantial anisotropy in the material properties underlying the reverberation of ultrasound was observed for plate E (see Figure 11). The largest error bar for the mean integrated reverberation level measured for plate E using four principal sound beam directions (x, -x, y and -y) is

attributed to the pronounced preferred orientation of the globular alpha microstructure of this plate due, presumably, to unidirectional processing. Figure 5 also shows that the alignment of the fine alpha-platelet colonies is the most random for plate C. This metallurgical finding is consistent with the ultrasonic results shown in Figure 11 in that the variance of the mean integrated reverberation level is minimum for the plate with the least amount of texture.

#### C. Correlation of Reverberation-Decay Statistics with Interstitial Oxygen Contamination

Dissolved oxygen is known to stabilize the alpha phase and increase the hardness of Ti-6211 alloys. However, no quantitative dependency of the sound-wave velocity on IOC has been established due to inconsistencies in the results of various investigators. As long as the alpha phase is low in oxygen, it is very tough. With increasing IOC, the alpha base becomes less tough until it is actually more brittle than the beta matrix.

The differences in mean integrated reverberation levels plotted in Figure 11 for the five contaminated plates, partitioned into three groups (plate A, plates B, C and D, and plate E), are significantly greater than the measurement error or the effects caused by texture and are, therefore, considered significant. Assuming that the five specimens differed only in dissolved oxygen,\* the significance of the apparent correlation between the reverberation and contamination levels seen in Figure 11 can be tested using rank-correlation and t-statistic analyses (2). Spearman's rank correlation coefficient is defined as

$$\rho_k = 1 - \frac{6}{k^3 - k} \sum_{i=1}^k d_i^2 \quad (1)$$

where k is the number of plates (k = 5) and  $d_i$  is the difference in ordering the i-th plate according to the contamination-level measurements and to the reverberation-level measurements. These orders are (1,2,3,4,5) and (1,3,2,4,5), respectively. The rank-correlation coefficient for the data shown in Figure 11 is 0.90. The standard error of  $\rho_k$  is given by

$$\sigma_\rho = \frac{1}{\sqrt{k-1}} \quad (2)$$

The value of  $\sigma_\rho$  is calculated to be 0.50, giving a t-value of 0.90/0.50 or 1.80. The resulting p-value is 0.08, meaning that there is only an 8-percent chance that the observed correlation between the reverberation and contamination levels is fictitious.

---

\*Clearly, the ultrasonic results do not order on the basis of IOC alone.

## V. CONCLUSIONS AND RECOMMENDATIONS

### A. Conclusions

The results of the reported experimental program are summarized as follow:

- (1) Surface-roughness conditions had no influence on the ultrasonic results obtained for the bulk of the five test specimens.
- (2) Substantial anisotropy in the material properties underlying the reverberation of ultrasound was observed for plate E due, presumably, to the extensive texture of this plate.
- (3) With one exception, the thickness of the alpha platelets in the test specimens increased with increasing oxygen contamination.
- (4) Several measures of the averaged reverberation decay curves proved to be sensitive and reliable indicators of the oxygen-induced microstructural changes among the test specimens.
- (5) The microstructure-sensitive ultrasonic results did not order perfectly on the basis of dissolved oxygen alone.
- (6) Metallographic results confirmed the ultrasonic results that the microstructures of plates A and C are closer to each other than those of plates A and B.
- (7) The probability that the observed correlation between ultrasonic-reverberation and oxygen-contamination levels is fictitious is merely eight percent.
- (8) Interstitial oxygen in these plates can be monitored through its microstructure-mediated effect on the reverberation of the focusable interrogating ultrasonic beam. In its current state of development, the reverberation-decay measurement system must be recalibrated for each new manufacturing condition (forging, welding, heat treating, etc.).

### B. Recommendations

The application of the reverberation-decay measurement technique to more realistic experimental situations is the main thrust of the recommended work. Follow-on work is needed since one is not yet prepared to argue that the monitored microstructural changes were due to variations solely in dissolved oxygen. The conclusions of this preliminary program must be considered tentative until all specimens are annealed and retested with 'blinded' ultrasonic examiners.

A more systematic, in-depth experimental study of the combined effects of thermomechanical processing and interstitial oxygen contamination on the microstructure of Ti-6211 alloys is in order. It would be of particular interest to learn what influence different forging conditions and welding procedures had on the microstructure of the test specimens aside from the microstructural effects attributable to the dissolved oxygen.

Because Ti-6211 alloys are both inhomogeneous and anisotropic, additional complications arise in the interpretation of the results of ultrasound-material interactions. A more analytical approach to the nondestructive characterization of interstitial oxygen contamination may place the investigated technique on a firmer theoretical base.

## REFERENCES

1. Goebbels, K., "Structure Analysis by Scattered Ultrasonic Radiation," in *Research Techniques in Nondestructive Testing*, R. S. Sharpe, editor, Academic Press, New York, 1980.
2. Kendall, M.G., *Rank Correlation Methods*, Hafner Publishing Company, New York, 1962.

## SECTION 5

# ACOUSTICAL CHARACTERIZATION OF Ti-6211 WELDMENTS AND OXYGEN CONTAMINATION Ti-6211 PLATE

Sanford R. Buxbaum and Robert E. Green, Jr.

*Materials Science and Engineering Department  
The Johns Hopkins University  
Baltimore, Maryland 21218*

The use of ultrasonic testing for the inspection of weldments in titanium alloys requires careful acoustical characterization of the materials and weldments in question. In the first part of the present work various ultrasonic tests were conducted on a series of test specimens of titanium alloy weldments and base plate material. Ultrasonic wave velocity and attenuation measurements were made in the low megahertz frequency range using both longitudinal and shear waves. Both the ultrasonic wave velocity and attenuation were observed to be lower in the weld region than in the base metal. Information provided by x-ray analysis helped to account for the observed wave velocity behavior. Changes in the attenuation were correlated to microstructural variations and hardness measurements in the weld region and base metal.

The second stage of the research focused on the problem of dissolved gas contamination of Ti-6211 welded joints. In order to evaluate the feasibility of ultrasonic testing for detecting quantitatively the presence of interstitial gas contamination in weldments of Ti-6211, ultrasonic wave velocity and ultrasonic attenuation measurements were performed on a series of five specimens with nominal oxygen levels of 0.1, 0.2, 0.3, 0.4, and 0.5 percent by weight. Careful density measurements in addition to the ultrasonic wave velocity data enabled accurate determination of elastic moduli. Variations in the ultrasonic data were correlated with results from scanning electronic microscopy, energy dispersive x-ray analysis, and hardness testing.

AD-P004 125

# ACOUSTICAL CHARACTERIZATION OF OXYGEN CONTAMINATED Ti-6211 PLATE

Sanford R. Buxbaum and Robert E. Green, Jr.  
Materials Science and Engineering Department  
The Johns Hopkins University  
Baltimore, MD 21218

## 1. INTRODUCTION

Titanium alloys exhibit high strength-to-weight ratios and good corrosion resistance and are, therefore, desirable for use in structural applications. The safe, in-service use of titanium alloy weldments in load-bearing parts requires the development of reliable nondestructive methods for inspecting the mechanical integrity of the weld region. Unfortunately, current nondestructive evaluation technology has proven inadequate for such alloys and applications. Since one of the primary nondestructive inspection techniques is ultrasonics, it is expedient to determine the usefulness and limitations of ultrasonic inspection for the materials in question. This requires careful acoustical characterization of these materials in order that appropriate accept/reject criteria be established.

## 2. RESEARCH OBJECTIVES

The mechanical properties of titanium alloys are known to be sensitive to oxygen content(1-26). Above a certain threshold concentration oxygen appears to have a severe embrittling effect on titanium alloys (6-8, 17, 20-26). Since gas tungsten-arc (GTA) and gas metal-arc (GMA) welding techniques are susceptible to

dissolved gas contamination, it is of specific interest to investigate methods for nondestructively determining the oxygen content of a Ti-6211 welded joint. The objective of this research was to evaluate the feasibility of ultrasonic testing for detecting quantitatively the presence of interstitial gas contamination in weldments of Ti-6211 by:

- (1) Performing ultrasonic wave velocity and ultrasonic attenuation measurements on a series of five specimens with varying oxygen contents.
- (2) Comparing variations in ultrasonic data with results of scanning electron microscopy and hardness testing.

### 3. BACKGROUND

Ultrasonic wave propagation analysis of a material is a nondestructive evaluation technique that provides information about the elastic properties and absorption characteristics of the material in which the wave propagates. Absolute measurements of shear and longitudinal wave speed can be used to calculate useful material parameters, such as the effective Young's modulus and the effective shear modulus. The term "effective modulus" refers to the fact that the modulus is calculated for a material that is assumed to be linear elastic, homogeneous, and isotropic, which is a fair approximation for some fine-grained polycrystalline materials. The energy loss, or ultrasonic attenuation of elastic waves propagating in a solid, may be divided into contributions from geometrical and intrinsic effects. Of interest here are the intrinsic effects, which include scattering of the ultrasonic wave by inhomogeneities, conversion of sound energy to heat as a result



of elastic deformation, interaction with thermal phonons, and dislocation damping(27).

Since the concentration of an alloying element, oxygen in this case, affects the same set of variables that determine ultrasonic wave propagation characteristics, it is expected that ultrasonic techniques will be suitable for determining oxygen concentration in "contaminated" Ti-6211 specimens. It has been shown that foreign solute atoms invariably change elastic moduli(5,10,11,18). Additionally, solute atoms can act as pinning points for dislocations and would, therefore, be expected to influence attenuation measurements.

Some previous studies of the effects of interstitial gases on elastic wave propagation also indicate the feasibility of this method for dissolved gas concentration determination. Zener(5) studied the relation between residual strain energy and elastic moduli and theoretically demonstrated that the presence of residual strain energy necessarily resulted in a lowering of the elastic moduli. Additionally, he derived a quantitative relation between the density of residual strain energy and the decrease in elastic moduli. However, the calculations of Zener are in conflict with experimental results for the titanium-oxygen system. It should be noted, though, that Zener(5) was trying to explain results for substitutional solid solution alloying. Apparently his explanation does not hold for interstitial solid solution alloying which occurs in the Ti-O, Ti-N, Ti-H, and Ti-C systems.

Hsu and Conrad(18) looked at the effect of oxygen on the elastic properties of titanium-oxygen alloys through ultrasonic wave velocity measurements performed on specimens with oxygen content

in the range of 0.04 weight percent to 2 weight percent and controlled impurity content. It was found that both density and longitudinal wave velocity increased with increasing oxygen content. Since the relative change in the wave velocity was greater than that in the density, the dynamic elastic modulus was increased by the oxygen in solid solution. Ultrasonic attenuation was also observed to increase with increasing oxygen content. The authors concluded that it was likely that the interstitial oxygen atoms actually increased the binding forces between the atoms.

The influence of oxygen content on the internal friction characteristics of titanium, particularly the modification of grain boundary relaxation phenomena was investigated by Pratt, Bratina, and Chalmers(10) with the objective of obtaining further information concerning the exact role of the interstitial solutes in alpha titanium. Measurements of internal friction were made by the standard method of studying the free decay of the oscillations of a simple torsional pendulum, the suspension of which consisted of a wire of the material in question. In the oxygen-containing alloys, the peak characteristic of grain boundary slip occurred at higher temperatures than in pure titanium and the heat of activation increased. The presence of oxygen resulted in an additional small peak not observed in the relaxation spectra of pure titanium. They also found that the addition of 4.5 atomic percent oxygen raised the rigidity modulus, which is consistent with the results of Hsu and Conrad(18).

## 4. EXPERIMENTAL PROCEDURES

### 4.1 Metallography

Metallographic specimens were cut from the oxygen contaminated Ti-6211 samples. The specimens were ground on successively finer silicon carbide papers down to 600 grit, and then polished on lapidary wheels using 15 micron and 0.05 micron compounds. A two step etching technique was used to reveal microscopic detail. In the first step, the polished specimen was briefly swabbed with a 2 ml HF, 98 ml water solution. This etched the alloy and stained the alpha phase. The second step, swabbing with a 1 ml HF, 2 ml HNO<sub>3</sub>, 97 ml water solution, removed the stain, leaving a light field of alpha phase material in which the beta phase appeared as finely dispersed dark lines when viewed through an optical microscope. When viewed through a scanning electron microscope (SEM), the beta phase appeared as finely dispersed light lines in a dark field of alpha phase material.

### 4.2 Ultrasonic Measurements

The oxygen contaminated specimens were unsuitable in the as-received condition for contact ultrasonic inspection due to poor surface finish. Flat parallel faces were machined on each specimen prior to performing both ultrasonic measurements and hardness measurements. A high degree of parallelism of specimen faces was required to minimize diffraction errors caused by divergence of the ultrasonic pulse as it propagated back and forth through the specimen.

Conventional pulse-echo overlap techniques(28) were used to measure the longitudinal wave velocities. In the pulse-echo

overlap technique, the specimen is pulsed with ultrasound and the subsequent echoes are monitored. The travel time, or periodicity, between two of the echoes is measured. If successive echoes are chosen, the travel distance is twice the specimen thickness. The wave velocity can then be calculated from the travel time and the travel distance. In the system used, shown schematically in Fig. 1, the inverse of the period, or the frequency was measured.

Referring to Fig. 1, the continuous wave (cw) oscillator provided an adjustable, continuous sync signal, the frequency of which was characteristic of the wave speed and thickness of the specimen under consideration. The frequency of the signal was measured and displayed by the frequency counter. The decade divider and dual delay strobe generator divided the frequency of the sync signal by selected powers of ten so that it was suitable for triggering the pulser-receiver and provided the strobed intensification required for the pulse-echo overlap technique. In the divided sync mode, one is able to tune the pulse-echo train, which is displayed on the oscilloscope screen. The direct mode enables one to overlap two echoes due to the persistence of the scope display. The pulser-receiver and transducer pulse the specimen with ultrasound and detect the subsequent echoes. Using an amplitude matching technique, radio frequency (rf) echoes were overlapped on the oscilloscope screen by adjusting the output of the cw oscillator. When successive rf echoes were properly overlapped, the frequency output of the cw oscillator multiplied by the travel distance between echoes, or twice the specimen

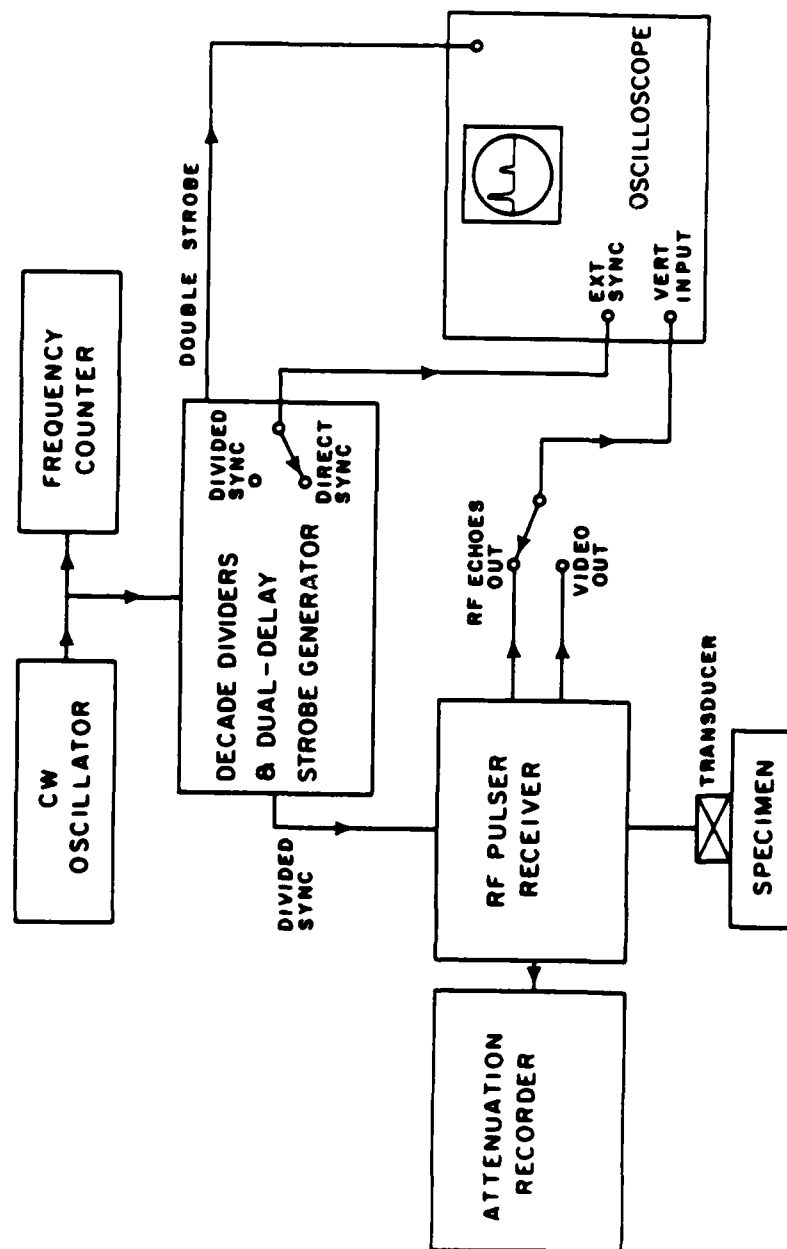


FIG. 1. ULTRASONIC WAVE VELOCITY AND ATTENUATION MEASURING SYSTEM

thickness, gave the sound wave velocity. The video output was used to properly align the strobes from the attenuation recorder before making the attenuation reading in units of decibels (dB's). The attenuation recorder includes a time gate permitting selection of any two echoes from the received wave train, an automatic gain control to stabilize the amplitude of the echoes, and circuitry to obtain the logarithm of the ratio of the selected echo amplitudes.

Commercial, longitudinal wave, ceramic transducers along with appropriate couplants were used in this research. Aerotech couplant (a light oil) was used for the wave velocity measurements. A 2 mm thick elastomer coating (developed by Martin Marietta Laboratories in Catonsville, MD) was applied to a 2.25 MHz, longitudinal wave, commercial transducer and was used to acoustically couple the transducer to the oxygen contaminated specimens for the attenuation measurements. The viscoelastic properties of this coating make it an ideal couplant for attenuation measurements. When subjected to low frequency stress cycles (low rates of deformation), the elastomer is flexible and can be forced down on a sample for a reproducible acoustical couple. When subjected to high frequency stress cycles (high rates of deformation) the coating behaves like a rigid body. The ultrasonic pulses effectively propagated through a rigid acoustical coupling media. This elastomer coating provided more reproducible attenuation measurements than was possible with conventional couplants. The thickness of the coating made it unsuitable for accurate velocity measurements.

#### 4.3 Hardness Measurements

Rockwell "C" hardness measurements were made on the oxygen

contaminated Ti-6211 specimens in accordance with ASTM Standard E18. A diamond tipped "Brale" indenter with a 150 kg load was used. Since Ti-6211 continued to exhibit plastic flow after the application of the major load, the dial indicator continued to move after the operating lever stopped. For this reason the operating lever was brought back to its latched position at an elapsed time of 30 seconds between application and removal of load.

#### 4.4 Density Measurements

Cubes nominally 1 inch on a side were machined from each of the oxygen contaminated Ti-6211 specimens. The volume was measured to an accuracy of  $0.001 \text{ cm}^3$ , and the mass was measured to an accuracy of 0.001 g. Two cubes were fabricated from each of the five oxygen contaminated specimens for mass density determination.

### 5. RESULTS AND DISCUSSION

To evaluate the feasibility of ultrasonic test methods for detecting quantitatively the presence of interstitial gas contamination in weldments of Ti-6211, various measurements were performed on a series of five specimens with approximate oxygen levels of 0.07, 0.14, 0.20, 0.24, and 0.29 percent by weight. The oxygen was introduced into the plate samples of Ti-6211 in the form of  $\text{Ti}_2\text{O}$  powder, and the plate samples were subsequently beta processed at  $1700^\circ\text{F}$  in a controlled, inert atmosphere for one hour. The samples were then air-cooled. Chemical analysis of the specimens is presented in Table I.

TABLE I. SPECIMEN COMPOSITIONS

SPECIMEN	COMPOSITION (weight percent)								
	Ti	Al	Cb	Mo	Ta	C	N	Fe	O
A	90.3	6.0	1.95	0.7	0.88	0.02	0.010	0.05	0.069
B	89.9	6.0	2.09	0.9	0.97	0.02	0.006	0.03	0.136
C	90.2	5.9	1.90	0.8	0.94	0.02	0.005	0.03	0.194
D	90.1	5.8	2.05	0.8	0.99	0.02	0.006	0.03	0.238
E	89.8	5.9	2.16	0.7	1.06	0.03	0.008	0.03	0.290

SPECIMEN	COMPOSITION (atomic percent)								
	Ti	Al	Cb	Mo	Ta	C	N	Fe	O
A	87.7	10.4	0.97	0.34	0.23	0.08	0.03	0.04	0.20
B	87.4	10.4	1.05	0.44	0.25	0.08	0.02	0.02	0.40
C	87.6	10.2	0.95	0.39	0.24	0.08	0.02	0.02	0.56
D	87.5	10.0	1.03	0.39	0.26	0.08	0.02	0.02	0.69
E	87.1	10.2	1.08	0.34	0.27	0.12	0.03	0.02	0.84



### 5.1 Metallography

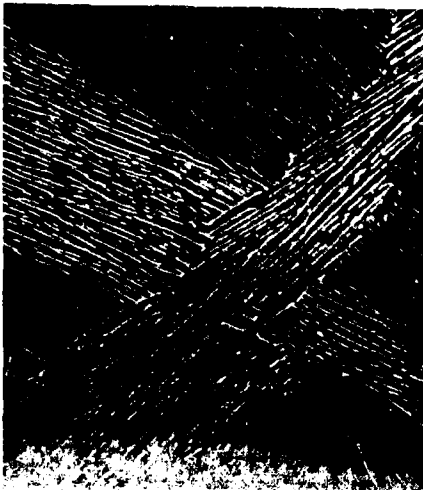
Metallographic analysis performed on the five specimens revealed significant microstructural differences. The photomicrographs (SEM) displayed in Fig. 2 show distinct changes in microstructure with increasing oxygen content. As the oxygen content increased, the alpha platelets became wider; hence, the separation of the layers of beta increased. Additionally, the beta layers thickened until they began to break up and become more globular in appearance. This is especially evident in the SEM photomicrograph of specimen E, the most heavily contaminated specimen. It should be noted that the microstructures of the oxygen-contaminated plates are not representative of those observed in the weld region of welded Ti-6211 specimens.

### 5.2 Density Measurements

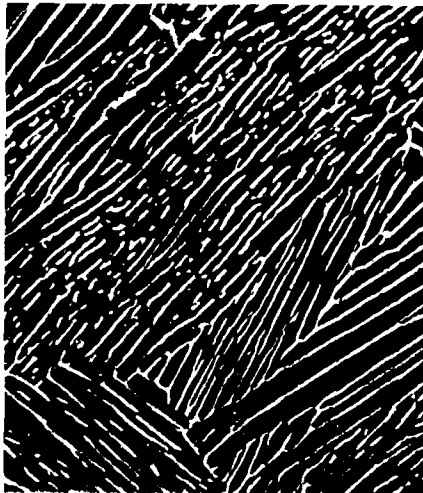
The results of density measurements performed on this series of five oxygen contaminated specimens are presented in Fig. 3. Note that density ( $\rho$ ) increases with increasing oxygen content because the oxygen enters the titanium lattice interstitially. These results are consistent with the results of Hsu and Conrad(18).

### 5.3 Ultrasonic Wave Velocity Measurements

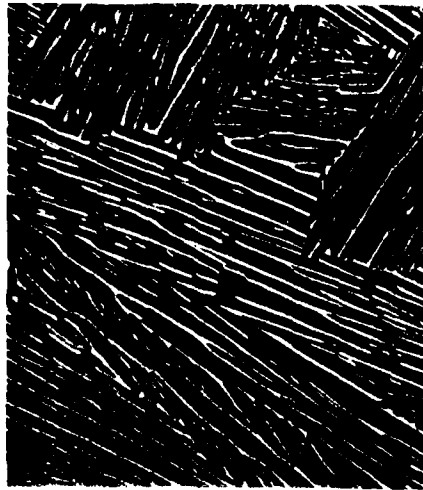
Longitudinal wave velocity ( $V_L$ ) was found to decrease with increasing oxygen content (see Fig. 4). Specimen C gave anomalous velocity results; it is suspected that this was due to improper thermomechanical preparation. Figure 5 is a plot of the average product  $\rho V_L^2$  (normalized) versus oxygen content for the five specimens. The behavior of the quantity  $\rho V_L^2$  is indicative of the



SPECIMEN A  
0.069 wt% OXYGEN



SPECIMEN B  
0.136 wt% OXYGEN



SPECIMEN C  
0.194 wt% OXYGEN



SPECIMEN D  
0.238 wt% OXYGEN



SPECIMEN E  
0.290 wt% OXYGEN

FIG. 2. SEM PHOTOMICROGRAPHS  
OF Ti-6211 PLATE WITH VARYING  
OXYGEN CONTENTS (1000X)

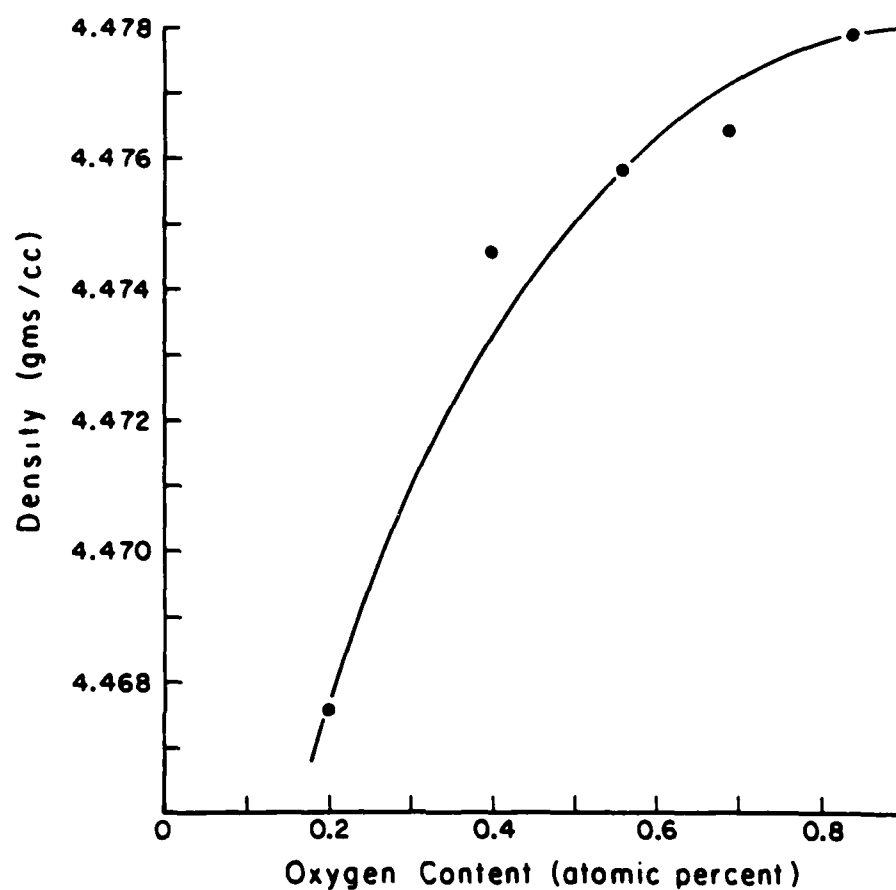


FIG. 3. DENSITY vs. OXYGEN CONTENT OF Ti-6211

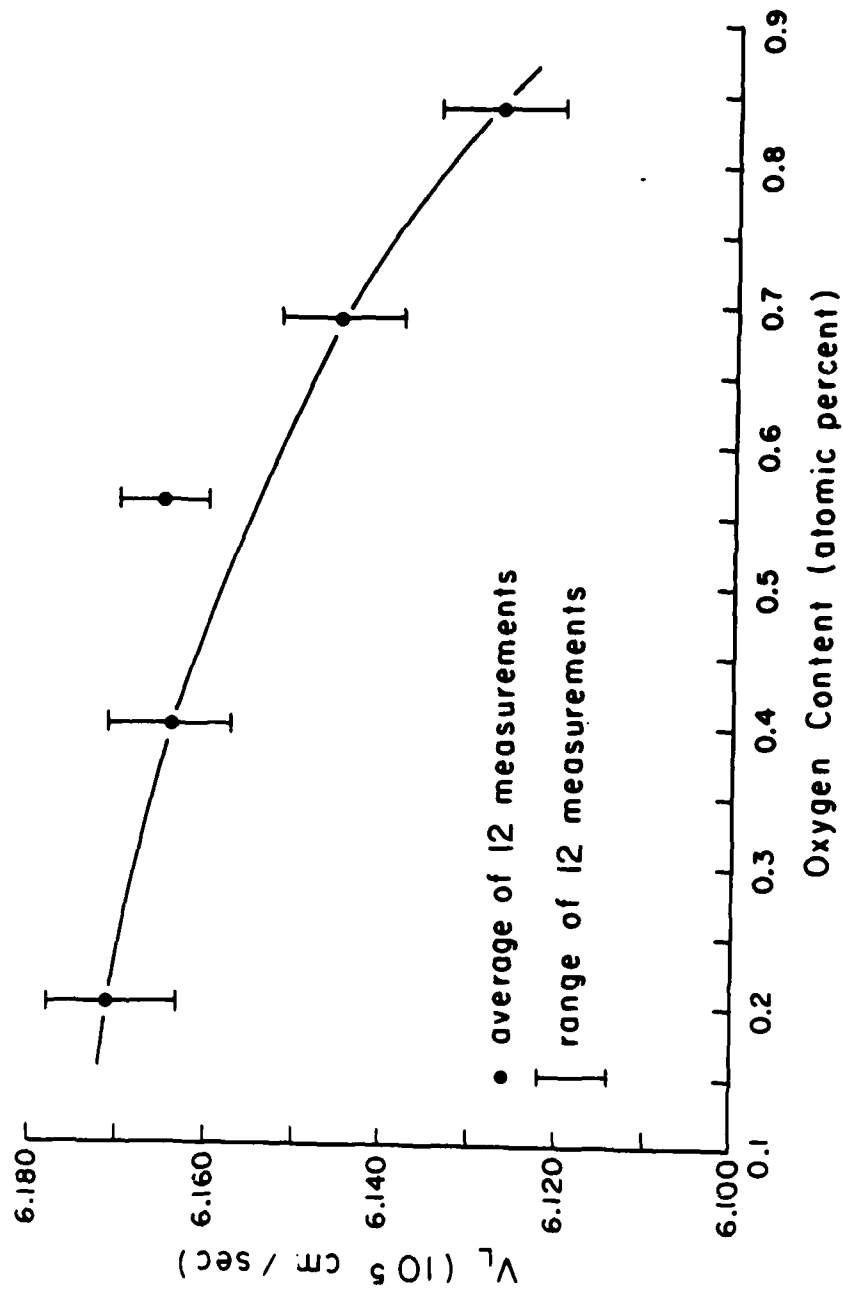


FIG. 4. LONGITUDINAL WAVE VELOCITY vs. OXYGEN CONTENT  
 (5 MHz TRANSDUCER)

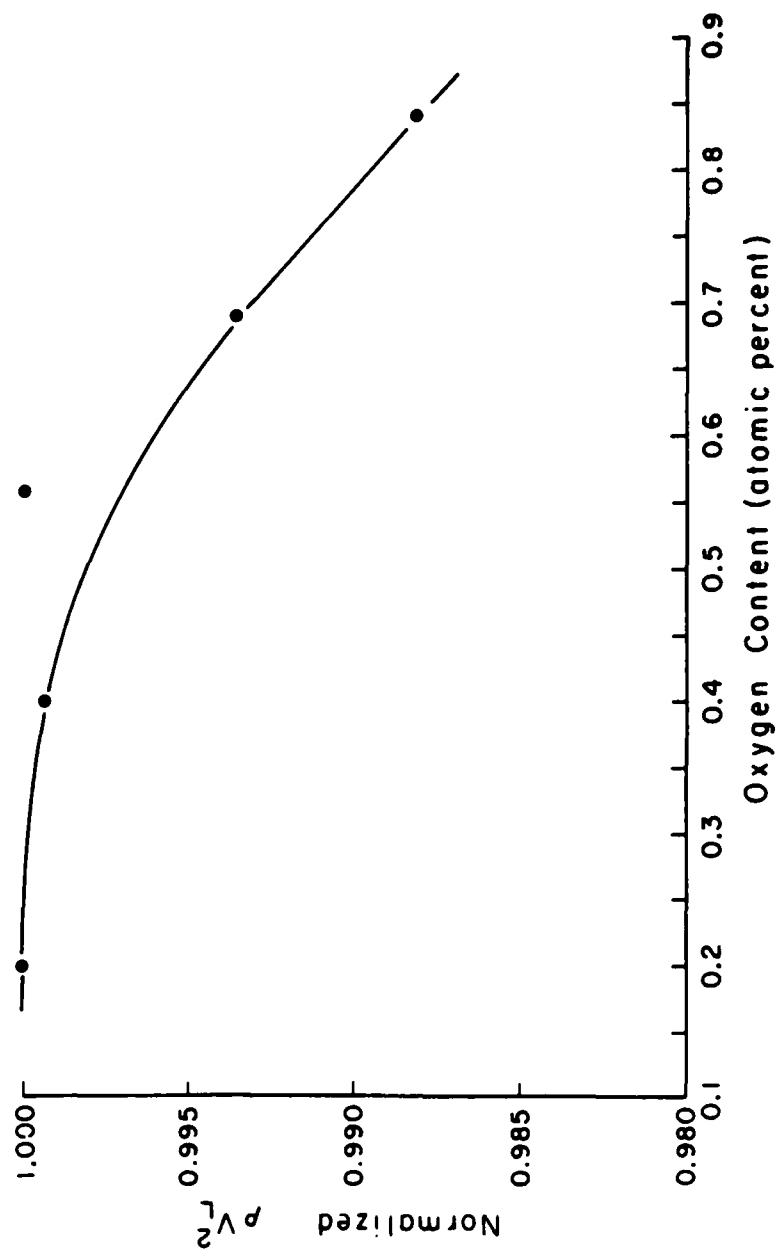


FIG. 5. NORMALIZED  $\rho V_L^2$  vs. OXYGEN CONTENT

behavior of the elastic moduli, so Fig. 5 shows that the elastic moduli tend to decrease with increasing oxygen content.

To explain the observation of a decrease in the longitudinal wave velocity and the elastic moduli, it is necessary to reconsider some of the literature discussed earlier. Zener (5) theoretically demonstrated that the residual stress introduced by slight interstitial or substitutional alloying in any metal necessarily reduces the elastic moduli. However, his theory was based on purely geometric considerations and did not consider the importance of the complex Ti-O electronic interaction. Additionally, Zener's conclusions were in conflict with the experimental results of Hsu and Conrad (18) who showed that in 100% alpha titanium, longitudinal wave velocity and, therefore, the elastic moduli, increased with increasing oxygen content. Hence, it is doubtful that the theoretical arguments of Zener (5) account for the results obtained here.

The Ti-6211 alloy is a near alpha alloy containing primarily alpha phase, hexagonal close-packed (HCP) metal with some beta phase, body centered cubic (BCC) metal. The sound wave velocity should be lower in the beta phase, because it has a more open crystal structure than the alpha phase. Hence, the decreasing sound wave velocity observed with increasing oxygen content could possibly be caused by an increasing amount of beta phase metal. X-ray diffractometer measurements were performed to test this hypothesis, but the results were inconclusive.

Under equilibrium conditions, oxygen, an alpha stabilizer in titanium, divides the single temperature for equilibrium solid state

phase transformation into two temperatures: (1) the alpha transus, below which the alloy is all alpha, and (2) the beta transus above which the alloy is all beta. Between these two temperatures both alpha phase and beta phase material are present. Increasing the oxygen content in titanium causes the alpha and beta transi to rise and the alpha plus beta region to broaden. Apparently, under nonequilibrium cooling conditions, such as air quenching from the beta region, the increasing transus temperature and the broadening of the two-phase region can result in increased retention of the beta phase. Assuming  $V_L$  tends to increase as oxygen content increases in 100% alpha titanium as per Hsu and Conrad (18), the influence of the oxygen on the alpha lattice was being masked by the larger decrease in  $V_L$  caused by retention of the beta phase.

#### 5.4 Ultrasonic Attenuation Measurements

Attenuation measurements were performed on the oxygen contaminated specimens to evaluate the usefulness of attenuation for quantitatively detecting the presence of oxygen. The results, shown in Fig. 6, demonstrate the inherent scatter present in attenuation measurements using contact transducers due to the sensitivity of this technique. The elastomer coating used to couple the transducer to the specimen provided a fairly reproducible transducer-specimen coupling and helped decrease the data scatter. Between 24 and 32 attenuation measurements were performed on each specimen. The average and range of these measurements are presented in Fig. 6, and the results do not look promising for quantitative oxygen analysis. However, simple statistical reduction of the attenuation data (see Fig. 7) highlights the enhancement of ultrasonic inspection data

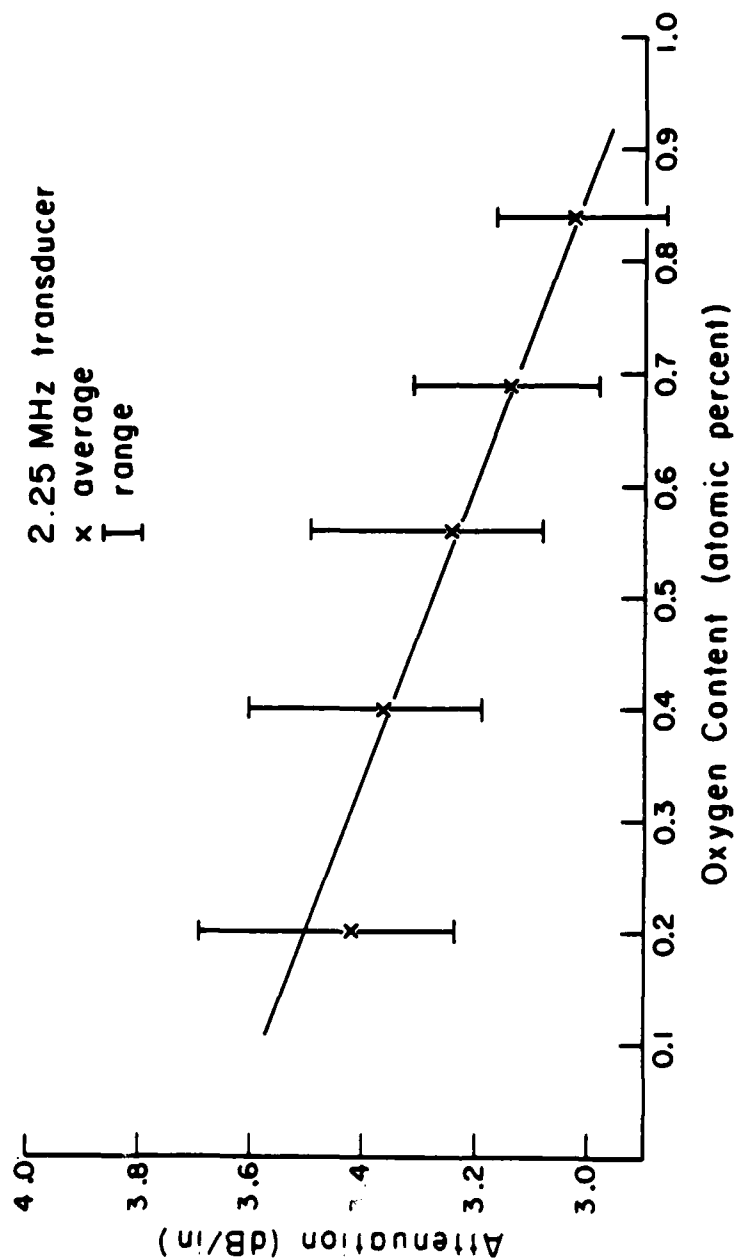


FIG. 6. LONGITUDINAL WAVE ATTENUATION vs. OXYGEN CONTENT



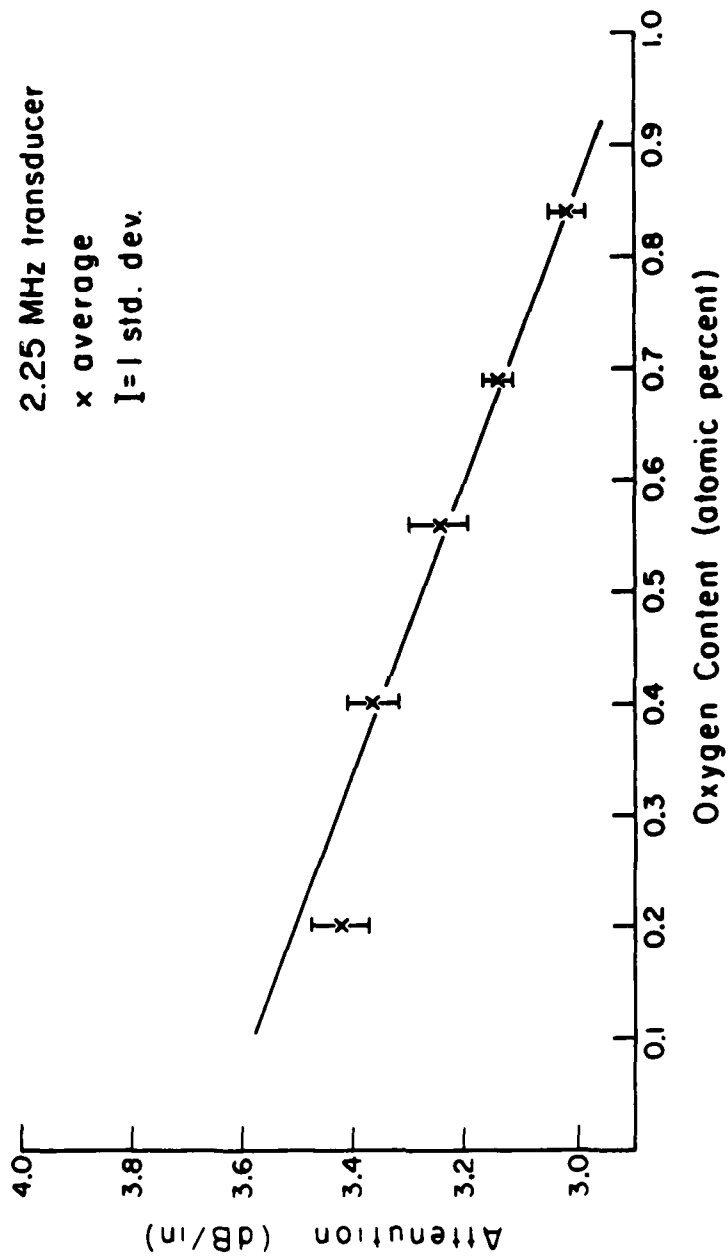


FIG. 7. LONGITUDINAL WAVE ATTENUATION vs. OXYGEN CONTENT

that is possible with statistical analysis. Furthermore, Fig. 7 indicates that ultrasonic attenuation has potential for quantitatively detecting the presence of oxygen in Ti-6211. It is not known whether the decrease in attenuation with increasing oxygen content is due to the effect of the oxygen on the alpha titanium lattice, the change in the amount of retained beta phase, or the microstructural variations induced by oxygen and thermal history.

### 5.5 Hardness Measurements

Rockwell "C" hardness, a measure of the material response to plastic deformation, was found to increase with increasing oxygen content (see Fig. 8). The increase was probably due to the solid solution strengthening provided by the interstitial oxygen, which partitions preferentially into the alpha phase. Statistical analysis was also shown to improve the usefulness of hardness testing for quantitatively detecting oxygen in the Ti-6211 alloy (see Fig. 9).

## 6. CONCLUSIONS

Analysis of the data collected from the oxygen contaminated specimens has highlighted some of the material effects that influence the ultrasonic testing of the Ti-6211 alloy. This analysis also indicated that ultrasonic attenuation shows promise as a non-destructive tool for quantitatively evaluating the amount of oxygen present in a Ti-6211 sample.

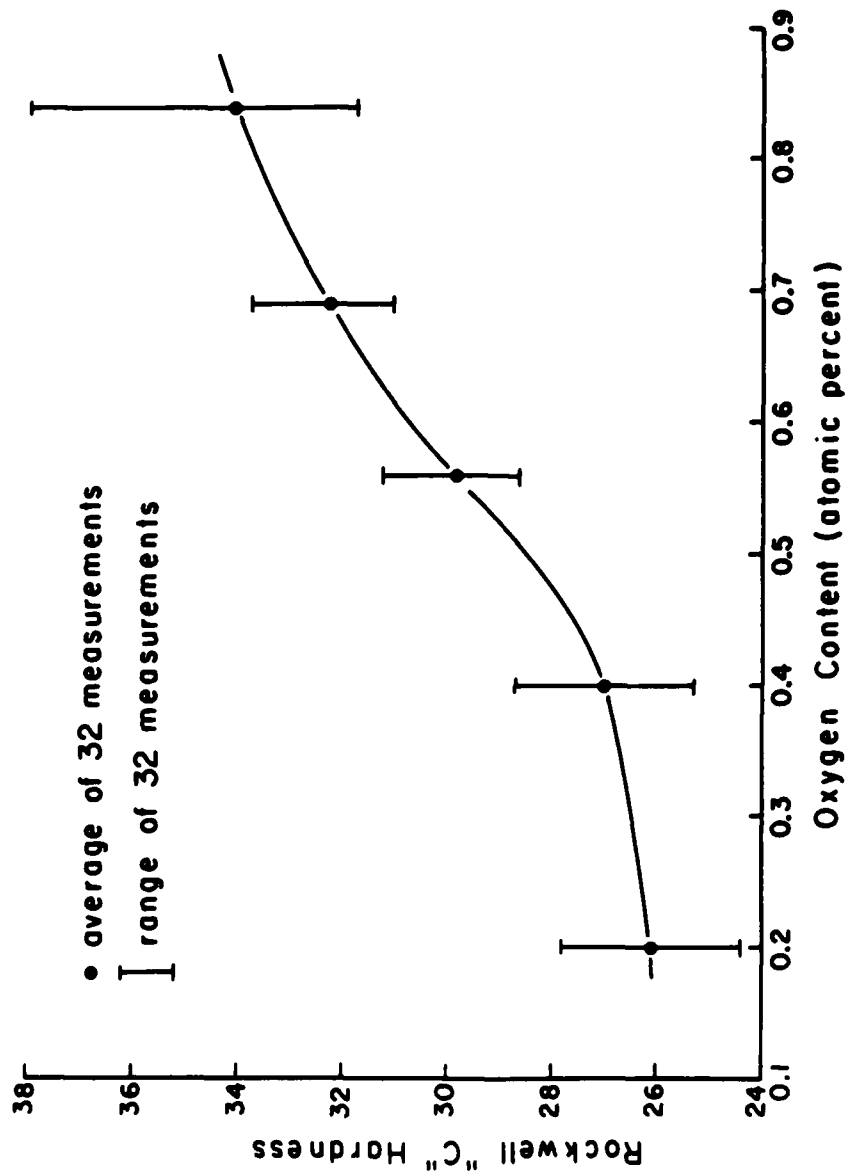


FIG. 8. ROCKWELL "C" HARDNESS vs. OXYGEN CONTENT

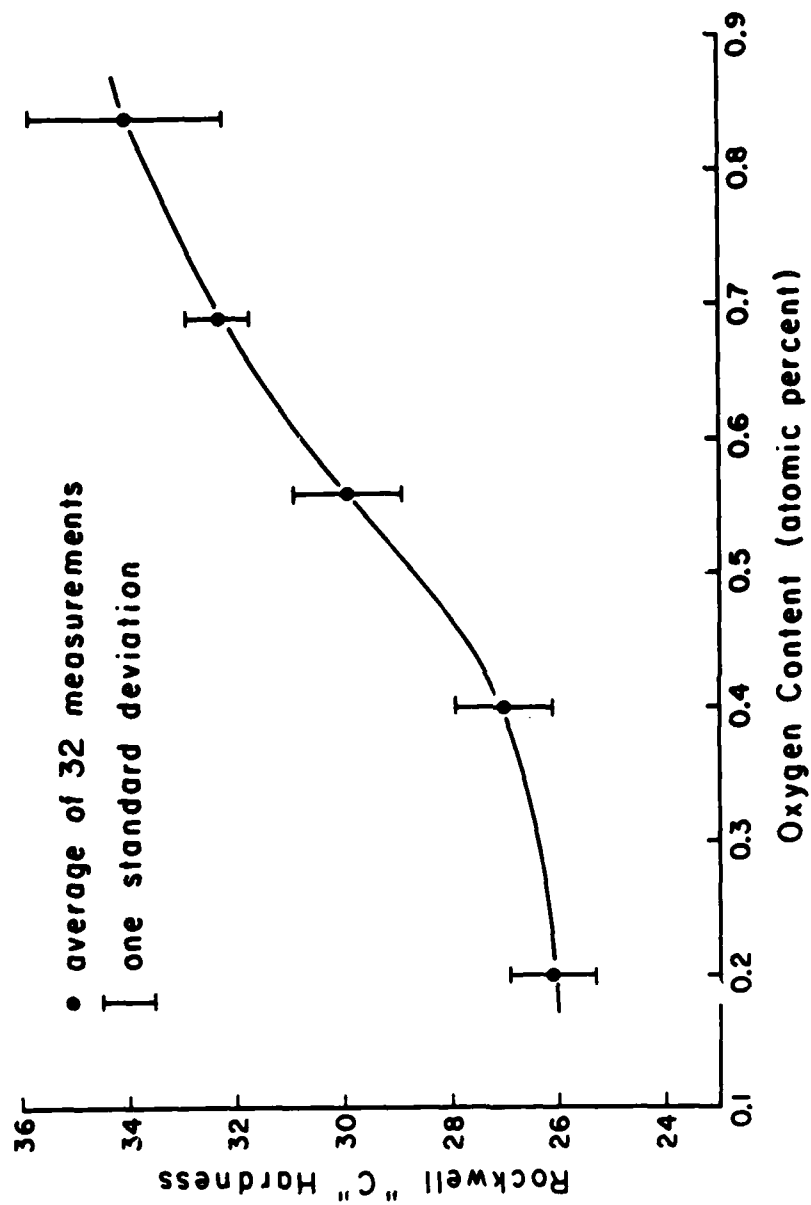


FIG. 9. ROCKWELL "C" HARDNESS vs. OXYGEN CONTENT

## BIBLIOGRAPHY

1. L. G. Carpenter and F. R. Reavell, *Metallurgia*, 39, 63, (1948).
2. H. T. Clarke, *Trans. AIME*, 185, 588, (1949).
3. E. A. Gulbransen and K. F. Andrew, *Trans. AIME*, 185, 741 (1949).
4. R. I. Jaffee and I. E. Campbell, *Trans. AIME*, 185, 646, (1949).
5. C. Zener, *Acta Cryst.*, 2, 163 (1949).
6. W. L. Finlay and J. A. Snyder, *Trans. AIME*, 188, 227, (1950).
7. R. I. Jaffee, H. R. Ogden, and D. J. Maykuth, *Trans. AIME*, 188, 1261, (1950).
8. A. E. Jenkins and H. W. Worner, *J. Inst. Metals* 80, 1337, (1951).
9. H. W. Worner, *Australian J. Sci. Research*, 4, 62, (1951).
10. J. N. Pratt, W. J. Bratina, and B. Chalmers, *Acta Met.*, 2, 204, (1954).
11. C. F. Ying and R. Truett, *Acta Met.*, 2, 374, (1954).
12. S. Andersson, B. Collén, U. Kuylenstierna, and A. Magnéli, *Acta Chem. Scand.*, 11, 1641, (1957).
13. R. J. Wasilewski, *Trans. AIME*, 224, 8, (1962).
14. H. Conrad, *Acta Met.*, 14, 1631, (1966).
15. W. R. Tyson, *Can. Met. Q.*, 6, 301, (1968).
16. J. Kratochvil and H. Conrad, *Scripta Met.*, 4, 815, (1970).
17. S. M. Gurevich, I. I. Kornilov, V. E. Blashchuk, V. V. Vavilova, and Y. A. Maksimov, *Metal Sci. H.*, 13, 271, (1971).
18. N. Hsu and H. Conrad, *Scripta Met.*, 5, 905, (1971).
19. G. A. Sargent and H. Conrad, *Scripta Met.*, 6, 1099, (1972).
20. S. M. Gurevich, V. E. Blashchuk, and L. M. Onoprienko, *Metal Sci. H.*, 15, 832, (1973).
21. I. I. Kornilov, *Metal Sci. H.*, 15, 826, (1973).
22. K. Okazaki, K. Morinaka, and H. Conrad, *Trans. JIM*, 14, 470, (1973).

BIBLIOGRAPHY (cont.)

23. T. A. Peradze and L. P. Fatkullina, Metal Sci. H., 15, 835, (1973).
24. V. V. Vavilova, Metal Sci. H., 15, 838, (1973).
25. V. V. Vavilova, T. A. Peradze, L. P. Fatkullina, and O.S. Korobov, Metal Sci. H., 17, 229, (1975).
26. J. Y. Lim, C. J. McMahon, Jr., D. P. Pope, and J. C. Williams, Met. Trans. A, 7, 139, (1976).
27. R. E. Green, Jr., Treatise on Materials Science and Technology, Vol. 3, (Academic Press, New York, 1973), 1-16, 145-151.
28. D. H. Chung, D. J. Silversmith, and B. B. Chick, Rev. Sci. Instrum., 40, 718, (1969).

AD-A147 626 PROCEEDINGS OF THE WORKSHOP ON NONDESTRUCTIVE  
EVALUATION (NDE) OF TITANIUM. (U) NAVAL RESEARCH LAB  
WASHINGTON DC N K BATRA ET AL. JUL 84

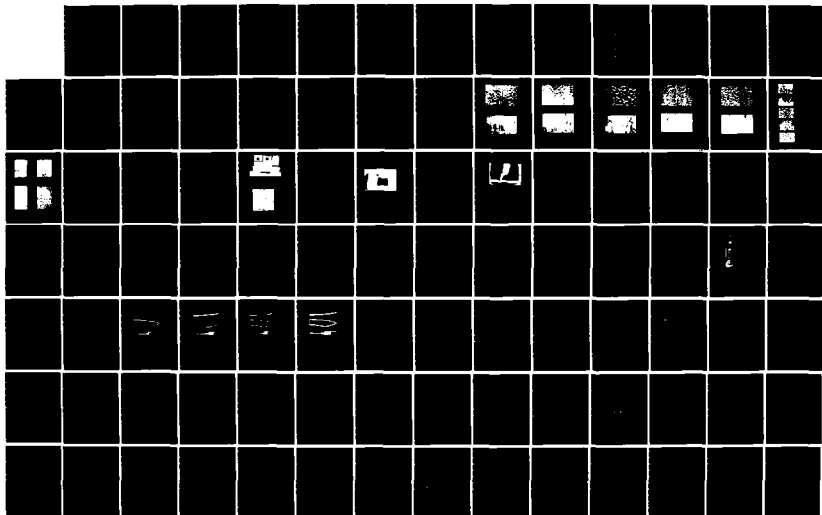
AD-A147 626 PROCEEDINGS OF THE WORKSHOP ON NONDESTRUCTIVE  
EVALUATION (NDE) OF TITANIUM. (U) NAVAL RESEARCH LAB  
WASHINGTON DC N K BATRA ET AL. JUL 84

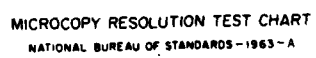
2/4

UNCLASSIFIED

F/G 11/6

NL





MICROCOPY RESOLUTION TEST CHART  
NATIONAL BUREAU OF STANDARDS-1963-A



**SECTION 6**  
**ULTRASONIC EVALUATION OF TITANIUM CONTAMINATION**  
**WITH CORRELATION TECHNIQUES**

E. S. Furgason, B. B. Lee, and G. O Deputy

*Purdue University*  
*West Lafayette, Indiana*

Direct ultrasonic evaluation of local variations in material composition is possible when these compositional variations induce measurable changes in the local elastic properties or microstructure of the material. In this study two standard classes of measurements are evaluated for their performance in the particular problem of quantitatively determining levels of interstitial oxygen contamination in titanium. The results of time-of-flight and frequency dependent attenuation measurements are presented for the case of finished flat titanium plates which have homogeneous interstitial oxygen contamination. These measurements were obtained using sensitive correlation techniques which were not required for these initial measurements, but which should prove beneficial in more practical contaminant situations. The applicability of such ultrasonic measurements are also examined for the case of more general inhomogeneous structures with rough surfaces.

AD-P004 126

# ULTRASONIC EVALUATION OF TITANIUM CONTAMINATION WITH CORRELATION TECHNIQUES

E. S. Furgason, B. B. Lee, and G. O. Deputy

Purdue University  
West Lafayette, Indiana

## ABSTRACT

Direct ultrasonic evaluation of local variations in material composition is possible whenever these compositional variations induce measurable changes in the local elastic properties or microstructure of the material. In this study, two standard classes of measurements are evaluated for their performance in solving the particular problem of quantitatively determining levels of interstitial oxygen contamination in titanium. The results of time-of-flight and frequency dependent attenuation measurements are presented for the case of finished flat titanium plates which are assumed to have homogeneous interstitial oxygen contamination. These measurements were obtained using sensitive correlation techniques which, although not required for these initial measurements, should prove beneficial in more practical situations of contaminant evaluation. The applicability of such ultrasonic measurements are also examined for the case of more general inhomogeneous structures with rough surfaces.

## INTRODUCTION

The effectiveness of all ultrasonic techniques in evaluating local variations in material composition is determined by the extent to which the compositional variations induce measurable changes in the local elastic properties of the material. The sensitivity of the ultrasonic technique to these variations is determined by two separate considerations, the electronic sensitivity of the ultrasonic system and the physical sensitivity of ultrasonic waves to the compositional variations. The objective of this study was to evaluate the extent to which two particular ultrasonic parameters of titanium are altered by the presence of oxygen contamination — velocity and attenuation. Variations in velocity and attenuation have previously been reported in the heat-affected-zone (HAZ) and welds of titanium plate due to the presence of large percentage changes in oxygen content and variations in microstructure [1]. However, a quantitative relationship between the observed changes and the oxygen content still remains to be determined.

Practical measurement of the oxygen contamination in and around welds will require an ultrasonic system with the highest possible sensitivity and resolution. For this reason, we chose to use a recently developed digital correlation flaw detection system [2] for these initial measurements, even though the use of other less sensitive systems would have been adequate for these initial tests.

A second practical consideration in the selection of a suitable technique arises from the need to evaluate the oxygen contamination during the fabrication process. In general, this requirement

precludes the use of exotic techniques or specially fabricated samples. In light of this constraint, the measurements reported are based on data extracted from conventional ultrasonic A-scans such as are routinely used to verify the structural integrity of the weld region.

## SYSTEM DESCRIPTION

The digital correlation flaw detection system used in these measurements overcomes the peak power limitations of conventional pulse-echo systems by transmitting long pseudo-random signals [3] and yet maintains the same high resolution as conventional systems through the use of pulse-compression in the sensitive correlation receiver. The signal-to-noise ratio enhancement, SNRE, achieved through band compression is given by,

$$\text{SNRE} = \alpha BT, \quad (1)$$

where  $\alpha$  is the duty cycle of the transmitted signal,  $B$  is the bandwidth of the transmitted signal, and  $T$  is the integration time of the output filter.

A diagram of the digital correlation flaw detection system is shown in Figure 1. This system, which is both microprocessor compatible and portable for field use, is described in further detail in reference [3].

## MEASUREMENT TECHNIQUE

In this study, five titanium samples containing differing degrees of oxygen contamination were tested. Each of the samples was a section of rolled plate nominally five inches square and one inch thick. As supplied, the broad rolled surfaces of the samples were very rough and the plates were arched along the rolling direction. The oxygen contamination levels of the five samples were reported to be approximately .07, .13, .17, .23, and .28 percent by weight [4].

For these initial measurements, a portion of the surface on each of the titanium samples was machined. First, a two inch wide strip along the rolling direction, was ground flat with a diamond grinder. The opposing face within each strip was then ground parallel to within approximately 1 mil. over the 5 inch plate length.

The first series of tests performed were immersion measurements using a commercial 5 MHz, one inch diameter disk transducer oriented with its face parallel to the machined region of the sample. The opposing face of the sample was isolated from the water bath by an air layer. The air pocket was maintained by clamping a thin sheet of Plexiglas over a large rubber O-ring. Since the back surface of the sample was isolated, the water bath served only to provide a convenient method of coupling the ultrasound into the sample.

To verify that the immersion method used was not essential to the experimental measurements, an alternate method using direct contact with shear wave couplant was also tested. The principal difference in the two techniques proved to be only a slight reduction in the available signal bandwidth due to constraints imposed by the couplant layer.

In all measurements, the position of the transducer was adjusted by hand so that the back surface echo was a maximum. After pulse-compression by the correlation receiver, the returning ultrasonic echoes were sampled by a microprocessor controlled A/D converter and stored for

later signal processing. An ultrasonic scan consisting of six reverberation echoes, typical of the scans stored for each titanium sample, is displayed in Figure 2.

### ULTRASONIC VELOCITY MEASUREMENTS

There exist several techniques for measuring the propagation velocity of ultrasound energy in solids. The most sensitive of these utilize a single frequency and are based on the mechanical resonance of the material. To take full advantage of such techniques, the mechanical resonance must be well defined and represent a single mode of vibration. This is achieved by fabricating samples of special shape having critically controlled dimensions.

One of our objectives was to evaluate the feasibility of estimating the ultrasound velocity utilizing only conventional ultrasonic measurement techniques. Consequently, our efforts centered on extracting the propagation velocity of longitudinal ultrasonic waves from A-scans of the type shown in Figure 2.

In principal, the velocity can be determined simply by measuring the time delay between successive reverberation echoes from the back surface of the sample and dividing by path length which is just twice the sample thickness. The difficulty in this procedure lies in uniquely identifying a particular point on the echo waveform and accurately determining the time delay. Since the ultrasonic wave suffers frequency dependent attenuation as it propagates through the material, the successive reverberation echoes are not identical in form. The starting point, or rising edge, of each echo is also not well defined due to the presence of clutter signals caused by the grains.

Fortunately, the goal of these measurements was not to accurately determine fundamental physical constants of the material, but rather to determine the variation of propagation velocity as a function of oxygen contamination. Consequently, it was not necessary to account for the systematic error resulting from dispersion introduced by attenuation. Thus for these measurements, the distance between the most prominent peaks of each echo was used to compute the propagation velocity.

The location of the peaks is easily accomplished by a computer search of the sampled data. Location of the peaks of the sampled data, however, does not by itself offer sufficient accuracy since the time resolution is limited by the sampling frequency. To increase the accuracy with which the echo peaks are located, a discrete Fourier transform was performed to obtain an analytic representation of the signal. This analytic representation of the signal allowed reconstruction of the ultrasonic signal between the sample points, permitting the exact location of the echo peaks to be determined.

Figure 3 presents the results of velocity measurements on all five samples obtained with this technique. The sample designations in this figure are those provided by NRL with A representing the sample with the least contamination and E corresponding to the sample with the highest level of oxygen contamination. From this graph, a clear trend of decreasing longitudinal ultrasound velocity with increasing levels of oxygen contamination is evident.

## ULTRASONIC ATTENUATION MEASUREMENTS

Absolute ultrasonic attenuation versus frequency was estimated from the standard A-scans, such as the one shown in Figure 2, by the following process. The reverberation echoes were first identified by locating major peaks of the data record by the same technique described above for the determination of the wave velocity. Based on the signal bandwidth, a zone was defined surrounding each peak which completely contained the reverberation echo and excluded as much background noise as possible. Figure 4 presents an A-scan upon which the zones containing the reverberation echoes has been identified by dashed lines.

The Fourier transform of the reverberation echo within each zone was then computed separately. As an example, the amplitude spectrum for each of the isolated sections shown in Figure 4 was computed. The computed amplitude spectra for all six of the reverberation echoes shown in Figure 4 are shown superimposed in Figure 5.

To determine the ultrasonic attenuation, an exponential curve was fit to the spectral data at each frequency within the usable bandwidth of the back surface echo signals. Different exponential decay constants were determined for each frequency component using a linear regression to obtain the best fit to the available information. Each of the data points used in the linear regression corresponded in position to a peak of one of the reverberation echoes and in amplitude to the amplitude of the specific Fourier frequency component.

Since the amplitude of the spectral components decreases both with increasing distance from the center frequency and with increasing depth into the sample, not all frequencies from every reverberation echo were of sufficient amplitude to be used in determining the attenuation constants. Attenuation constants were computed using only those spectral data points which were known to be higher in amplitude than the background noise. As a result, the number of data points contributing to the linear regression was a function of frequency with the greatest number of points, and therefore the greatest accuracy, occurring in mid-band. The ultrasonic attenuation versus frequency for the typical scan shown in Figure 4 and the spectra shown in Figure 5 is presented in the log-log plot of Figure 6. The straight line in Figure 6 is the best least squares fit to the log-log attenuation plot.

The oscillation in the computed frequency dependent attenuation is believed to be due to beam spreading as the ultrasound wave reverberates within the sample. This effect could be compensated using the results of simple geometrical calculations. The jump discontinuities which appear in Figure 6 are the result of changes in the number of spectral data points used to calculate the ultrasonic attenuation coefficient at different frequencies.

To demonstrate the reproducibility of these measurements, several scans were made of each sample. The results for samples A and E, the two extreme cases are presented in Figure 7. This plot clearly demonstrates the consistency of the measurement technique and its ability to easily differentiate between the extreme cases of contamination. Not only is the attenuation greater in sample A, the slope (rate of increase with frequency) is also substantially greater. For that component of the total attenuation due to scattering, the slope of the loss is dependent upon the grain size relative to the ultrasonic wavelength. Therefore, the slope of these attenuation plots contains additional information about the microstructure.

Figure 8 presents a comparison of the attenuation measurements on all five titanium samples at two particular frequencies, 4 MHz and 6 MHz. Also plotted in Figure 8 are the slopes of the

straight lines which best fit, in the sense of the least square error, the experimentally measured frequency dependent attenuation.

The measured ultrasonic attenuation at both frequencies clearly demonstrates a trend to lower attenuation in the more heavily contaminated samples, decreasing by approximately a factor of four over the range of materials tested. The variation of attenuation seen in Figure 8 is large enough to provide a means of identification of the various titanium samples.

Although the apparent dependence of ultrasonic attenuation on the degree of oxygen contamination seems to be quite strong, the direct application of this technique is, at present, limited by the scatter in the experimental data. This variation in measured attenuation is due in part to uncertainty in the experimental measurements and the computed results, however, a very significant component appears to depend on the measurement location. In particular, the data for sample D is shown clustered in two distinct groups. The group of three higher values for each quantity applies to measurements in the center of the sample, whereas the lower three values were obtained near the edge of sample D. This observation suggests that sample D, and perhaps also sample C, are inhomogeneous, though not necessarily in terms of the distribution of interstitial oxygen.

Final measurements were performed to determine the effect of surface finish on the measurement of ultrasonic attenuation. Since only a portion of each original sample had been ground smooth, it was possible to repeat the attenuation measurements using the rough surfaces of the titanium samples. Using direct contact measurement, an example of the effect of the rough surface on the measurement of attenuation in sample A was obtained and appears as the uppermost trace in Figure 7. This plot shows that the rough surface increases the signal loss through scattering, thus increasing the apparent attenuation of the material. The plot also shows, however, that the scattering is not strongly frequency dependent so that the identity of sample A can still be deduced from the frequency dependence of the curve which has the same slope as previous measurements on the smooth surfaces of sample A.

## DISCUSSION AND RESULTS

It has been demonstrated that by properly processing conventional A-scan ultrasonic data, it is possible to extract two parameters — velocity and attenuation — which permit a quantitative estimate of the degree of oxygen contamination in titanium samples. The results presented in Figures 3 and 8 suggest that the resolution of these quantitative determinations is approximately  $\pm 0.04$  percent oxygen by weight. Such resolution is not quite high enough to always unambiguously distinguish between nearest neighbors in the sample set provided, although it is easily sufficient to distinguish next nearest neighbors, such as samples C from A or E from C. Since the measurements presented are based on conventional ultrasonic A-scans, they can be straightforwardly extended to those situations where ultrasonic testing is already being used to detect internal defects and determine the structural integrity of welds.

The use of ultrasonic velocity measurements for the evaluation of oxygen contamination does, however, seem to suffer from some disadvantages. First, the sensitivity to variations in oxygen content seems to be very low. Our measurements suggest an overall variation for longitudinal velocities of approximately one percent for the range of samples tested. Although a slightly greater sensitivity has been reported for shear wave velocities [4], the use velocity measurements, obtained either by through transmission or pulse-echo methods, requires knowledge of the

sample dimensions or path length to approximately 1 part in 10,000. This may prove to be a severe restriction in many practical applications.

Another significant difficulty arises from the fact that the velocity measurements yield a single numerical result. This result includes the effect of all material along the propagation path and is surely sensitive to parameters other than oxygen contamination.

Ultrasonic attenuation measurements seem to avoid the difficulties associated with the measurement of velocity. The attenuation measurements show substantial variation with levels of oxygen contamination making knowledge of the sample dimensions less critical. In addition, the attenuation measurement offers not a single number to represent the measurement, but an entire function over any chosen frequency range. Realizing that ultrasonic measurements will be sensitive to microstructure variations in the HAZ and weld as well as to contaminants other than oxygen, the wealth of information offered by frequency dependent ultrasonic attenuation measurements should make practical the separate identification of these various effects.

The attenuation results presented suggest that the choice of a slightly higher frequency range and broader signal bandwidth might enable a clearer distinction to be drawn between the results of the various samples supplied. Since ultrasonic wavelength is reduced as the transmitted frequency increases, and the interaction between the ultrasound and the material reaches a maximum for ultrasonic wavelengths comparable to the grain size, higher frequencies should be more sensitive to subtle changes in microstructure.

The measurements presented were all based on the use of ultrasonic reverberations within a relatively thin plate. The use of reverberation echoes may not be essential to these measurements, particularly for the case of thick sections. Since the grain boundaries reflect the ultrasound energy as the wave passes through the bulk, the attenuation of the ultrasonic wave could be deduced as a function of depth from the backscattered grain echoes. For this type of approach to be practical, an extremely high signal-to-noise ratio, such as that provided by the correlation system used in these measurements, would be required to recover the ultrasonic signals directly backscattered by the grain boundaries.

#### REFERENCES

1. ONR/NRL Titanium NDE Workshop, 9-10 December 1980.
2. B. B. Lee and E. S. Furgason, "A New Digital Correlation Flaw Detection System," J. Nondestructive Evaluation, Vol. 2, No. 1, pp. 57-63, 1981.
3. N. M. Bilgutay, E. S. Furgason, and V. L. Newhouse, "Evaluation of a Random Signal Correlation System for Ultrasonic Flaw Detection," IEEE Trans. Sonics Ultrasonics, Vol. SU-23, No. 5, pp. 329-333, 1976.
4. ONR/NRL Titanium NDE Workshop, 3-5 February 1982.

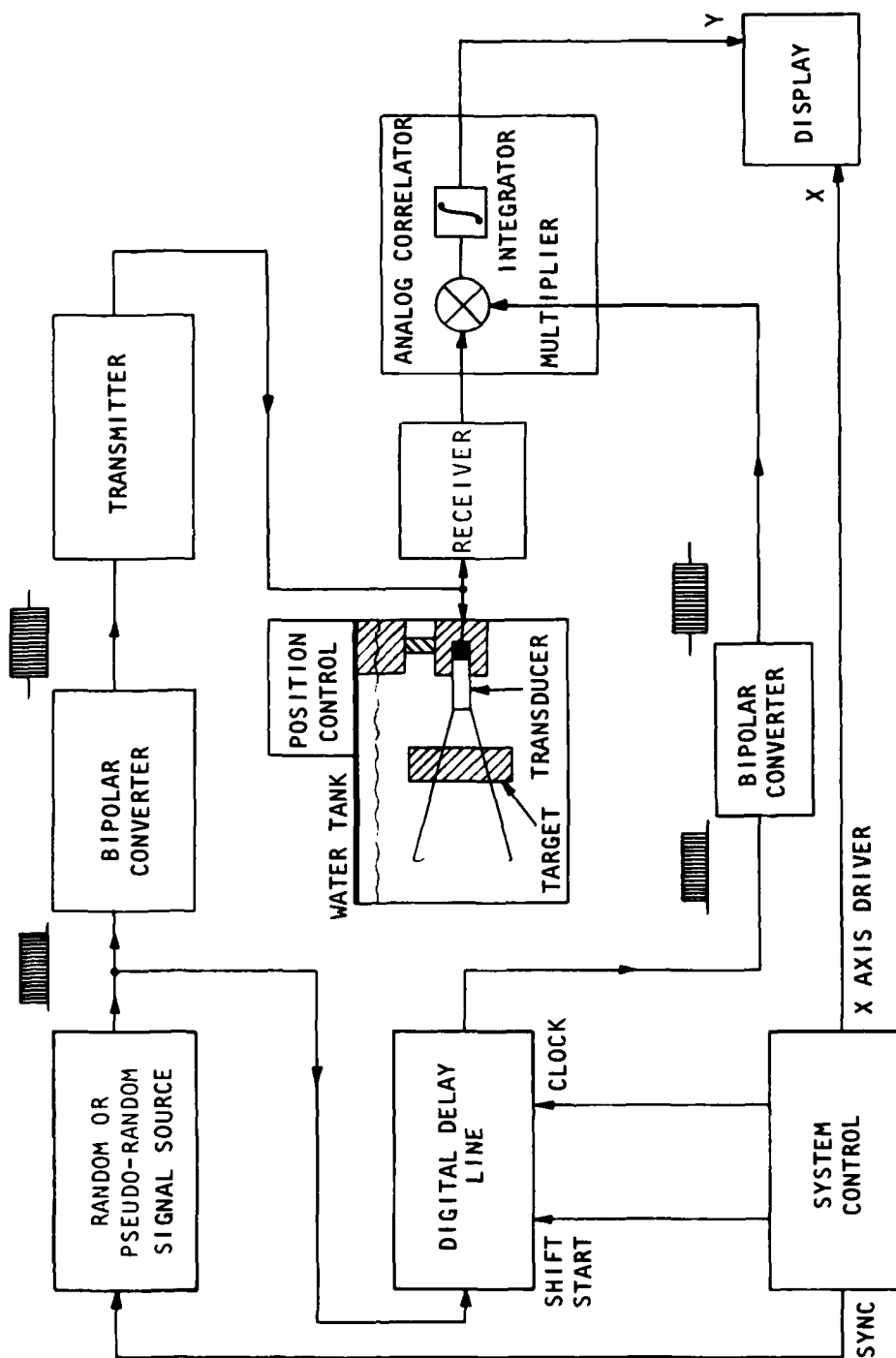


Figure 1. Block diagram of the digital correlation flow detection system.



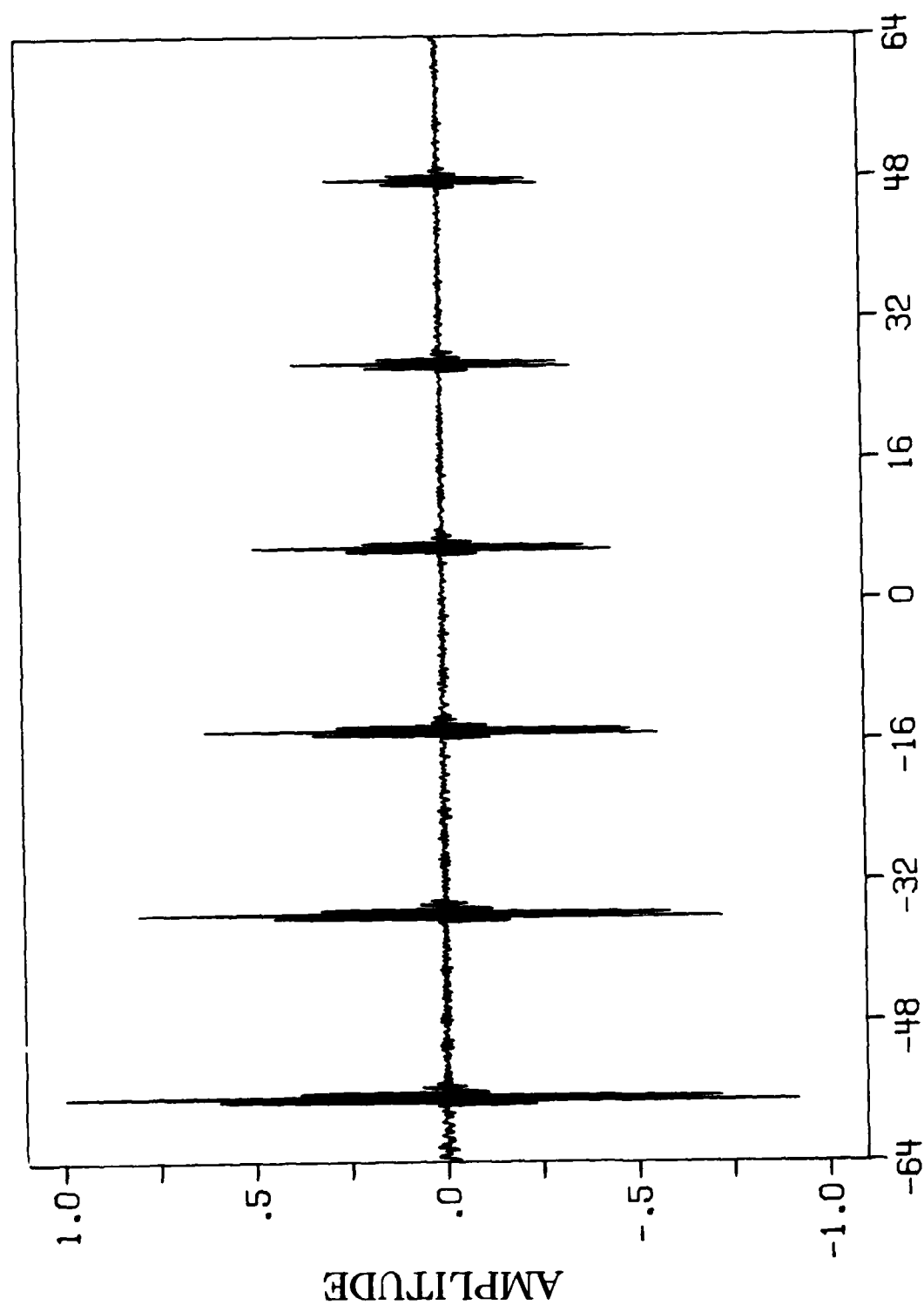
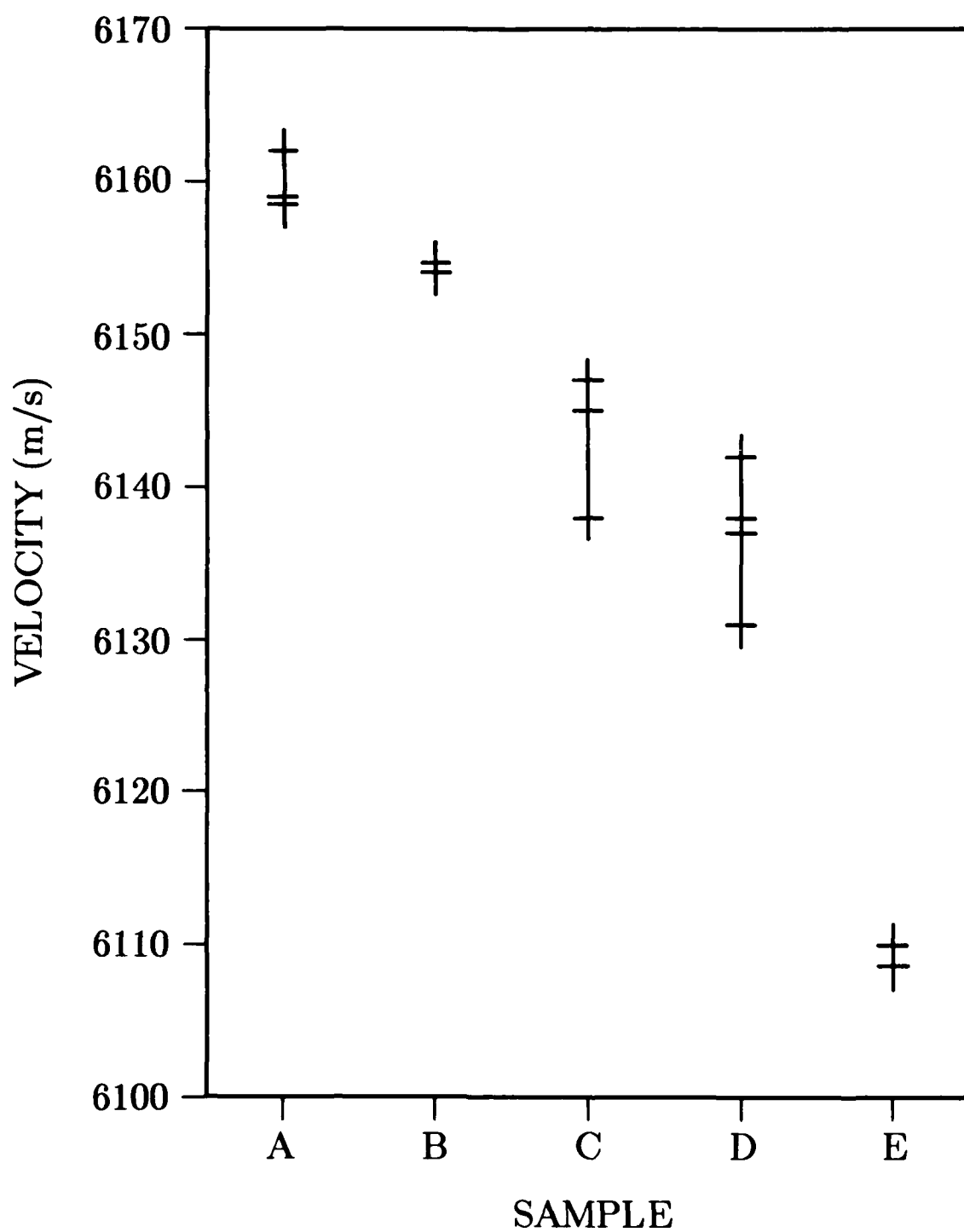
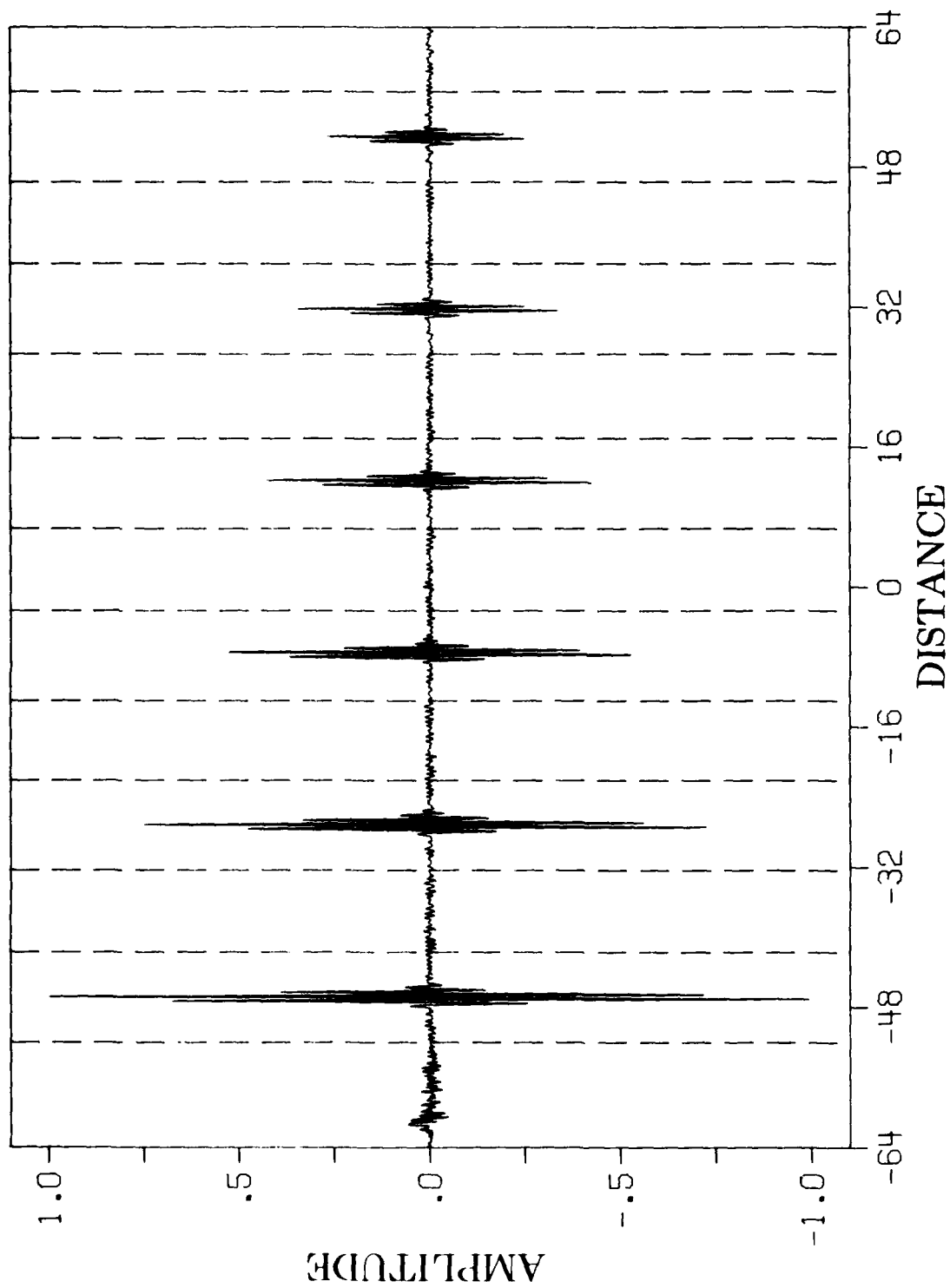


Figure 2. Typical ultrasonic A-scan of titanium sample E, showing six reverberation echoes.



**Figure 3.** Experimentally determined longitudinal wave propagation velocity in oxygen contaminated titanium samples. Crosses indicate measured values.



**Figure 4.** Typical ultrasonic A-scan of titanium sample C. Dashed lines indicate the region surrounding each reverberation echo which was isolated for further signal processing.

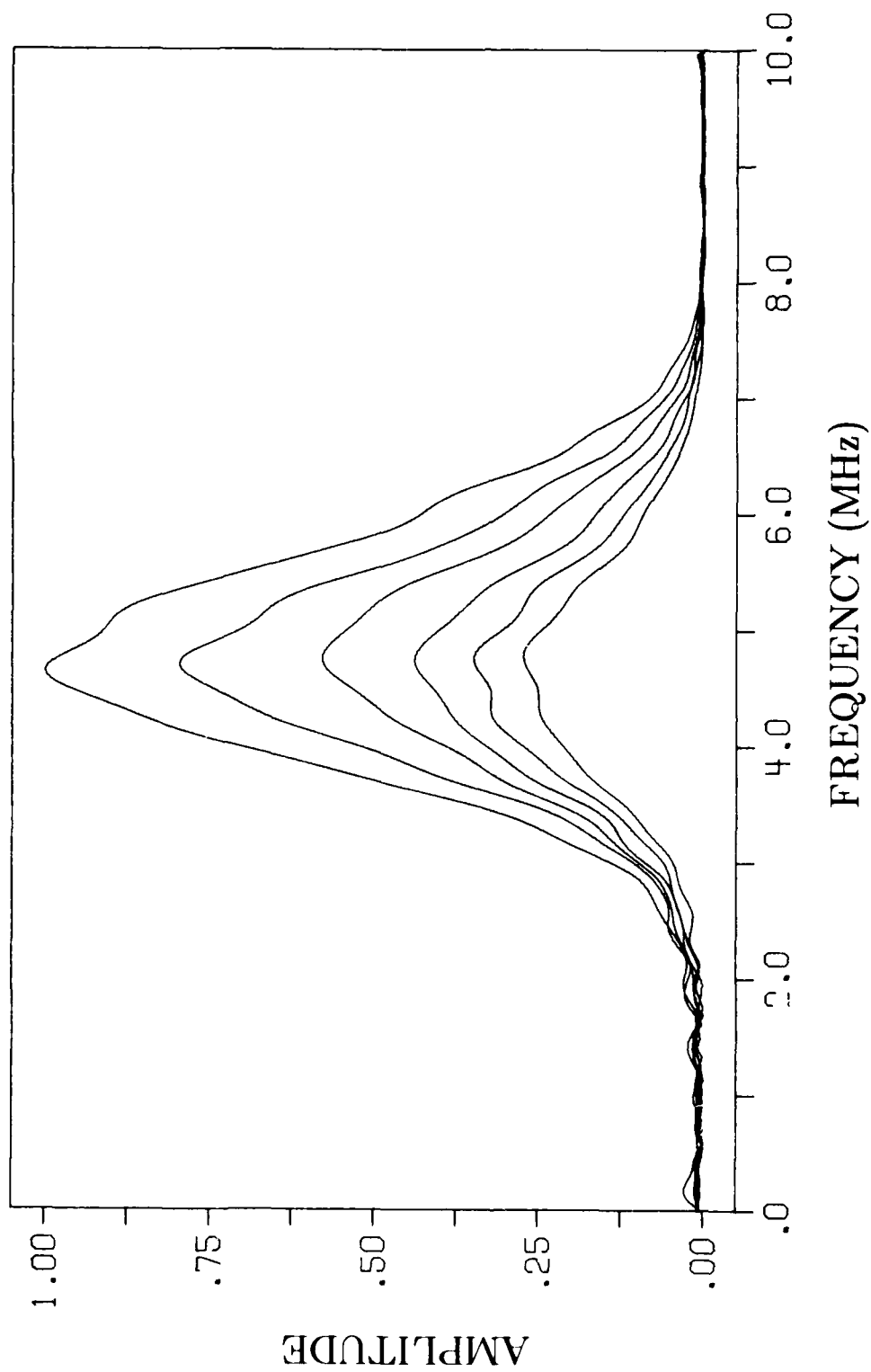


**Figure 5.** Amplitude spectra from the six signal zones containing reverberation echoes shown in Figure 4.

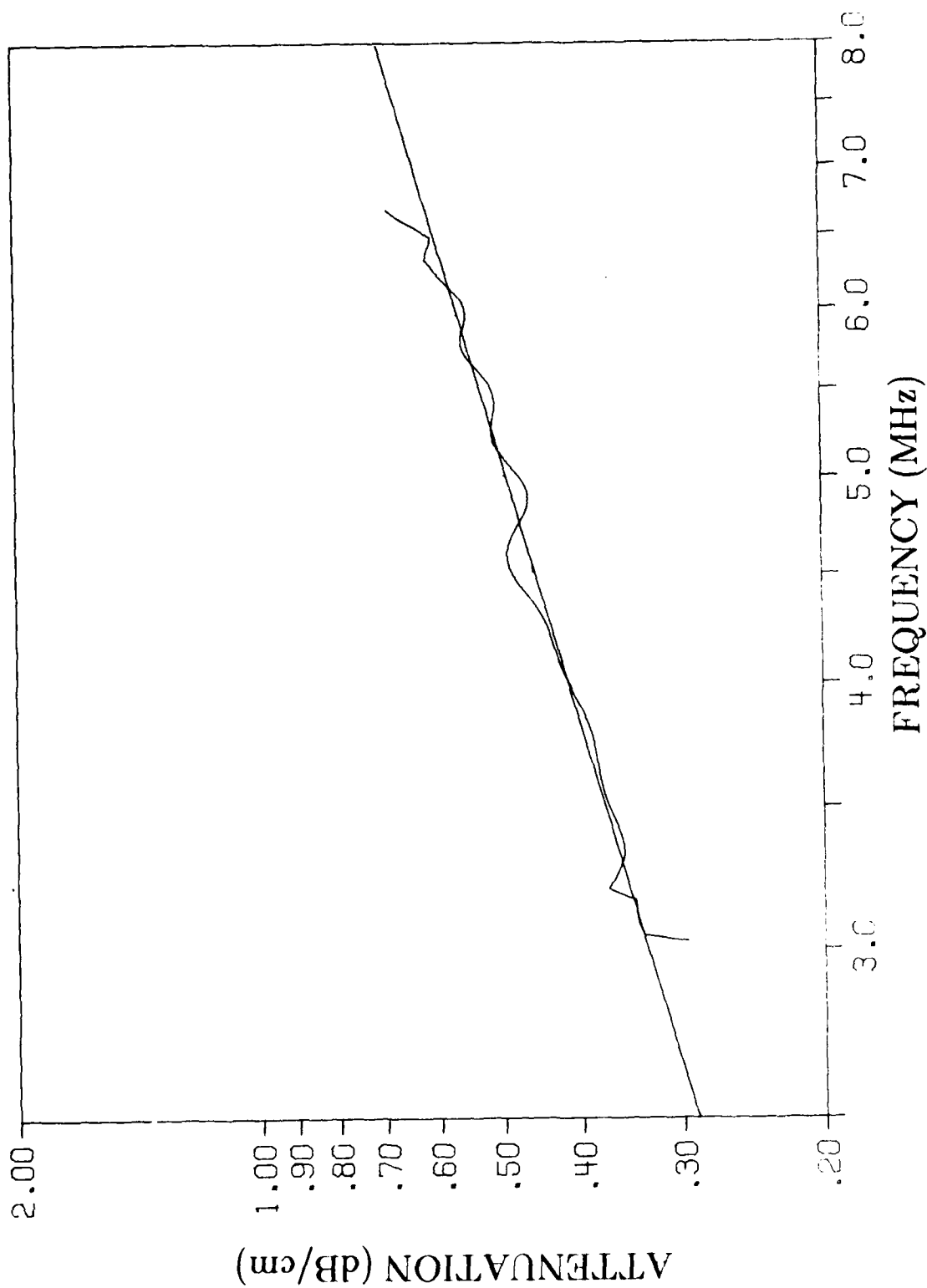


Figure 6. Ultrasonic attenuation as a function of frequency for sample C, calculated from the experimentally measured spectra in Figure 5.

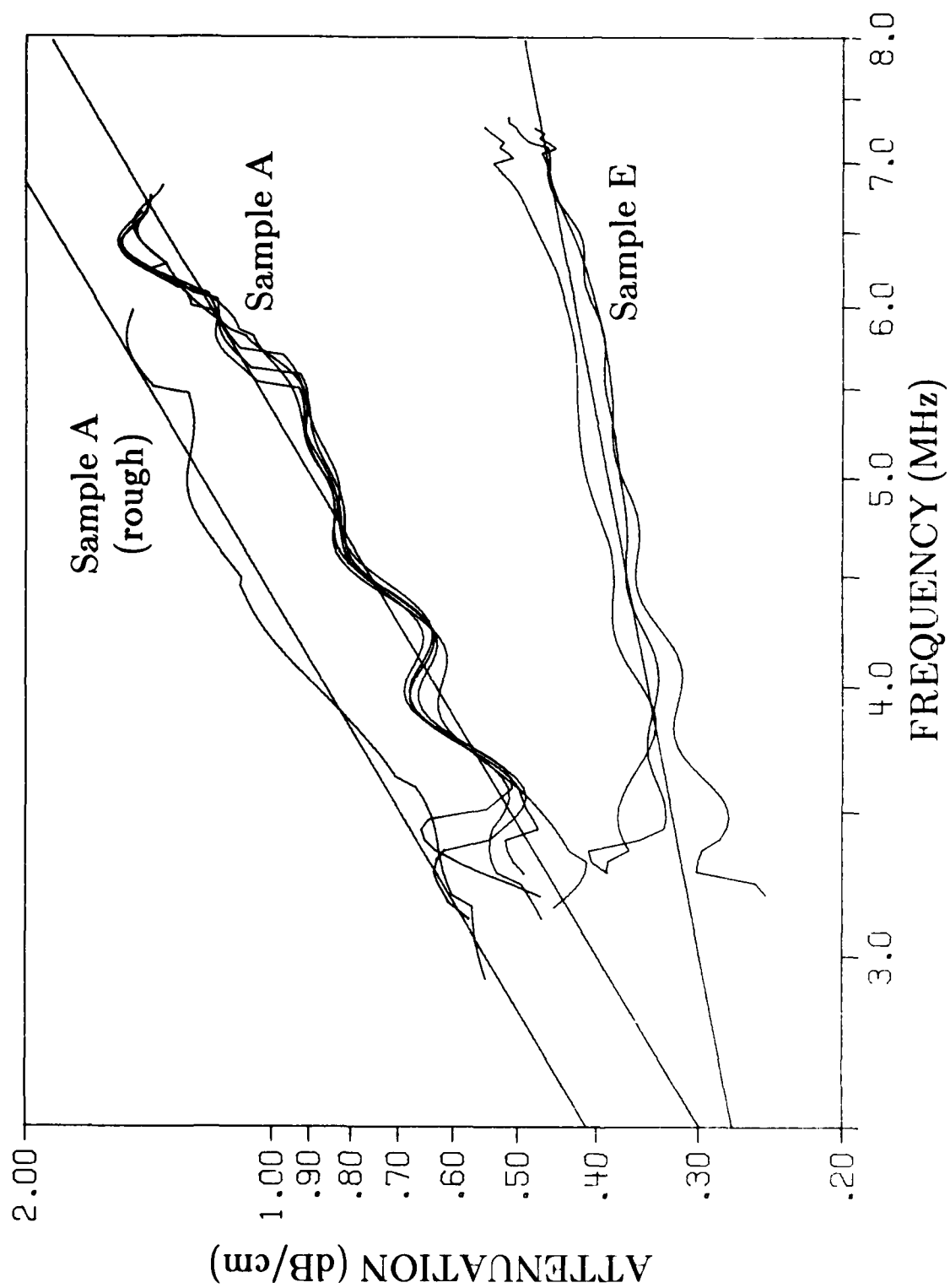
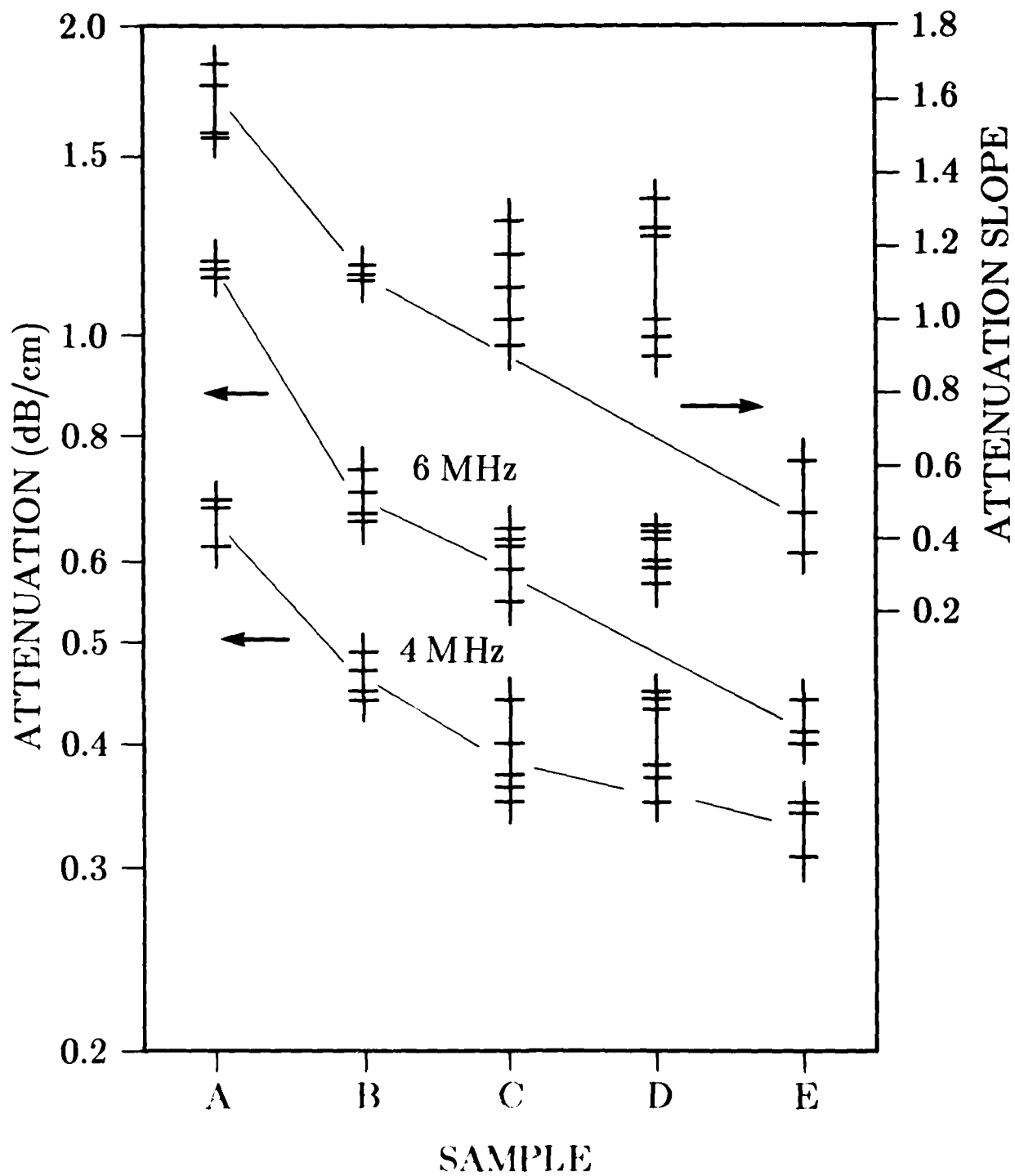


Figure 7. Comparison of ultrasonic attenuation as a function of frequency for several independent measurements on samples A and E.



**Figure 8.** Experimentally measured ultrasonic attenuation at 4 MHz and 6 MHz for oxygen contaminated titanium samples. Uppermost trace presents the variation in attenuation slope for different degrees of oxygen contamination.

**SECTION 7**  
**PHOTOACOUSTIC MICROSCOPY OF OXYGEN**  
**CONTAMINATED TITANIUM ALLOYS**

R. L. Thomas and L. D. Favro

*Department of Physics, Wayne State University  
Detroit, Michigan 48202*

↓  
The photoacoustic microscope is a device which uses a chopped laser beam as a modulated heat source and an acoustic cell and a detector to measure the microscopic thermal properties of materials. The result is a micrograph of the variations of the near surface thermal properties of the sample. As such it is a useful device for observing defects and the near subsurface grain structure of materials. Such structure is expected to be affected by nonsubstitutional impurities such as oxygen in titanium.

We have applied this technique to the five samples of titanium alloy. The samples were first machined flat and polished to remove the disturbed surface region and tool marks which were present when they were received. Individual photoacoustic micrographs were taken of each sample and then comparative photoacoustic micrographs were taken of pairs of samples within the same cell to eliminate systematic errors due to variations of cell properties.

These micrographs indicated small differences in the microscopic structure in the various samples but these differences appear to be overwhelmed by the gross variations in grain structure apparently induced by the rolling processes, etc. Rather large variations in structure were observed from point to point in the same sample, making it difficult to make meaningful comparison between samples. Micrographs which indicate the differences and similarities of the samples will be presented. ↑

AD-P004 127



Five samples of gas-contaminated Ti-6211 Alloy were examined with a photoacoustic microscope which images the near-subsurface variations in thermal properties. A schematic diagram of the microscope appears in Fig. 1. A focused laser beam, which is chopped at an audio frequency serves as a local a.c. heat source on the surface of the sample. The heating results in a localized a.c. temperature distribution which is determined by the chopping frequency of the laser, and by the optical absorptivity, heat conductivity, and specific heat of the material just under the surface. The a.c. surface temperature (which contains information about the subsurface properties) is detected by means of the resultant heating of the air over the surface, which in turn is detected by a microphone placed near the heat source. Both the microphone and the heated laser spot are inside an enclosed cell, which serves both to reduce outside noise and to increase the signal pressure at the microphone. As the laser spot is scanned over the sample surface, the microphone output is digitally recorded for later display as a photoacoustic picture on a CRT or for signal processing by a computer. The penetration depth of the a.c. temperature can be derived from the equation for thermal diffusion and is given by  $(2k/\omega c \rho)^{1/2}$  where  $k$  is the thermal conductivity,  $\omega$  the circular frequency,  $c$  the specific heat and  $\rho$  the density of the material. For typical materials and low audio frequencies this depth can be of the order of a millimeter, but in our experiments on the Ti test bars (done at 1 kHz) the penetration depth is of the order of 100 to 200  $\mu\text{m}$ .

The test bars as received showed gross tool marks and surface damage on the scale of a millimeter or so. To remove this damaged area the surfaces

were first ground flat and then buffed to a relatively smooth surface. Photoacoustic micrographs of this surfaces still showed surface scratch marks against the background of the subsurface structure. Hence, small portions of the surfaces were further cleaned by etching to obtain clear areas with no obvious surface damage.

Figure 2 shows a scanning photoacoustic microscope (SPAM) micrograph of sample A, as well as an optical picture of the same region of the sample. The dimensions of the region are 1.91x1.27 mm. Although some surface tool scratches still show in the SPAM picture, it is immediately apparent that it shows features which are not visible in the optical micrograph. At this point one can only speculate about the origin of these features. They may be grains which differ in composition and crystallographic orientation or crystal structure. Each of these properties could affect the thermal parameters and cause contrast variations in the photoacoustic picture.

Figures 3 through 6 are similar SPAM-Optical comparison pictures for each of the other test bars in increasing order of nominal oxygen concentration. All of these micrographed regions are of the same size as the original one on sample A. Of particular interest is a vertical band of higher contrast in the center of the SPAM picture of sample C (Fig. 4). This band is a surface oxidized strip caused by a previous photoacoustic scan with the laser power set too high. Notice that many photoacoustic features can be traced across the boundaries of this region into the neighboring unoxidized area. This would seem to indicate that the increased contrast stems not from changes in underlying structure but from the increased optical absorptivity of the oxide layer. (This layer is visible under a low power microscope as a yellowish patch on the surface). Sample D (Fig. 5), and to a somewhat lesser extent also sample E (Fig. 6), shows a much finer grain structure in the photoacoustic micrograph. This presumably

reflects a greater point-to-point metallographic variability in these samples and may be the result of increased gas contamination. The SPAM pictures are all displayed together in Fig. 7 to facilitate visual comparison of the various samples. In Fig. 8 we show photoacoustic and optical pictures of two different regions on Sample D, which have quite different visual appearances, but very similar photoacoustic micrographs. Therefore we believe that the fine grain structure in the photoacoustic micrograph is intrinsic to the sample.

In summary, the SPAM technique shows differences in subsurface thermal properties among the five samples studied. In each case, structure is observed photoacoustically which is not evident in the optical micrographs. The apparent granularity of the SPAM micrographs varies from sample to sample, with the finest scale granularity obtained for sample D. Although the statistical sample is much too small to make a meaningful correlation, it would not be physically unreasonable for these trends to be the result of increasing gas contamination.

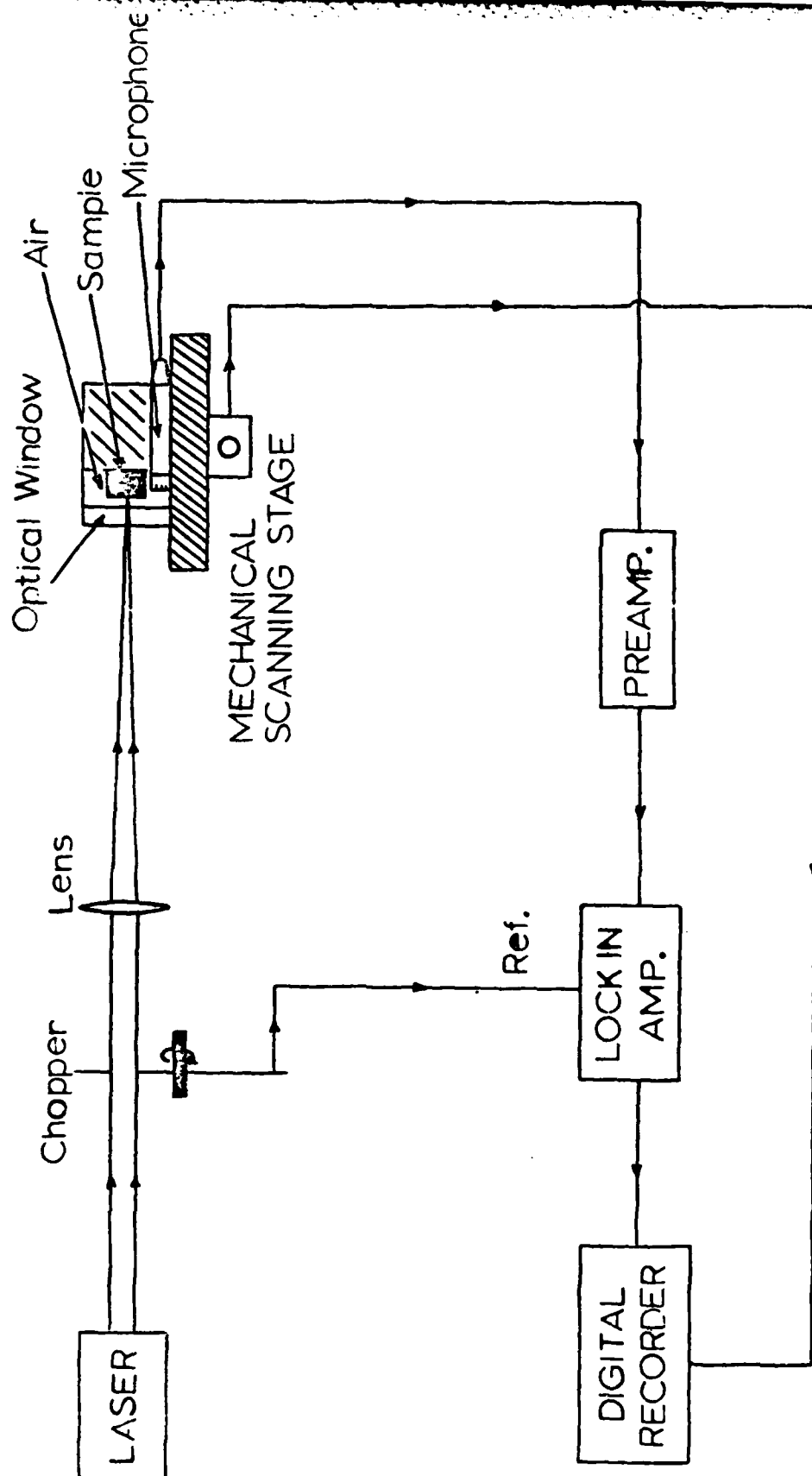
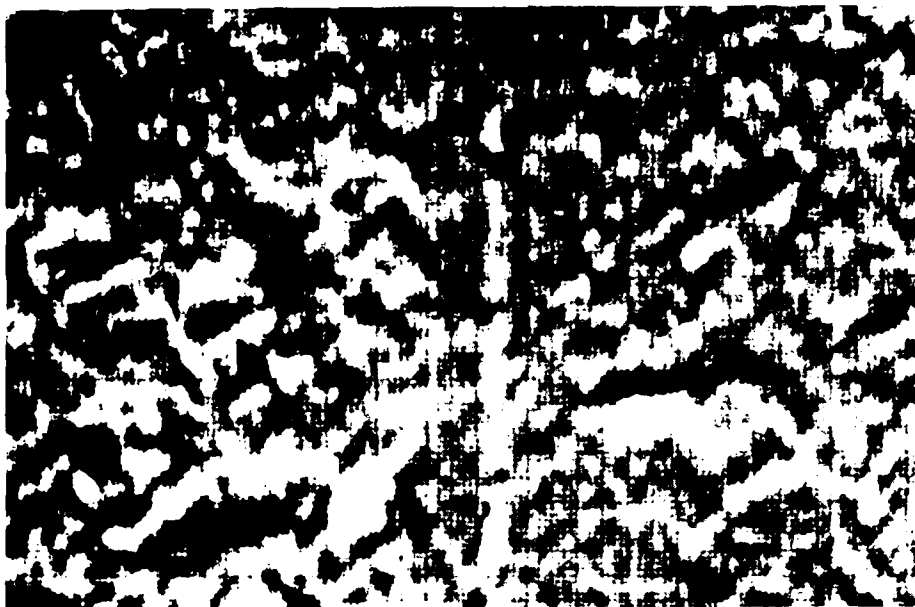


Fig. 1 Block diagram of the apparatus

Fig. 2



SPAM

1.91 mm



1.27 mm

OPTICAL

#A 5-7

118

Fig. 3



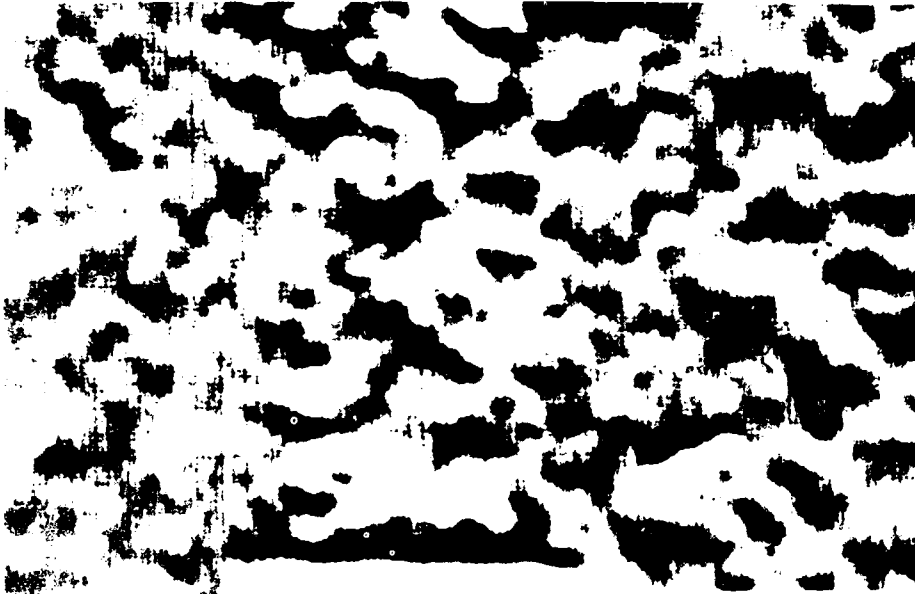
SPAM



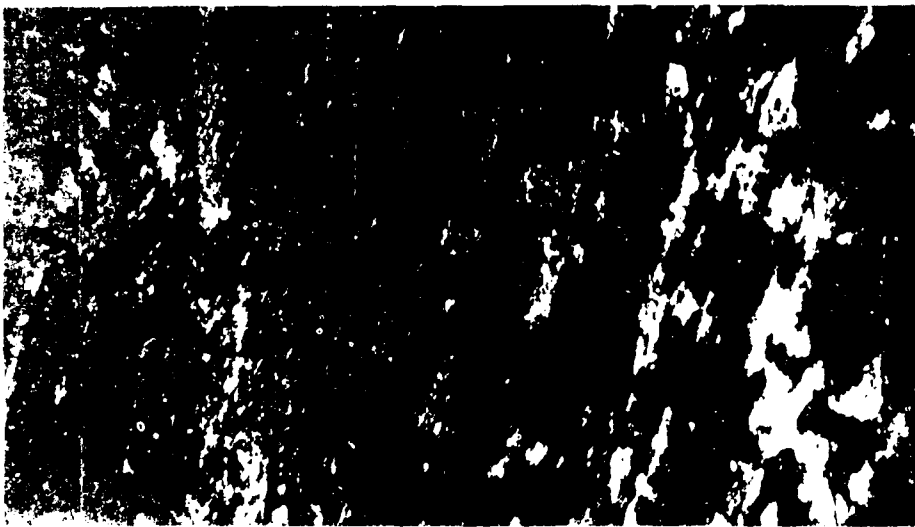
OPTICAL

#B 5-7

Fig. 4



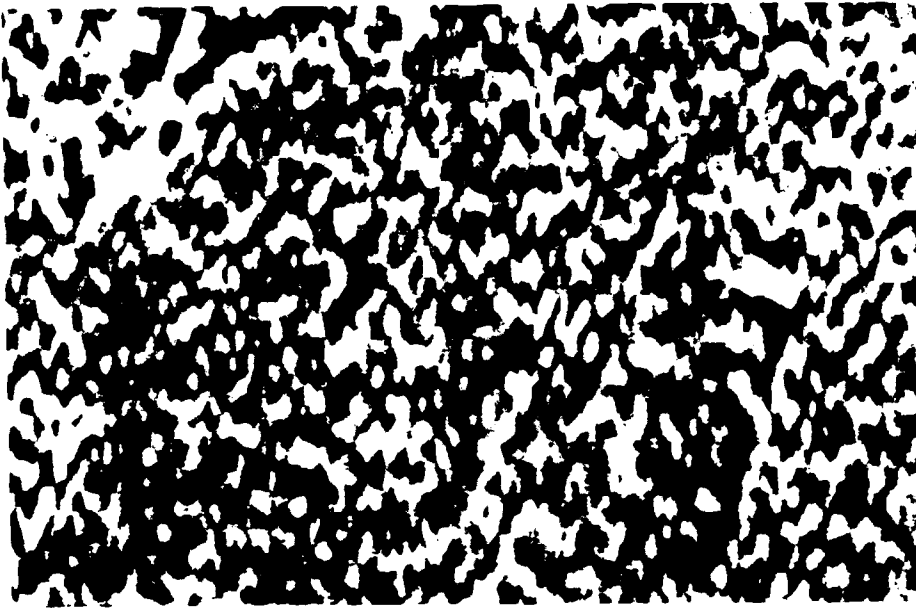
SPAM



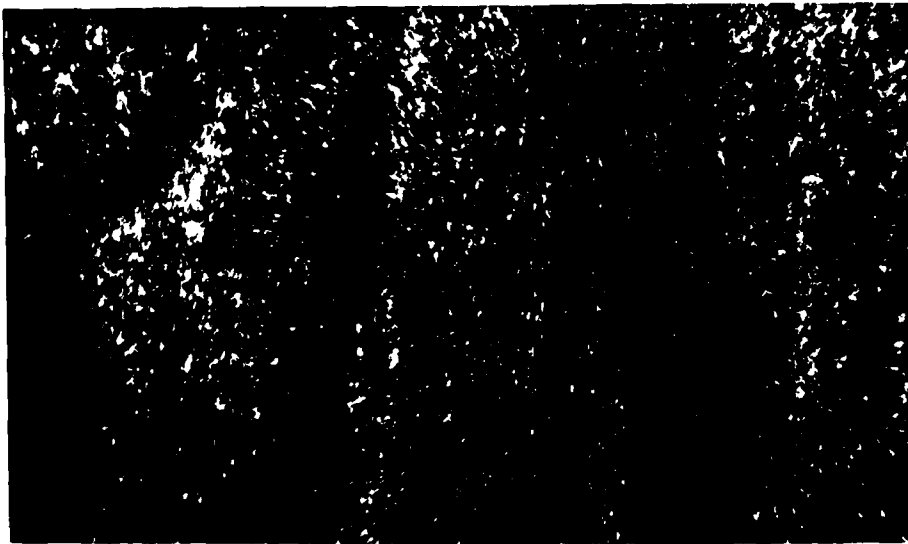
OPTICAL

#C 5-7

Fig. 5



SPAM

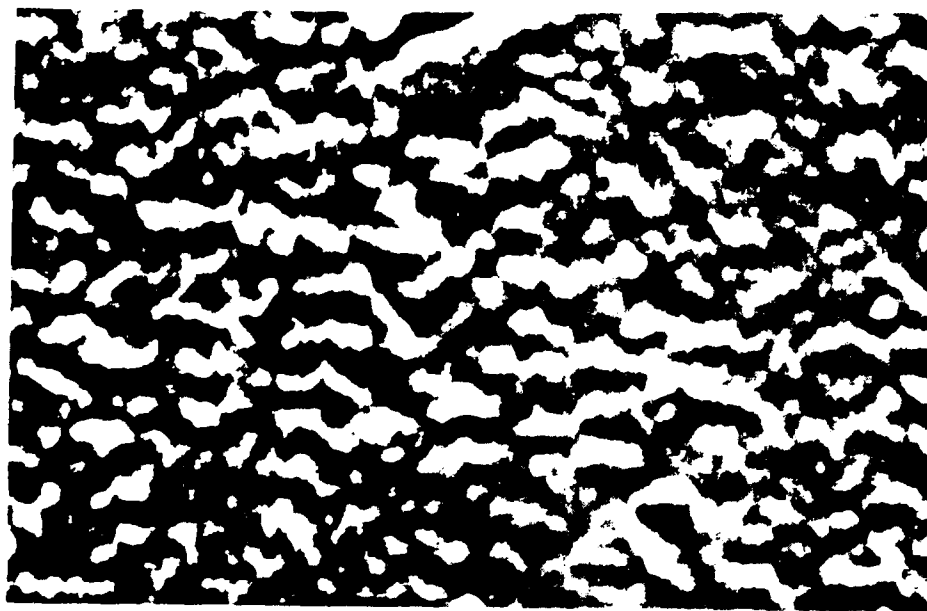


OPTICAL

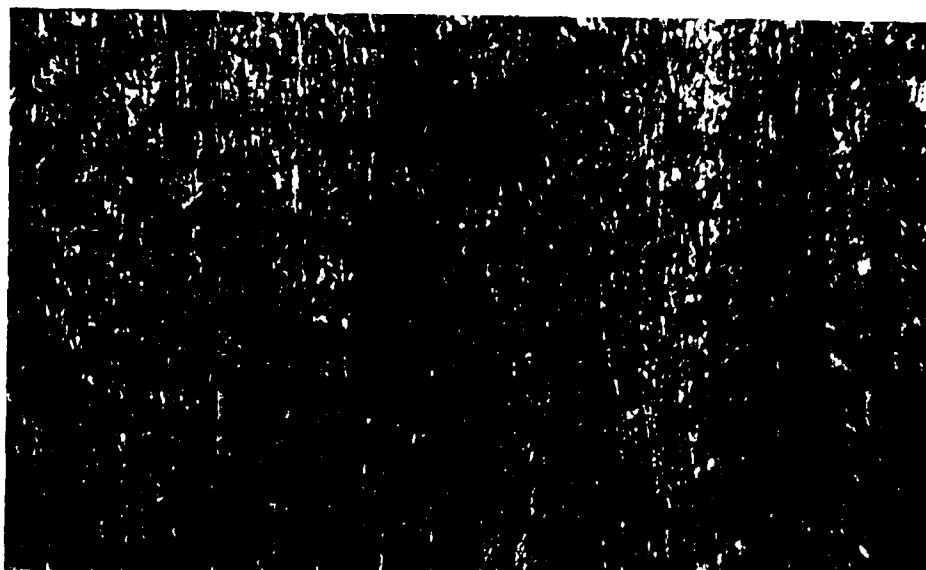
#D 5-7



Fig. 6



SPAM



OPTICAL

Figure 7

0(%)

H(ppm)

SPAM

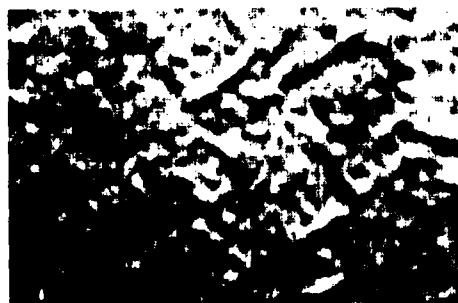
A



0.075

40

B



0.136

49

C



0.194

42

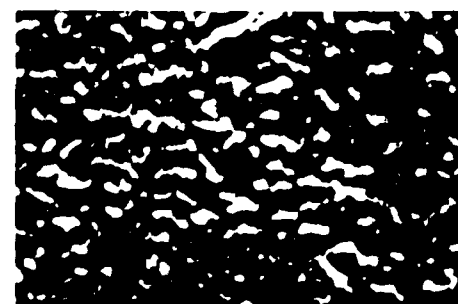
D



0.238

61

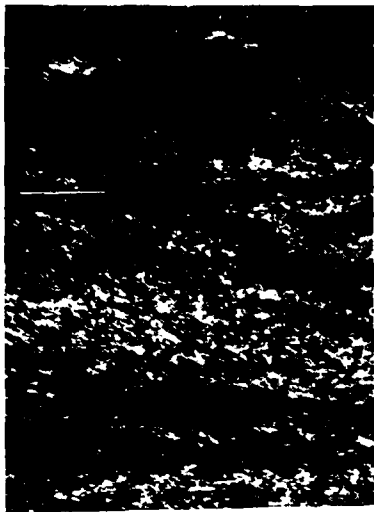
E



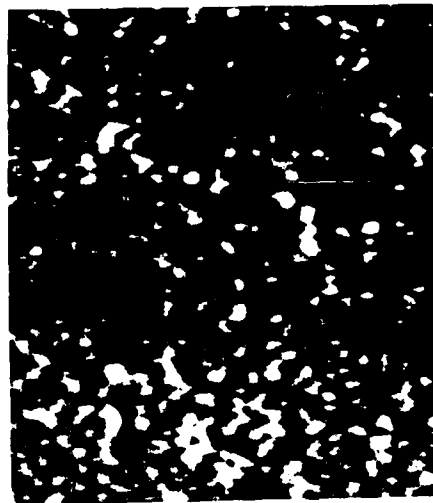
0.290

54

Figure 8



OPTICAL



SPAM



Photoacoustic and Optical Micrographs of Two  
Different Regions of Sample D

SECTION 8

**HIGH RESOLUTION ACOUSTIC MICROSTRUCTURAL  
CHARACTERIZATION OF TITANIUM  
WITH INTERSTITIAL CONTAMINATION**

Alan M. Greenburg

*General Dynamics/Electric Boat Division  
Eastern Point Road  
Groton, Connecticut 06340*

and

Donald E. Yuhas and Michael G. Oravec

*Sonoscan, Inc.  
530 East Green Sheet  
Bensenville, Illinois 60106*

This investigation deals with observations relating to the acoustic characterization of the microstructure of titanium. The main idea is to relate weld integrity, or in this particular case, the level of interstitial gas contamination contained in titanium to variations in acoustic properties. The Scanning Laser Acoustic Microscope was used to obtain both images and quantitative attenuation and velocity data. Acoustic frequencies of 100 MHz and 30 MHz were used. Two different titanium alloys were tested. These include nonwelded Ti-6211 alloy as well as welded Ti-6AL4V alloy. Results indicate that substantial variations in acoustic characteristics are observed and can be correlated with the level of interstitial gas contamination. Specifically, the average acoustic attenuation is found to increase with the level of interstitial contamination. Also, the acoustic characteristics of the sample become more nonuniform or inhomogeneous with increasing contamination level. This is evidenced by large variations in the local attenuation properties (on scale of a few hundred microns). Associated with the inhomogeneous attenuation characteristics are large, discontinuous sonic velocity variations.

AD-P004 128

---

\*This work was sponsored by General Dynamics/Electric Book Division under IRAD Project 82007129 "Development of a Non-destructive Test Method for Detecting Contamination in Titanium Weldments"

### Introduction

This work involves the high frequency, high resolution acoustic characterization of titanium using the scanning laser acoustic microscope. The main emphasis is the detection and the quantification of several acoustic characteristics of titanium. Variations in these acoustic parameters are then related to the level of gas contamination (oxygen). The emphasis differs from standard non-destructive testing applications. Here, material integrity is related to measurements of the overall characteristics of acoustic transmission, rather than to the detection of localized flaws, e.g., cracks.

The result of this work provides a better understanding of titanium's properties, particularly in terms of the variations that result from gas contamination. Also, the information gathered through careful acoustic characterization provides rigid guidelines for developing non-destructive test methods for on-line weld evaluation.

## Background

The instrument used in these investigations is a scanning laser acoustic microscope (SLAM). The SLAM is a high frequency ultrasonic imaging instrument which enables one to test the mechanical or acoustic characteristics of a material non-destructively. Using the acoustic images it is possible to determine uniformity in elastic properties, such as density and elastic modulus. A key feature of the instrument is the high operating frequency, typically 100MHz. This provides image resolution and sensitivity to structure on the size scale of tens of microns.

In figure 1, we show a picture of the scanning laser acoustic microscope used in this investigation. Figure 2 is a simplified schematic which will serve to illustrate the imaging geometry and the basic operating principles of the SLAM. As shown, a standard transmission acoustic imaging geometry is used where the sound is incident on the bottom of the sample. After traversing the sample where it is scattered and refracted by structural defects, the sound is received by a detector that is represented in the figure by a mechanical receiving transducer.

The use of a mechanical receiver is a perfectly viable and acceptable way to produce acoustic images, however, it suffers in two respects. First, the resolution is limited by the size of the receiver in the system shown in Figure 2. Since mechanical receivers usually have a large spatial extent, it is difficult to obtain wavelength limited acoustic resolution using high sonic frequencies. Secondly, the only way to produce an image is to mechanically move the receiver across the face of a sample, and record image data, in a step by step fashion. This tends to be slow.

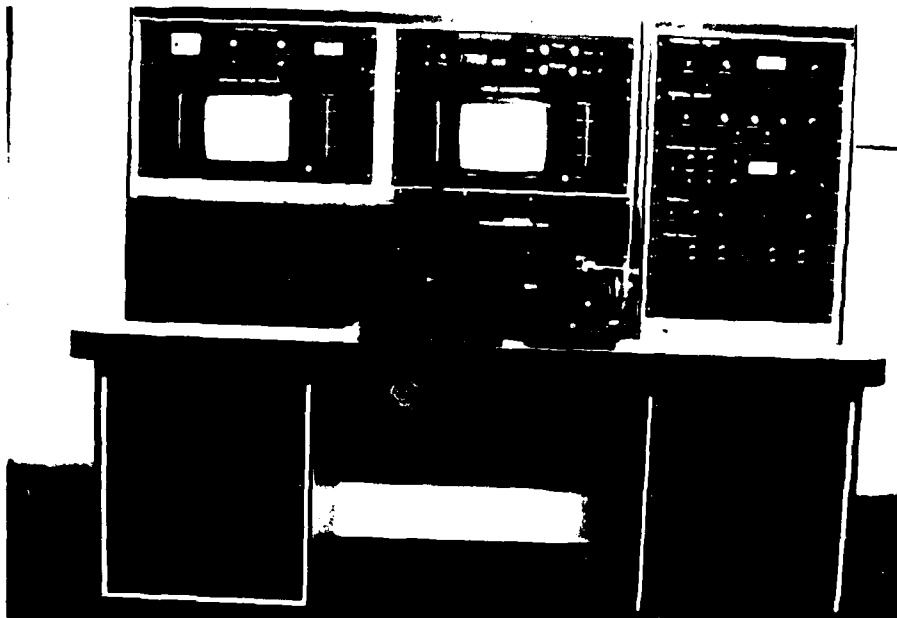


Figure 1 A commercially available scanning laser acoustic microscope.

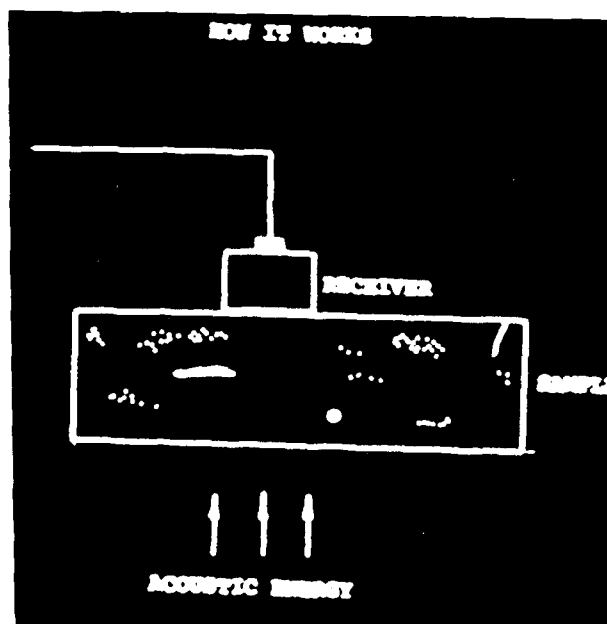


Figure 2 Schematic illustrating imaging geometry for transmission imaging.

In the scanning laser acoustic microscope system, the mechanical detector is replaced by a focused laser beam. The laser beam picks up and detects the small minute acoustic vibrations as it scans across the face of the sample. In this way, it can be used to produce a rapid, full grey scale, acoustic image. Resolution is controlled by the receiver size (laser spot size) and is adjusted to give wavelength limited resolution over the range of acoustic operating frequency of 30 to 500 MHz.

By combining an ultrasound source similar to that depicted in figure 2 with the scanning laser detector, SLAM images can be produced at very rapid rate, specifically 30 frames per second. The ultrasonic image consists of 40,000 points and is displayed on a CRT monitor. The bright areas of micrographs correspond to levels of high acoustic transmission found in regions where there is good mechanical continuity throughout the sample. The grey to black areas indicate progressively more attenuating zones from the standpoint of mechanical continuity.

Figure 3 is a photograph of a titanium sample being investigated on the scanning laser acoustic microscope at a frequency of 30 megahertz. For larger samples, tests are performed at 30 MHz in an immersion system as shown. The sound source, i.e. the transducer, is underneath the sample and does not appear in the photograph. The region scanned by the laser, and thus acoustically imaged, is located just under the anodized aluminum tube.



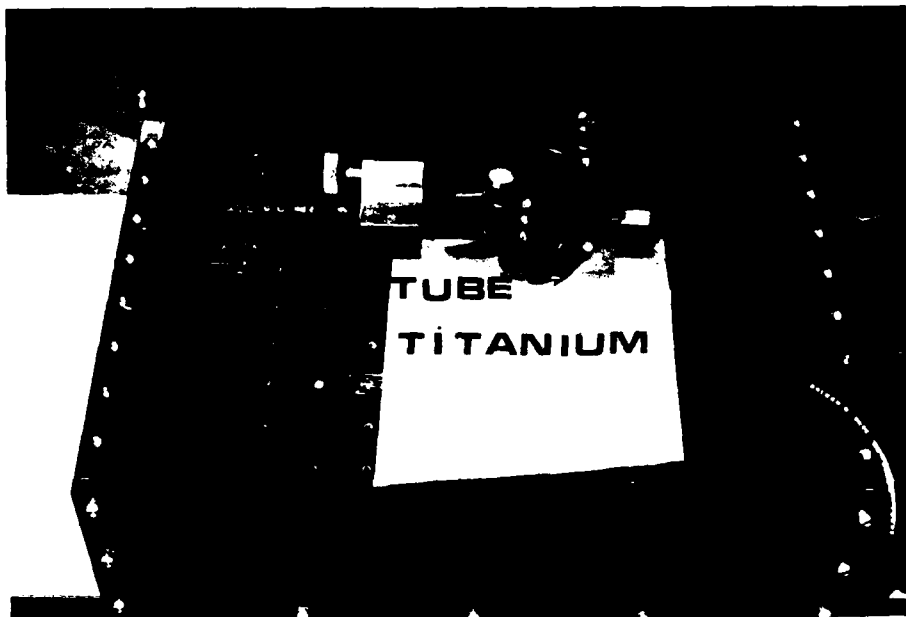


Figure 3 Sample mounted for the SLAM imaging. Transducer is hidden by the 5 inch square titanium sample.

## ACOUSTIC MICROSCOPE DATA

The approach adopted in this study involves using the real-time imaging capabilities of the SLAM to develop some general ideas of how sound propagates in the various titanium samples. Analytical methods are then developed and implemented in order to quantify the image information. Acoustic image interpretation as well as some of the quantitative techniques are illustrated in Figures 4 to 6.

Figure 4 shows a 30 MHz acoustic micrograph of a crack which is found in a welded section of titanium 6Al 4V that had been heavily contaminated with gas (nitrogen). The interest here is not flaw detection, although the micrograph shows an obvious crack. The image serves to illustrate both the flaw detection capabilities and material characterization methods that are available with the microscope image data.

Flaw detection inside materials involves the interpretation of the structures visible in acoustic micrographs. The structure in Figure 4 can best be understood with reference to the schematic shown in Figure 5. The drawing shows the sound incident on the bottom of the sample and refracting as it enters the sample. As it propagates, it interrogates an entire volume of material. Thus, the three dimensional character of the flaws appear in the images. For example, cracks such as that illustrated in Figure 4 are characterized by dark shadows whose width is directly related to the extension of the crack beneath the surface. Near the bottom of the micrograph, (Figure 4) the extension of the crack is rather shallow (small shadow). Toward the top of the micrograph the shadowed zone gets larger, indicating the crack extends more deeply beneath the surface. The shadow arises because of the high attenuation of sound as it tries to propagate across the gap where no



Figure 4 Acoustic image (30MHz) showing the shadow of a crack found in welded titanium. The width of shadow measures crack extension beneath the surface.

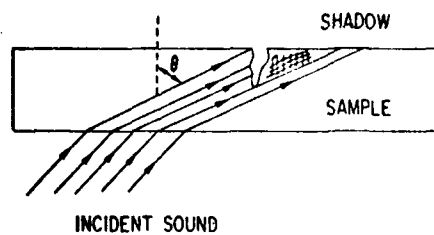


Figure 5 Schematic the shadowing effect for cracks.

mechanical contact exists.

The acoustic characterization of the material essentially involves quantifying the structure and the levels of white and black as they appear on the acoustic micrographs. The micrographs are used to guide the data recording process, but are not themselves used. Quantitative measurements are recorded electronically by selecting a single line of video information while viewing the real-time image. The operator selects the desired line from the image and records the acoustic transmission at points along the line.

In Figure 6, the insertion loss (energy lost in transversing the sample) is plotted on the ordinate while the distance along the weld is on the abscissa. Results presented here were obtained at 100 MHz on welded titanium 6Al 4V. Figure 6 shows a line scan in the vicinity of a crack similar to that shown in Figure 4. The connection between the graph and micrograph is straight forward. The darker zones correspond to the higher insertion loss numbers while the lighter portions of the micrographs correspond to the lower insertion loss values.

The most dominant feature in this graph is the presence of the crack shadow. From a characterization standpoint, it is perhaps more interesting to analyze the regions away from the crack. This line scan data, once recorded, can be manipulated to derive a number of parameters.

In the "characterization region" of the line scan shown in Figure 6, two very useful characterization parameters have been derived. First, the average insertion loss is determined by computing the mean of a portion of the line scan. Second, the standard deviation provides a quantitative measure of image contrast. The image contrast parameter is particularly important since it may be more amenable to measurement in on line imaging situations.

LONGITUDINAL SCAN

TI 6AL-4V

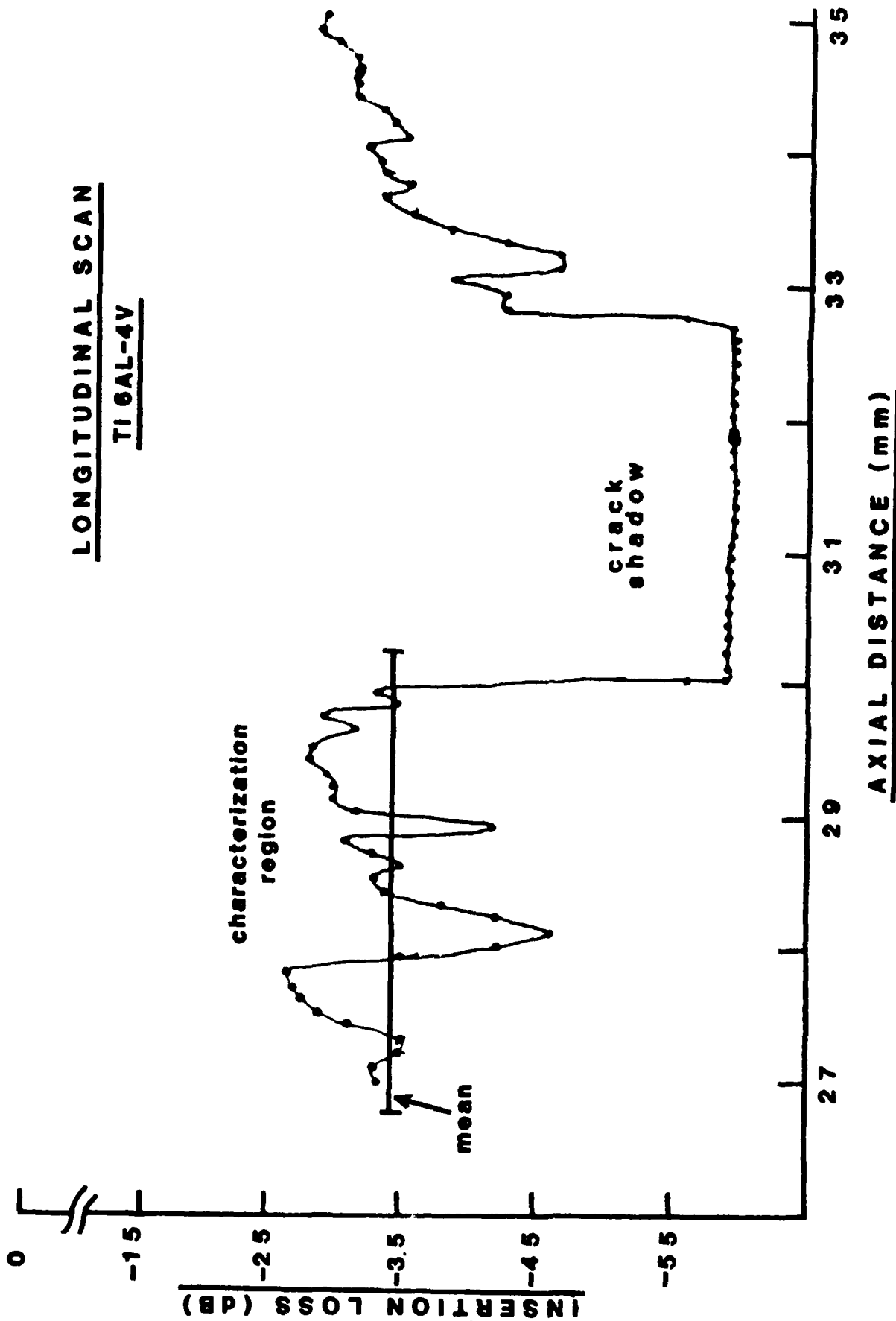


Figure 6 Line scan showing quantitative insertion loss data in the vicinity of a crack. The amplitude variations in the "Characterization zone" yield a unique material signature.

## OBSERVATIONS TITANIUM 6211

Five different samples were provided to EB Div. with oxygen contamination levels varying from the 0.074% found in Sample A, up to a high of 0.29% in Sample E. Table 1 describes the chemistry of the titanium 6211. All samples were 5" by 5" rectangular blocks of the same thickness. Measurements were made on these samples with "as cast" surface finish. In addition, a small portion of the surface of three samples was machined, and some measurements were made on the SLAM for purposes of comparison.

All five samples were first imaged. Observations of the acoustic transmission characteristics in real-time made it possible to qualitatively assess which acoustic parameters can be associated with oxygen contamination. Quantitative measurements were obtained by methods described in the previous section.

Figure 7 shows a plot of the attenuation data as a function of oxygen contamination. On the vertical axis, we have insertion loss, while on the abscissa the sample identification and the level of oxygen contamination is plotted. The curves are shown. The upper curve corresponds to results obtained on the machined surface, while the lower curve shows insertion loss data obtained on samples with the "as cast" surfaces. These measurements are made by recording the average acoustic loss over a field of view (square centimeter). Each point plotted represents an average of several determinations. The vertical axis is labeled as insertion loss, in that we are measuring the amount of acoustic amplitude lost or attenuated in the material. The shapes of the two curves are similar, however, there is approximately a 10dB difference in the absolute insertion loss numbers. The difference can be attributed to the surface conditions with the "as cast" surface showing more attenuation or insertion loss. There is a very

clear trend in both curves. Sample A, the sample with the least amount of contamination shows greater insertion loss, while Sample E, the sample with the highest oxygen contamination, shows the least insertion loss (most transparent). The trends in both curves are almost identical in terms of the shape of the curve.

An alternate means for characterizing the material involves looking in detail at the structure of the images. Figure 8 shows acoustic line scan data obtained on Samples A, C, and E. The tracings give a quantitative measure of acoustic transmission as a function of distance along the sample. A variety of methods are available for quantification of the line scan data. The image contrast, for example, can be easily quantified by computing the standard deviation. It is quite clear that the raw line scan data show distinct variations between samples A, C, and E. The standard deviation, a quantitative measurement of acoustic contrast, has been calculated from these curves and is plotted in Figure 9. These results indicate that significant variations in the scattering characteristics are associated with the percentage of oxygen contamination.

TABLE 1

## CHEMICAL ANALYSIS OF 5 TITANIUM 6211 SAMPLES

CHEMISTRY	SAMPLE NUMBERS				
	NRL A-4	NRL B-4	NRL C-4	NRL D-4	NRL E-4
C %	0.02	0.02	0.02	0.02	0.03
N %	0.010	0.006	0.005	0.006	0.008
Fe %	0.05	0.03	0.03	0.03	0.03
Al %	6.0	6.0	5.9	5.8	5.9
Co %	1.95	2.09	1.90	2.05	2.16
Ta %	0.38	0.97	0.94	0.99	1.06
Mo %	0.70	0.9	0.8	0.8	0.7
O %	0.074	0.136	0.194	0.238	0.290
H (ppm)	40	49	42	61	54



# INSERTION LOSS T16211

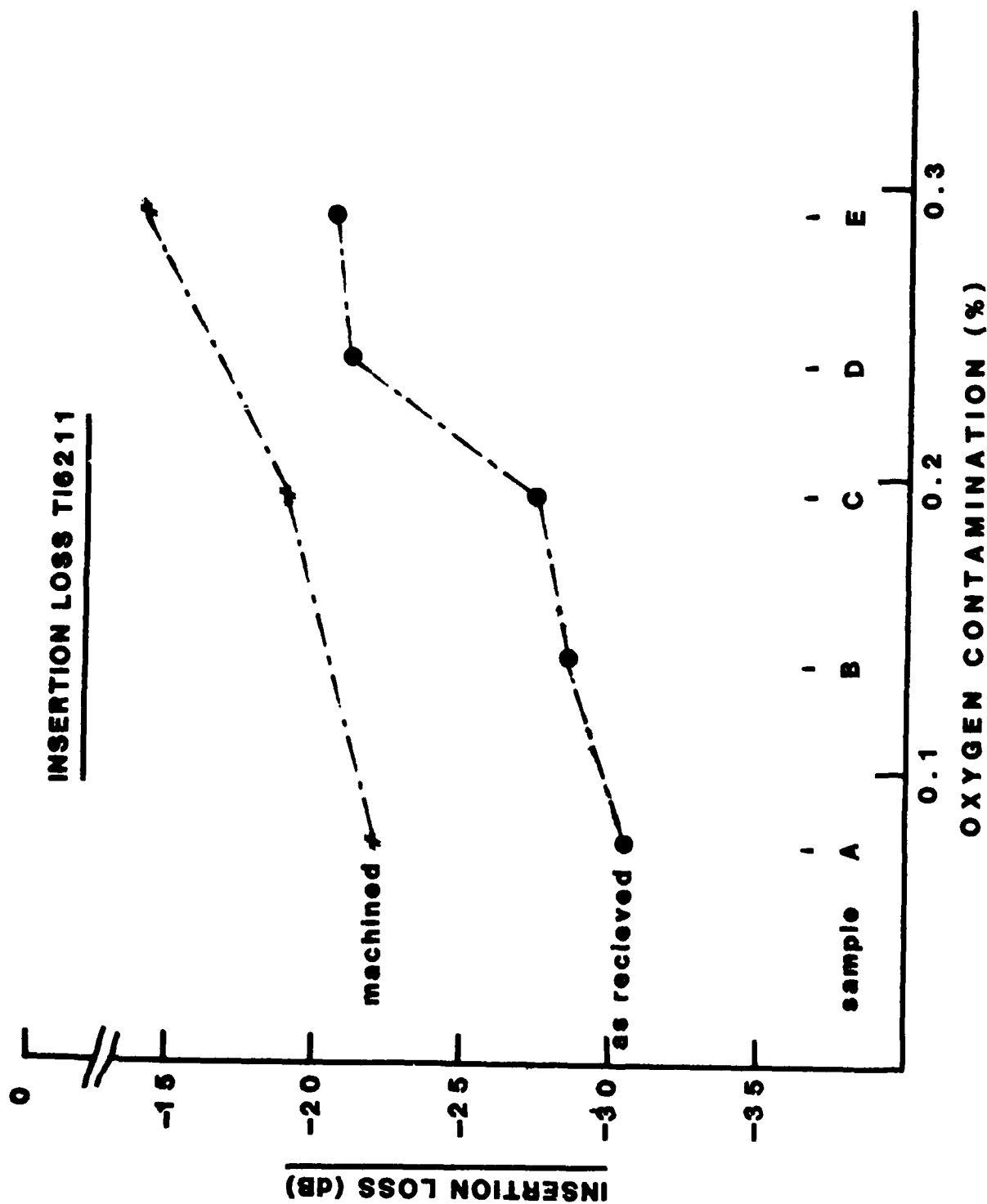


Figure 7 Average insertion loss data for machined and "as received" surfaces.  
The trend toward decreased insertion loss with increasing oxygen contamination is apparent.

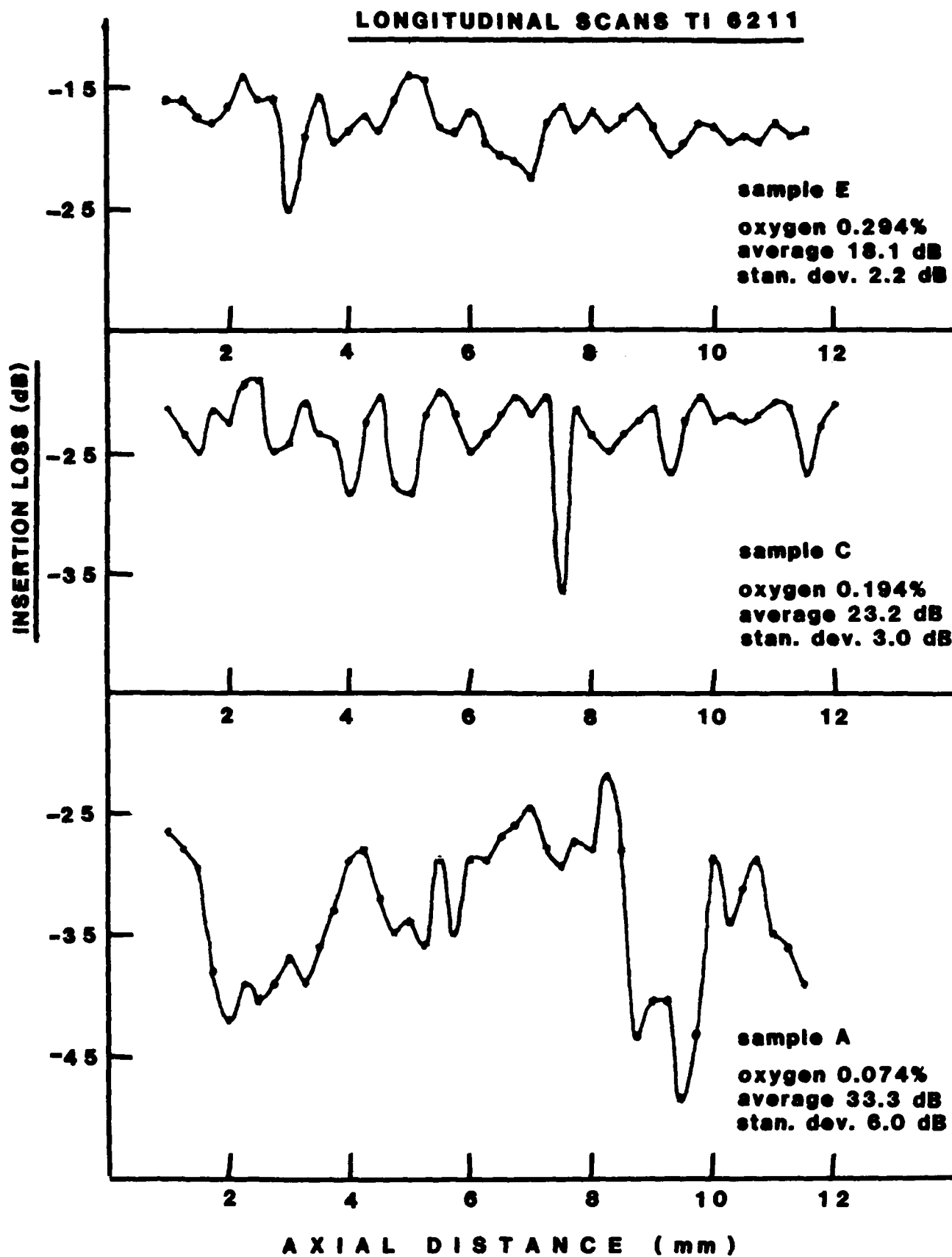


Figure 8 Acoustic line scan data comparing typical acoustic scattering characteristics of titanium 6211 samples A, C, and E.

IMAGE CONTRAST TI 62111

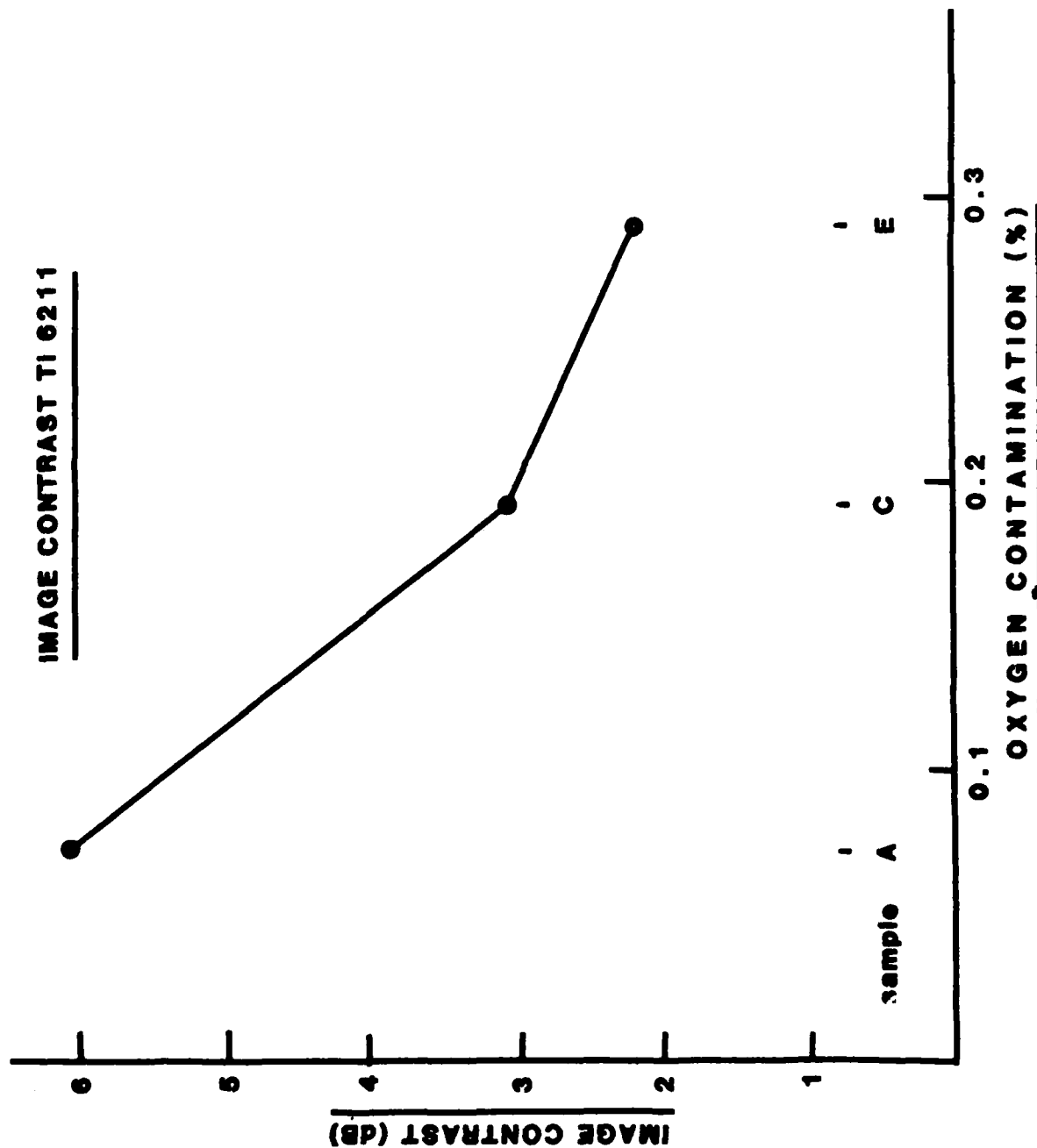


Figure 9 Image contrast data (standard deviation) of titanium 6211 as a function of oxygen contamination.

## CONCLUSION

Results presented in this report show the qualitative and quantitative variations in titanium 6211 which can be associated with gas contamination. Data on the average acoustic attenuation at 30 MHz and attenuation inhomogeneity are in agreement with results of others presented at the February, 1982 Orlando Meeting.\* Data on the average attenuation show a clear correlation with the level of gas contamination. Specifically, the average attenuation was found to decrease with the measured oxygen content. This result is similar to that reported by others at lower acoustic frequencies, although the differences are not as great, owing to the lower frequency and interference, due to phase-cancellation effects.

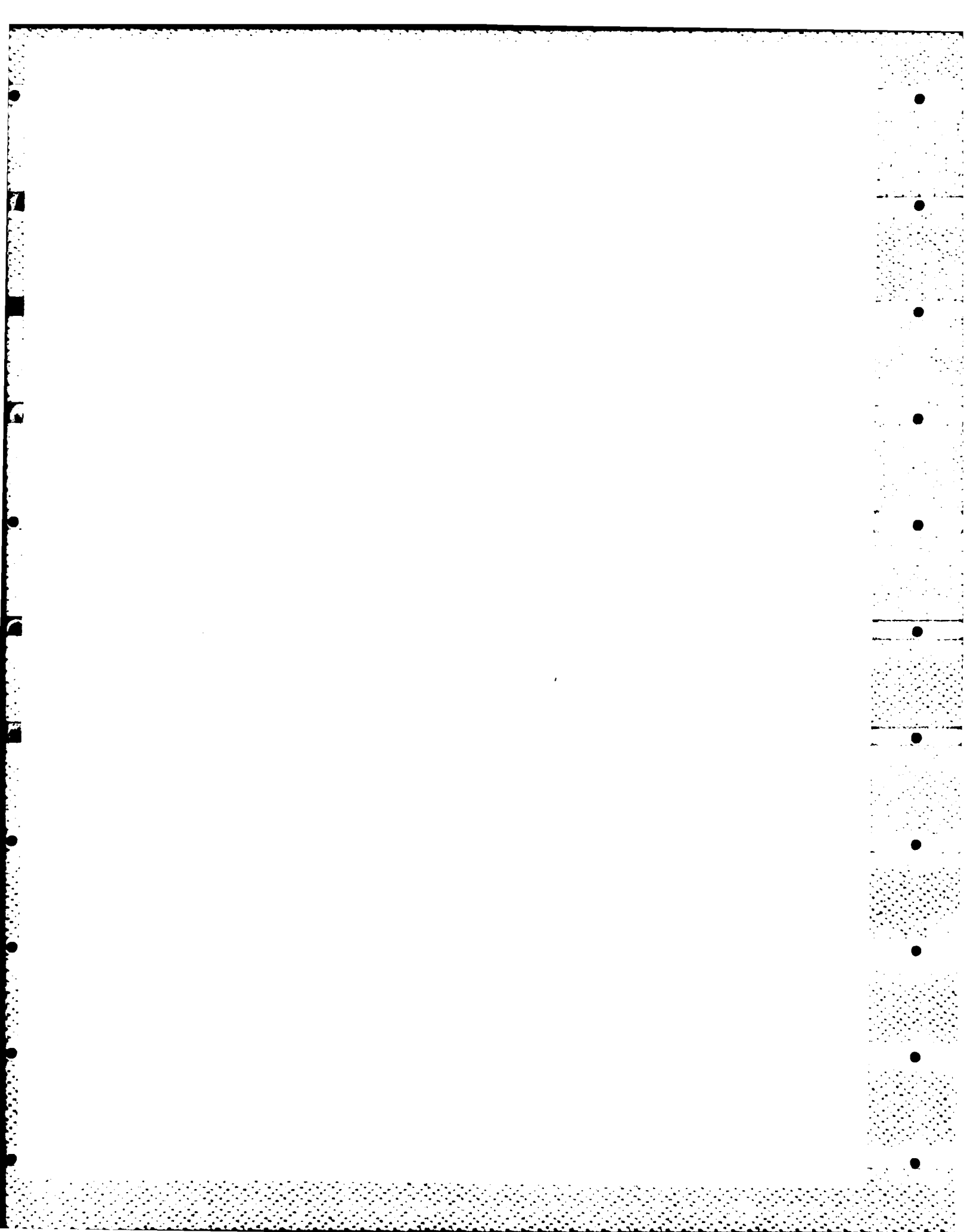
The special inhomogeneity of both the attenuation and sonic velocity (compressional) was found to decrease with the level of gas contamination. These parameters are unique to the SLAM method, e.g., high frequency imaging and, thus, are not directly comparable to the results obtained by others. These characterization parameters are important because they will be the easiest to quantify in an on line weld evaluation system.

Although clear correlation between acoustic parameters and oxygen contamination was found, a more fundamental question arises of whether the acoustic changes are the result of direct detection of the gas contamination or the microstructural changes associated with the gas contaminate.

The answer to this question has a direct bearing on the specificity of any non-destructive test. For this reason, an important next step would be the direct comparison of weld samples which contain various levels of gas contamination.

\* Workshop on "Non-destructive evaluation (NDE) of Titanium Alloys" Feb. 2-4, 1982 Orlando, Florida

**PART C**  
**ELECTROMAGNETIC TECHNIQUES**



SECTION 9  
FEASIBILITY STUDY TO DEMONSTRATE DETECTION OF LOW  
LEVELS OF OXYGEN CONTAMINANT IN TITANIUM USING  
EDDY CURRENT AND ULTRASONIC NDE TECHNIQUES

Susan N. Vernon, John M. Jamieson, and Anthony N. Mucciardi

*Adaptronics, Inc.  
1750 Old Meadow Road  
McLean, VA 22102*


An eddy current and two ultrasonic techniques were employed to establish the feasibility of detecting low levels of oxygen contaminant in 6-2-1-1 titanium plates.

The eddy current technique consisted of two probes used in a transmit/receive mode. The transmitter was stationary and generated eddy currents at driving frequencies between 250 kHz and 1 MHz. The receiver was varied in distance from the transmitter over a 0.125" to 1.0" range. It was found that the eddy current response was independent of oxygen content over the frequency and distance range considered.

One ultrasonic technique measured the ratio of longitudinal velocities at 5 MHz and 20 MHz. No strong correlation was found between the velocity ratio and oxygen content.

The second ultrasonic technique measured the ratio of the shear wave velocity to the longitudinal wave velocity at 5 MHz, where each wave traveled normal to the surface of the plate. A strong correlation was found between this velocity ratio and oxygen content.

It is concluded that the shear/longitudinal velocity is related to the oxygen content. A proposed field implementation using this technique is presented.



AD-P004 129

## 1. INTRODUCTION

The eddy current technique, applied to detect quantitatively the presence of oxygen as a bulk contaminant in titanium plates, employed two probes in a transient/receive mode, respectively. The goal was to generate a surface by varying the distance,  $d$ , between the probes on the surface of the plate and by varying the carrier frequency,  $f$ , at each value of  $d$ . The horizontal and the vertical components of the impedance plane were recorded at each value of  $f$  and  $d$ . The hypothesis was that computed features of the surface could be related to the oxygen content of the plates. Frequencies from 10 Hz through 1 MHz were examined. At frequencies of 1 kHz and below, there was no difference between the impedance value in air and in titanium, and the difference was very slight below 250 kHz. For each test block, the proposed surface was generated for frequencies from 250 kHz through 1 MHz and distances between 0.125" and 1.000". It was found that the variation in the horizontal and vertical components with distance was independent of oxygen content and of frequency, except at 3 kHz and 1 MHz where there was no variation with distance.

Two ultrasonic techniques were also tested. In the first, the time between the back-wall and front-wall reflections of a longitudinal wave was measured on each block at transducer frequencies of 5 MHz and 20 MHz. The hypothesis was that the oxygen content would have a different effect on the velocities at the two frequencies. This effect would result in a correlation between oxygen content and the ratio of the 5 MHz travel time to the 20 MHz travel time. No strong correlation was found (the correlation coefficient was 0.146).



The second ultrasonic technique was successful. A 5 MHz shear wave was launched into each block in a direction normal to the back surface. The travel time,  $T_S$ , between front- and back-wall reflections was measured and compared with the corresponding longitudinal wave travel time,  $T_L$ . Since the distance traveled by the shear wave was the same as the distance traveled by the longitudinal wave, the ratio,  $T_L/T_S$ , is equivalent to the ratio of the shear wave velocity to the longitudinal wave velocity. Because of time and cost constraints, only blocks A, B, and E had their surfaces prepared for use in the experiments. The correlation coefficient between oxygen content and the velocity ratio was 0.941. This technique should be pursued further.

## 2 EDDY CURRENT TECHNIQUE

### 2.1 OVERVIEW

The eddy current technique employed two probes in a transmit/receive mode. The goal was to generate some feature of the eddy current signal by varying the distance,  $d$ , between the probes on the surface of the plate at several different frequencies  $f$ . The horizontal and vertical components of the impedance plane recorded at each value of  $f$  and  $d$ . The hypothesis was that computed feature(s) of the eddy current response would be related to the oxygen content of the plate. The concept is illustrated in Figure 2.1.

### 2.2 EQUIPMENT

The oxygen content of the five plates is given in Table 2.1.

TABLE 2.1: OXYGEN CONTENT OF FIVE TITANIUM PLATES

<u>Plate</u>	<u>O<sub>2</sub> Weight %</u>
A	0.075
B	0.136
C	0.194
D	0.238
E	0.290

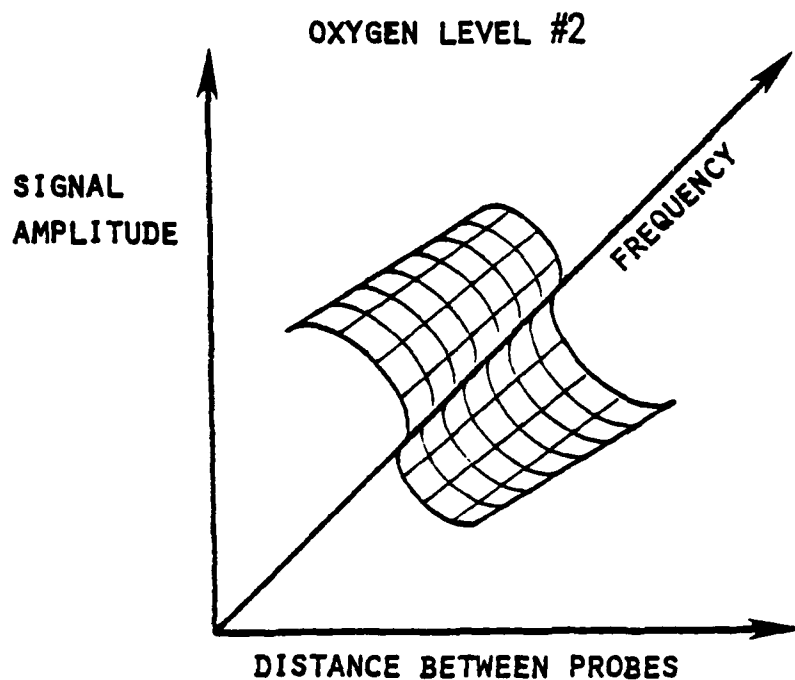
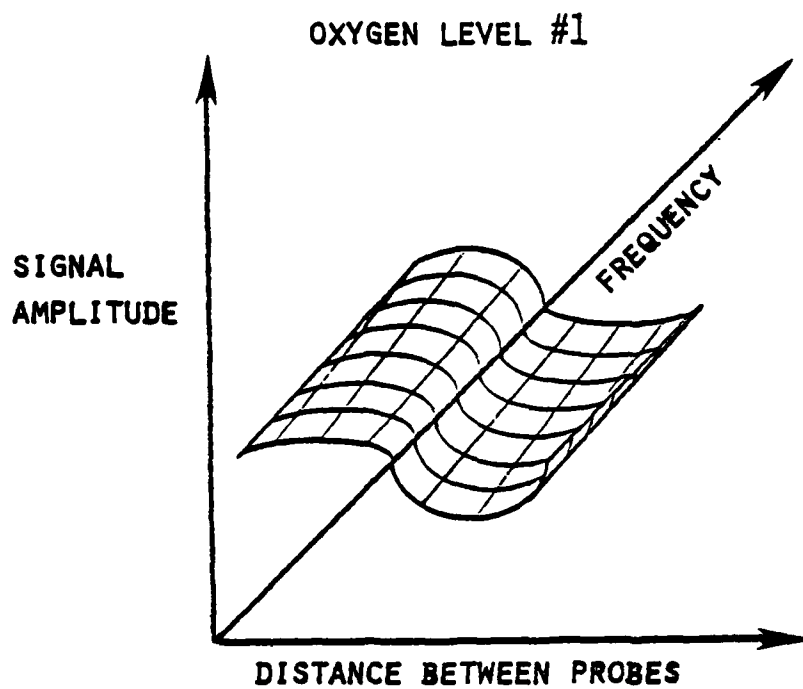


FIGURE 2.1: ILLUSTRATION OF POSSIBLE EDDY CURRENT SIGNALS WHICH MIGHT BE GENERATED BY TWO PLATES CONTAINING DIFFERENT LEVELS OF OXYGEN CONTAMINANT

A schematic of the equipment is shown in Figure 2.2 and the probe arrangement is illustrated in Figure 2.3. Two Zetec coils were used with the Aeromaster G eddy scope. An electromagnetic field was generated (transmitted) by one probe. The eddyscope was wired so that the second probe was used to measure the field generated by the first. One probe was held stationary on the plate, and the second probe was mounted on an automatic scanner which moved the probe on the surface of the plate. The distance between the probes,  $d$ , could vary from about  $1/4"$  to  $3"$ .

A stepping motor-driven scanner was used to position the probes, and the scanner was controlled by an Adaptronics ALN 4033 digital Interface/Controller.

The x- and y-channel outputs of the eddyscope were connected through a junction box to the ALN 4000 Multi Purpose Processing System.

A spatial encoder, mounted next to the stepping motor, was also connected via the junction box to the ALN 4000. The encoder triggered the ALN 4000 to record analog data at a spatial frequency of 500 points per inch.

The analog data were digitized by the ALN 4000 and recorded on a cassette tape. The x- and y-channels of digitized data were also displayed on the oscilloscope connected to the ALN 4000. After completion of the data collection, the digitized data were transferred to a Data General Eclipse AP/130 computer for further analysis.

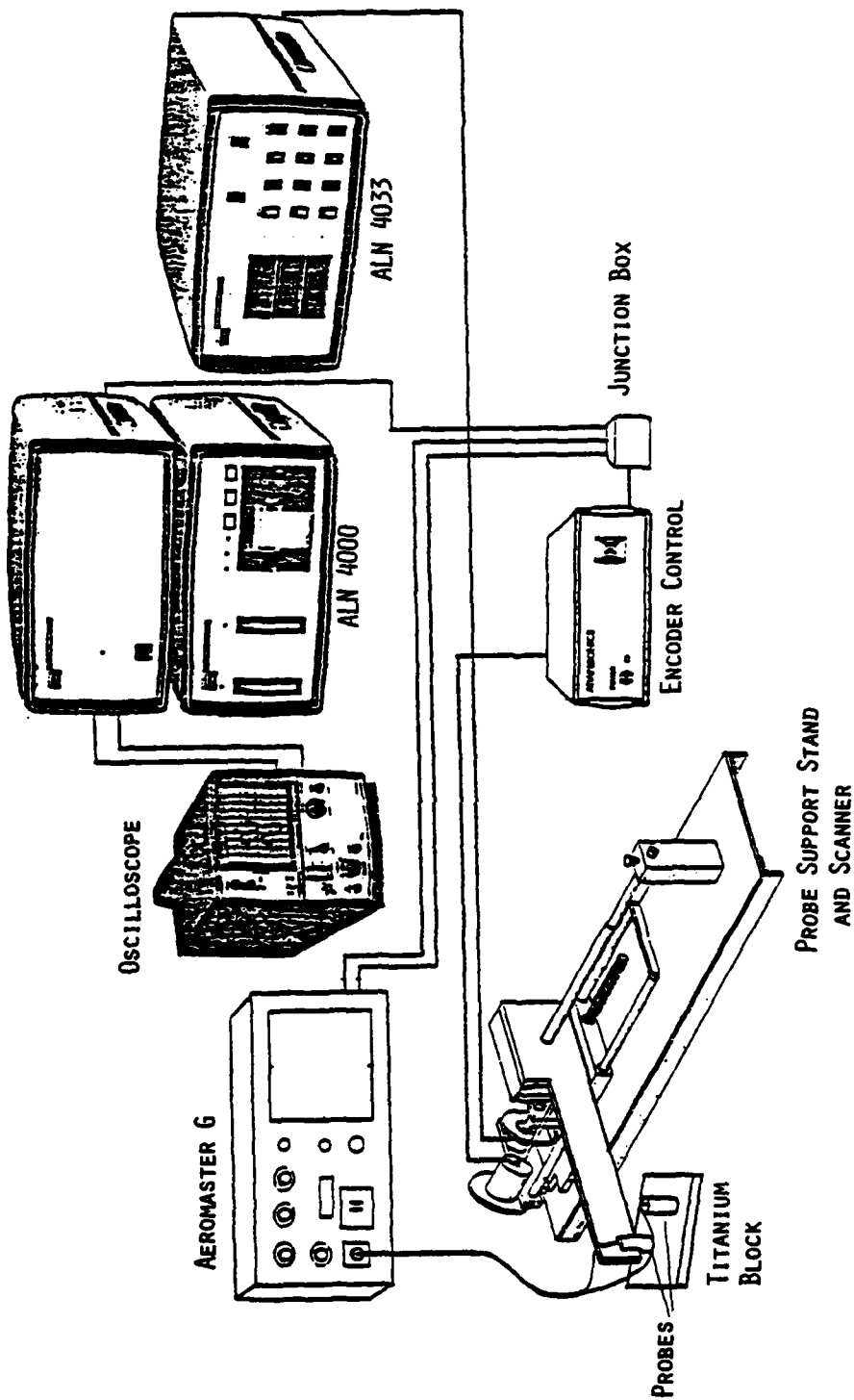


FIGURE 2.2: SCHEMATIC OF THE PROBE MOUNT, SCANNER, AND ASSOCIATED CONTROL AND DATA COLLECTION EQUIPMENT

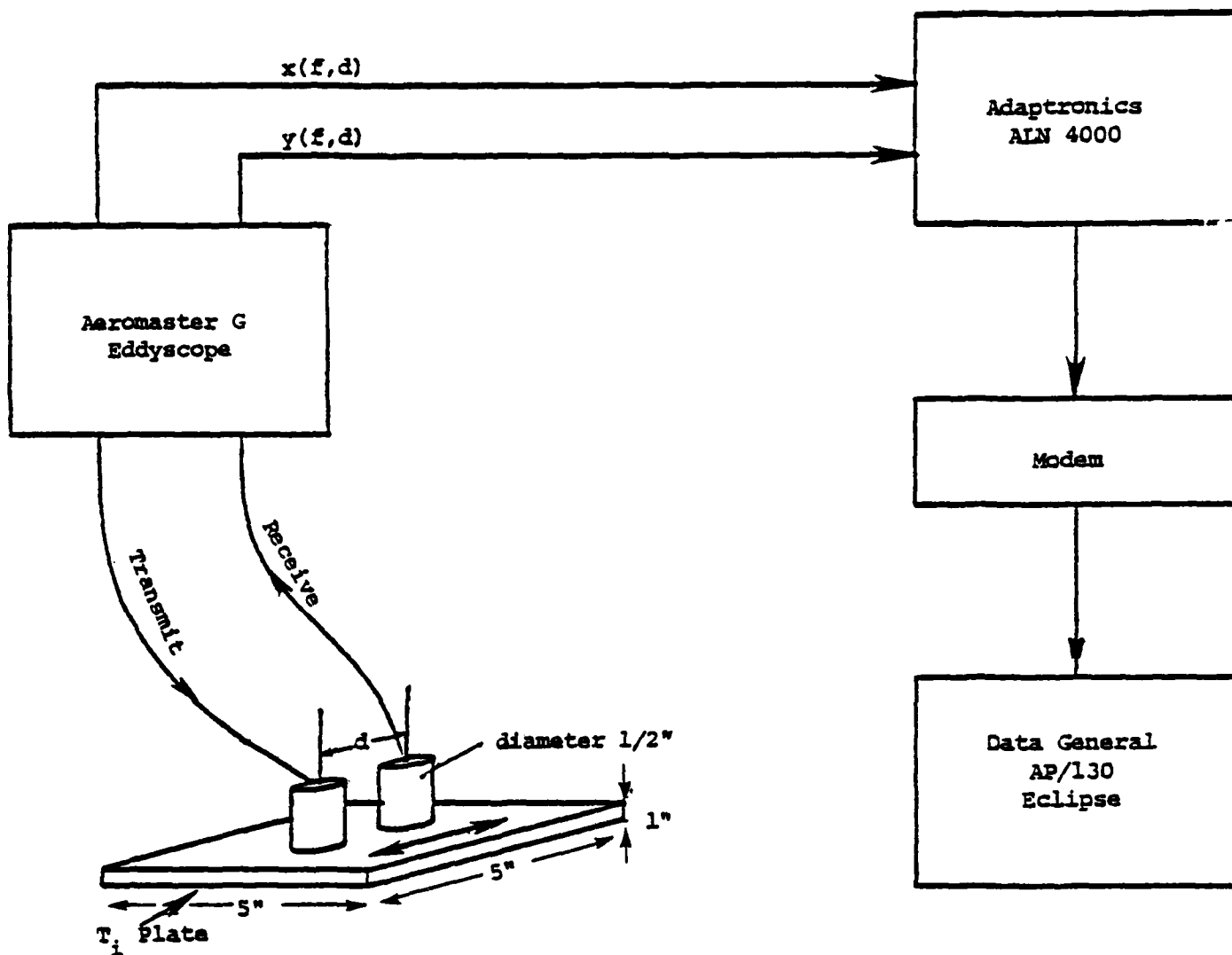


FIGURE 2.3: EXPERIMENTAL EQUIPMENT FOR RECORDING AND ARCHIVAL STORAGE OF TITANIUM ALLOY EC SIGNALS

The transmit probe can be varied in frequency,  $f$ .  
 The receive probe can be varied in  $f$  and distance,  $d$ .  
 The complex impedance is recorded as a function of  $f$  and  $d$ .

### 2.3 EXPERIMENTAL PROCEDURE

As a first step, it was decided to examine only the two plates (A and E) which represented the boundary amounts of oxygen (.075% and 0.29%, respectively). One large surface of each of these plates was machined smooth. To determine the frequencies which might yield meaningful information, frequencies from 10 Hz through 1 MHz were examined with suitable coils. At frequencies of 1 kHz and below, titanium made negligible contributions to either the amplitude or phase of the received signal.

At 3 kHz through 100 kHz, there was a difference between the signals in air and in titanium; however, there was no measurable difference in the values from plates A and E, nor was there a variation with distance between the probes for either plate. At 3 kHz, the skin depth (distance beneath the surface at which the eddy current density is 37% of the density at the surface) is 0.270" in commercially pure titanium and 0.473" in titanium-6-2-1-1.

At frequencies between 250 kHz and 1 MHz, inclusive, the difference between the air and metal indications were larger, and the values varied with distance up to about a one-inch separation between the probes. Consequently, data were collected over a distance between the coils varying from the minimum of about 1/4-inch up to 1 1/4-inch, at frequencies of 250 kHz, 500 kHz, and 1 MHz.

To determine the effect of surface roughness, data were also collected on the rough surface of plate E.

## 2.4 RESULTS

The relative received signal was found to depend on the distance between the probes but to be independent of both oxygen content and frequency. The surface roughness of the unmachined surface of plate E only increased the noise level; it did not affect the average signal values.

The results are illustrated in the x-channel, y channel, amplitude, and phase waveforms shown in Figures 2.4 through 2.7. The 250 kHz data from the machined surface of plate A and two sets of data from the unmachined surface of plate E are superimposed in Figure 2.4. The 500 kHz data from the machined surface of plate A, the machined surface of plate E, and the unmachined surface of plate E are superimposed in Figure 2.5. The corresponding 1 MHz data are superimposed in Figure 2.6. The superimposition of all the data at the three frequencies is shown in Figure 2.7. Schematics of the types of surfaces generated are shown in Figure 2.8.

## 2.5 CONCLUSIONS

Within the limitations imposed by coil and equipment sensitivities, the eddy current technique investigated would not be adequate to discriminate among titanium plates having oxygen contents of 0.075% and 0.29%, the extremes of the samples investigated.

The variation of signal amplitude with distance between the probes would be expected to be more sensitive to discontinuities in a material than to varia-



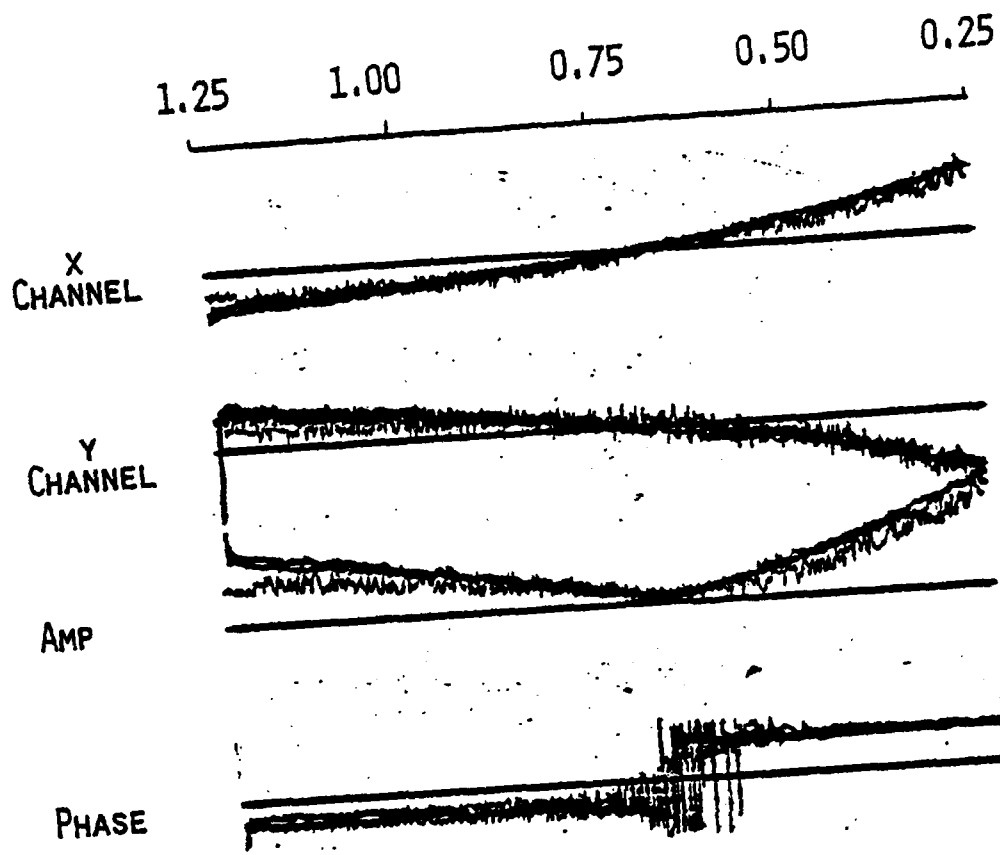


FIGURE 2.4: SUPERIMPOSITION OF 250 kHz DATA FROM MACHINED PLATE A, AND 2 SETS OF 250 kHz DATA FROM UNMACHINED PLATE E

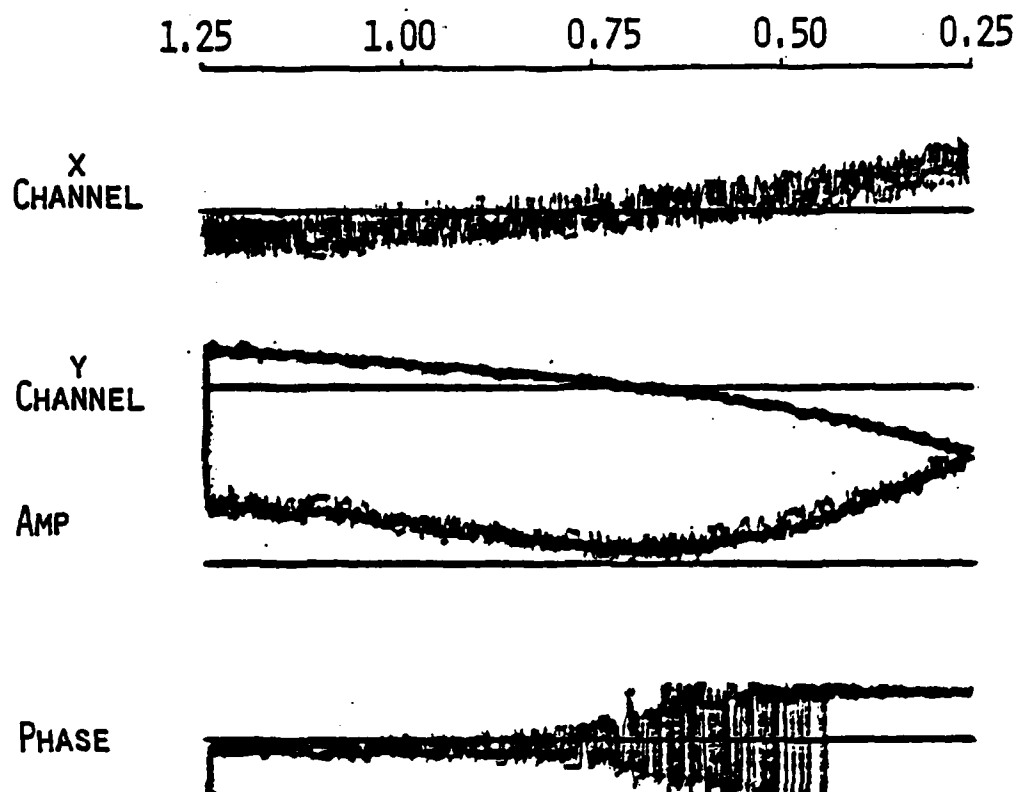


FIGURE 2.5: SUPERIMPOSITION OF 500 kHz DATA FROM MACHINED  
PLATE A, POLISHED PLATE E AND UNMACHINED PLATE E

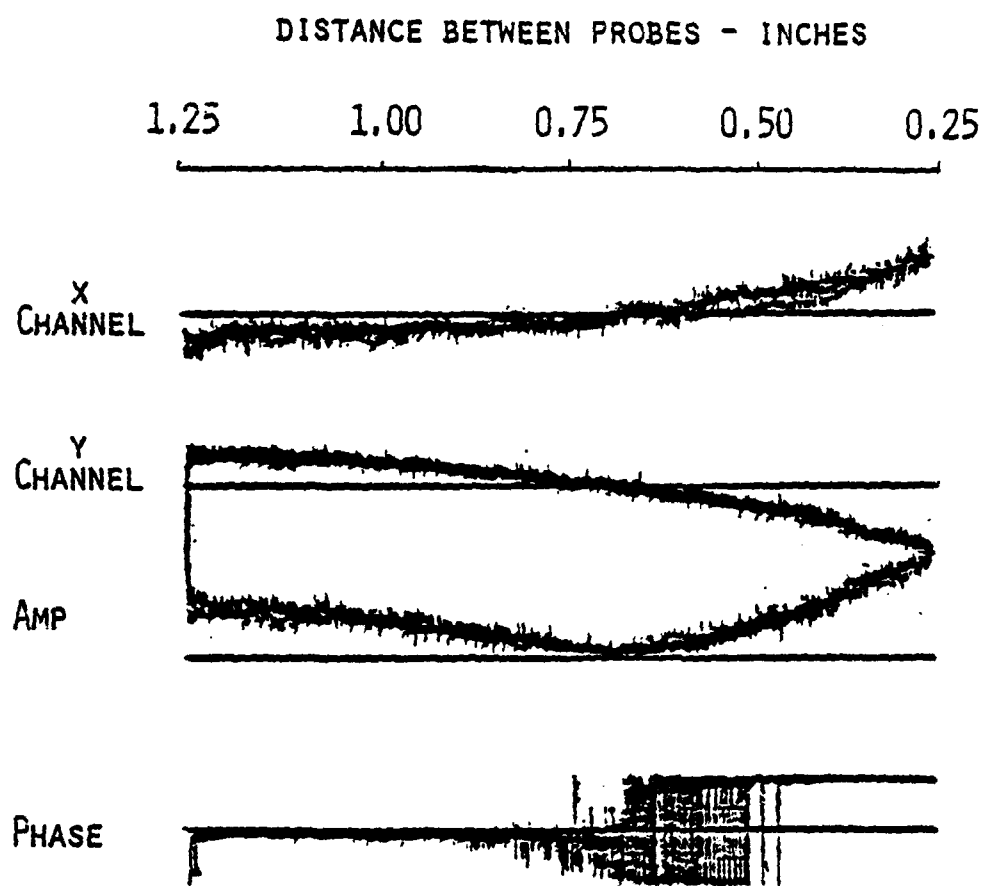


FIGURE 2.6: SUPERIMPOSITION OF 1000 KHz DATA FROM MACHINED  
PLATE A, POLISHED PLATE E AND UNMACHINED PLATE E

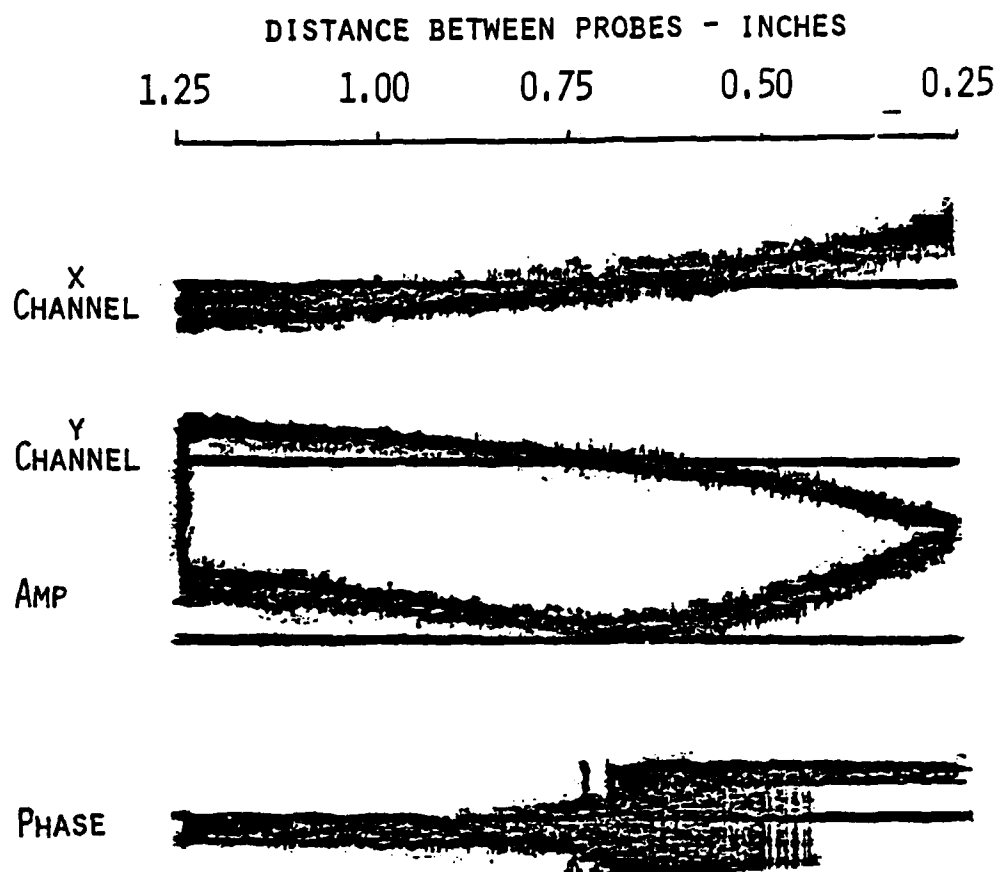


FIGURE 2.7: SUPERIMPOSITION OF 250 kHz, 500 kHz and 1000 kHz  
DATA FROM PLATES A AND E

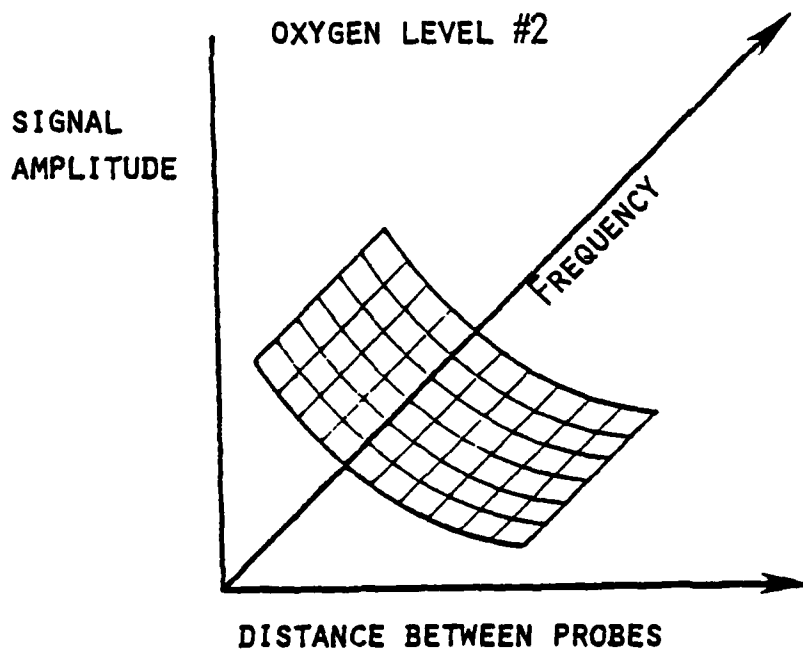
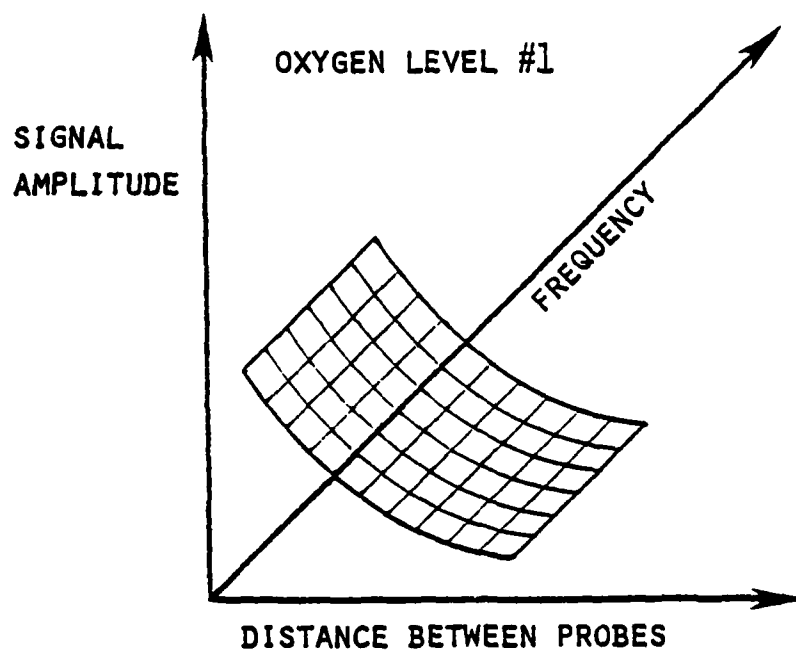


FIGURE 2.8: ILLUSTRATION OF THE SURFACES ACTUALLY GENERATED. THE SHAPES OF THE SURFACES ARE INDEPENDENT OF OXYGEN CONTENT.

tions in bulk properties of the material. Since the oxygen is uniformly distributed in the material, it would be expected to affect the bulk properties. Consequently, this technique would not be sensitive to varying levels of oxygen.

It is possible that a coil could be developed which would be sensitive to small variations in material conductivity. If these small differences in oxygen content affect the conductivity of titanium, it might be worthwhile to direct efforts toward the development of such a coil.

### 3. ULTRASONIC TECHNIQUES

Two ultrasonic techniques were also tested. The results of the first served to eliminate another technique from the list of possible solutions to the oxygen detection problem. The second is considered worthy of further investigation.

#### 3.1 COMPARISON OF THE EFFECT OF OXYGEN CONTENT ON THE RATIO OF 5 MHZ AND 20 MHZ LONGITUDINAL WAVE VELOCITIES

The first technique was based on the hypothesis that the velocities in titanium of a 5 MHz ultrasonic wave and a 20 MHz wave would be affected differently by the oxygen content of the titanium.

##### 3.1.1 Equipment

K-B Aerotech wideband transducers were used in conjunction with a Panametrics pulser/ receiver. The output of the pulser/receiver was connected to the ALN 4000 Multi Purpose Processor System where it was digitized at a 20-MHz rate and stored on cassette tape. As with the eddy current data, the digitized data were transferred to the Data General computer for further analysis.

##### 3.1.2 Experimental Procedure

The transducers were coupled with a liquid couplant directly to the titanium plates, so that the longitudinal wave travel time between the front and back surfaces could be measured. This arrangement is illustrated in Figure 3.1. To maintain a constant travel distance, the 5 MHz transducer and the 20 MHz transducer were placed alternately on the same spot on a given plate. Since

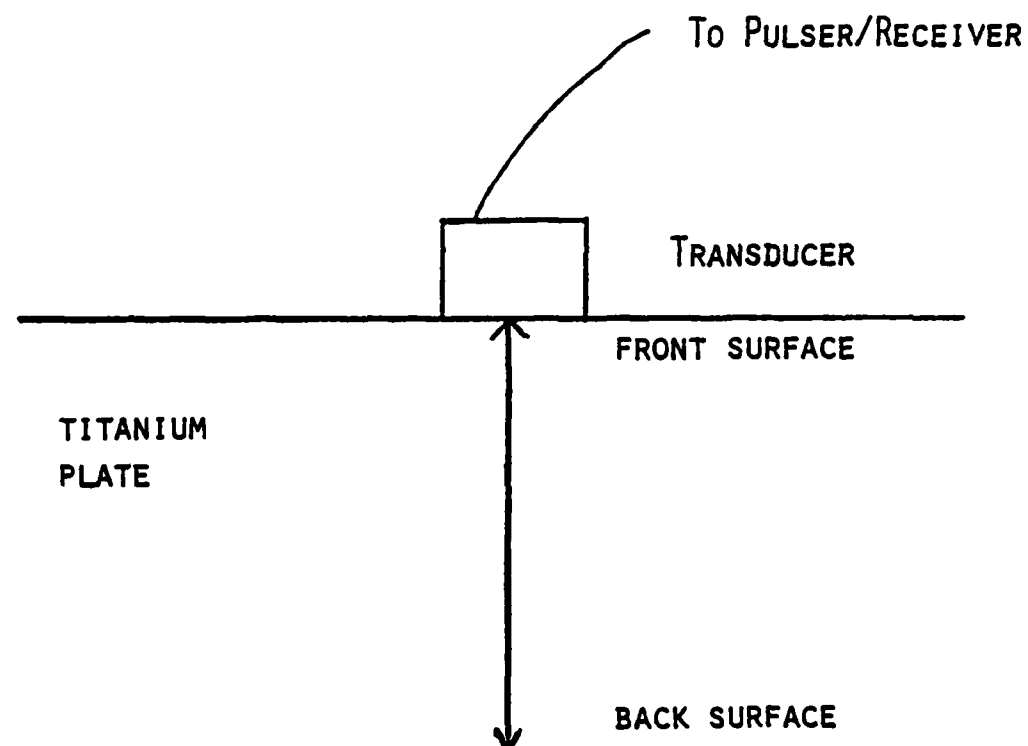


FIGURE 3.1: ILLUSTRATION OF SOURCES OF REFLECTIONS OF 5 MHz and 20 MHz LONGITUDINAL WAVES IN TITANIUM PLATES



the distance was constant, the travel time was inversely proportional to the velocity. Data collection started after 5  $\mu$ seconds and 2048 points (102.4  $\mu$ seconds) of data were collected. Typical waveforms are shown in Figure 3.2. Figure 3.2(a) shows the 20 MHz signal from plate E and Figure 3.2(b) shows the 5 MHz signal from plate E. Aliasing of the 20-MHz returns contributed to the weaker surface reflections in the high-frequency signals. However, the times between reflections were easily measured.

The ratios of the 5 MHz travel time to the 20 MHz travel time (or the ratio of the 20 MHz wave velocity to the 5 MHz wave velocity) for each plate were compared with the oxygen content of the plate.

### 3.1.3 Result

No correlation was found between oxygen content and velocity ratios.

## 3.2 COMPARISON OF THE EFFECT OF OXYGEN CONTENT ON THE RATIO OF THE SHEAR WAVE VELOCITY TO THE LONGITUDINAL WAVE VELOCITY

This approach was based on the hypothesis that the oxygen content in titanium would have a different effect on the shear wave velocity than on the longitudinal wave velocity.

### 3.2.1 Equipment

The experimental setup was the same as described in Section 3.1 above. An exception was the transducer shoe, wedge, and coupling arrangement (Figure 3.3) required to launch a shear wave into the titanium so that it would be reflected normally from the back surface. This was necessary to insure that

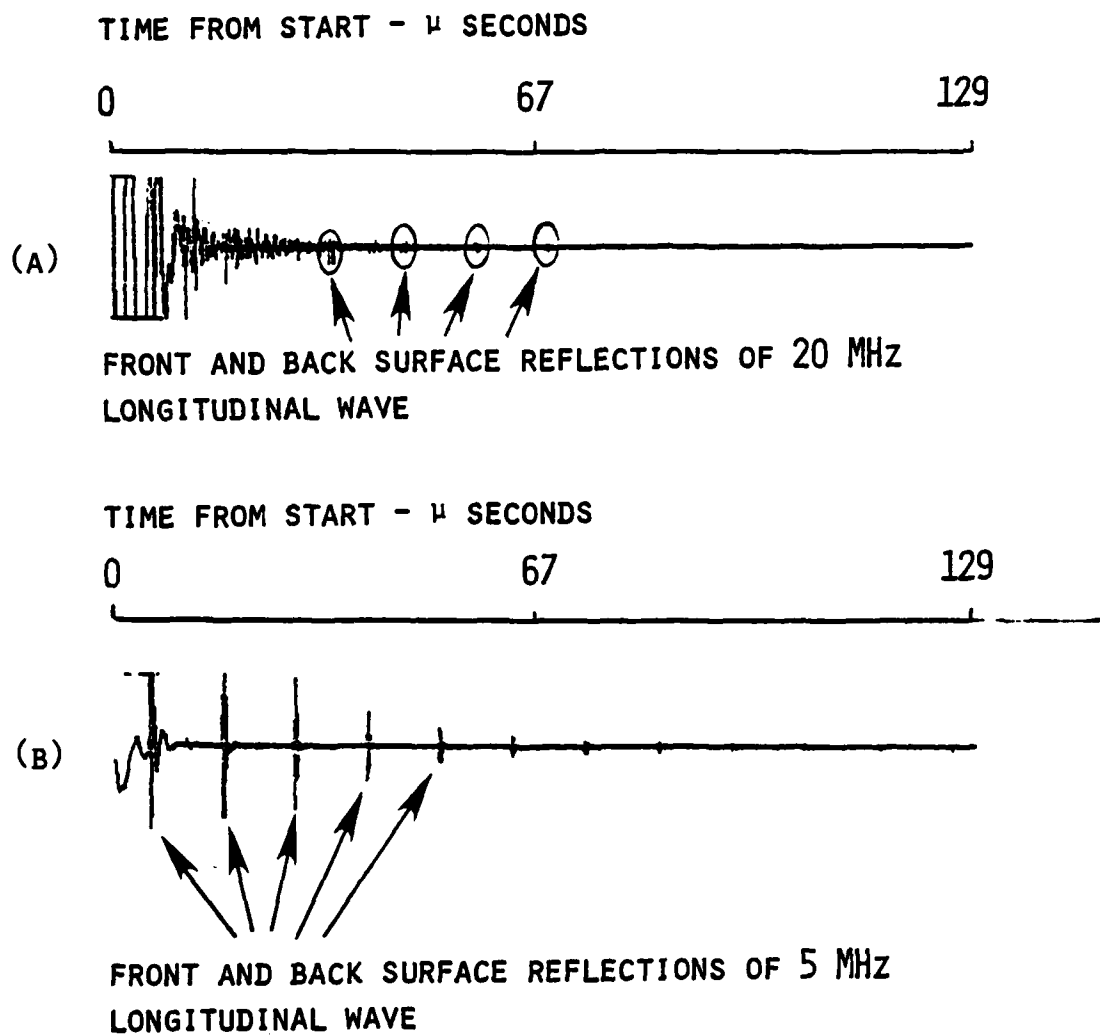


FIGURE 3.2: ULTRASONIC SIGNALS FROM PLATE E

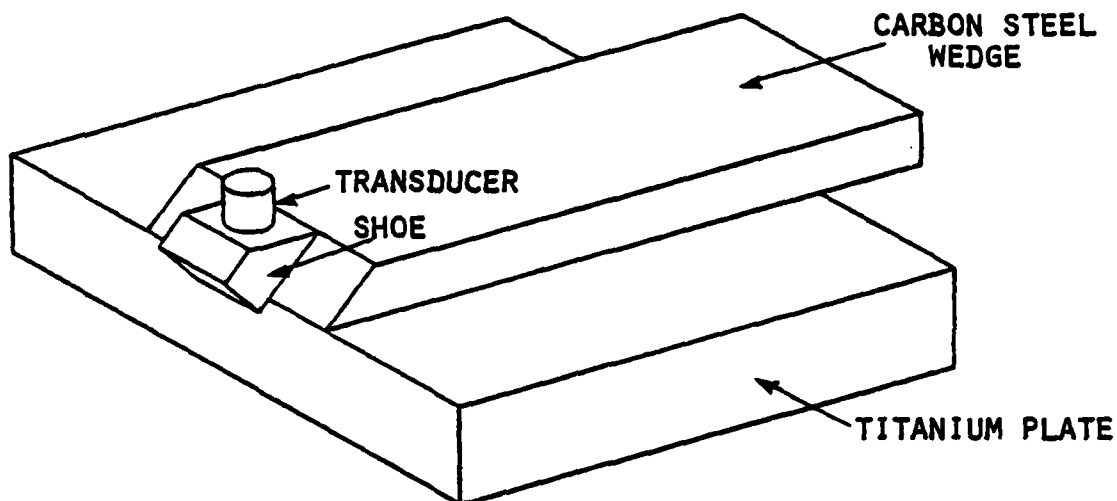


FIGURE 3.3: THE COMBINATION OF TITANIUM PLATE, CARBON STEEL WEDGE, TRANSDUCER AND SHOE USED TO LAUNCH SHEAR WAVE INTO TITANIUM PLATE

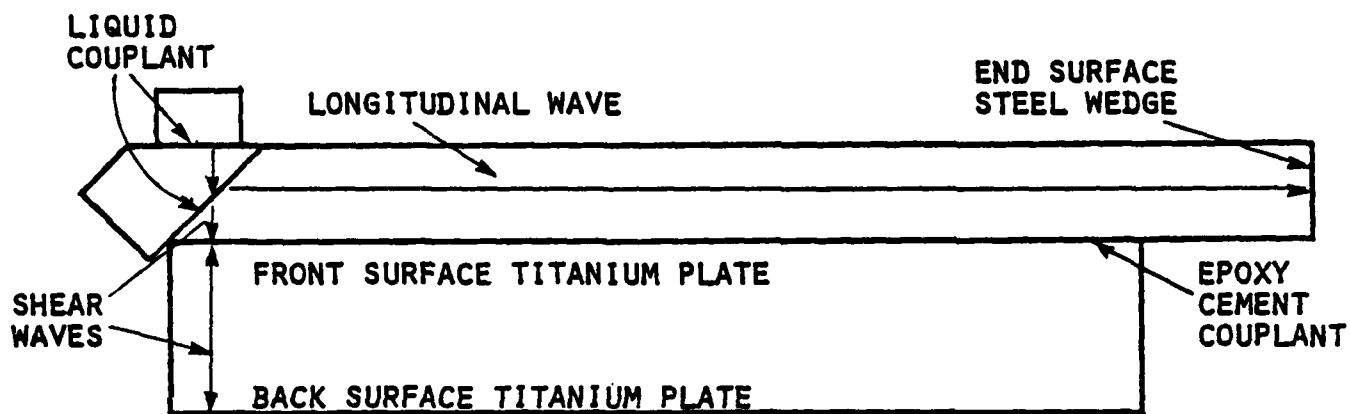


FIGURE 3.4: SCHEMATIC SHOWING DIRECTIONS OF TRAVEL OF LONGITUDINAL AND SHEAR WAVES IN THE TRANSDUCER SHOE, CARBON STEEL WEDGE AND TITANIUM PLATE

the distance traveled between front and back surfaces of the plate was the same for both the longitudinal and shear waves used in this experiment.

The longitudinal wave generated by the transducer passed through a lucite shoe and into a carbon steel 45° wedge. A liquid couplant was used between the transducer and the shoe and between the shoe and the wedge. Mode conversion took place at the lucite-steel surface, sending a shear wave in a direction normal to the carbon steel-titanium interface and a spurious longitudinal wave down the length of the steel plate (Figure 3.4).

Because a liquid will not sustain shear waves, a rigid couplant between the carbon steel wedge and the titanium was required to transmit the shear wave into the titanium. This need was met by cementing the steel wedge to the titanium plate with epoxy and allowing it to set overnight. In addition, to make good contact, the plate surface was machined. Due to approaching deadlines, only plate B was machined to give a third data point. (Plate B was selected because it, like plate A, had no coalescence. Plates A and E had been machined previously for the eddy current experiment described in Section 2.)

### 3.2.2 Experimental Procedure

As with the previous UT experiment, 2048 points (102.4  $\mu$ sec) of data were collected, starting at 5  $\mu$ sec. At least two sets of shear wave data and two sets of longitudinal wave data were collected from each plate. Data from plate B, typical of the machined plate data, are shown in Figure 3.5 where the front and back surface reflections are indicated.

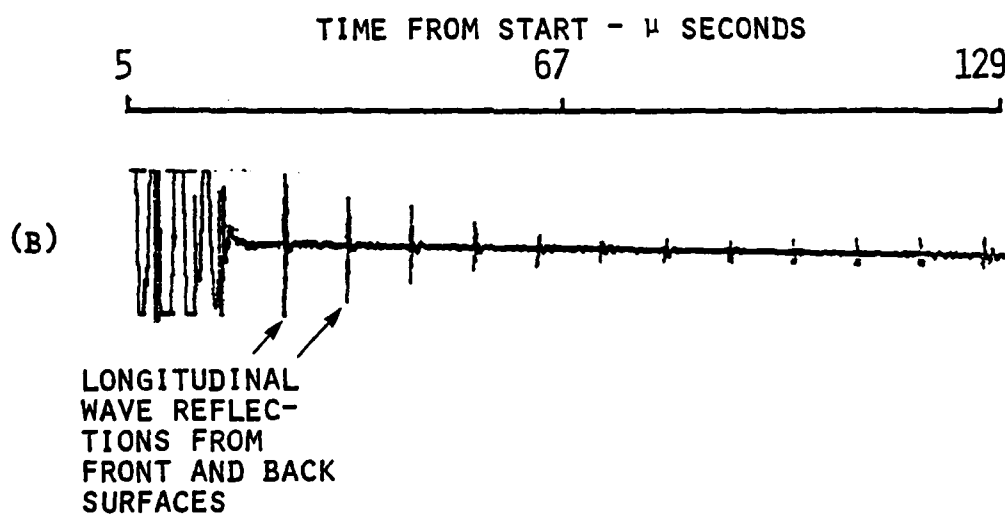
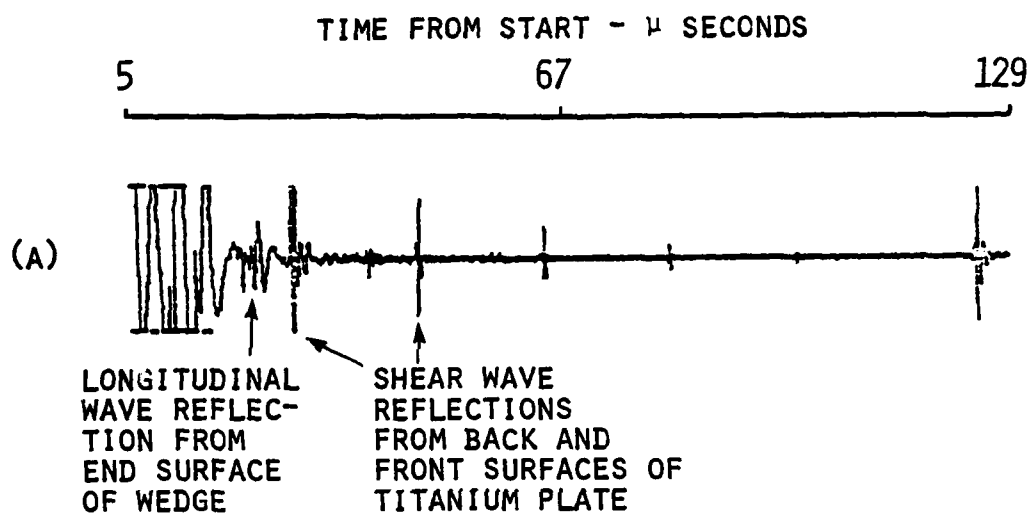


FIGURE 3.5: 5 MHz ULTRASONIC DATA FROM PLATE B

It was found that the travel times between the first two or three reflections were sometimes slightly different than the travel times between later reflections. Since the first two or three were also the stronger responses, these values were used in the calculations. The ratio of the longitudinal wave travel time to the shear wave travel time, equal to the ratio of the shear wave velocity to the longitudinal wave velocity, was compared with the oxygen content of the plates.

### 3.2.3 Results

The results are shown in Figure 3.6. The handbook values of the velocities of the two types of waves in commercial pure titanium were used to calculate the value of the ratio for .0% oxygen. There is a definite trend in the relationship between the ratio of the velocities and oxygen content as supported by the high correlation coefficient.

### 3.2.4 Conclusions

This technique is advantageous in that it is independent of both rolling direction and material thickness up to a value at which attenuation would mask the echoes of interest. In the absence of a parallel back-reflecting surface, a pitch-catch arrangement could be used.

Furthermore, there are special transducers which generate a 90° shear wave. We used the carbon steel wedge and a normal transducer because they were readily available. Epoxy cement was used as coupling because it was also expeditious and promised success in shear-wave coupling. Rubber cement and some waxes will also adequately couple shear waves between rigid materials.

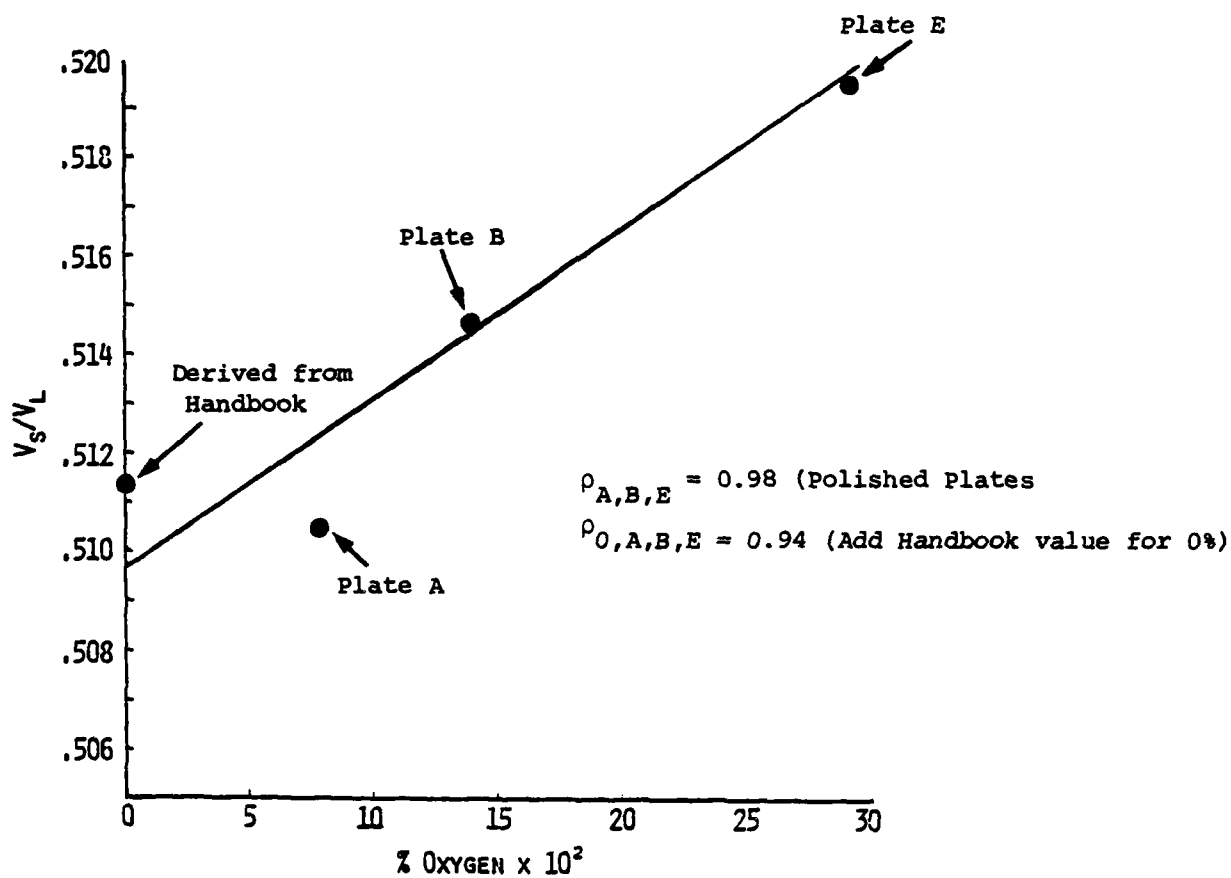


FIGURE 3.6:  $\frac{V_S}{V_L}$  VS. PERCENT OXYGEN CONTENT IN TITANIUM PLATES

This could be a quick and simple method for measuring the level of oxygen content in titanium. The equipment would consist of: (1) a probe containing both shear wave and longitudinal wave transducers and, (2) a portable pulser/receiver combined with a signal processing unit which would calculate wave velocity ratios and relate them to oxygen content.

The application of this proposed field equipment is illustrated in Figure 3.7. Figure 3.7(a) shows the travel paths of the two types of waves when the front and back surfaces are parallel. Because the travel distance is the same for each wave, and the ratio of the travel times (or velocities) are calculated, the results are independent of plate thickness. If the configuration of the material were unknown and no back-wall response was measured, it could be assumed that front and back surfaces were not parallel. A second transducer could be moved over the surface until the back-wall response was received. Travel times of the two waves would be measured. In this case, the travel distances would not be the same, so it would be necessary to rotate the dual transducer probe 180° to reverse the paths of the two waves. Travel times would again be measured. Ratios would be calculated using the travel times for which the distances were the same. In this situation, illustrated in Figure 3.7(b), rolling direction would be a factor.



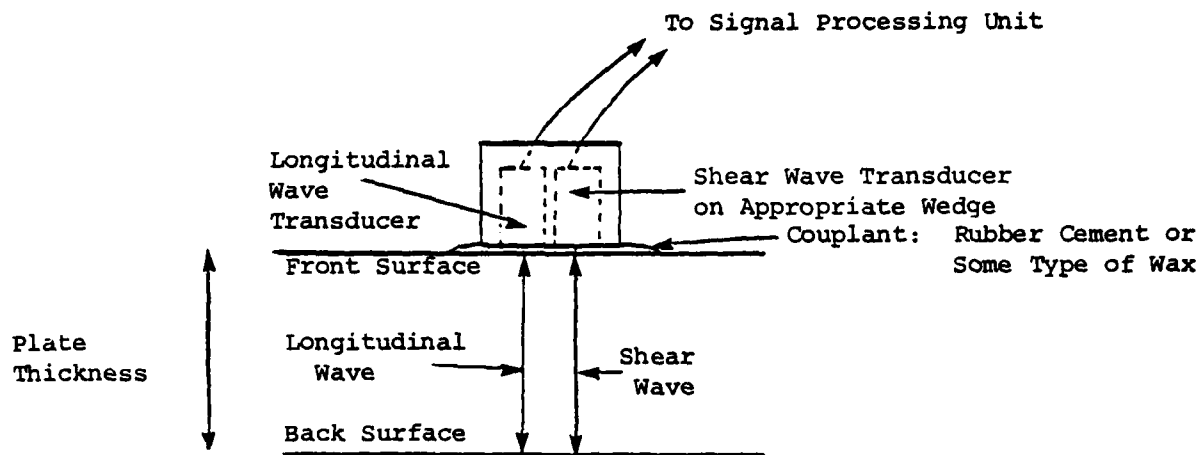


FIGURE 3.7(a) SCHEMATIC SHOWING USE OF PROBE CONTAINING BOTH A SHEAR WAVE TRANSDUCER AND A LONGITUDINAL WAVE TRANSDUCER: BACK AND FRONT SURFACES PARALLEL. Since the ratio of the wave velocities are measured, and both waves travel normal to the surface, the results are independent of plate thickness and rolling direction.

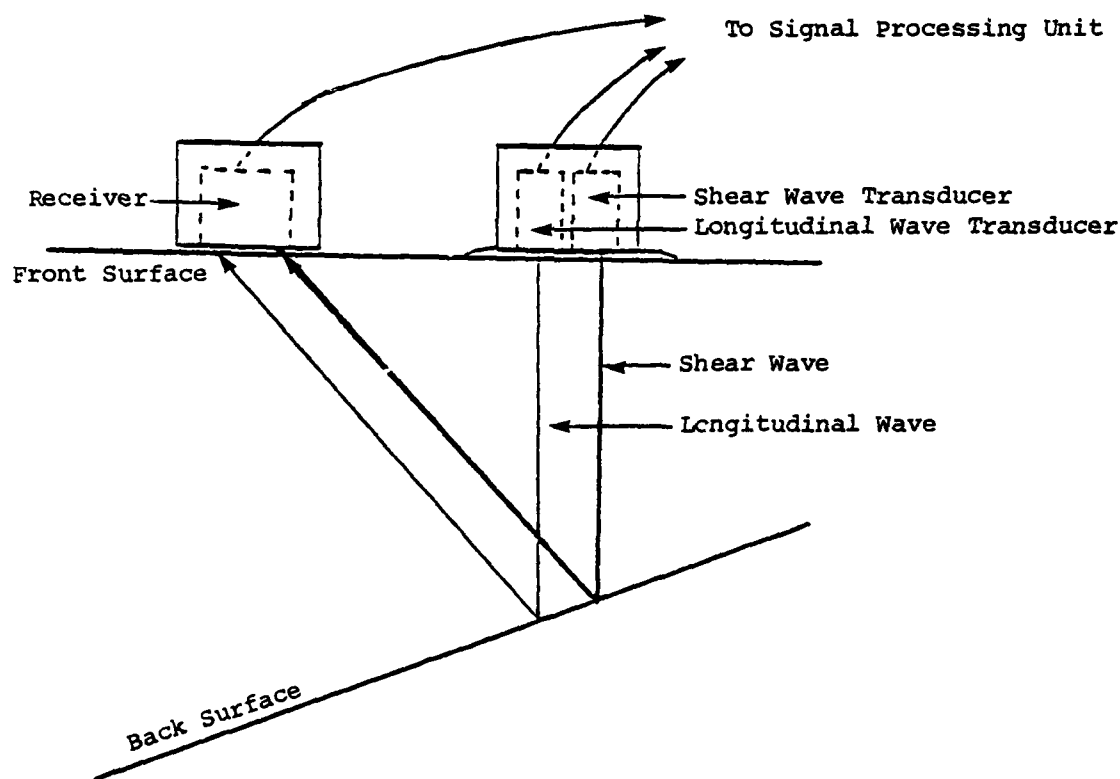


FIGURE 3.7(b) SCHEMATIC SHOWING USE OF DUAL TRANSDUCER PROBE: BACK AND FRONT SURFACES NOT PARALLEL. In this situation the back-wall reflection would not be received by the transmitting probe. A second probe consisting of a receiver would search until a signal was received. The travel times would be measured. The position of the transmitting device would be rotated 180° so the travel paths of the two waves would be reversed. Travel times would again be measured and ratios calculated using shear/longitudinal times involving the same distance.

## SECTION 10

# EVALUATION OF INTERSTITIAL GAS CONTAMINATION IN TITANIUM ALLOYS USING INDUCED MAGNETIC FIELD ANALYSIS

Kenji J. Krzywosz

*Southwest Research Institute  
San Antonio, TX 78284*

The use of induced magnetic field and the resultant material reaction from titanium alloys containing interstitial gas contamination was evaluated. This presentation discusses the material conductivity changes noted as evaluation of five titanium specimens was conducted. The oxygen contamination levels in the specimens ranged from 0.075 percent by weight to 0.290 percent by weight. A quantitative evaluation was conducted with difficulty due to inhomogeneity of contamination levels noted from some of the evaluated specimens. Consequently, an averaged signal response from the specimen surface was necessary. The averaged signal response corresponding to material conductivity changes was then correlated to various levels of oxygen contamination.

AD-P004 130

### EXECUTIVE SUMMARY

Although it was difficult to quantify the exact levels of oxygen contamination, the results of the experimental investigation conducted at Southwest Research Institute indicated that it was possible to obtain approximate levels of contamination using a nondestructive electromagnetic testing method. The contamination in the form of dissolved oxygen was introduced in Titanium-6211 alloys during the welding and forging processes.

A quantitative analysis was conducted by correlating a specific bulk material conductivity to different levels of oxygen contamination in Titanium-6211 alloys. This was accomplished first, by inducing eddy currents in the material and then monitoring the amount of reaction field generated by the induced currents. The amount of reaction field received was directly proportional to the amount of induced eddy currents. Consequently, the amount of reaction field received was correlated to variations in the material conductivity caused by the oxygen contamination.

The experimental results indicated that the material conductivity decreased with the increase in oxygen contamination levels. The intensity of reaction field received decreased accordingly with the increased oxygen contamination levels.

## II. TECHNICAL DISCUSSION

During the evaluation program, two different types of electromagnetic methods were investigated in correlating the material conductivity changes to oxygen contamination levels. This was accomplished, in both cases, by introducing ETs into the Ti-6211 specimens. The primary approach, which was originally proposed, utilized a Hall sensor to directly monitor the amount of magnetic reaction field generated by the induced ETs. The results of this investigation was highly encouraging. The second approach relied on a pulsed ET method to evaluate the duration of buildup and decay of induced ETs. The ET decay time to variations in material conductivity was correlated, however, with inconclusive results. The results obtained were not correlatable due primarily to coil heating effect which resulted in inconsistent readings of decay time. Additional investigations, we feel, are needed to fully evaluate this second approach. Consequently, the rest of the report is focused on the first method, which used the combination of ET/Hall sensor probe arrangement.

### A. Material Specimens

As mentioned previously, the Ti-6211 specimens were approximately five inches square by one inch thick. The 'as received' material surfaces were rough which was caused by the forging process. The specimens were not equal in thickness nor were the surfaces exactly flat. Some specimens had a slight curvature on one of their surfaces. To minimize the introduction of additional variables caused by the effect of rough and curved surfaces, the "as received" sample specimens were machined-finished on both sides of the square surfaces. One side was grind-finished to a smooth surface. Table 1 indicates the "as finished" average thickness obtained from five specimens. The thickness measurements were obtained ultrasonically from nine locations as indicated, using a Nova digital thickness instrument. Experimental measurements were obtained from these locations.

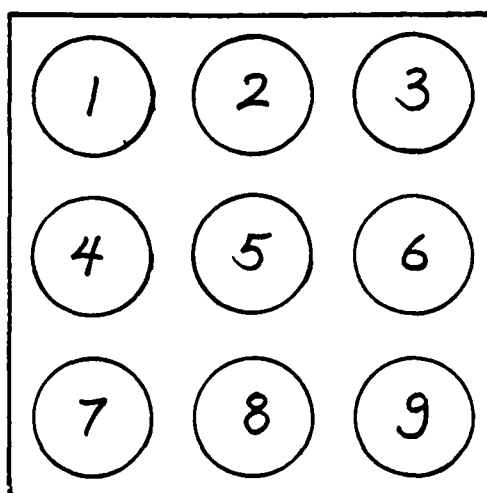
### B. Magnetic Reaction Field Analysis

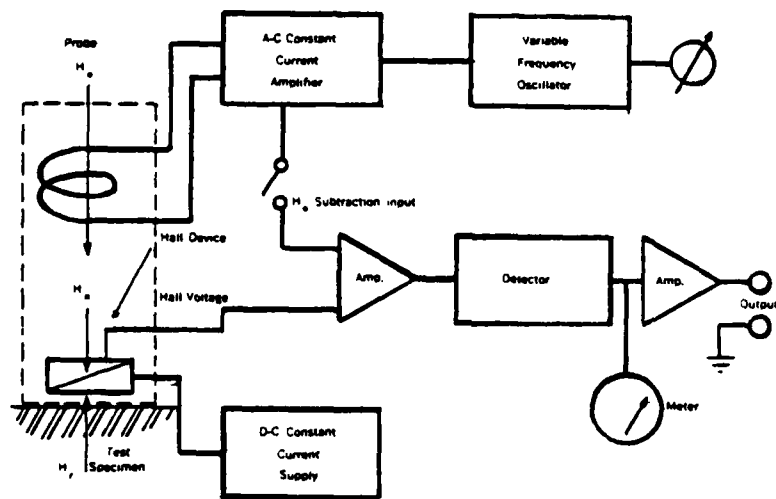
The task of analyzing the magnetic reaction field was accomplished by using a sensitive instrument called the Magnetic Reaction Analyzer. This instrument was capable of measuring both the magnetic and electrical properties of metallic materials using an operating frequency range of 10 Hz to 100 KHz. The basic schematic of the instrument is shown in Figure 1. The probe assembly, shown in Figure 2, consisted of a pancake-type ET coil encircling a Hall detection sensor. The 1-1/4-inch-diameter coil was excited by using a variable-frequency, constant-current oscillator. The oscillator provided a highly stabilized magnetizing current through an ET coil. Detection of the ET reaction field was accomplished by using a 1/4-inch diameter Hall sensor. The detection sensor measured the normal component of a magnetic field along the coil axis and perpendicular to the surface of the plate specimen. The Hall sensor output was then displayed as standardized meter readings in "magnetic reaction units." These readings represented the magnitude or vector quantity of the magnetic reaction field.

TABLE 1

Thicknesses of Ti-6211 Alloy Specimens  
used to Obtain Test Results

SPECIMEN NO.	AVERAGE THICKNESS	LOCATION OF MAX. THICKNESS	LOCATION OF MIN. THICKNESS
NRL A-3	0.843 "	(1) (4)	(3)
NRL B-3	0.850 "	(2)	(7)
NRL C-3	0.843 "	(4)	(8) (9)
NRL D-3	0.840 "	(1) (3) (6)	(5)
NRL E-3	0.852 "	(1) (4) (5) (8) (9)	(3)





BLOCK DIAGRAM MRA 1090

FIGURE 1. BASIC SCHEMATIC OF MAGNETIC REACTION ANALYZER

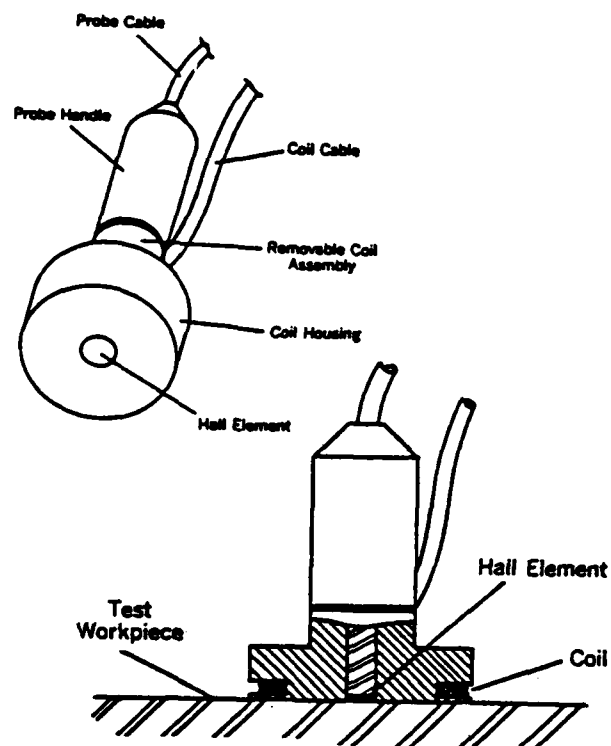


FIGURE 2. PROBE ASSEMBLY

Compared to the conventional impedance monitoring ET method, this technique was found to be more sensitive and versatile, especially in the lower frequency range. This was made possible by using a Hall detection sensor which can detect a minute change in the ET reaction field. This minute change, especially in the lower frequency range of 10 Hz to 50 KHz, would not have produced an appreciable impedance change using a conventional ET method.

C. Effect of the Operating Frequency

Basically, the ET penetration depth was inversely proportional to the operating frequency. Thus, by lowering the operating frequency, the penetration depth increased. Based on the standard depth of penetration where density of ET has decreased to 37 percent of the surface density, the penetration depth in Ti-6211 alloys ranged from 0.082 inch at 100 KHz to 1.50 inches at 0.3 KHz. Consequently, at the lower frequency range, the bulk material conductivity changes attributed either directly to the different levels of oxygen contamination or to the microstructure changes caused by the oxygen contamination can be monitored. In either case, the ET reaction field obtained at 100 KHz and below presented definite changes in the overall material conductivity as oxygen contamination levels increased.



### III. TEST RESULTS

The ET reaction field, obtained from each of the five specimens, was monitored at the excitation frequencies of 0.3 KHz, 0.5 KHz, 1 KHz, 5 KHz, 10 KHz, 50 KHz, and 100 KHz. Based on the notable variations detected within the specimen of known oxygen contamination levels, it was necessary to obtain averaged meter readings. This was accomplished by obtaining nine different readings from the face of each smoothed surface. The results of averaged "magnetic reaction units" from each of five specimens are presented in Table 2. It should be noted that the averaged value and the standard deviation presented were based on readings from nine different locations on a sample and not from nine separate readings obtained from the same location on the sample. The averaged "magnetic reaction units" of each respective frequencies were also plotted as shown in Figures 3 through 9. A definite decrease in the readings of "magnetic reaction units" was obtained as oxygen contamination levels increased. This decrease in the "magnetic reaction units" corresponded to a decrease in the material conductivity. The results obtained agreed with the finding of Arieli, Bar-Cohen, and Blas, that the material conductivity decreased as oxygen contamination levels increased (3).

Significant conductivity changes were noted within the specimen having the specified oxygen contamination levels. This suggests possible inhomogeneity of microstructure within the specimen caused by the oxygen contamination. Consequently, more than one reading per specimen was definitely needed to obtain the positive correlation between the material conductivity change and the oxygen contamination level.

According to the correlation curves presented in the figures, the best correlation was obtainable in the 5 to 10 KHz range. The correlation curves at these frequencies had the highest slope which allowed more accurate correlations to be made. The slope flattened out above and below the 5 to 10 KHz range. Unfortunately, there is a major drawback in the 5 to 10 KHz range. Specimens B and C cannot be separated because they exhibited similar material conductivities despite the difference in the oxygen contamination levels. Consequently, the next best slopes were found in the frequency range of 0.3 to 1.0 KHz. This choice was confirmed to be best when the averaged "magnetic reaction units" were normalized when using the magnetic reaction readings from specimen A. This specimen had the least amount of oxygen contamination. This step was taken to determine which frequencies brought the maximum changes in the reading between the least and most oxygen-contaminated sample specimen. The normalized results are presented in Figure 10.

TABLE 2  
AVERAGED MAGNETIC REACTION  
UNITS VS FREQUENCIES

FREQ (DEPTH)	NRL A-3	NRL B-3	NRL C-3	NRL D-3	NRL E-3
0.3 KHZ (1.50")	3.50 $\pm$ 0.13	3.48 $\pm$ 0.12	3.44 $\pm$ 0.16	3.42 $\pm$ 0.13	3.40 $\pm$ 0.14
0.5 KHZ (1.16")	5.70 $\pm$ 0.16	5.65 $\pm$ 0.17	5.62 $\pm$ 0.18	5.57 $\pm$ 0.19	5.55 $\pm$ 0.17
1.0 KHZ (0.821")	10.87 $\pm$ 0.18	10.82 $\pm$ 0.16	10.77 $\pm$ 0.25	10.67 $\pm$ 0.18	10.61 $\pm$ 0.20
5.0 KHZ (0.367")	36.01 $\pm$ 0.12	35.82 $\pm$ 0.16	35.86 $\pm$ 0.11	35.60 $\pm$ 0.14	35.48 $\pm$ 0.18
10 KHZ (0.260")	52.50 $\pm$ 0.10	52.24 $\pm$ 0.10	52.23 $\pm$ 0.10	52.07 $\pm$ 0.13	51.94 $\pm$ 0.10
50 KHZ (0.116")	83.53 $\pm$ 0.07	83.42 $\pm$ 0.12	83.32 $\pm$ 0.10	83.31 $\pm$ 0.17	83.20 $\pm$ 0.10
100 KHZ (0.082")	86.53 $\pm$ 0.12	86.53 $\pm$ 0.08	86.43 $\pm$ 0.13	86.48 $\pm$ 0.11	86.36 $\pm$ 0.10

FIGURE 3. OXYGEN CONTAMINATION LEVEL VS  
AVERAGED MAGNETIC REACTION UNITS - 0.3 KHE

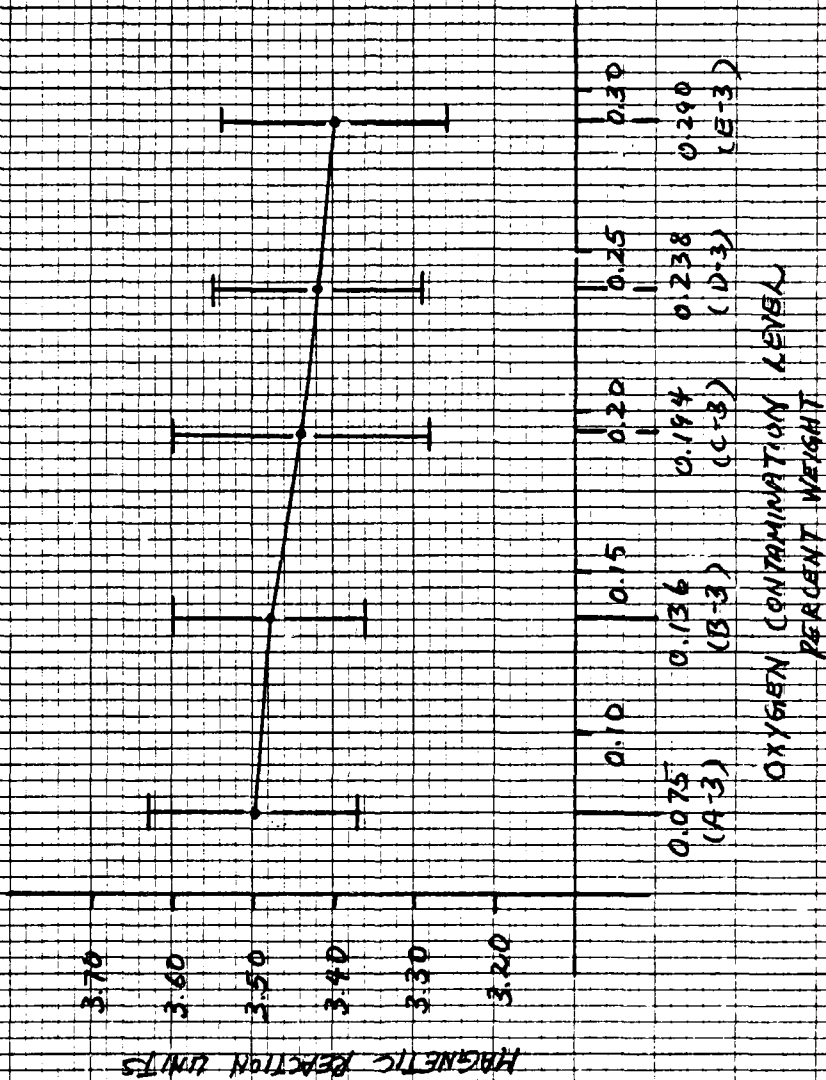


FIGURE 4. OXYGEN CONTAMINATION LEVELS VS  
AVERAGED MAGNETIC REACTION UNITS - 0.5 KHZ

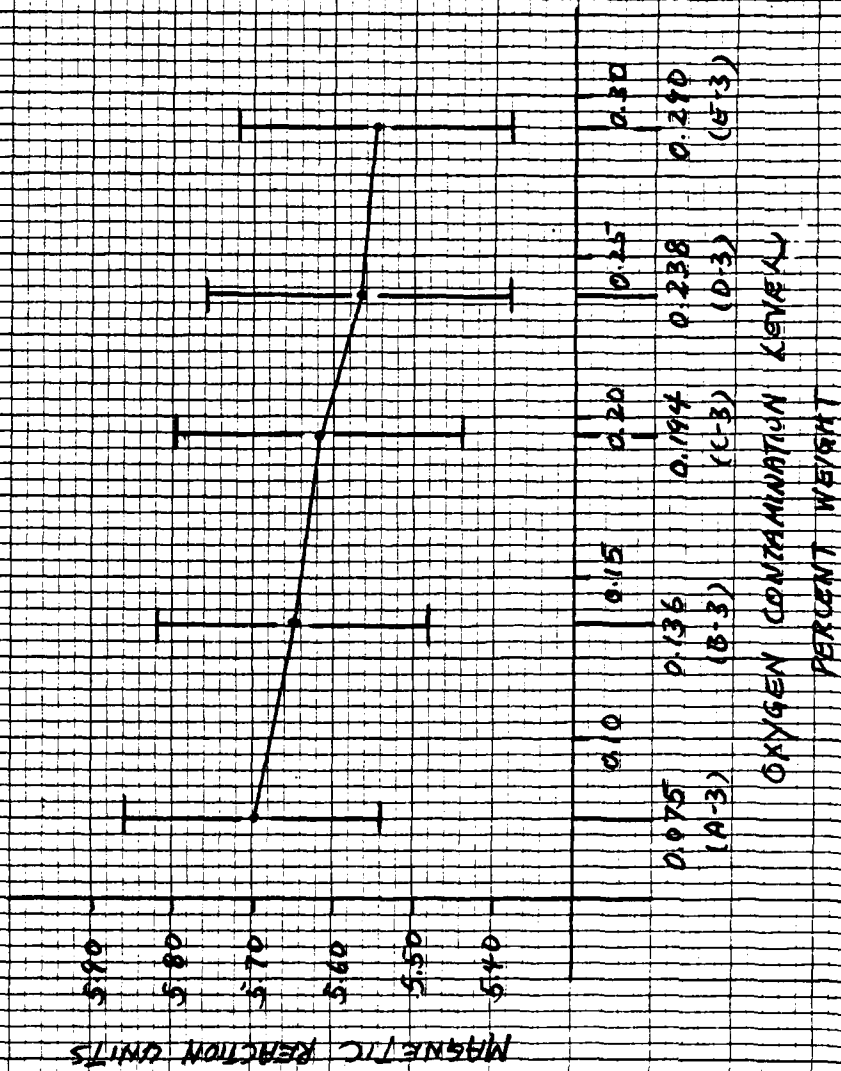


FIGURE 5. OXYGEN CONTAMINATION LEVEL VS  
AVERAGED MAGNETIC REACTION UNITS = 1.0 KHZ

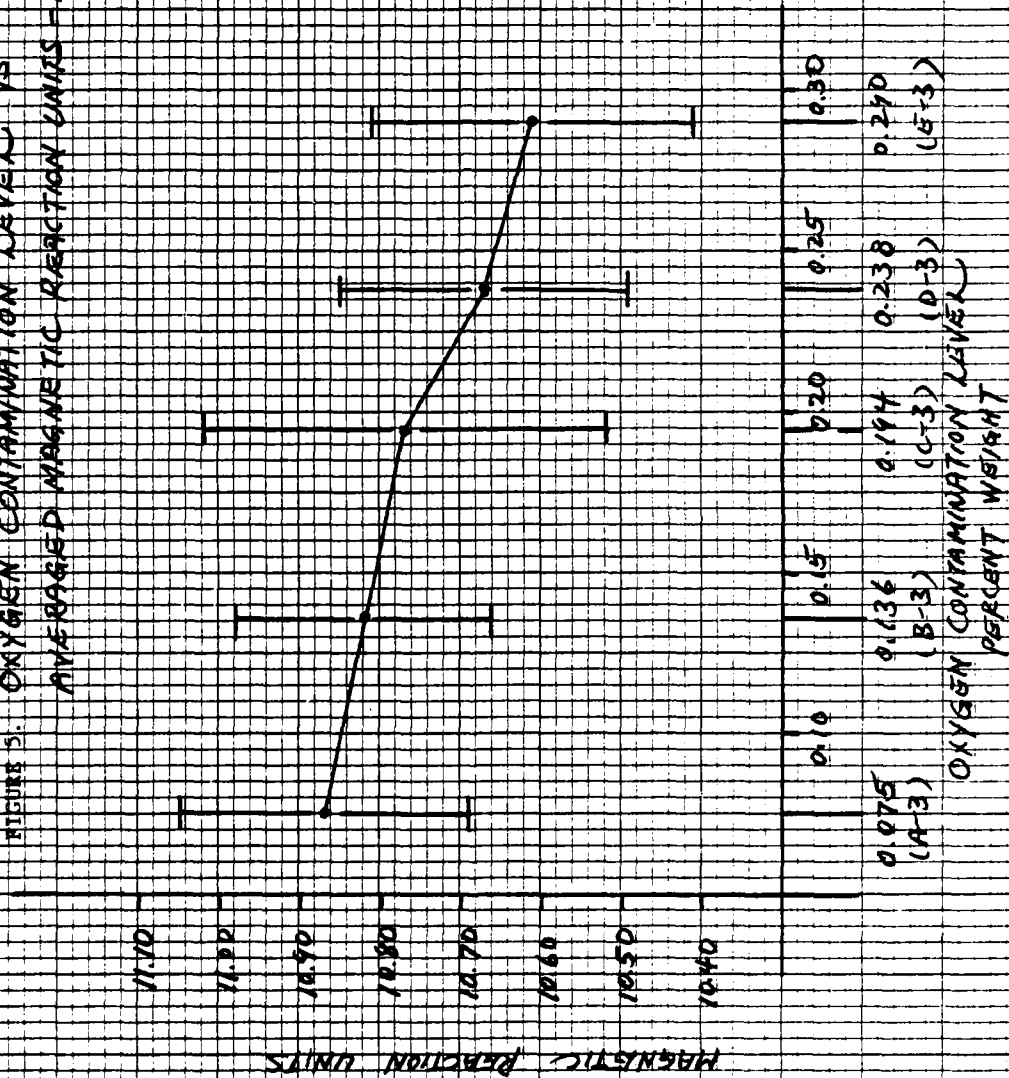
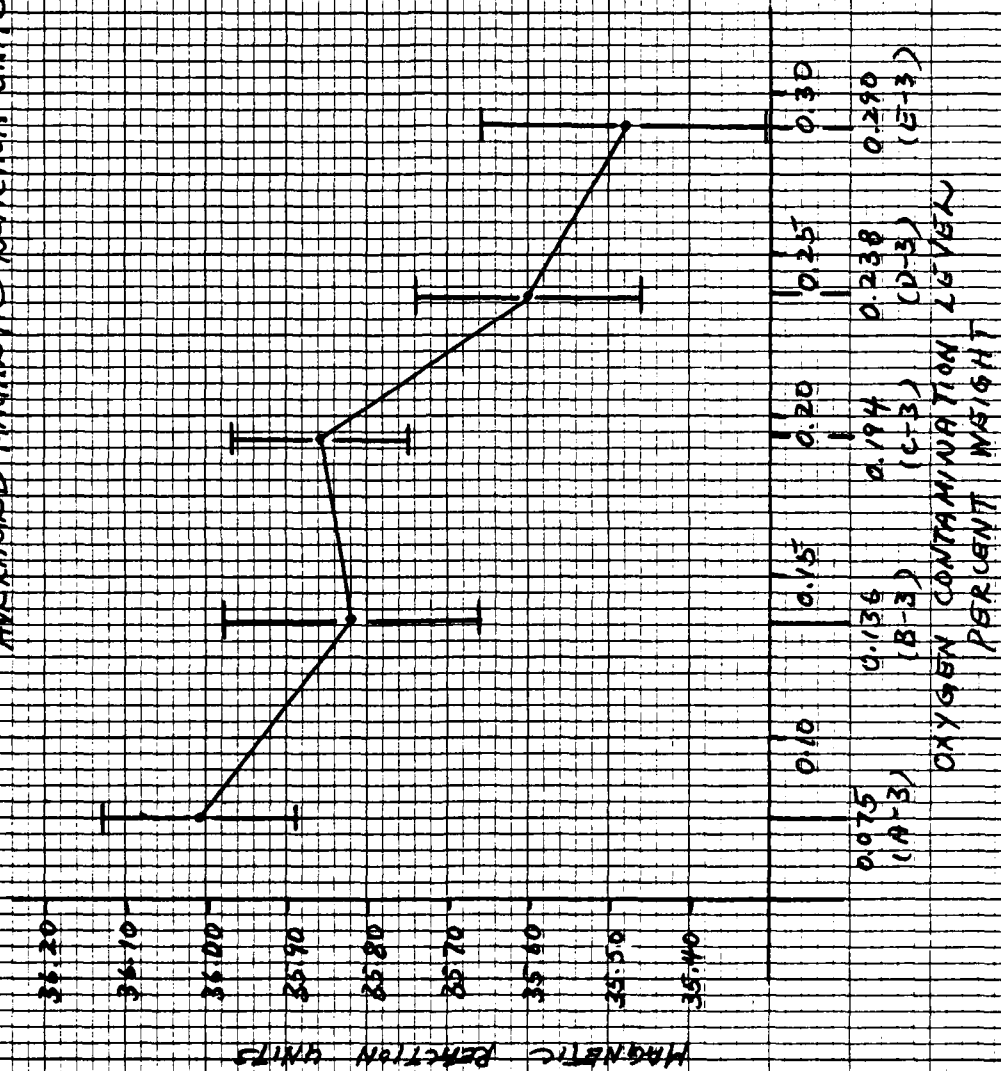


FIGURE 6. OXYGEN CONTAMINATION LEVELS VS  
AVERAGED MAGNETIC REACTION UNITS - 5.0 KHZ



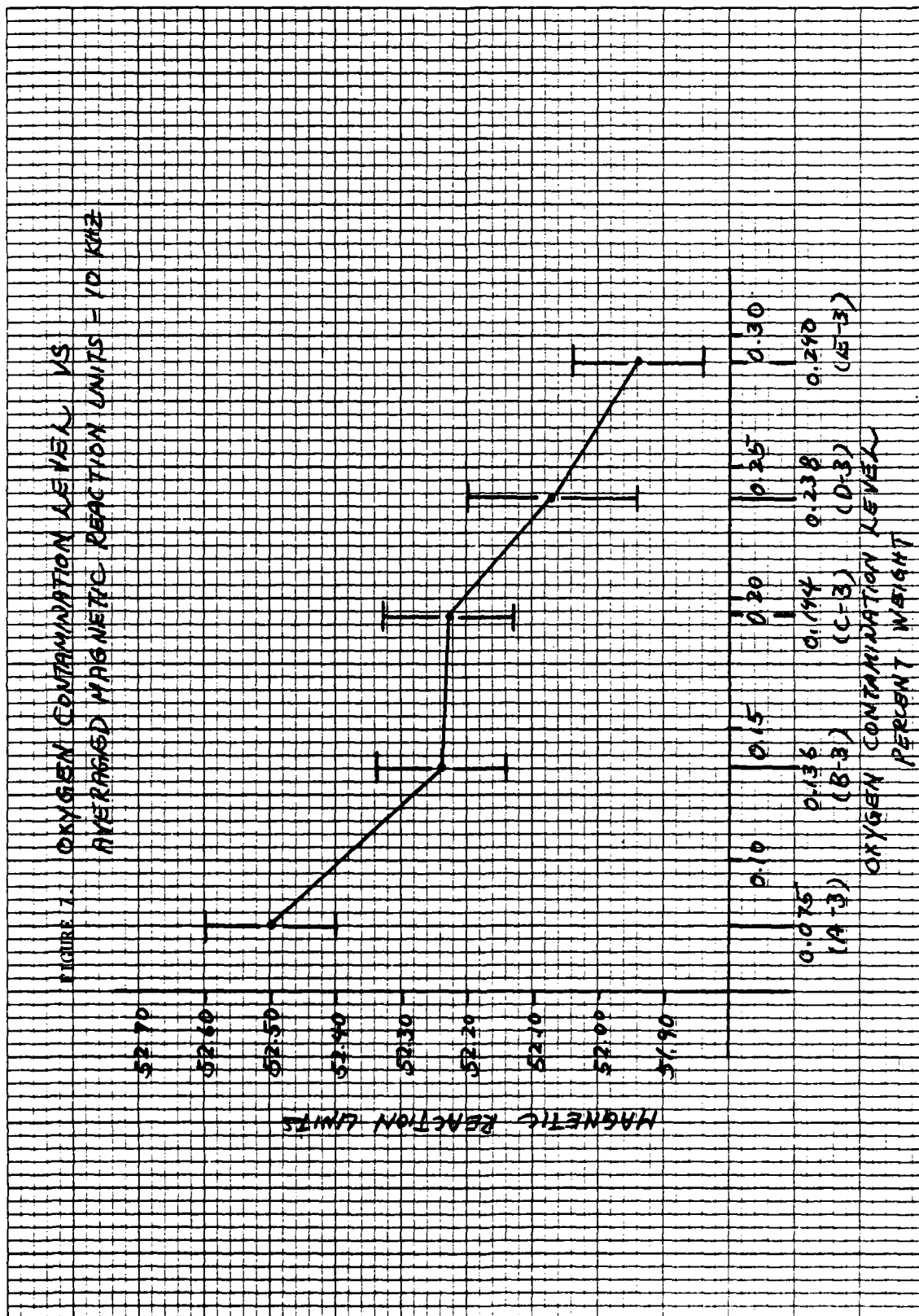


FIGURE 8. OXYGEN CONTAMINATION LEVEL VS  
AVERAGED MAGNETIC REACTION UNITS - 50 KHZ

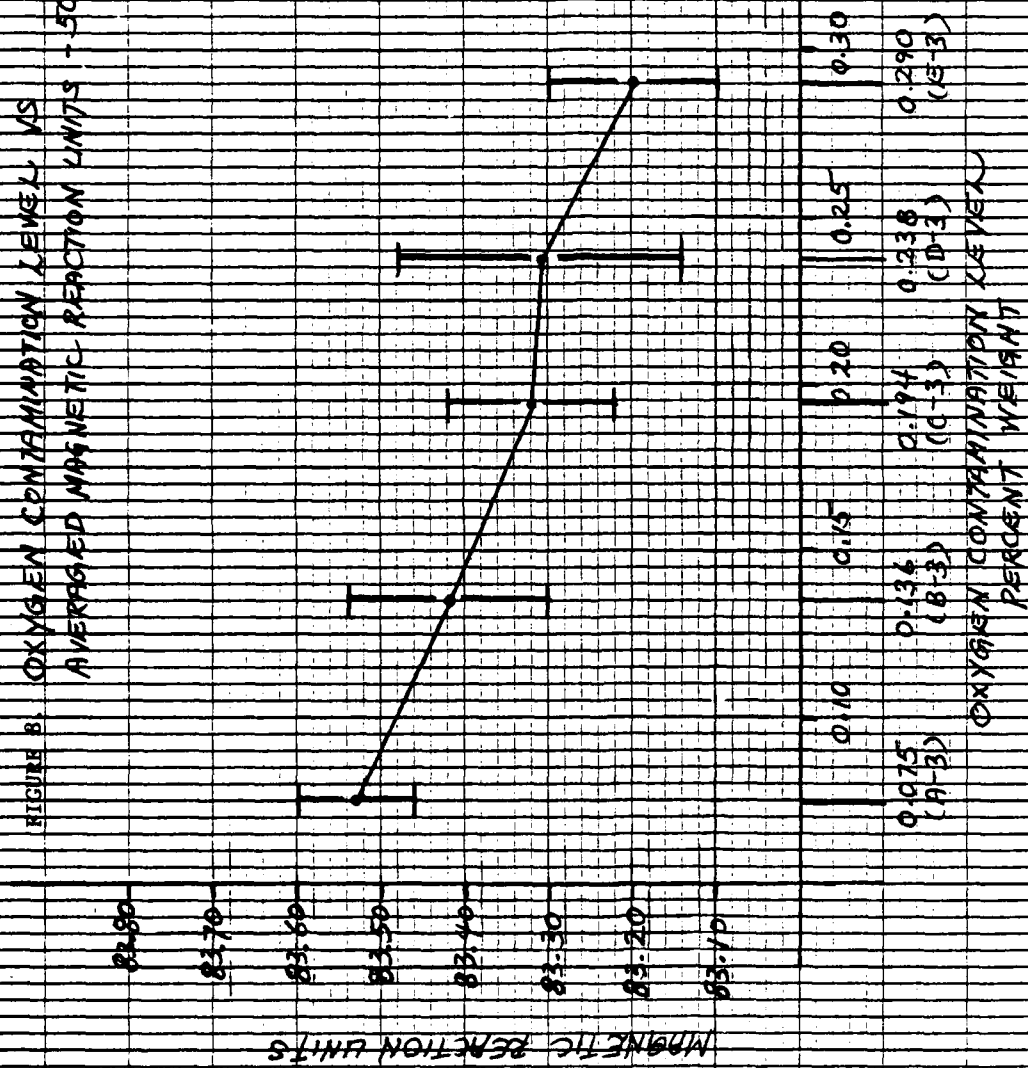




FIGURE 9. OXYGEN CONTAMINATION LEVEL VS  
AVERAGED MAGNETIC REACTION UNITS - 100 KHZ

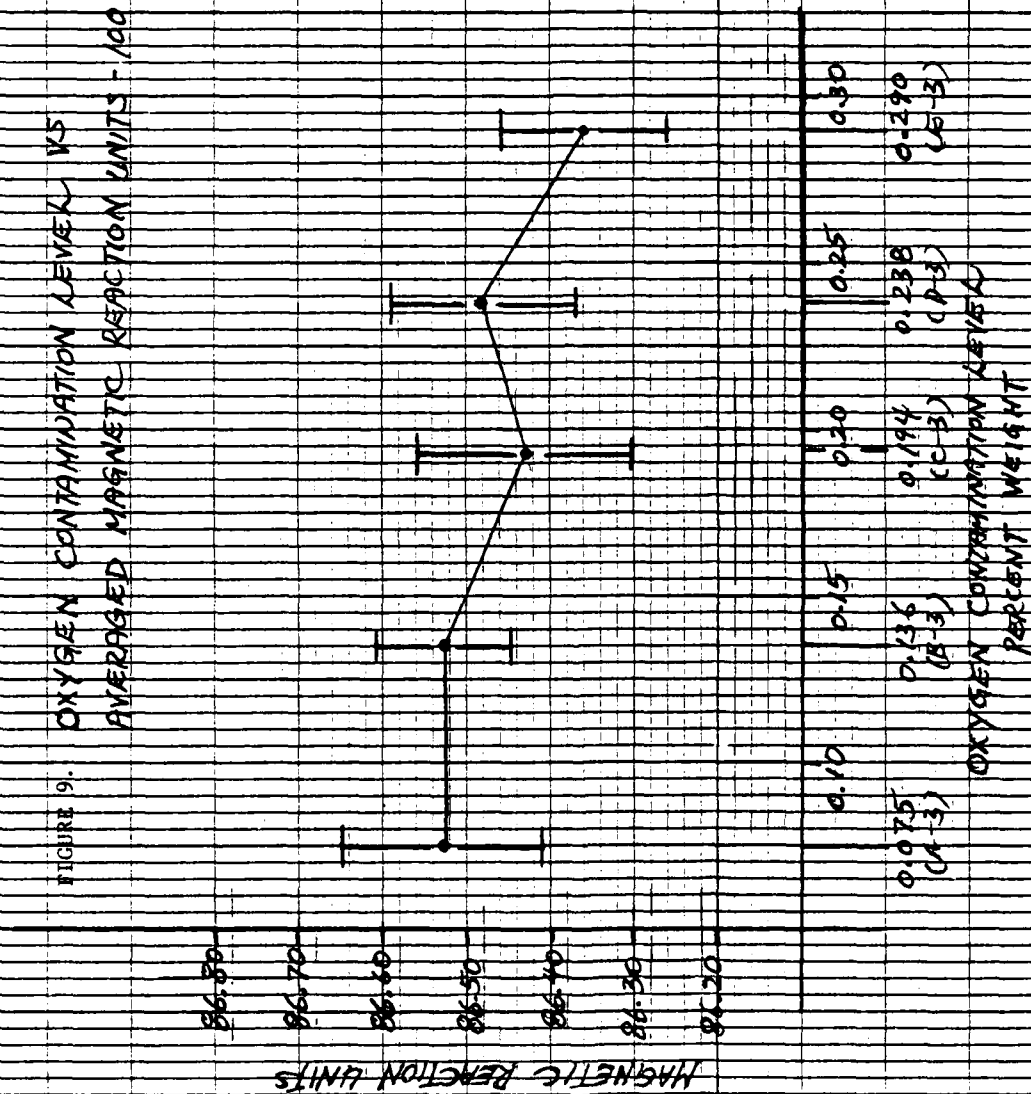
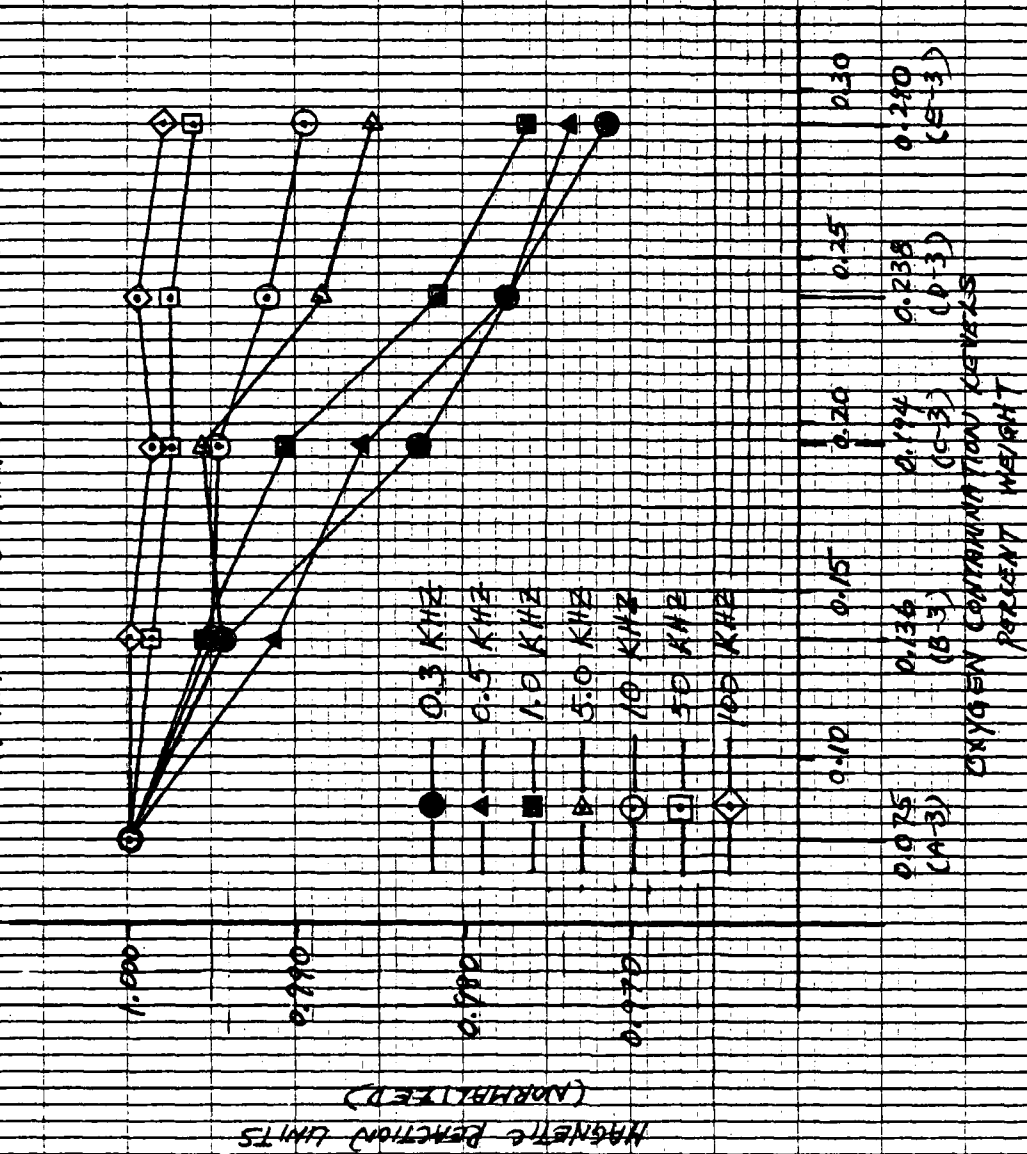


FIGURE 10. OXYGEN CONTAMINATION LEVEL, VS  
NORMALIZED MAGNETIC REACTION UNITS



#### IV. CONCLUSIONS

Based on the evaluation of Ti-6211 specimens using a magnetic reaction analyzer, the following conclusions are made:

- Magnetic reaction field analysis was used successfully in detecting bulk material conductivity changes in Ti-6211 caused by oxygen contamination.
- Approximate levels of oxygen contamination can be determined based on the averaged magnetic reaction units obtained at 1 KHz and below.
- Conductivity of Ti-6211 alloys decreased as the oxygen contamination level increased.
- Probe lift-off must be maintained to obtain repeatable test results.
- Based on the conductivity variance noted within the specimen of known oxygen contamination level, the contamination affected the specimen nonuniformly throughout the volume.

## V. RECOMMENDATIONS

Because of the encouraging results obtained, it is recommended that the magnetic reaction analysis method be investigated further using an actual welded specimen. Due to the portability of the instrument, it is highly adaptable to either shop or field use in evaluating the oxygen contamination levels. A minimal modification allowing the probe assembly to follow the specimen contour to include the welded region, is all that is required.

Since the evaluation of the oxygen contamination levels was dependent on a comparative analysis, the electromagnetic method was as reliable as the standard used to make the analysis. Consequently, a well-defined standard, which is representative of the type of material to be investigated, should be used in quantifying the oxygen contamination levels.

## VI. REFERENCES

1. Hagemaiier, D. J., "Nondestructive Detection of Hydrides and Alpha-Case in Titanium Alloys," Materials Evaluation, December 1972.
2. Rosen, A., Nativ, S., and Bohrer, M., "The Effect of High Temperature Exposure on Mechanical and Electrical Properties of Ti-6Al-4V Sheet," Materials Evaluation, June 1975.
3. Arieli, A., Bar-Cohen, Y., and Blas, A., "The Effect of High Temperature Oxidation on the Eddy Current Conductivity of Ti-6AL-4V Alloy," Materials Evaluation, May 1978.

SECTION 11

**ELECTROMAGNETIC NDE OF INTERSTITIAL CONTAMINATION  
IN TITANIUM ALLOY WELDMENTS**

Robert M. Rose, Sc.D

*Department of Materials Science and Engineering  
Massachusetts Institute of Technology  
Cambridge, MA 02139*

↓  
The direct effect of dissolved oxygen and other interstitials on the electrical resistivity of titanium alloys is generally small relative to the resistivity of the alloy itself. However, there are special cases where the microstructural effects (e.g., alpha precipitation of the oxygen may be large enough to cause detectable changes in the resistivity. We have measured this effect, by four-point probe and ac susceptibility, in five Ti-6211 specimens and seven Ti-6Al-4V weldments provided by an ONR-sponsored project at M.I.T. In the forged and annealed Ti-6211 specimens, there was no detectable relationship between the resistivity/susceptibility and the oxygen content. On the other hand, the weld metal specimens did exhibit measurable oxygen sensitivity, approximately 7% of the base resistivity per pct. oxygen. Control experiments on the base metal from the weldments showed a resistivity variation of 1% or less. We conclude that microstructural effects of oxygen contamination on electrical resistivity of weldments are large enough to measure; these effects are wiped out by annealing. Thus, the resistivity/susceptibility method cannot be used generally on Ti alloys regardless of history but is a valid and convenient specific approach to NDE of Ti welds.

*Present*

AD-P004 131

# ELECTROMAGNETIC NDE OF INTERSTITIAL CONTAMINATION IN TITANIUM ALLOY WELDMENTS

Robert M. Rose, Sc.D.

M.I.T.

## SUMMARY

Detection of oxygen contamination of Ti-6211 by electromagnetic methods depends crucially on the sensitivity of the electrical resistivity of that alloy to the oxygen content. We had previously measured the absolute resistivity of seven Ti-6Al-4V weldments provided by an ONR-sponsored project at M.I.T. The result was that when the weldments had been produced by essentially the same technique (three of the seven), a clear relationship may exist, but when techniques differ, considerable scatter occurred. For the five plates, two methods were used: AC susceptibility and four point probe. The latter was developed to the necessary level of precision; the former is still being improved. By using the probe we found that, for the five Ti-6211 plates the resistivity increased 6% per percent oxygen by weight with a correlation coefficient of 0.8. These measurements were confirmed by absolute resistivities determined from small bars cut from the plates. It is significant that the variation is very

similar to that of the weldments, and that control experiments on the base metal from the weldments shows no variation. We conclude that the structure sensitivity of the electrical resistivity of this alloy precludes the use of electromagnetic methods as general analytical approaches. However for a well characterized process for which standards can be generated, the electromagnetic methods should be valid and extremely convenient to use.



AD-A147 626

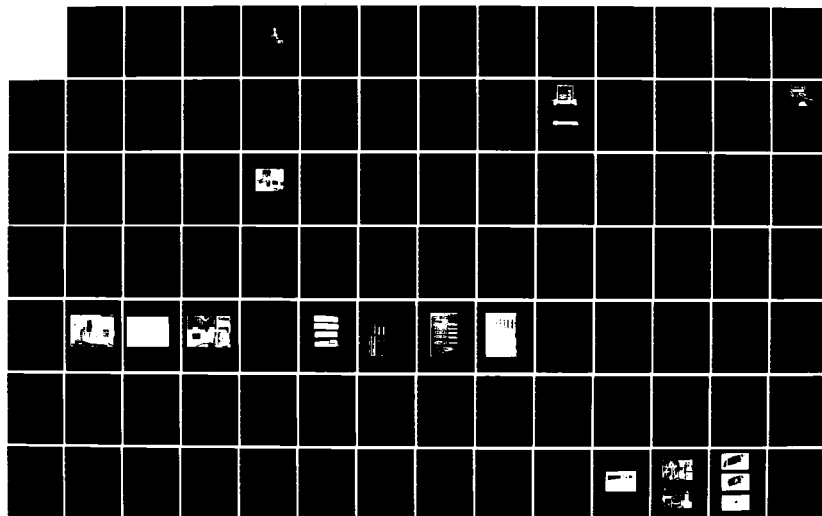
PROCEEDINGS OF THE WORKSHOP ON NONDESTRUCTIVE  
EVALUATION (NDE) OF TITANIUM (U) NAVAL RESEARCH LAB  
WASHINGTON DC N K BATRA ET AL. JUL 84

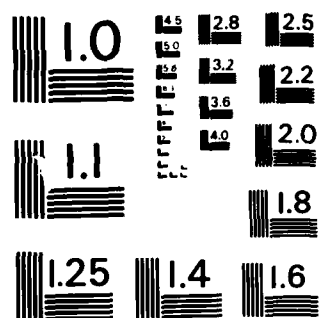
3/4

UNCLASSIFIED

F/G 11/6

NL





MICROCOPY RESOLUTION TEST CHART  
NATIONAL BUREAU OF STANDARDS-1963-A

## INTRODUCTION

Two assumptions underlie our approach:

- 1) that oxygen contamination has a measureable effect on the electrical resistivity of the Ti alloys of interest; and,
- 2) that the resistivity changes are practically measurable by nondestructive techniques.

Oxygen has a pronounced effect on the resistivity of pure transition metals with reasonable solubility for that element [1,2]. For the Ti alloys of interest, the situation is more complex and unclear. However, oxygen is a potent alpha stabilizer in Ti alloys and, therefore, there should be microstructural consequences of oxygen contamination. The question then is whether or not the changes induced by the oxygen will measurably affect the resistivity. If the answer is positive, then resistivity measurement affords a very convenient NDE approach to oxygen, particularly if noncontact techniques are developed which can deal with changes in shape and liftoff.

## EXPERIMENTAL

### Methods

#### A. Noncontact (susceptibility)

This was done by the use of a single coil driven by a Princeton Applied Research Model 110 tuned amplifier/oscillator in the oscillator mode, with a series resistor; a double coil (driver and detector) was also used.

The coil signal was detected by a PAR Model 129 two-phase lock-in amplifier; the output of the latter was filtered with a Frequency Devices Model 901F active filter and measured with a Doric integrating microvoltmeter. Frequencies of 1, 10 and 100 KHZ. were used. Both in-phase and quadrature components were monitored.

#### B. Contact

A four-point probe with spring-driven contacts, shown in Figure 1, was used. DC current up to one ampere was provided through the outer contacts and voltage and current measured with digital voltmeters and (for the current) shunts.

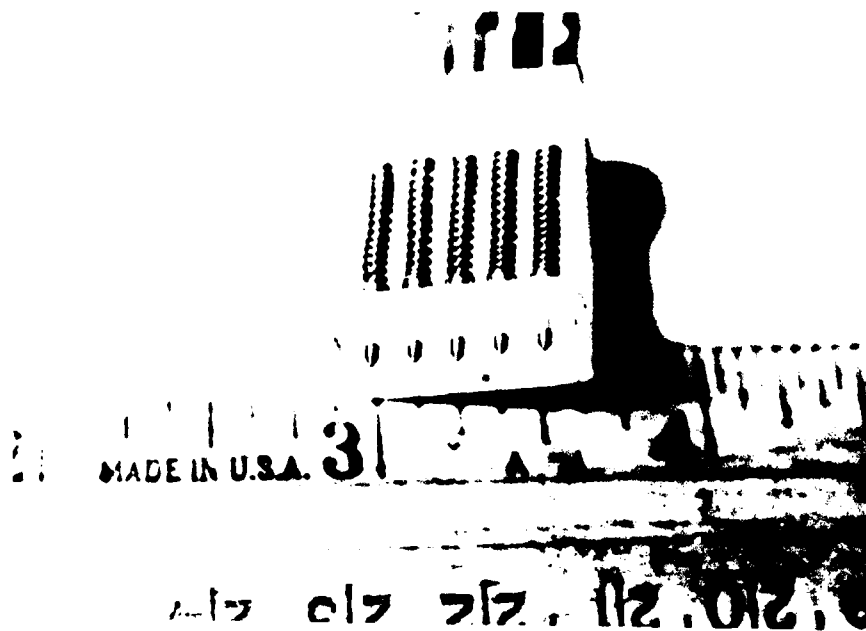


Figure 1. "Five point" probe, used to measure relative resistivity; any four terminals may be used.

### C. Destructive

From the various weldments used, specimens were cut and precision-ground to right cylinders whose exact dimensions depended on the shape of the weldment involved; all were near  $1/8" \times 1/8" \times 1"$ . Resistivity was measured by the four-point probe technique as above, but with spot-welded nickel wire connections as well.

### Materials

The five plate specimens were used. In addition, resistivity was measured by method C (above) the other specimens. Three of these specimens had been produced under nearly identical welding conditions; the others had been produced with different fluxes and widely different procedures.

### Procedure

One side of each plate was machined flat to facilitate measurement; at that time, susceptibility and four-point probe measurements were made. Finally,  $0.1" \times 0.1" \times 1"$  test bars were taken from the corner of each plate and measured by Method C. Weld metal specimens were all done by Method C, as discussed above.

## RESULTS AND DISCUSSION

The susceptibility measurements showed no measurable dependence on oxygen content, for the five plates. A brief check of precision shows that the lock-in amplifier approach is no better than 1-2%. Consequently we are preparing to use larger coils (requiring less sensitivity) and a bridge which is good to 1 part in  $10^4$ . We do not expect to have this apparatus ready before this contract terminates. The four-point probe method initially showed scatter such that no useful relationship was apparent. However, when the apparatus was upgraded by using lower probe currents, a high stability power supply (an EDC current standard), polarity reversal and shielding of leads and probe, the correlation coefficients improved immediately. Figures 2-4 show the results of the probe measurements with currents of 1 amp, 500 ma and 100 ma. respectively. The quality of the measurement degrades sharply between 500 ma. and 1 amp.

On the other hand, the resistivity of the three "identical" welds is apparently much better behaved, as shown in Figure 5, at least as far as three points may be trusted. On the basis of these three rather lonely points, differences of 0.1% in oxygen content should be readily detectable. Finally, Figure 6 shows the three points above together with four others, where these were widely different with regard to fluxes and welding conditions, as mentioned above. There is now

considerable scatter. The regression line has the Equation,

$$10^4 \rho = 1.67 + 0.137 (\% \text{ oxygen})$$

with a deviation of  $\pm 0.034 \times 10^{-4}$  about the line. Such a slope is easily exploitable, given modern electronics, as a change in oxygen of 0.1% changes the resistivity by 0.82%. The deviation corresponds to 0.25% oxygen; however, the deviation should be much less, as Figure 5 implies, when only one type of weld is evaluated. The slope in this figure is ca.  $2.5 \times 10^{-5}$  ohm-cm/percent O; given the weld metal resistivity itself, differences of the order of 0.01-0.05% should be detectable. Control experiments, performed on base metal from these weldments, showed the resistivity to be constant to within 1%. Finally, absolute resistivity measurements were made, using (see above) the bar specimens taken from each plate. The results are shown in Fig. 7. One caveat is necessary with regard to this data: it was taken without the stable power supply and shielding, and without polarity reversal and as is now known, this arrangement degrades the data. The regression line is

$$10^4 \rho = 1.65 + 0.16 x$$

with a correlation (!) coefficient of 0.38. We also performed a correlation calculation with the probe measure-



ments using the same electronics and operating procedure; the correlation coefficient was 0.97. Thus, whatever our reservations about our method and the statistical validity of our results, we are indeed measuring resistivity with the probe.

The shortcoming of this approach is that the sensitivity of resistivity to oxygen level is mediated by microstructure. Since many factors determine the microstructure it will not be possible to use this method without detailed knowledge and control of the specific manufacturing procedure. For a given welding procedure a calibration process would be necessary in order to determine the resistivity vs. oxygen relationship. The reward for such pains is that NDE methods based on resistivity are very convenient and very rapid, and involve inexpensive and reliable apparatus. Both the four-point probe and the susceptibility method are adaptable to irregular shapes, the former by variants of van der Pauw's theorem[3], and the latter by detailed analysis of both components of the susceptibility.

It is apparent that much of the remaining scatter, perhaps all of it, stems from the microstructural variability of the plates, particularly since the measurements of the base metal from the weldments were quite consistent. In this respect the plates supplied may be more complicated, for our purposes, than actual weld

metal, which is now consistent over relatively long seam lengths.

#### CONCLUSIONS

1. There is a correlation between resistivity and oxygen content which can be used to detect weld contamination in the 0-1% range.

2. There is considerable residual scatter in our data which is probably due to microstructural variability rather than our method. Under controlled welding conditions this scatter may be reduced, perhaps eliminated, judging from the limited data points available.

3. The resistivity/susceptibility approach cannot be used unless it is integrated with process characterization and control as the resistivity is too sensitive to microstructural variables other than oxygen content.

## REFERENCES

1. C. S. Tedmon, R. M. Rose and J. Wulff, Trans. Met. Soc. AIME 230, 1733 (1964).
2. C. S. Tedmon, R. M. Rose and J. Wulff, J. Appl. Phys. 36, 164 (1965).
3. J. Van der Pauw, Phillips Tech. Rev. 13, #1 (1964).

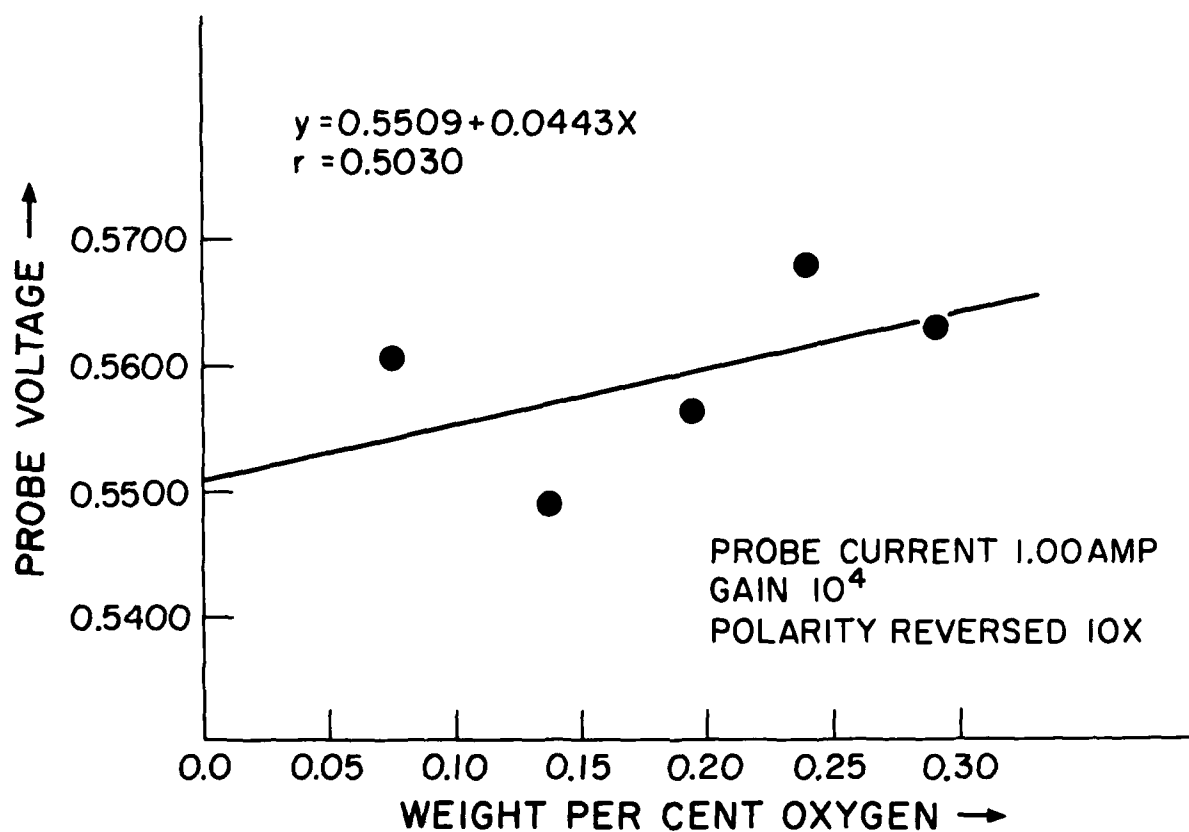


Figure 2. Four-point probe measurements, 1 ampere probe current, on five Ti-6211 specimens.

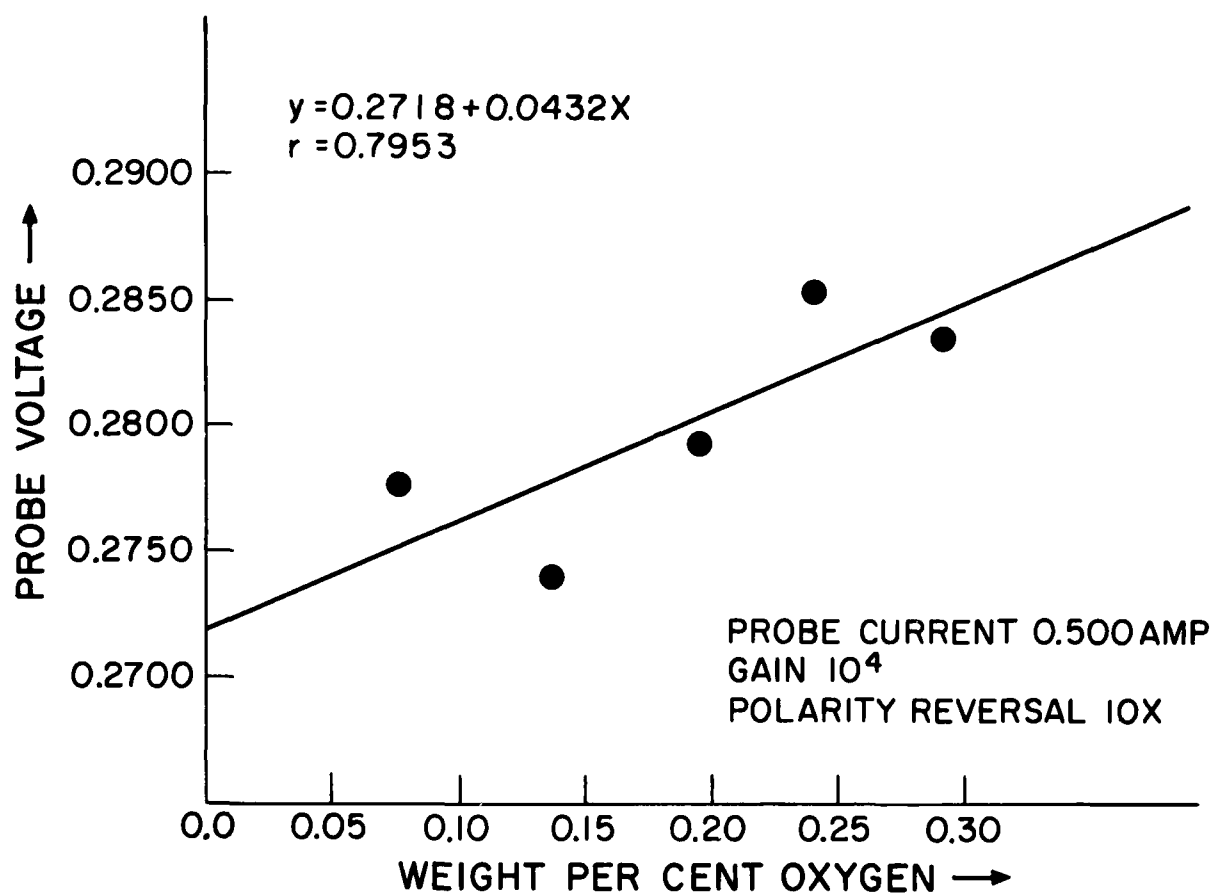


Figure 3. Four-point probe measurements, 500 ma probe current, same specimens as Fig. 2.

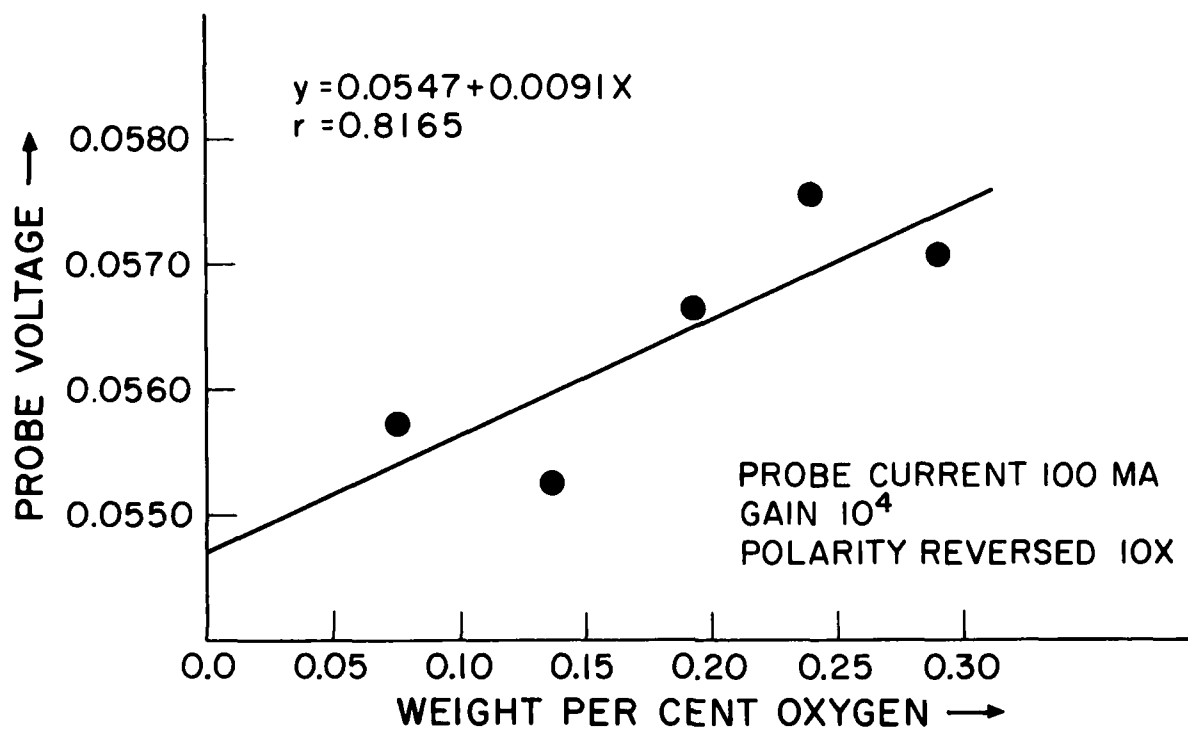


Figure 4. Four-point probe measurements, 100 ma.  
probe current, same specimens as Figs. 2 and 3.

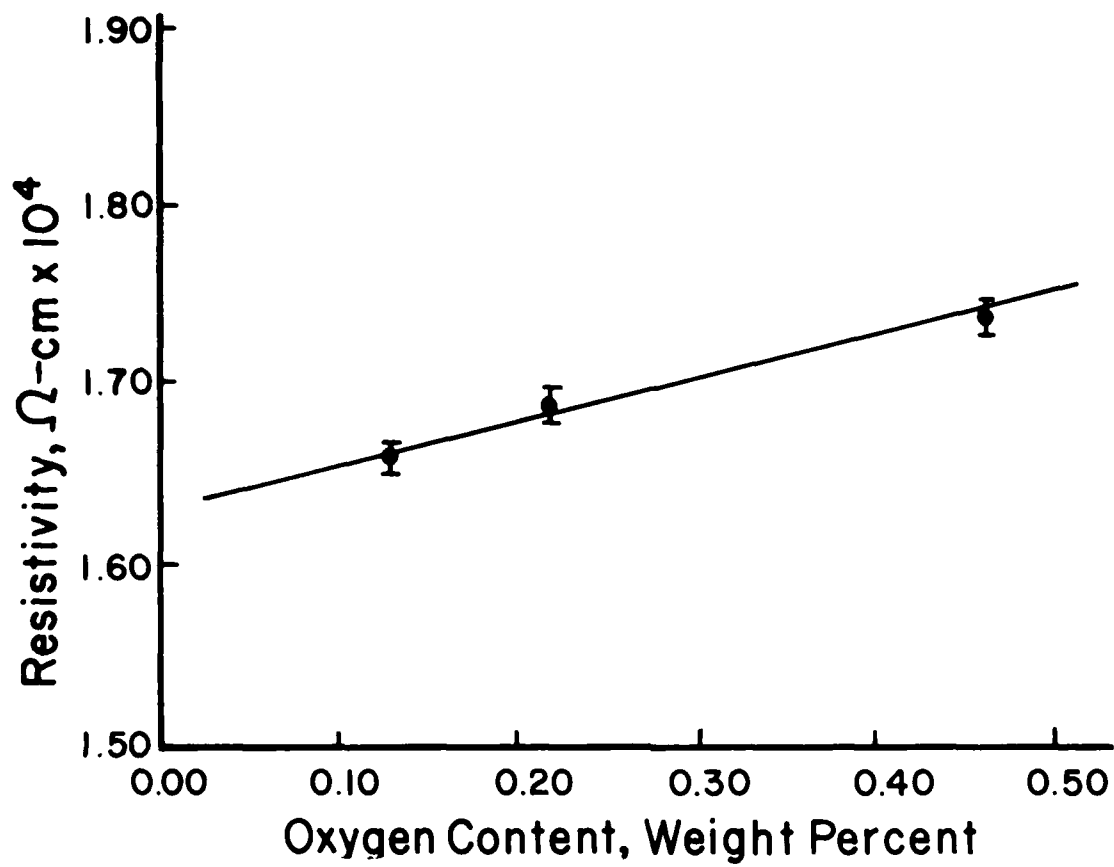


Figure 5. Resistivity vs. oxygen content for "identical" welds.

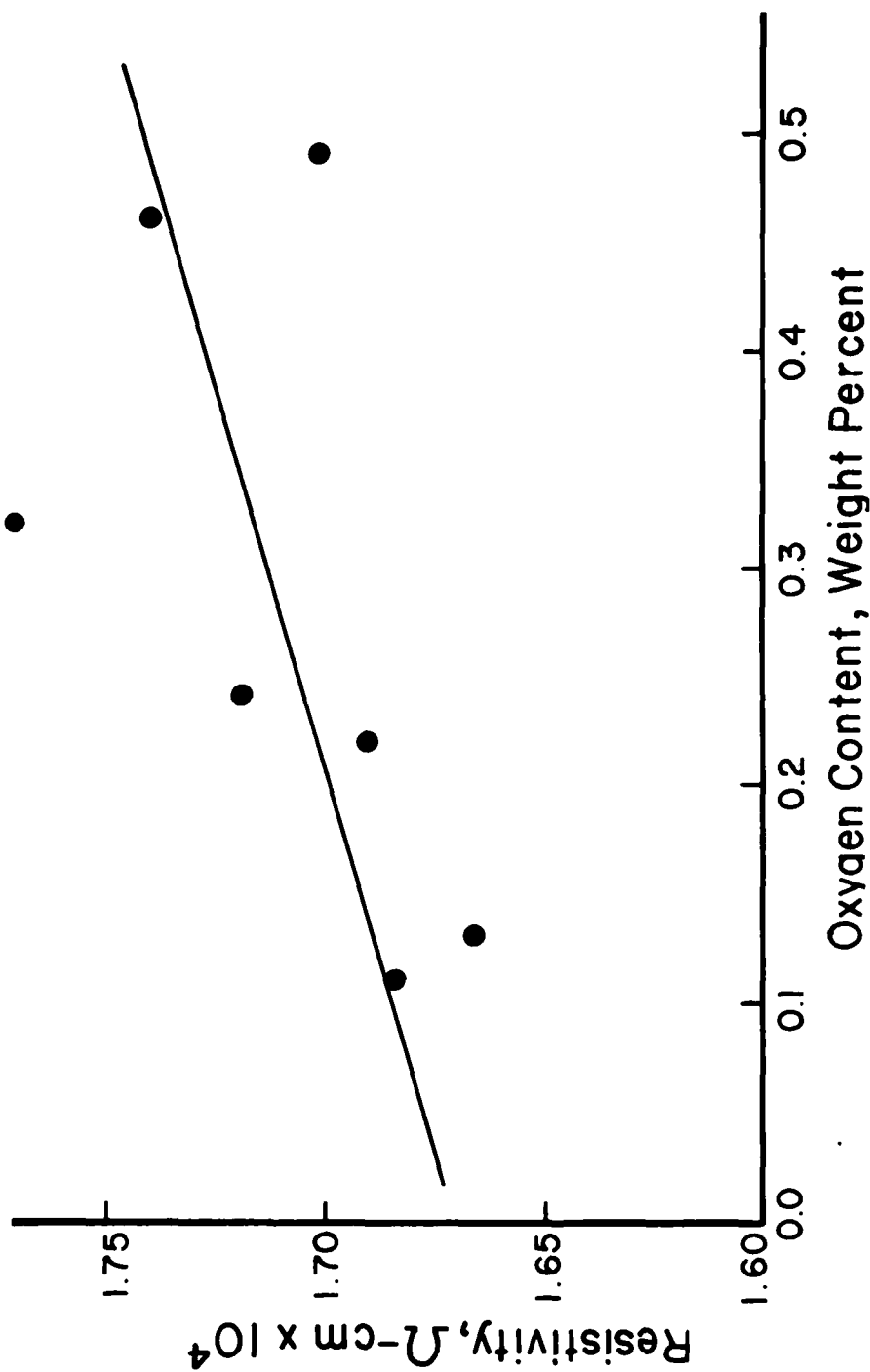


Figure 6. Resistivity vs. oxygen content for seven weldments; five different procedures used.



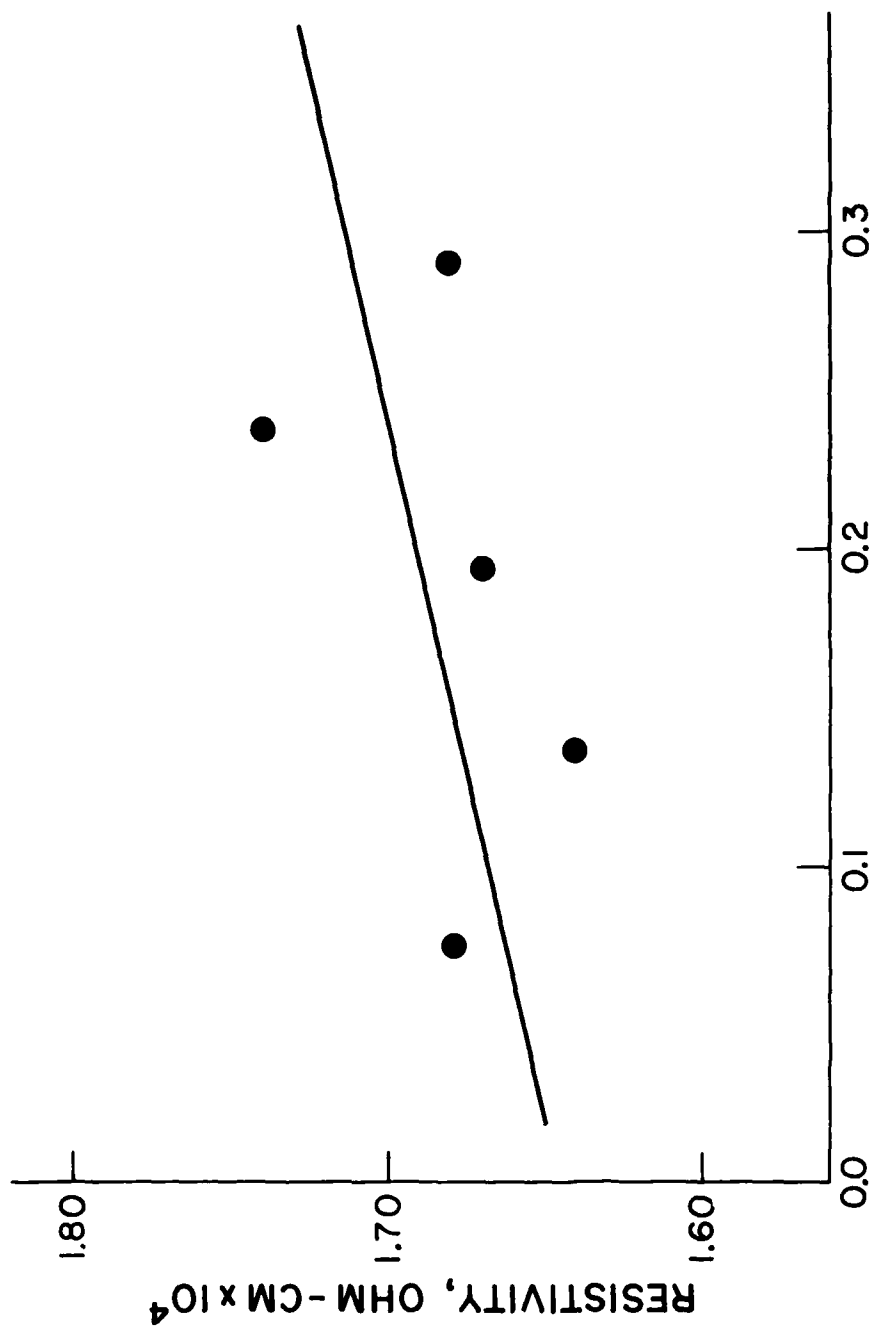


Figure 7. Resistivity measurements on Ti-100 plate specimens.

## APPENDIX

### Noncontact Method

After some experimentation a coil with much greater sensitivity was devised. In essence, the coil has a cylindrical driving element and a "pancake" sensing element, and a ferrite core. Figures A1 and A2 are typical results at drive frequencies of 5 KHz and 10 KHz, using the phase shift as a measure of bulk resistivity. It was necessary to place the probe at or near the center of each plate as edge effects caused very large phase shifts; small lateral displacements near the center had no measurable effect. Table AI contains the statistics for these data. It is apparent that the correlation is very poor, despite smaller relative standard deviations. The explanation for this is specimen inhomogeneity; for the non-contact method as we used it, the averaging procedure as used with the "five-point" probe was not possible, as we had to stay near the center of the plate. This would also explain the relatively poor correlation of the test bar resistivities and the oxygen content.

TABLE AI: Analysis of experimental errors for each of the nondestructive testing methods

Testing Method	Specimen	Average Value	Std. Dev.	Std. Dev./ $\Delta_{max}^*$
Surface 4-pt. probe, 0.50 amp.	A	0.2775 V	0.0041 V	0.3661
	B	0.2739 V	0.0046 V	0.4107
	C	0.2792 V	0.0033 V	0.2946
	D	0.2851 V	0.0048 V	0.4286
	E	0.2837 V	0.0042 V	0.3750
Surface 4-pt. probe 0.10 amp.	A	0.05580 V	0.00117 V	0.5295
	B	0.05530 V	0.00075 V	0.3409
	C	0.05654 V	0.00064 V	0.2886
	D	0.05750 V	0.00079 V	0.3577
	E	0.05694 V	0.00096 V	0.4364
Surface 4-pt. probe 1.0 amp.	A	0.5603 V	0.0061 V	0.3098
	B	0.5485 V	0.0087 V	0.4450
	C	0.5558 V	0.0166 V	0.8505
	D	0.5680 V	0.0061 V	0.3123
	E	0.5632 V	0.0084 V	0.4275
Eddy Current Measure- ment 5 KHz Frequency	A	-10.945°	0.0168°	0.1167
	B	-10.987°	0.0249°	0.1729
	C	-11.029°	0.0319°	0.2215
	D	-10.885°	0.0419°	0.2910
	E	-10.897°	0.0289°	0.2007
Eddy Current Measure- ment 10 KHz Frequency	A	-15.872°	0.0274°	0.1337
	B	-15.918°	0.0257°	0.1254
	C	-16.017°	0.0226°	0.1102
	D	-15.873°	0.0189°	0.0922
	E	-15.812°	0.0199°	0.0971

\*  $\Delta_{max}$  is defined as the greatest difference between the average for two specimens (within the testing method used).

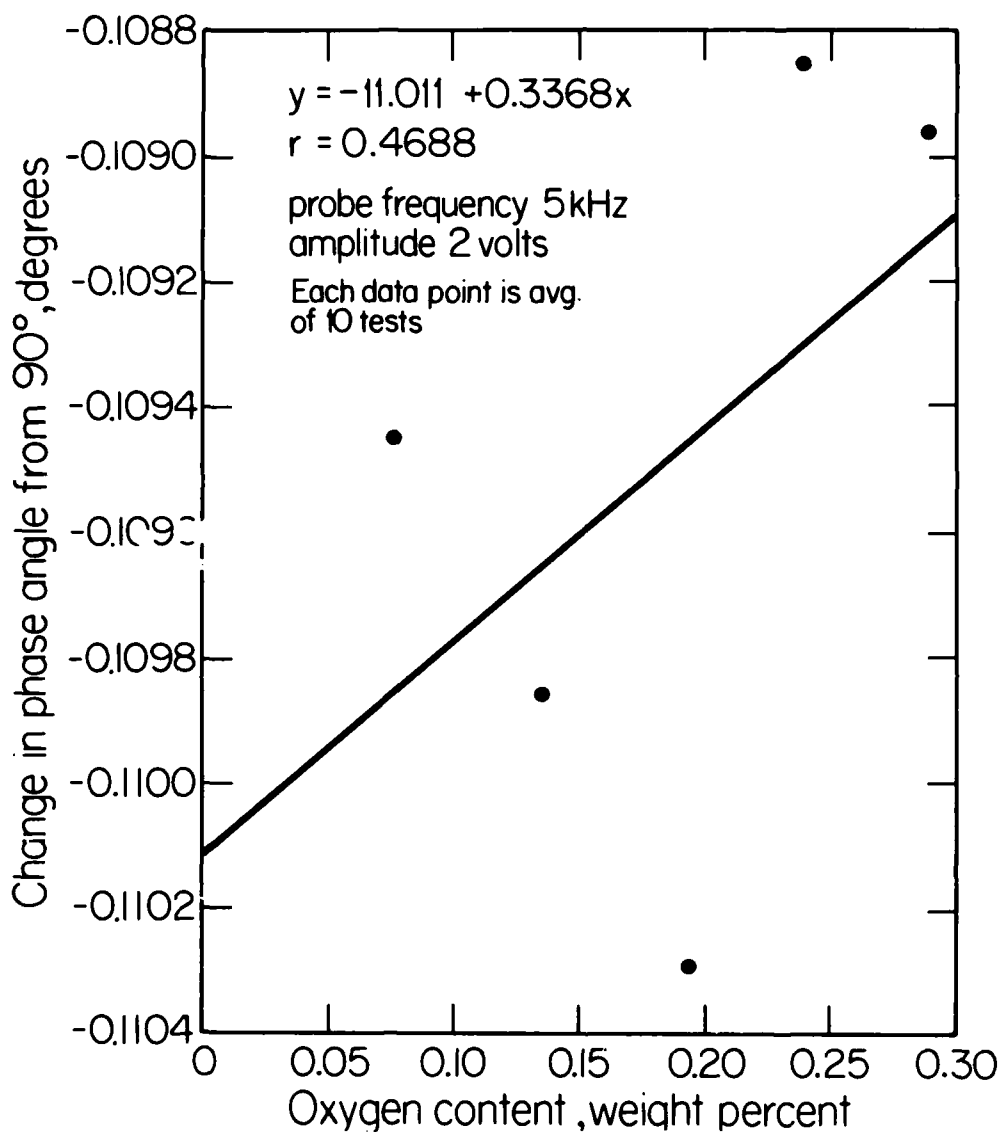


Figure A1. Phase shift versus oxygen content, non-contact method at 5 KHz.

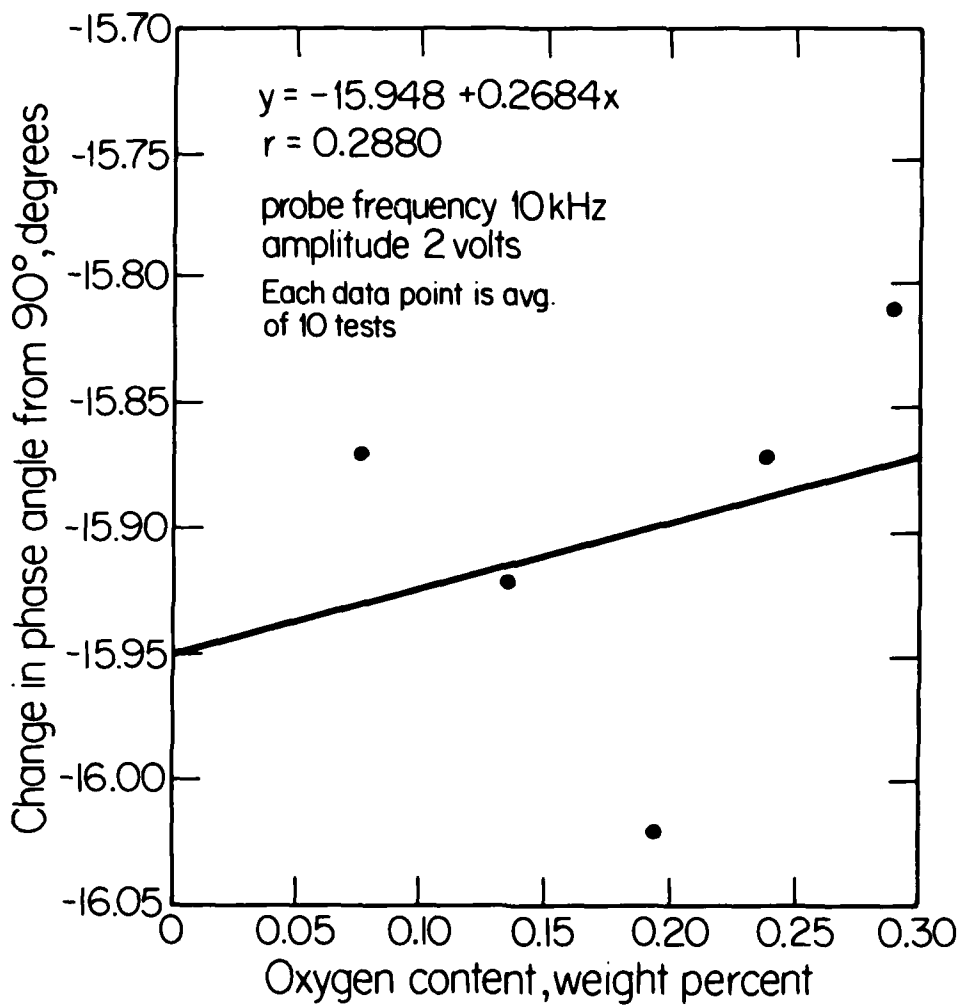


Figure A2. Phase shift versus oxygen content, non-contact method at 6 KHz.

**SECTION 12**  
**EVALUATION OF THE THERMOELECTRIC METHOD FOR DETERMINATION  
OF INTERSTITIAL GASES IN TITANIUM**

Harry J. Marks and Francis G. Karchnak

*Allis-Chalmers Corporation  
Nuclear Components Division  
York, Pennsylvania 17405*

Allis-Chalmers (A-C) investigated the use of a thermoelectric method for determining interstitial gases in titanium. The test method measured the thermoelectric effect generated between the test metal and a heated, constant temperature, electrode. Various contact probe materials were evaluated. No correlation could be drawn between the controlled variable (oxygen) and the thermoelectric results. The inconsistent variation in the chemical composition of the test specimens is considered the cause for an indeterminate test.

AD-P004 132

## I. STATEMENT OF WORK

Allis-Chalmers will investigate the feasibility of detecting and evaluating interstitial (dissolved) gas contamination in titanium using a thermoelectric technique. A metal testing device, TEVOTEST 3.205 (Figure 1), is to be used for this application.

This instrument works on the principle of measurement of the thermoelectrical effect which is generated between the test metal and a heated, constant temperature, electrode. Allis-Chalmers currently utilizes this instrument for alloy identity weld wire verification and other "difficult to sort" applications such as traceability. The advantage of this instrument is its portability, speed, and independence of the shape of the test specimen.

The objective is to quantitatively detect the presence of oxygen as a bulk contaminant in titanium alloy plate specimens (Figure 2). Five such specimens will be supplied with nominal oxygen levels of 0.1, 0.2, 0.3, 0.4 and 0.5 by weight. Each plate will be of nominal one inch (2.54 cm) thickness and a maximum six inches (15.24 cm) square.

INSTRUMENT 3-105  
METAL TESTING  
DEVICE WITH  
PROBES

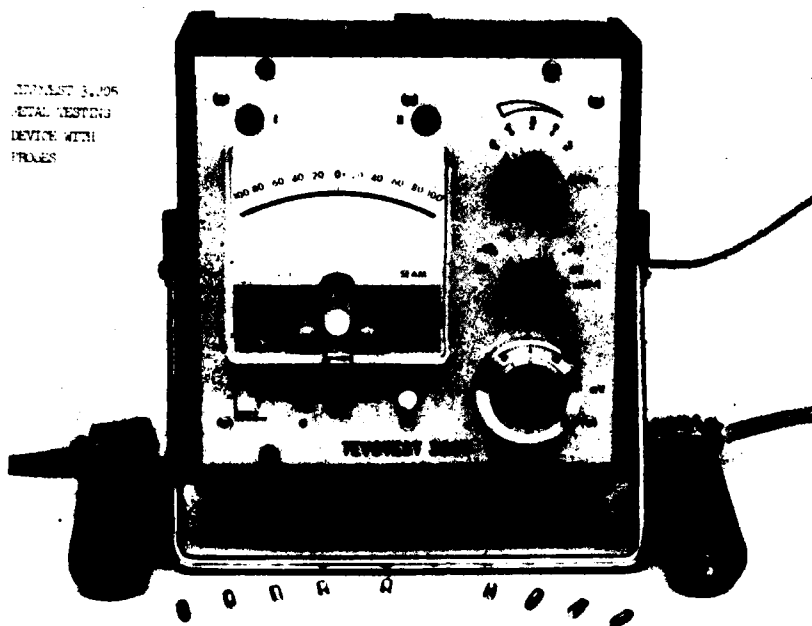


FIGURE 1

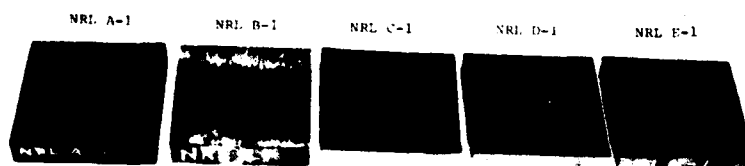


FIGURE 2  
METAL TESTING  
RESULTS

FIGURE 2



### III. INTRODUCTION

Pure titanium metal is soft, weak and extremely ductile. However, through appropriate additions of other elements, the titanium metal base is converted to a high strength metal. The problem is that, in fabrication and welding, titanium must be protected against atmospheric contamination (i.e. oxygen) at any temperature above 1100°F because it reacts with atmospheric gases. Although such contamination may increase its strength, it reduces its ductility, toughness and corrosion resistance to unusable levels.

As a general approximation, it is desirable to keep the level of oxygen below 0.08% (800 ppm). Toughness deteriorates rapidly with increasing oxygen above 0.08%. The critical level of oxygen appears to vary slightly for different alloys. This atmospheric contamination, also known as interstitial gas contamination, is the most serious presently perceived problem in the NDE (non-destructive examination) of titanium alloys. Moreover, such an NDE technique is needed for bulk plate acceptability and for repair welds.

This paper deals with applying the TEVOTEST 3.205 metal testing device as an NDE candidate for identifying the level of oxygen contamination in titanium test specimens, (Fig. 1). The TEVOTEST 3.205 instrument is made by the "Institut Dr. Forster," a German organization known to most American Nondestructive Test Engineers for its

eddy current equipment. The instrument is marketed in the Pennsylvania area by Forster Instruments, Coraopolis, PA. The instrument, from here on referred to as the TEVOTEST, works on the principle of the thermoelectric effect.

Electrical energy can be transformed into thermal energy, and vice versa. We know this works because every day many of us see thermocouples in use. It all started in the early 1820's, when Thomas Johann Seebeck discovered that an EMF (electromotive force) could be produced by purely thermal means in a circuit composed of two different metals A and B, whose junctions are maintained at different temperatures. This circuit is shown in the following sketch.

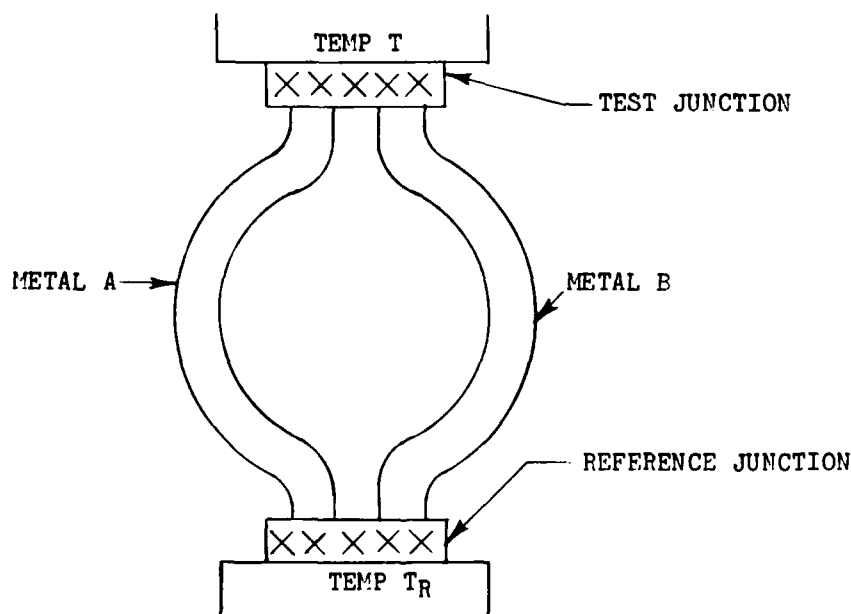


FIGURE 2 (a)

When the temperature of the reference junction  $T_R$  is kept constant, the thermal EMF ( $E_{AB}$ ) is found to be a function of the temperature  $T$  of the test junction. The thermal EMF arises from the fact that the density of free electrons in a metal differs from one metal to another and, in a given metal, depends on the temperature. When two different metals are connected to form a junction, electrons diffuse from one into another, either liberating or absorbing energy in the form of heat.

The TEVOTEST operates on this thermoelectric principle, that is, an EMF is generated between a test metal and a heated, constant temperature, electrode. (See Figure 1). The hot probe operates at a temperature difference of  $55^\circ\text{C}$  above the cold probe. (See Figure 3 for a close-up of the probes). Note the removable tips (Figures 3 and 4) which allow different probe materials to be used. The basic experiment is carried out according to the following scheme.

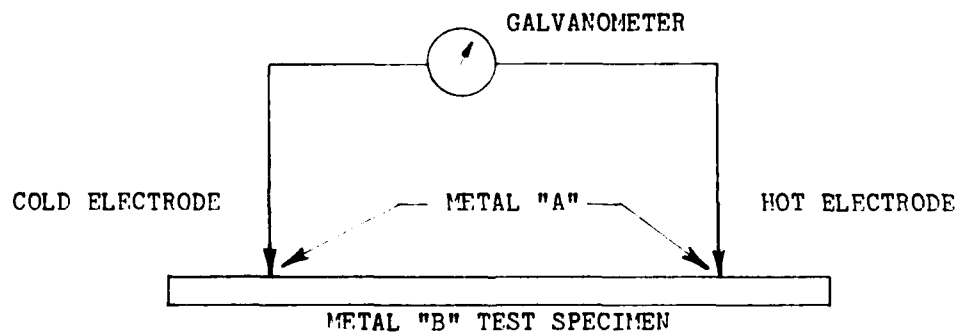
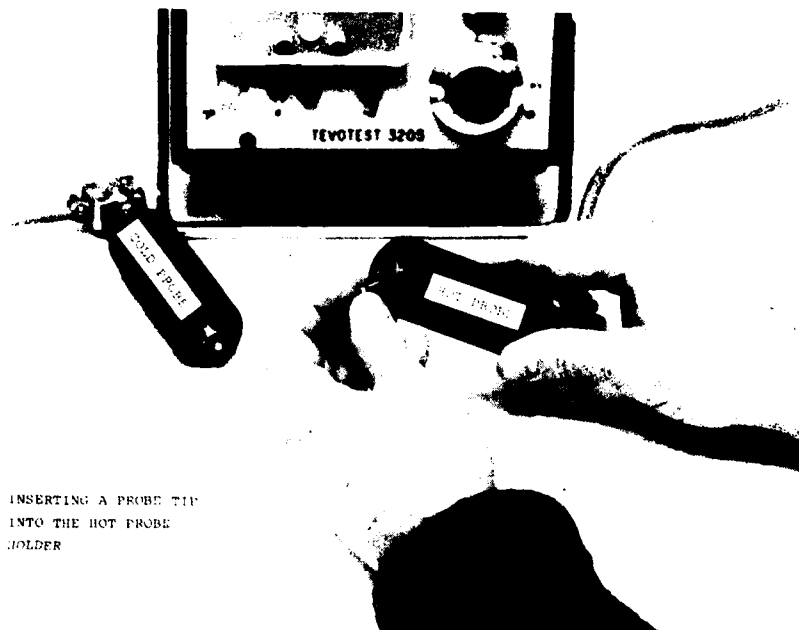


FIGURE 2 (b)



INSERTING A PROBE TIP  
INTO THE HOT PROBE  
HOLDER

FIGURE 3

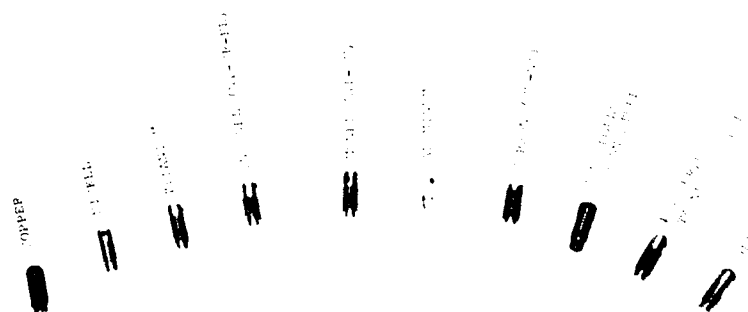
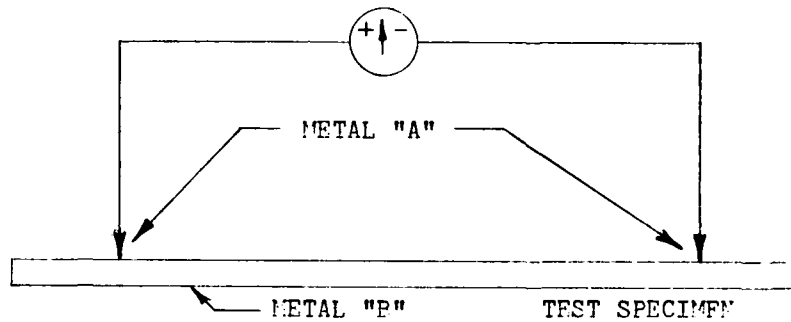


FIGURE 4

The voltage produced depends essentially upon the temperature differential between the two electrodes and the type of the respective metals.

If we want to look at the scheme in passive terms consider the same material in the hot tip, the cold tip and the test specimen.



If Metal A and Metal B are identical, no thermoelectric effect is generated, no current is produced, and the galvanometer scale remains at zero.

#### IV. TECHNICAL APPROACH

The approach was to utilize different probe tips in the probe holder of the TEVOTEST and establish a combination of probe tips that would detect the slight thermoelectric difference due to the dissolved gas contamination in the five titanium. A correlation between the dissolved gases and the millivolt readings from the TEVOTEST was the objective of this investigation. Specifically, the following probe tips were evaluated (Figure 4).

- a. Copper
- b. Brass
- c. Inconel (Ni-Cr-Fe)
- d. Cold Rolled Carbon Steel
- e. Cupron (Copper-nickel)
- f. Aluminum
- g. 400 Series Stainless Steel
- h. Nickel
- i. Monel (Nickel-copper)
- j. Titanium

Reviewing the chemical analysis certification for the titanium specimens, it is evident that the major chemical elements (other than oxygen) are not uniform for the five samples. This situation of chemical nonuniformity is certainly not desirable and presents a complex variable in the evaluation of the test results.

The five titanium specimens were initially cleaned thoroughly with acetone. The electrodes and specimens were then locally cleaned by rubbing with a soft ink eraser and

wiped with Kaydry. The ink eraser was found to be a suitable nonabrasive material for removing dirt and surface oxidation. The use of abrasive materials was avoided to preclude wearing down the probe tips.

The following discussion is a detailed step by step description of the TEST SET-UP and TEST PROCEDURE:

#### TEST SET-UP

Connect the cable and probe holders and allow the TEVOTEST to warm up fifteen minutes before using. The amber "HEATER" indicator light should be cycling "on-off" at regular intervals. The TEVOTEST is now ready for use. It should be noted here that during the upcoming tests, the values recorded will not be the deflections of the galvanometer, but rather the millivolt readings from a vernier control used to null the galvanometer.

#### TEST PROCEDURE

1. Insert copper probes in both hot and cold probe holders (Figure 3).
2. With the machine properly warmed up, ("on-off" light cycling) put the copper probes together and zero the meter by using the adjustment on the back of the machine. This compensates for the slight potential differences between the two probe tips.

3. Place both probes firmly against the first titanium specimen, about 3 inches apart (Figure 5). The distance apart can be varied with no change in results. Press the integral button on the hot probe. Allow approximately five seconds for the meter to stabilize. If a deflection occurs, null the galvanometer, read the control setting (in mv) and record.

NOTE: If there is a deflection, it can be readily verified by altering probe distance. Changing probe spacing does not change the reading.

4. Repeat Step 3 for all five specimens.
5. Next change the hot probe tip only, use all other tips in the hot probe side, one at a time, repeating Steps 3 and 4 for each tip combination. Do not change the zero on the back of the machine.
6. Repeat Steps 2 through 6 using as many probe combinations as possible. Remember to zero the adjustment on the back of the machine whenever the cold probe is changed, and that both tip materials must be identical when this adjustment is made.





FIGURE 5

## V. TEST RESULTS

Tables 1 through 5 document the readings taken for the various combinations of hot and cold probes. As can be seen from the results, no obvious trends could be drawn. Examination of all the values showed that a monel hot probe and a titanium cold probe produced the largest millivolt difference in the test specimens, from + 0.412 to 0.470. (See Table 3 -- also note the specific monel readings are not a linear progression or regression as opposed to the oxygen concentration having a linear progression).

Evaluating the situation further and as noted in Appendix 2, the substantial elements in monel are nickel and copper. The various tables show that using copper either as a cold probe, or in a hot probe combination, the difference in readings of the copper tips was less than that for monel. Nickel was tried only in a hot probe combination since only one nickel probe was available.\* Again, the difference was less than that for monel.

Graphs were made of the test results to see if any correlation could be made. Graph 1 reflects the amount of each element in the five different specimens. Graph 2 is a plot of actual millivolt readings for the four probe combinations which produced the largest responses. Graph 3 is a plot of the four probe combinations producing the largest "delta" mv responses.

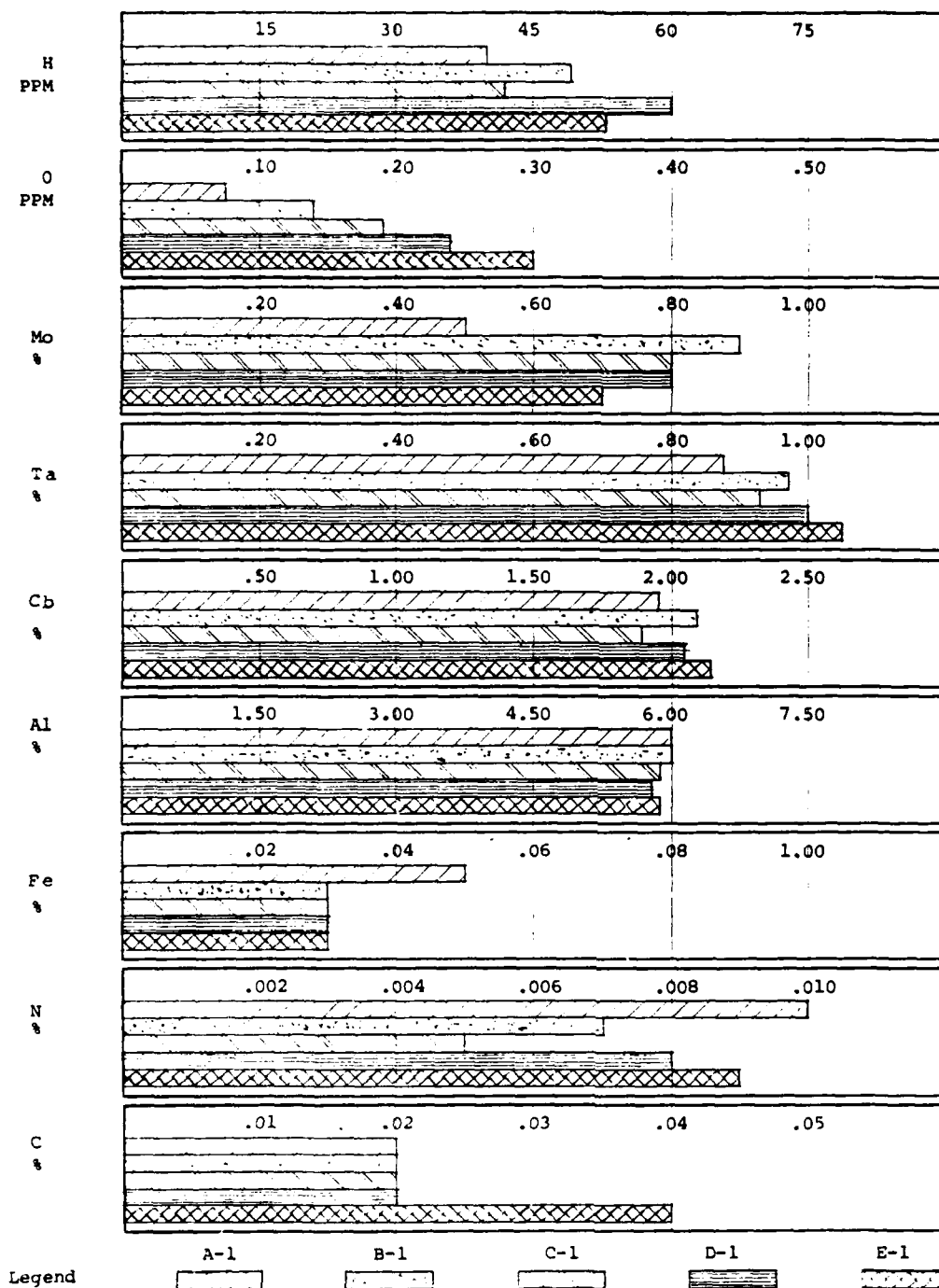
\*Two probe tips of identical material are needed to initially zero the system. See Step 6 of the test procedure.

None of the graphs correlate with the oxygen concentration as listed on the material test reports.

A graph was also made comparing the three gases, nitrogen, hydrogen and oxygen, individually and as a whole (see Graph 4). The total of these three gases was compared with Tables 1 through 5 and Graph 3. No correlation was found.

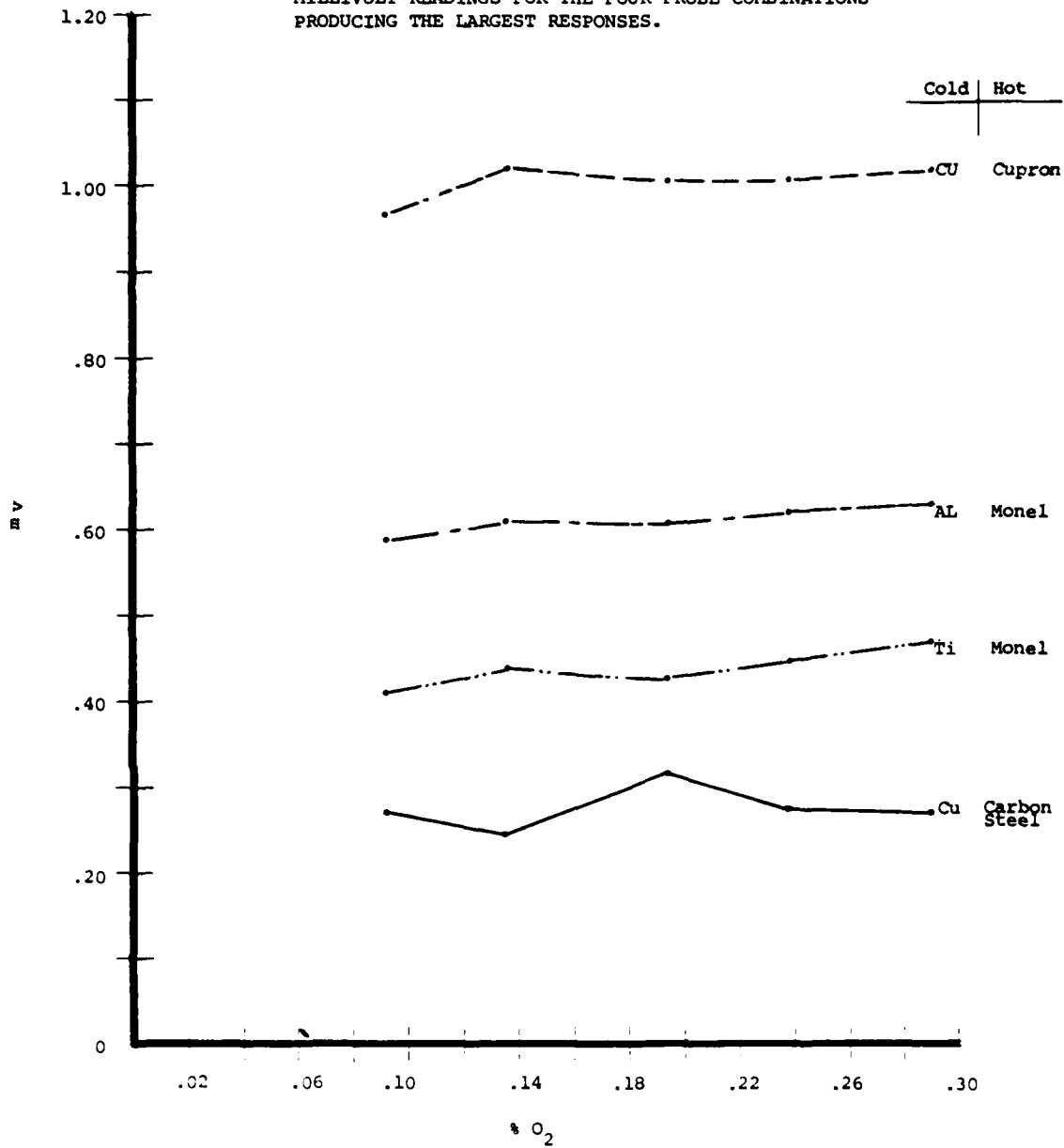
It is concluded, therefore, that the TEVOTEST is unable to quantitatively detect the dissolved oxygen in these titanium specimens. However, some of the readings correspond to the different elements in the specimens. For example, with a titanium cold probe and monel hot probe, the mv readings shown in Graph 6 correlate with % Tantalum (Ta) atomic number 73 plotted as Graph 5. Comparing Graph 7 to Graph 6 shows a similar trend for Columbium (Cb) atomic number 41.

GRAPH 1  
CONCENTRATION OF ELEMENTS IN NRL SPECIMENS



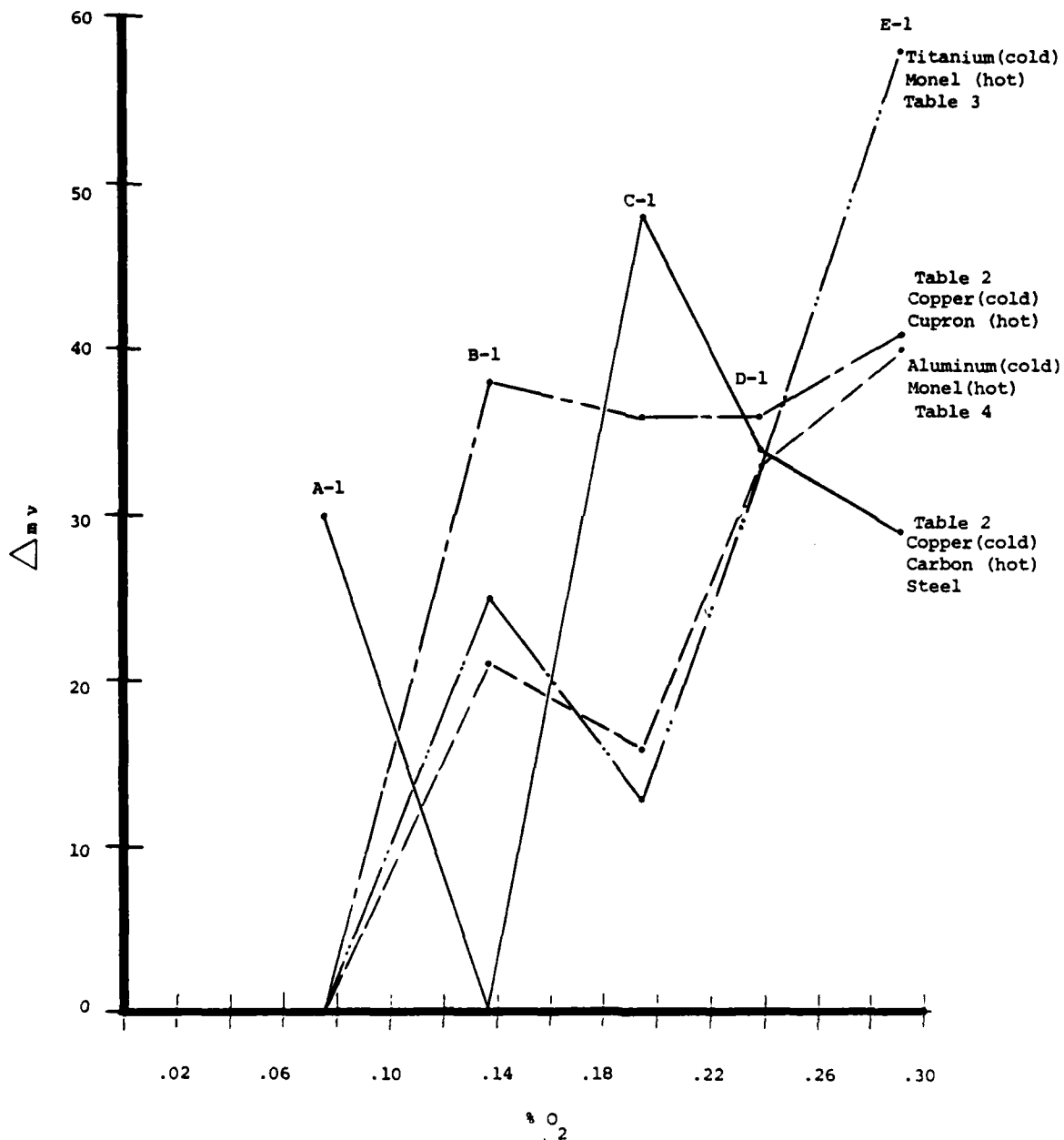
GRAPH 2

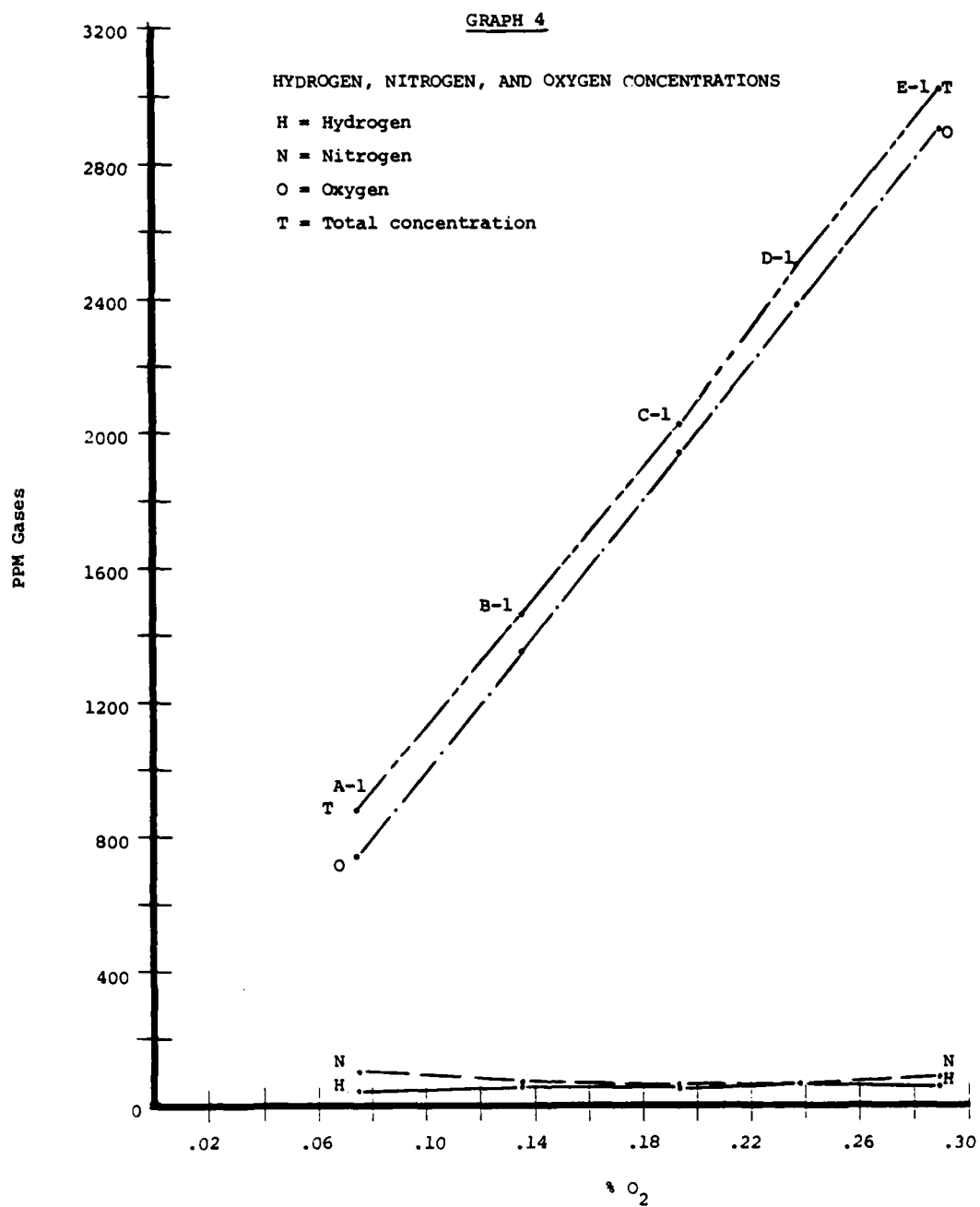
MILLIVOLT READINGS FOR THE FOUR PROBE COMBINATIONS  
PRODUCING THE LARGEST RESPONSES.

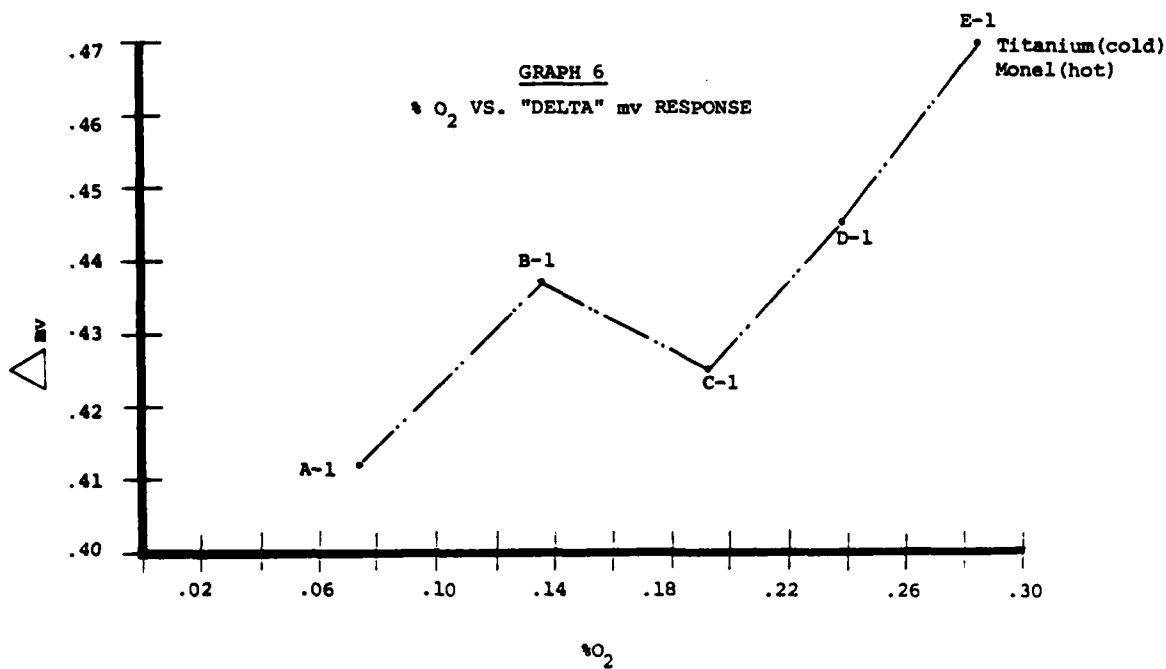
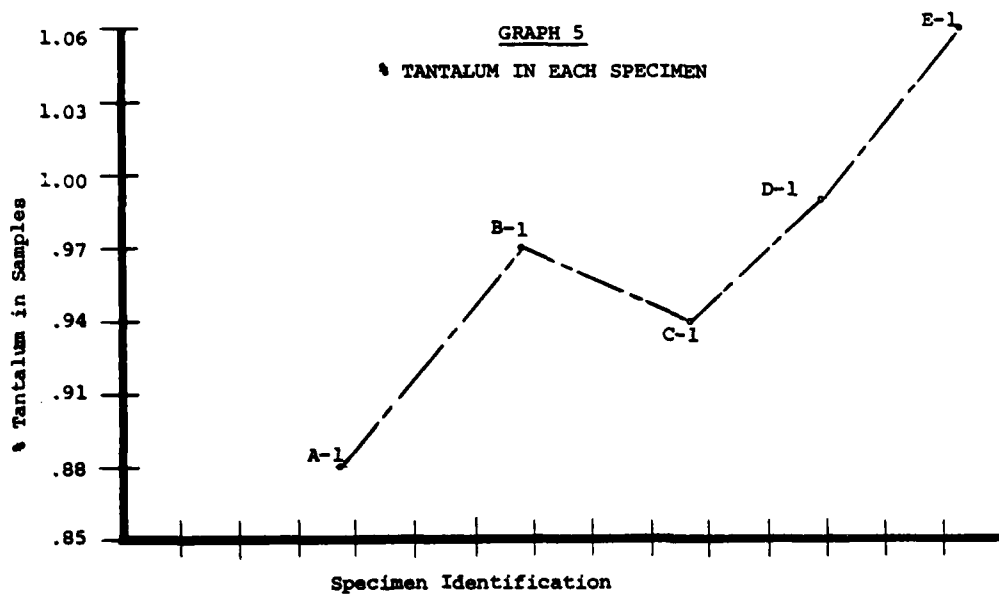


GRAPH 3

"DELTA" MILLIVOLT READINGS FOR THE FOUR PROBE  
COMBINATIONS PRODUCING THE LARGEST RESPONSES









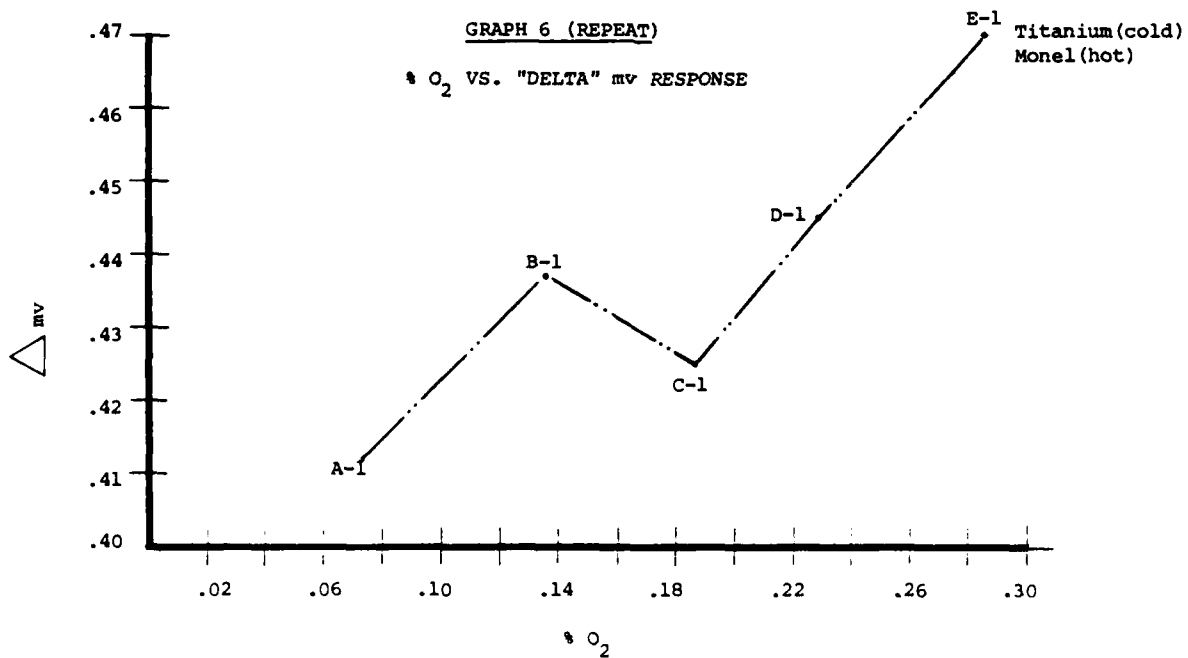
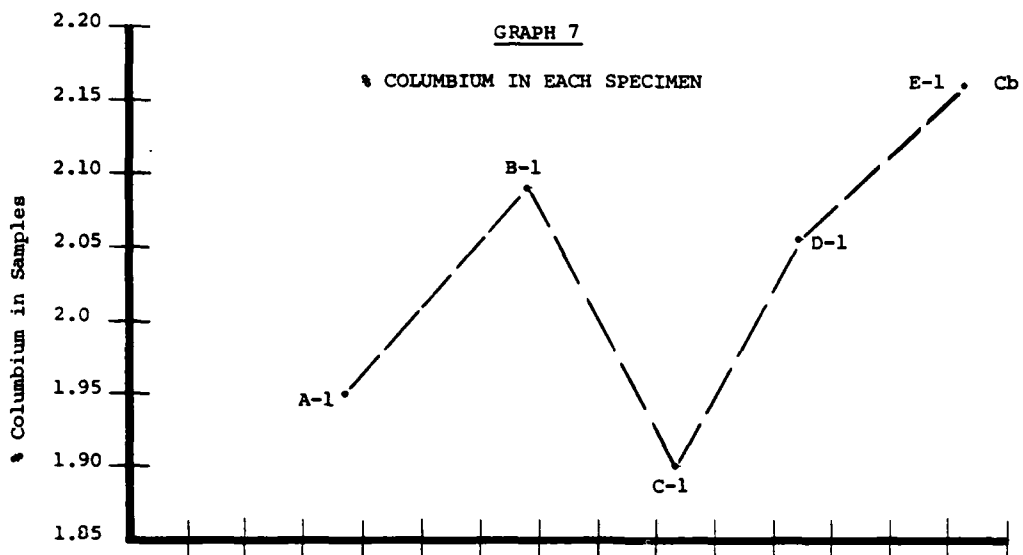


TABLE 1  
MILLIVOLT READINGS

COLD PROBE - COPPER  
GAIN = 4

VARIABLE HOT PROBE TIPS	TITANIUM SPECIMENS (% OXYGEN) *				
	A-1 (0.75%)	B-1 (0.136%)	C-1 (0.194%)	D-1 (0.238%)	E-1 (0.290%)
Nickel	+.467	+.467	+.494	+.494	+.472
Brass	+.349	+.355	+.369	+.373	+.358
Monel	+.790	+.790	+.790	+.790	+.790
Inconel	+.091	+.080	+.080	+.080	+.075
Copper-Nickel	+.481	+.481	+.477	+.477	+.467
Aluminum	+.409	+.409	+.409	+.409	+.409
Cold Roll Carbon Steel	+.280	+.280	+.284	+.278	+.275
Titanium	+.353	+.364	+.370	+.370	+.370
400 Series Stainless Steel	+.106	+.106	+.106	+.106	+.107
Copper	+.374	+.374	+.374	+.374	+.374

\*The tables identify specimens A-1 thru E-1 by oxygen content as a variable; however, oxygen is not the only chemical variable.

TABLE 2  
MILLIVOLT READINGS

COLD PROBE - COPPER  
GAIN = 5

VARIABLE HOT PROBE TIPS	TITANIUM SPECIMENS (% OXYGEN) *				
	A-1 (0.75%)	B-1 (0.136%)	C-1 (0.194%)	D-1 (0.238%)	E-1 (0.290%)
Nickel	+.492	+.514	+.508	+.508	+.508
Brass	+.364	+.364	+.378	+.378	+.370
Monel	+.790	+.814	+.803	+.807	+.796
Inconel	+.070	+.060	+.085	+.080	+.080
Copper-Nickel	+.968	+1.06	+1.04	+1.04	+1.09
Aluminum	+.400	+.400	+.400	+.400	+.400
Cold Roll Carbon Steel	+.271	+.241	+.288	+.275	+.270
Titanium	+.377	+.377	+.377	+.377	+.377
400 Series Stainless Steel	+.106	+.108	+.107	+.107	+.108
Copper	+.382	+.382	+.382	+.382	+.382

\*The tables identify specimens A-1 thru E-1 by oxygen content as a variable; however, oxygen is not the only chemical variable.

TABLE 3  
MILLIVOLT READINGS

COLD PROBE - TITANIUM  
GAIN = 5

VARIABLE HOT PROBE TIPS	TITANIUM SPECIMENS (% OXYGEN) *				
	A-1 (0.75%)	B-1 (0.136%)	C-1 (0.194%)	D-1 (0.238%)	E-1 (0.290%)
Nickel	+ .115	+ .115	+ .115	+ .115	+ .115
Brass	- .019	- .019	- .019	- .019	- .019
Monel	+ .412	+ .437	+ .425	+ .445	+ .470
Inconel	+ .293	+ .293	+ .293	+ .293	+ .293
Copper-Nickel	+ .578	+ .578	+ .578	+ .578	+ .578
Aluminum	- .011	- .002	- .003	- .001	- .010
Cold Roll Carbon Steel	- .122	- .146	- .124	- .126	- .124
Titanium	0	0	0	0	0
400 Series Stainless Steel	- .278	- .278	- .278	- .278	- .278
Copper	0	0	0	0	0

\*The tables identify specimens A-1 thru E-1 by oxygen content as a variable; however, oxygen is not the only chemical variable.

TABLE 4  
MILLIVOLT READINGS

COLD PROBE - ALUMINUM  
GAIN = 5

VARIABLE HOT PROBE TIPS	TITANIUM SPECIMENS (% OXYGEN) *				
	A-1 (0.75%)	B-1 (0.136%)	C-1 (0.194%)	D-1 (0.238%)	E-1 (0.290%)
Aluminum	+.212	+.212	+.212	+.212	+.212
Cold Roll Carbon Steel	+.180	+.165	+.180	+.170	+.183
Titanium	+.200	+.200	+.200	+.200	+.200
Monel	+.589	+.610	+.605	+.622	+.629

\*The tables identify specimens A-1 thru E-1 by oxygen content as a variable; however, oxygen is not the only chemical variable.

TABLE 5  
MILLIVOLT READINGS

COLD PROBE - COLD ROLL CARBON STEEL  
GAIN = 5

VARIABLE HOT PROBE TIPS	TITANIUM SPECIMENS (% OXYGEN) *				
	A-1 (0.75%)	B-1 (0.136%)	C-1 (0.194%)	D-1 (0.238%)	E-1 (0.290%)
Aluminum	+ .926	+ .940	+ .935	+ .928	+ .930
Cold Roll Carbon Steel	+ .800	+ .790	+ .800	+ .800	+ .793
Titanium	+ .918	+ .918	+ .918	+ .918	+ .918
Monel	+1.34	+1.40	+1.40	+1.41	+1.40

\*The tables identify specimens A-1 thru E-1 by oxygen content as a variable; however, oxygen is not the only chemical variable.

## VI. CONCLUSIONS

The TEVOTEST metal testing device which operates on the thermoelectric principle could not correlate between the various (controlled) oxygen concentrations in the five test specimens. The lack of correlation between the controlled variable (oxygen) and the thermoelectric results is attributed to the nonuniform distribution of the other major chemical elements. These other chemical elements act as a bulk matrix and influence the thermoelectric potential difference. It is understood that in practical applications, nonuniform chemistry similar to that found in the five specimens is expected.

## VII. RECOMMENDATIONS

1. Future development specimens should be homogeneous, except for the property (in this case, oxygen) being investigated.
2. Since the atmospheric contaminants (oxygen, hydrogen, nitrogen) are present in the atmosphere in uniform proportions, future development should center around the total dissolved gas concentration.
3. As part of the scope of development, it is recommended that the investigative organization perform an independent chemical analysis for the elements which would influence this method.
4. Finally, it is recommended that the thermoelectric method not be pursued further for quantitative detection of oxygen. However, the thermoelectric method should be recognized as a possible candidate for NDE application for evaluating Columbium and Tantalum concentrations in Titanium.



VIII. REFERENCES

- A. J. Insheep and J. A. McMaster, Titanium Fabrication Corp.,  
and N. Normando, Airco Welding Products.  
How to Weld Titanium Alloys - Special Report #662,  
December 10, 1973
- B. WRC (Welding Research Council) Bulletin  
Procedures for Fracture Toughness Characterization and  
Interpretations of Failure-safe Design for Structural  
Titanium Alloys.  
R.J. Goody, R.W. Judy and R.W. Huber, Bulletin No. 134,  
October 1968.
- C. Annual Book of ASTM Standards 1981. Part 8, by American  
Society for Testing and Materials.

**PART D**  
**NUCLEAR TECHNIQUES**

SECTION 13  
MEASUREMENT OF OXYGEN CONTAMINATION  
IN TITANIUM ALLOY INGOTS BY  
FAST NEUTRON ACTIVATION ANALYSIS

Adel Abusamra

*Science Applications, Inc.*  
*San Diego, CA 92121*

*016(N,P)N16*

↙ The total oxygen content of five titanium samples was determined using activation analysis with fast neutrons. The method utilizes the nuclear reaction  $^{16}\text{O}(n, p)^{16}\text{N}$ . The produced  $^{16}\text{N}$  has a half-life of 7.2 seconds and decays by emitting 6.1 MeV gamma rays.

Titanium samples of variable oxygen content and benzoic acid standards incapsulated in polyethylene vials were irradiated simultaneously with 14.3 MeV neutrons produced from a fast neutron generator. They were transferred to two NaI (TL) gamma-ray counting systems and were simultaneously counted. The 6.1 MeV gamma-ray counts produced by both titanium sample and standards were compared. The values of oxygen in the five titanium samples were 0.067%, 0.127%, 0.165%, 0.231%, and 0.27% with relative error of less than 5%. *Percent*

↙ The analysis is nondestructive, fast, accurate, practically interference free, and can reach 100 ppm level.

AD-P004 133

## 1.0 INTRODUCTION

This final technical report describes the progress made at Science Applications, Inc., in demonstrating a capability to measure the total oxygen content of titanium alloy using nondestructive nuclear techniques.

The oxidation of titanium alloys, caused by interstitial oxygen contamination is a serious problem that causes metal fatigue. Should the welding process of a titanium alloy be interrupted, oxygen from air can get into the weld area and start the oxidation process. Hence, it is important to be able to certify, with high degree of certainty, the assurance of the noncontamination of a weld area with oxygen, and to point out the region of the welds which do not meet the desired specifications. The method used should meet the following criteria:

1. Nondestructive
2. Quantitative
3. Reliable
4. In-Process
5. Fast
6. Safe
7. Cost-Effective

While other efforts related to this measurement determine changes in electrical resistivity, transit time of shock wave transmission, or thermoelectric currents, etc., due to increase or decrease in oxygen content of titanium alloy, they do not produce absolute values of oxygen. False measurements, due to some unknown factor related to changes in crystalline structure of titanium alloy, can result if some of the previously mentioned techniques are used. However, the nuclear technique probes into the very structure of matter, inducing nuclear transformation of oxygen atoms and signaling, with gamma-ray emission, their absence or presence in the metal analyzed. The activation analysis of oxygen with 14 MeV neutrons is a well established and validated analytical technique; it is a rare example of an analytical method that is virtually free of interferences and gamma-ray attenuation effects that utilizes short-lived isotopes, thus permitting a very rapid analysis.

In this report, the determination of oxygen content of titanium alloy - 6211 - will be demonstrated with a great deal of accuracy and reliability. The ultimate goal is to develop a safe and reliable portable unit that can measure oxygen levels in titanium or metallic welds, and indicate whether to accept such a weld or reject it based on its oxygen content.

## 2.0 SURVEY OF LITERATURE

Fast neutron activation analysis has proven to be a highly sensitive and precise method for bulk oxygen measurement (1-4). The technique is based on inducing a nuclear transformation of the oxygen atoms in the matrix by the use of  $^{16}\text{O}(n,p)^{16}\text{N}$  reaction initiated by a flux of 14 MeV neutrons. Blake et al <sup>(5)</sup> utilized this technique to measure oxygen contamination in high-purity beryllium samples and were able to detect 20 parts per million (ppm) oxygen in specimens analyzed. Vogt and Ehmann, <sup>(6)</sup> determined non-destructively the level of oxygen in meteorites using fast neutron activation to <sup>(7)</sup> Word et al, used fast neutron activation analysis to determine the oxygen content of steel samples and were able to perform 600 measurements per day with a detection limit of 10 ppm. Wood and Pasztor <sup>(8)</sup> used fast neutron activation analysis to determine oxygen in steel samples, compared the results with those obtained using vacuum fusion techniques, and concluded that nuclear methods were much faster and more reliable than conventional methods.

Bryne et al, <sup>(9)</sup> devised an automatic system to determine oxygen in beryllium metal components that weight 500-2000 gms, using fast neutron activation techniques. Their results compared favorably with those obtained with existing chemical methods.

### 3.0 THEORY OF ACTIVATION ANALYSIS

Neutron activation analysis is a nuclear method for quantitative elemental analysis. It is a sensitive, accurate and reliable analytical technique. It involves the irradiation of a sample with neutrons from a nuclear reactor or fast neutron generator, then measuring the intensity of the characteristic gamma-rays emitted by the produced radioactive atoms. The elemental composition of the sample is obtained by comparing the intensities of the gamma-rays emitted by the sample to the intensities of the gamma-rays emitted by irradiated elemental standards. The measurement of gamma-rays is accomplished by using a high-resolution Ge(Li), or NaI(TL) detector coupled with a gamma-ray spectrometer.

The determination of oxygen by fast neutron activation makes use of the  $^{16}\text{O}(n,p)^{16}\text{N}$  nuclear reaction initiated by a flux of 14 MeV neutrons. The unstable  $^{16}\text{N}$  nucleus, formed in the reaction, decays with a half-life of 7.3 seconds and emits gamma-rays of 6.1 and 7.1 MeV of energy.

These gamma-rays are detected by a NaI(TL) detector and their number is proportional to the oxygen content of the irradiated specimen. The governing equation for fast neutron activation analysis:

$$D = \frac{Nf\sigma\epsilon}{\lambda} (1 - e^{-\lambda t_b}) (e^{-\lambda t_w}) (1 - e^{-\lambda t_c}) \quad (1)$$

where

- D = counts recorded by the detector
- N = the number of nuclei in a sample which can undergo a given reaction
- f = the neutron flux (neutron/cm<sup>2</sup>/sec)
- σ = the isotopic reaction cross section
- ε = the efficiency of the radiation detection including geometric factors
- λ = the decay constant of the radioactivity produced
- t<sub>b</sub> = duration of neutron bombardment
- t<sub>w</sub> = arbitrary waiting time
- t<sub>c</sub> = arbitrary counting time

Comparison of the gamma-ray yield obtained from a sample to that obtained from a reference standard, provides a measure of the oxygen content of the sample as stated by the following relationship:

$$\frac{\text{counts of sample}}{\text{counts of standard}} = \frac{\text{weight of oxygen in sample}}{\text{weight of oxygen in standard}} \quad (2)$$

The fast neutron generator is actually a deuteron accelerator used to produce 14 MeV neutrons by means of the  $^3\text{He}(d,n)^4\text{He}$  nuclear reaction. It is a commercially available unit with accelerating energies of 100-600 KeV and a deuteron beam of 1-5 milliamps and a total neutron output of  $10^9$ - $10^{11}$  n/second.

As 14 MeV neutrons interact with other components of the Ti-alloy such as V or Nb, any produced gamma-ray has much lower energy than 6.1 MeV produced by  $^{16}\text{N}$ . Lower gamma-ray energies are not counted and are discriminated against in the single channel gamma-ray spectrometer. The presence of elemental fluorine in the matrix can produce  $^{16}\text{N}$  by the nuclear reaction of  $^{19}\text{F}(n,\alpha)^{16}\text{N}$ . The probability of interaction for this reaction is low and if the ratio of oxygen to fluorine is 10:1, the error produced is 5%. It is very unlikely for fluorine to be present in any significant level in titanium, or metals in general, to cause any serious errors to the oxygen measurements.



## 4.0 EXPERIMENTAL

### 4.1 Instrumentation

The fast neutron generator available to SAI is a product of Kaman Science, Inc. (Fig 1). It produces a total of  $10^{11}$  n/sec in  $4\pi$  geometry or a neutron flux of  $10^8$  n/cm<sup>2</sup>/sec at the sample's irradiation position. The system is equipped with a dual automatic counting and transfer system (Fig 2). Samples to be irradiated are encapsulated in 3 1/2" x 3/4" polyethylene, which are sent by pressurized air to the irradiation position in the generator. The gamma-ray counting setup (Fig 3) consists of two 4" x 4" NaI(TL) detectors in a lead shield connected separately to a single-channel analyzer and a total count printer. Counts of both sample and standard are printed out after each irradiation. The fast Neutron generator is shielded with concrete to prevent fast neutrons from reaching operating personnel.

### 4.2 Procedure

#### A - SAMPLE AND STANDARD PREPARATION

SAI received five titanium bars of alloy Ti-6211 (Fig 4). The bars had dimensions of 1" x 1" x 6" and were numbered as follows:

NRL-A-5-1

NRL-B-5-1

NRL-C-5-1

NRL-D-5-1

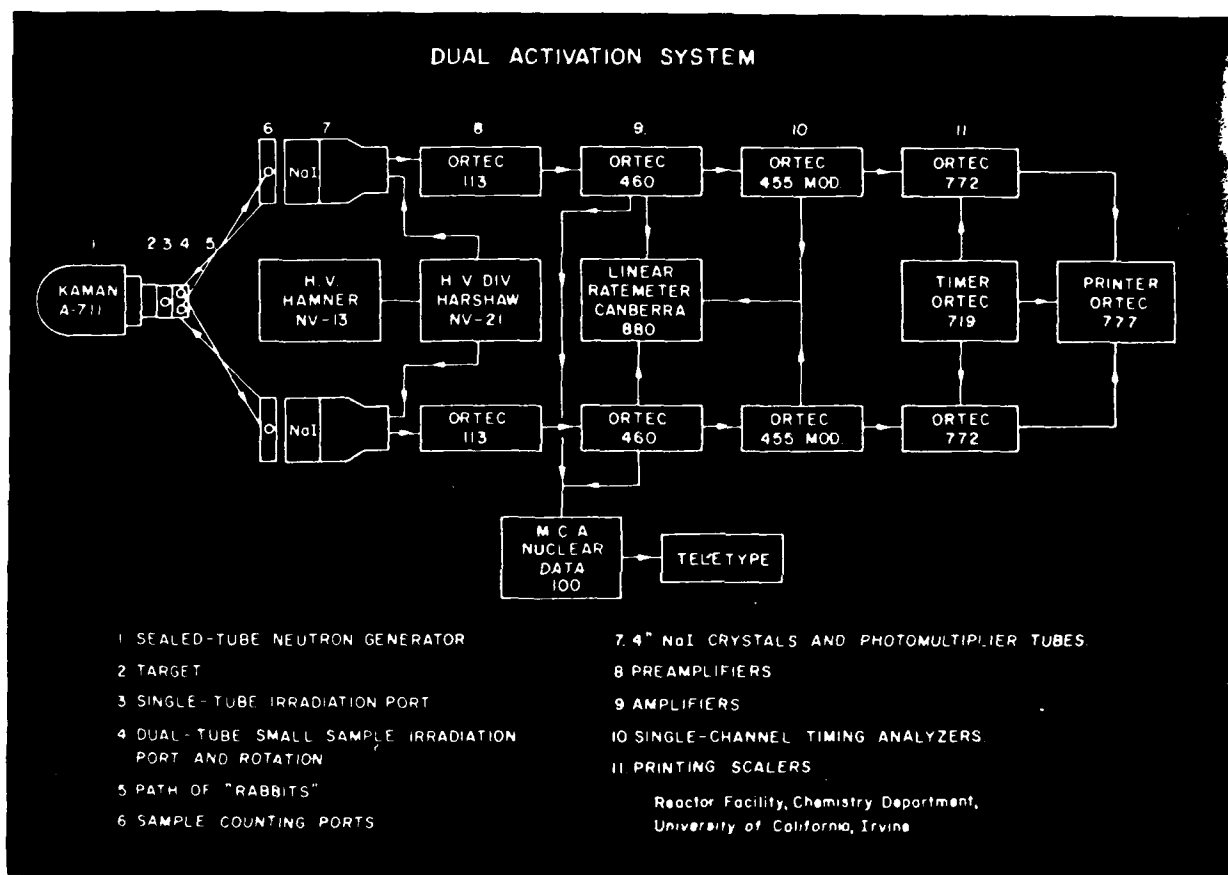
Each of these titanium alloy bars were fabricated into five cylinders, each of which had 0.79 cm diameters and a length of 3.75 cm. Extreme care was exercised in the machine shop to prevent the mixing of the different titanium alloys. In order to remove any possible surface contamination, each fabricated titanium cylinder was washed with the following reagents in this numerical order:

1. carbon tetrachloride
2. reagent-grade acetone
3. distilled deionized water
4. concentrated nitric and hydrofluoric acid mixture 4:1



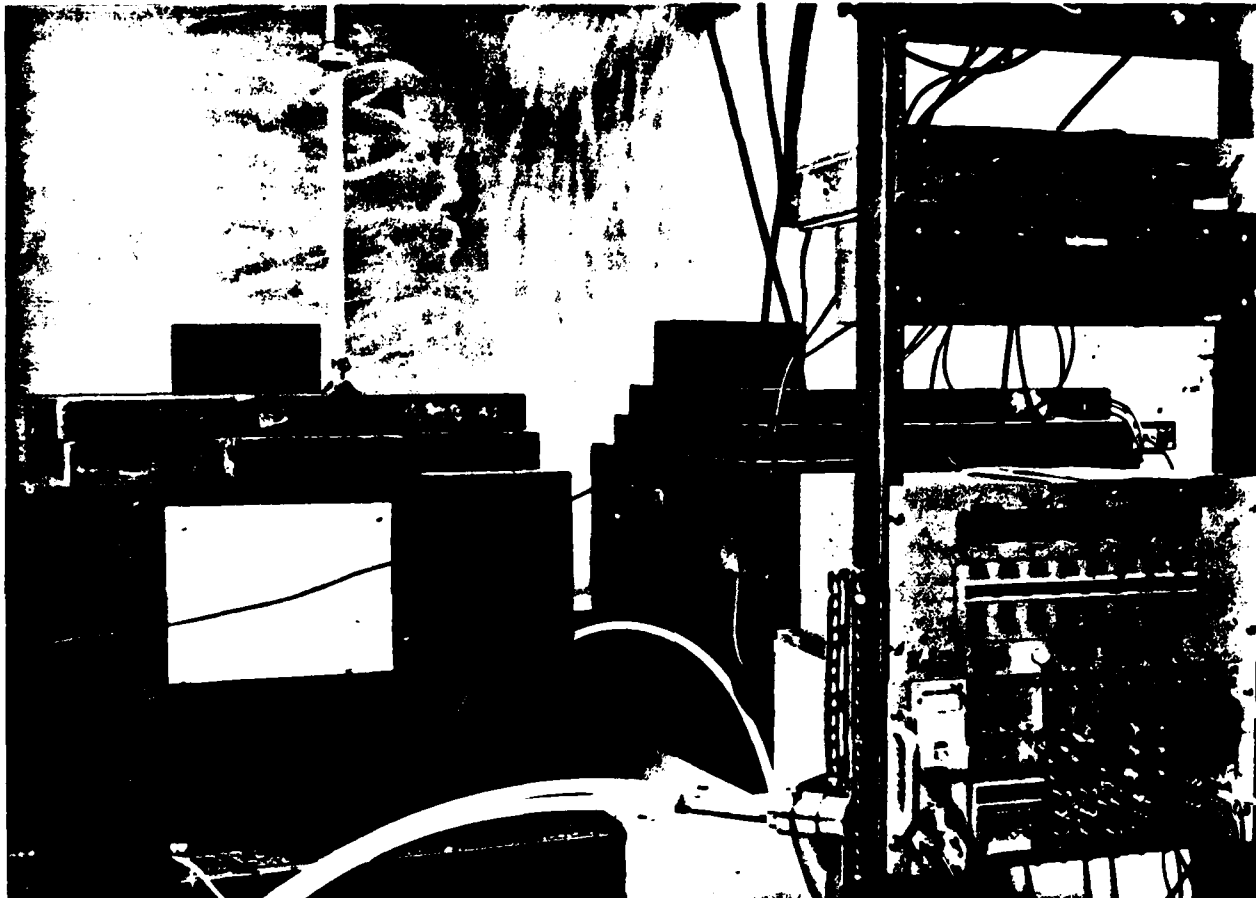
SAI-82AA-14

Figure 1. Fast Neutron Generator.



SAI-82AA-15

Figure 2. Dual Activation and Transfer System.



SAI-82AA-16

Figure 3. Gamma-Ray Counting System.

5. distilled deionized water
6. reagent-grade acetone
7. dried with heat lamp

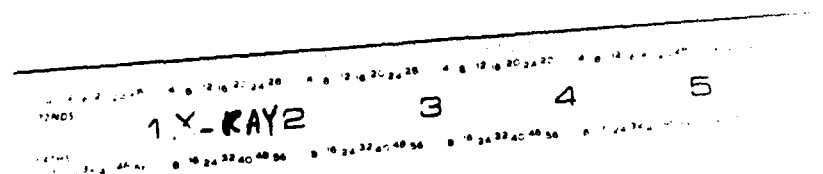
It was then encapsulated and neat sealed in 1 3/4" x 3/4" polyethylene irradiation vials as shown in Figure 5, 6. Five oxygen standards were prepared by filling each polyethylene irradiation vial with two grams of benzoic acid of known oxygen content and sealing them. Blanks (empty polyethylene irradiation vials) were prepared by flushing them with nitrogen gas and heat sealing them. (Fig. 7)

#### B - IRRADIATION AND COUNTING

Titanium alloy samples and benzoic acid standards were transferred together by pressurized air to the irradiation position in the fast neutron generator. They were irradiated for 20 seconds at a flux of  $1 \times 10^8$  n/cm<sup>2</sup>/sec. During irradiation, they were rotated along their axis to receive a homogeneous exposure of neutrons.

After irradiation, they were allowed to decay for 3 seconds and were transferred by pressurized air into two separate NaI(TL) gamma-ray detectors, each connected to a single-channel gamma-ray analyzer and a line printer.

Each sample and standard were counted for 20 seconds. The counts, due to oxygen activation in the titanium alloy and oxygen activation of the benzoic acid standard, were recorded on two separate printers. The operation of irradiating and counting was repeated several times on each sample in order to get a good replication of results.



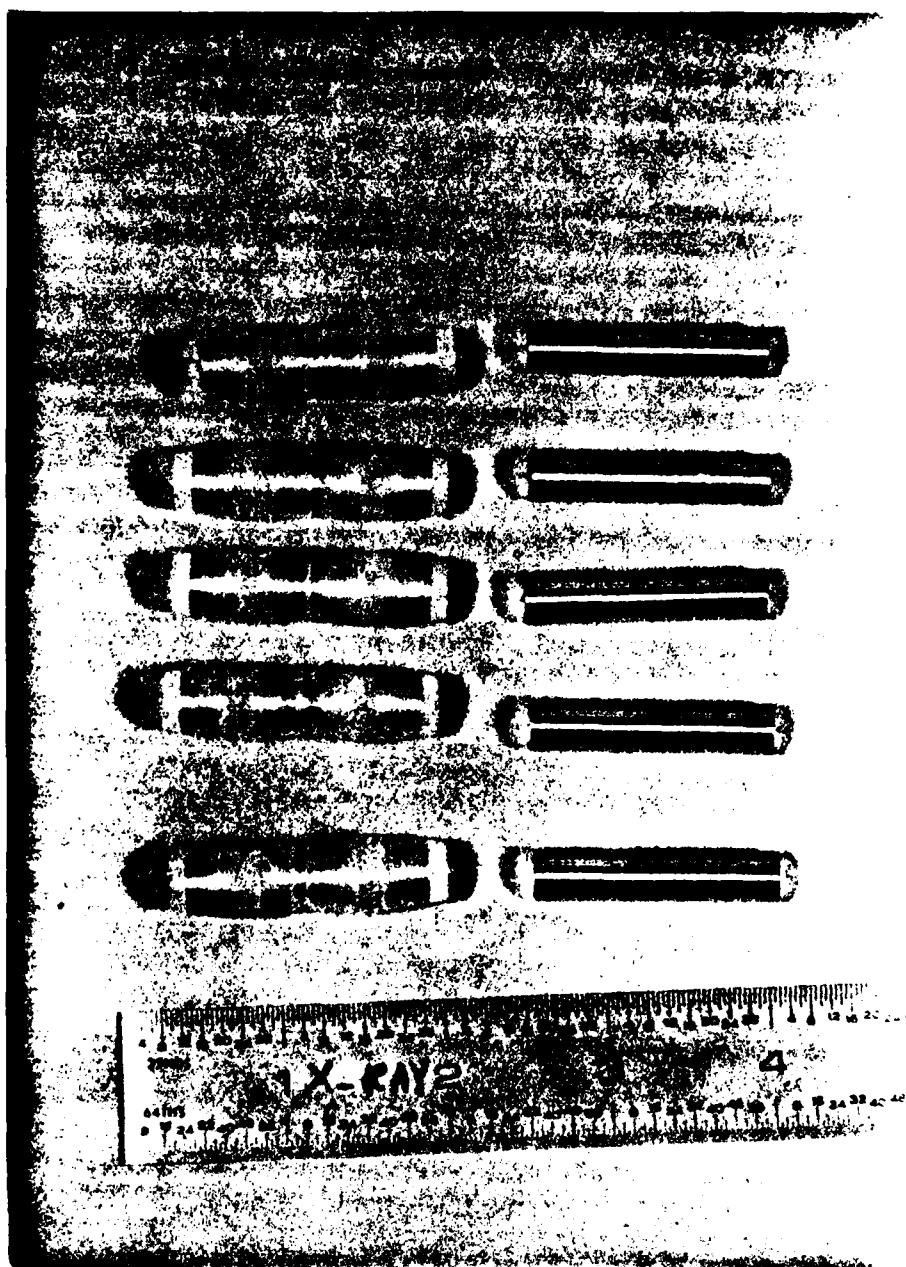
SAI-82AA-11

Figure 4. Titanium Alloy-6211.



SAI-82AA-12

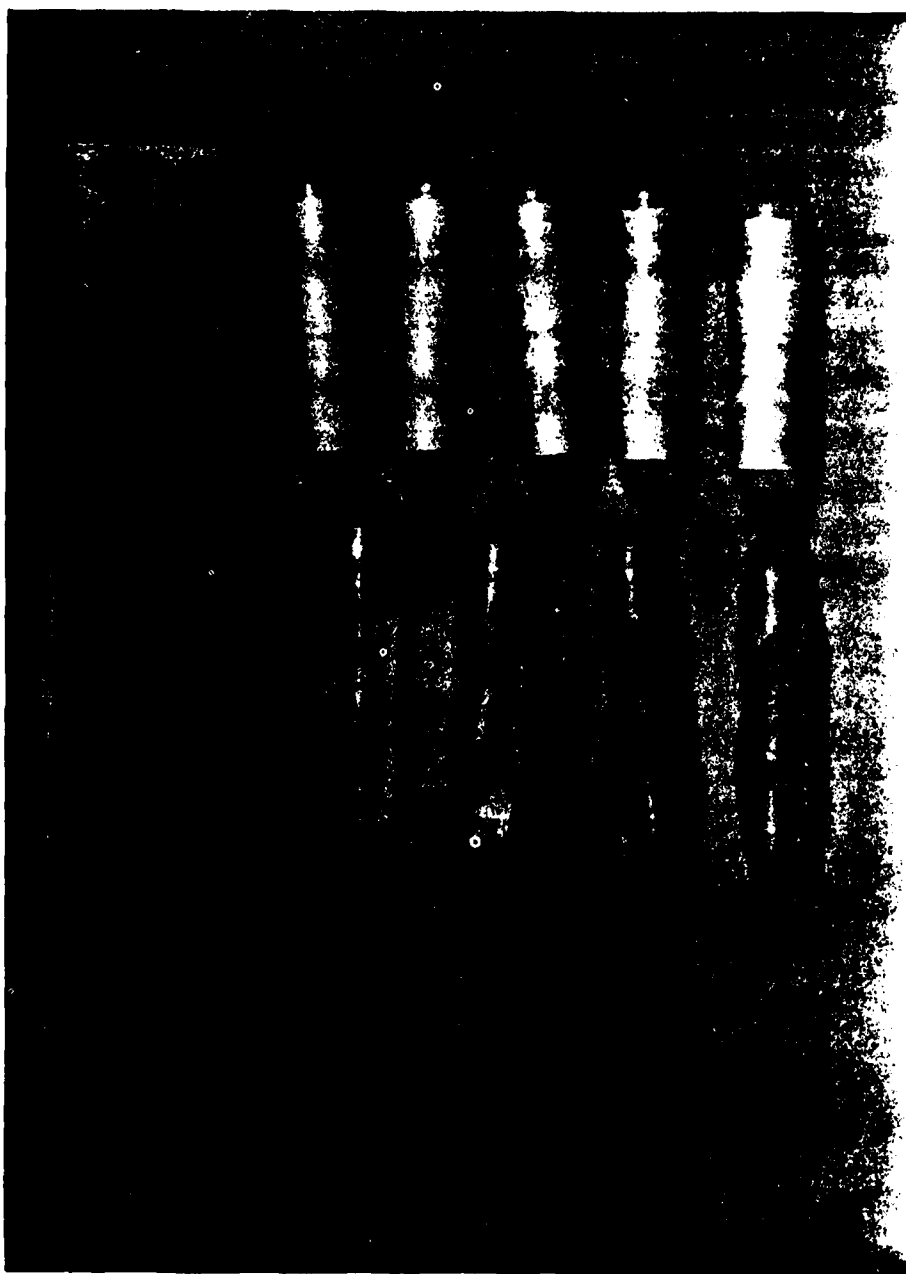
Figure 5. Irradiation Capsul



SAI-82AA-13

Figure 6. Titanium alloy bone fixation capsule





SAI-82AA-10

Figure 7. Oxygen Standards of Benzoic Acid.

## 5.0 EVALUATION OF RESULTS

Knowing the oxygen content, and the count rate in the benzoic acid standards, and the count rate of each irradiated titanium cylinder, the mass of oxygen in each irradiated titanium cylinder was calculated. Table (1) shows a very good replication of the percentage of oxygen in each titanium cylinder analyzed. Table (2) shows the average oxygen content of five replicates from each of titanium bar A, B, C, D, and E. The relative error in these determinations is small and ranges between 2.8% and 3.9%.

More confidence in the accuracy of the oxygen values obtained by fast neutron activation is derived when the obtained results agree very well with those using vacuum fusion, Table (2). A correlation coefficient of 0.994 between the two sets of independent oxygen analysis is obtained. Furthermore, when 1 gm of  $H_2O$  sample was analyzed by fast neutron activation using benzoic acid as standards, water was experimentally found to contain 89.36% oxygen while theoretically it contains 88.88%.

SAMPLE		% OXYGEN		$\sigma$
A <sub>1</sub>	=	0.0661 %	$\pm$	0.0013
A <sub>2</sub>	=	0.0708 %	$\pm$	0.0011
A <sub>3</sub>	=	0.0667 %	$\pm$	0.0014
A <sub>4</sub>	=	0.0674 %	$\pm$	0.0015
A <sub>5</sub>	=	0.0668 %	$\pm$	0.0014

Average = 0.0675 %  $\pm$  2.8 %

B <sub>1</sub>	=	0.125	$\pm$	0.0016
B <sub>2</sub>	=	0.125	$\pm$	0.0020
B <sub>3</sub>	=	0.126	$\pm$	0.0036
B <sub>4</sub>	=	0.126	$\pm$	0.0021
B <sub>5</sub>	=	0.134	$\pm$	0.0034

Average = 0.127 %  $\pm$  3.0%

C <sub>1</sub>	=	0.160	$\pm$	0.0027
C <sub>2</sub>	=	0.167	$\pm$	0.0029
C <sub>3</sub>	=	0.170	$\pm$	0.0027
C <sub>4</sub>	=	0.168	$\pm$	0.0022
C <sub>5</sub>	=	0.161	$\pm$	0.0019

Average = 0.165 %  $\pm$  2.7 %

D <sub>1</sub>	=	0.226	$\pm$	0.0061
D <sub>2</sub>	=	0.234	$\pm$	0.0041
D <sub>3</sub>	=	0.235	$\pm$	0.0017
D <sub>4</sub>	=	0.239	$\pm$	0.0041
D <sub>5</sub>	=	0.224	$\pm$	0.0041

Average = 0.231 %  $\pm$  2.7 %

E <sub>1</sub>	=	0.253	$\pm$	0.0034
E <sub>2</sub>	=	0.268	$\pm$	0.0028
E <sub>3</sub>	=	0.278	$\pm$	0.0022
E <sub>4</sub>	=	0.278	$\pm$	0.0047
E <sub>5</sub>	=	0.275	$\pm$	0.0038

Average 0.270 %  $\pm$  3.9%

TABLE 1 Oxygen Content of Ti-6211

<u>SAMPLE</u>		<u>NAA MEASURED % OXYGEN</u>		<u>RELATIVE ERROR</u>	<u>VACUUM FUSION % OXYGEN</u>
NRL-A-5-1	=	0.0675	<u>+</u>	2.8 %	0.075
NRL-B-5-1	=	0.127	<u>+</u>	3.0 %	0.136
NRL-C-5-1	=	0.165	<u>+</u>	2.7 %	0.194
NRL-D-5-1	=	0.231	<u>+</u>	2.7 %	0.238
NRL-E-5-1	=	0.270	<u>+</u>	3.9 %	0.290

Correlation Coefficient = 0.994

Slope = 1.038

Intercept = 0.0081

TABLE 2 Agreement of Oxygen Values Produced  
By NAAI with Those by Vacuum Fusion

## 6.0 CONCLUSION

It can be concluded from this study that fast neutron activation analysis provides a nondestructive analysis for oxygen content in titanium alloys. This analysis proved to be interference-free, to reach parts per million sensitivity, and to provide fast, accurate, and reliable results.

## 7.0 BIBLIOGRAPHY

1. S. S. Nargolwalla, E. P. Przybylowicz, Activation Analysis with Neutron Generators, Wiley, New York, 1973.
2. D. E. Wood, Nucl. Instr. Methods, 92 (1971).
3. R. L. Schulte, E. A. Kamykowski, J. of Radioanalytical Chem., 43 (1978) 233.
4. S. S. Nargolwalla, E. P. Przybylowicz, J. E. Suddueth, and S. L. Birkhead, Modern Trends in Activation Analysis (1968), NBS S. P. 312, p. 879.
5. Blake, K. R. ; Martin, T. C.; Morgan, I. L.; Houston C. D., Measurement of Contamination of High-Purity Beryllium Samples. Proceedings of International Conference on Modern Trends in Activation Analysis, pp 76-81, (1965).
6. Vogt, J. R. and Ehman, W. D., "Nondestructive Determination of Silicon and Oxygen in Meteorites by Fast-Neutron Activation Analysis". Proceedings of the International conference on Modern Trends in Activation Analysis, pp 82-85, (1965).
7. Wood, J. D.; Downton, D. W.; and Blake, J. M., "Fast-Neutron Activation Analysis System with Industrial Applications." Proceedings of the International Conference on Modern Trends in Activation Analysis, pp 175-181, (1965).
8. Wood, P. E. and Paztor, L. C. "A Comparison of Neutron-Activation Analysis and Vacuum-Fusion Analysis of the Oxygen Content of Steel". Proceedings of the International Conference on Modern Trends in Activation Analysis, pp 259-264, (1965).
9. Bryne, J. T.; Illslay, C. T. and Price, H. J., "An Automatic System for the Determination of Oxygen in Beryllium Metal Components". Proceedings of the International Conference on Modern Trends in Activation Analysis, pp 304-309, April (1965).

## SECTION 14

# NEUTRON ACTIVATION ANALYSIS OF TITANIUM WITH OXYGEN CONTAMINATION

I. L. Morgan

*Scientific Measurement Systems, Inc.*  
*Austin, TX 78759*

Measurement of trace amounts of elements in a given composition is of great interest in many areas of industrial as well as academic activities. There are a number of methods available, such as chemical analysis, gas chromatography, etc., which are capable of yielding a high degree of accuracy. However, these procedures necessarily destroy the sample. Neutron activation analysis for the trace elements is an attractive and accurate method, where no destruction of the sample is warranted.

The present investigations were conducted for assessing the  $O_2^N$  content in titanium metal samples via neutron activation analysis. The  $O_2^N$  content was measured to a few hundred parts per million with an accuracy of  $\pm 5\%$ .

Availability of high energy and high flux neutron generators, in addition to the results of this study, indicate that the neutron activation analysis approach to nondestructive assessment of object compositions is not only feasible but could provide an advanced, accurate and rapid technology.



AD-P004 134

## I. Introduction

In many areas the measurement of trace amounts of elements present in a given composition is of great interest and significance. Such a measurement is possible to a high degree of accuracy through conventional methods such as chemical analysis, gas chromatography, etc. Although accurate, such techniques necessarily entail destruction of the sample during the testing procedure. There is a wide field of activities where a nondestructive measurement technique is of great need. Of many such nondestructive methods relevant to the measurement of trace amounts of elements, the neutron activation analysis provides an attractive, rapid and accurate approach.

The present study involves measurements of trace amounts of oxygen present in Titanium metal. The determination of  $O_2$  content, in the samples of Ti provided, was made using the method of neutron activation. The  $O_2$  content down to a few hundred parts per million were measured.

This report is organized as follows: Section II presents a brief theoretical discussion of the underlying physical principles of the technique. In Section III a description of the experimental setup is provided. The experimental procedure is described in Section IV. Section V contains the data obtained on various samples. In Section VI the procedure for data analysis is included along with the final results. Section VII summarizes the conclusions.



## II. Theory

Neutron activation technique for qualitative, as well as quantitative analysis, was first reported<sup>1</sup> as early as in 1936; however, it did not receive a widespread application until the mid-50s when the sources for neutron irradiation became more easily available.

Several monographs and texts on activation analysis are available<sup>2-8</sup>. These primarily discuss the activation analysis using reactor neutrons as opposed to isotopic neutron sources. In the present report we restrict ourselves only to the discussion of the principles underlying the technique, omitting discussions on the neutron sources.

Neutron activation analysis essentially involves bombardment of a sample with a flux of neutrons which, upon interaction, converts the elements present in the sample to various radionuclides. These nuclides decay through emission of characteristic radiation at a rate well defined for the nuclide. The resultant emission energy spectrum and the associated half-life permit the unambiguous identification of the elements present in the sample.

The activity of a particular radionuclide produced by such a nuclear reaction from a nucleus N can be expressed in terms of the operational parameters of the technique as follows:

$$A = B \cdot \epsilon \cdot N \cdot \sigma \cdot \phi \cdot \left\{ 1 - e^{-\frac{0.693 t_a}{T_{1/2}}} \right\} \cdot \left\{ e^{-\frac{0.693 t_d}{T_{1/2}}} \right\} \quad (1)$$

where

$A$  = the measured count-rate at time  $t_d$ , in counts/sec

$B$  = the branching ratio for the emission being measured

$\epsilon$  = the detection efficiency of the counter

$N$  = the number of target nuclei of element  $N$  exposed to the incident neutron flux.

$\sigma$  = the activation cross section of the particular reaction for element  $N$  at the given incident particle energy ( $\text{cm}^2$ )

$\phi$  = the particle flux of constant intensity and energy, (particles/ $\text{cm}^2$  - sec)

$t_a$  = irradiation time

$t_d$  = decay time from the termination of the irradiation to the start of counting.

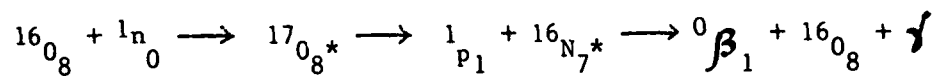
$T_{1/2}$  = the half-life of the product nuclei.

The factors,  $\epsilon$ ,  $\sigma$  and  $\phi$  can vary considerably with sample size, time, irradiation conditions, counting arrangement, etc. Hence, during a particular analysis these are not evaluated specifically. Instead, a comparative method is used which provides higher accuracy.

In this method a set of standards, containing a known amount of the unknown element,  $N$ , is first irradiated. The activity of these standards is then compared with the activity of the sample and the amount of the unknown element,  $N$ , in the sample is determined from the relation,

$$\frac{\text{Amount of element } N \text{ in the sample}}{\text{Activity of the sample}} = \frac{\text{Amount of } N \text{ in the standard}}{\text{Activity of the standard}} \quad (2)$$

For the unknown element in the present case, namely, oxygen, the following reaction yields the information required.



$^{16}_{N7}$ , produced in this reaction, undergoes a gamma decay with a 7.35 sec.

half-life. The gamma emissions are at 7.1 MeV and 6.1 MeV.

### III. Experimental Setup

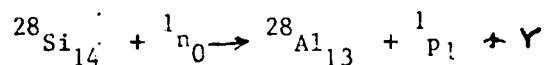
A schematic of the experimental apparatus and the peripheral equipment is shown in Figure 1. The system consists of a neutron generator, a NaI scintillation detector, a multichannel pulse-height analyzer and a data storage facility.

A Texas Nuclear, Inc. neutron generator, which is a part of the facilities at the Balcones Research Center of The University of Texas at Austin, was utilized for the set of experiments conducted during this study. This generator produces 14 MeV neutrons via the nuclear reaction,



The activity of the irradiated sample was examined through an Isotopes Inc. 3" x 3" NaI(Th) crystal detector with a phototube voltage of 600-800 V. The output signal from the phototube was preamplified through an Ortec 118A Preamplifier unit and the final amplification was made through a Canberra 1417 Spectroscopy Amplifier. The amplified signal was analyzed on a TN 1750 Multichannel Analyzer.

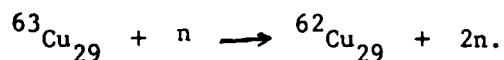
The system was calibrated with a  ${}^{137}\text{Cs}$  source which provides 0.661 MeV gamma rays. Another calibration source used was  ${}^{28}\text{Al}$  ( $\sim 1.78$  MeV gamma rays), obtained from silicone via the reaction



Since the neutron flux during any experiment varies, the flux was monitored continuously during the experiments.

Two techniques were employed for monitoring the neutron flux. One technique employed a simultaneous irradiation of a copper foil along with the sample and the other one employed a Texas Nuclear Neutron Dosimeter.

The copper foil approach to the flux measurements utilized a set of Reactor Experiments, Inc. high purity copper foils of mass  $\sim 0.3$  gms each. During an irradiation by a neutron flux, copper undergoes the nuclear reaction



The resultant radionuclide,  ${}^{62}\text{Cu}_{29}$ , subsequently undergoes a  $\beta^+$  decay with a half-life of 9.73 minutes. The positron annihilations produce 0.511 MeV gamma rays, the intensity of which is a measure of the irradiation flux.

The neutron dosimeter consists of a  $\text{Li}_6\text{I}$  detector, embedded centrally within a 12-inch diameter polyethelyn sphere. A pair of Canberra Scalar/Timer counters was used for counting the output from this dosimeter. The counts obtained are directly proportional to the neutron flux during any irradiation interval.

#### IV. Neutron Activation Analysis

##### Experimental Procedure

A. Samples: Five Titanium samples of dimensions 0.25" x 1" x 5" were received for the activation analysis. Each sample was cut into three equal sized pieces to permit a complete irradiation exposure.

B. Preparation of Samples: The samples were treated for the surface contaminations using a standard procedure termed "etching". The etching procedure consisted of cleansing the samples with a 50:1:1 solution of  $H_2O$ , HF and  $HNO_3$ . The etching compound was then removed by rinsing the samples in aqueous NaOH solution, followed by rinsing with alcohol. The samples were treated for the contaminations immediately prior to the irradiation.

C. Activation: Cleaned samples were each irradiated for a fixed duration of 60 secs; and then transferred to the NaI detector assembly. The delay time, from the end of the irradiation period to the start of the counting procedure, was preset to be 10 seconds. For each case, cumulative counts for 30 seconds duration were collected using the multichannel analyzer, (MCA). The resultant gamma emission spectra, collected on the MCA, were stored on a magnetic tape recorder unit, for each experiment. As explained in Section III, simultaneous measurements on copper foils were made to monitor the neutron flux. The delay time before the commencement of the counting was selected to be seven minutes for all copper foil measurements.

For the measurements on the oxygen content, the gamma emission spectra of the samples were analyzed with an energy window spanning a 4 MeV - 7.7 MeV range. As discussed in Section II, this energy window covers the  $^{16}\text{N}_7$  gamma emission lines. The lower energy cutoff of 4 MeV is above the emission spectra of the other elements present in the sample.

After performing a number of pilot experiments on the flux monitoring technique, the  $\text{Li}_6\text{I}$  dosimeter approach was selected as the more convenient and accurate method.

## V. Data

The raw data obtained from the activation analysis of the five samples are given in Table I. For each of the samples, the activation time,  $t_a$ , was 60 seconds, the delay time,  $t_d$ , was 10 seconds and the activity counts were collected for 30 seconds, ( $t_c$ ). The neutron flux was measured with a Bonner Ball  $Li_6I$  dosimeter.

A Borax ( $Na_2 B_4 O_7 \cdot 10 H_2O$ ) sample was used as the standard. The data obtained from the activation of the standard are given below.

Molecular weight of the standard	= 382
Mass of the standard	= 3.8211 gm
$O_2$ - content of the standard	= 2.7208 gm
Activating time ( $t_d$ )	= 60 sec
Delay time ( $t_d$ )	= 8.1 sec
Counting time ( $t_c$ )	= 30 sec
Bonner Ball counts	= 34527
Activity counts (gross)	= 31724
Background counts	= 306
Net activity counts (gross - background)	= 31418



Table I

<u>Sample</u>	<u>Mass (gm)</u>	<u>BB counts</u>	<u>Activity (net) Counts</u>
A	99.3199	31 820	675*
B	93.69	15 080	1165*
C	31.1336	17 318	408**
D	65.7811	17 057	1027***
E	63.3323	16 971	1100***

\* Average of six experiments

\*\* Average of two experiments

\*\*\* Average of four experiments

## VI. Data Analysis

The net counts obtained in all experiments need to be corrected for the delay times involved. In terms of the time intervals involved, the activity counts are related to the initial activity by

$$\text{counts} = (\text{initial activity}) \times \text{correction factor (CF)}$$

where,

$$\text{CF} = (1 - e^{-\lambda t_a}) e^{-\lambda t_d} \cdot (e^{-\lambda t_1} - e^{-\lambda t_2})$$

$t_1$  is the time at which the count measurement begins and  $t_2$  is the end of the measurement interval.  $\lambda = \ln 2 / T_{1/2}$ , is the decay constant.

After correcting the data for the delay, the counts obtained for each sample were normalized to a reference Bonner Ball count (RBBC). In this analysis we have taken the Borax case Bonner Ball counts as the reference. Thus the corrected normalized activity counts (CNC) are given by,

$$\text{CNC} = \frac{\text{Sample activity counts} \times \text{RBBC}}{(\text{CF}) \cdot (\text{Sample Bonner Ball Counts})}$$

The  $O_2$  contents of the samples was determined using two different standards. One was the Borax standard and the other one was selected to be the sample #E. From the chemical assays which were provided with the samples, the  $O_2$  content of the sample #E was known to be 0.29% by weight.

The calculations for the  $O_2$  contents of the samples were made using the relation

$$\text{Mass of } O_2 \text{ in Sample} = K \cdot (\text{CNC of samples})$$

where,

$$K = \frac{\text{Mass of } O_2 \text{ in Standard}}{\text{CNC of Standard}}$$

For Borax,  $K = 4.34 \times 10^{-7}$ . For the sample #E as the standard,  $K = 4.3 \times 10^{-7}$ .

The results of these calculations are given in Table II.

For the case of Borax standard, corrections were made to account for the differences in the detection geometry. The distance of the Borax sample from the detector front was twice the distance at which all other samples were placed. Thus a correction was required for the difference in the solid angles subtended by the samples and the standard. This correction is already included in the computation of the K factor above.

Table II

Sample	CNC ( $\times 10^5$ )	% Oxygen by Weight			
		Borax std.	#E std.	Error*	Chemical assay
A	1.29173	0.0607	0.06025	$\pm 0.0023$	0.075
B	3.04753	0.1410	0.13990	$\pm 0.0041$	0.136
C	1.54570	0.2151	0.21350	$\pm 0.0107$	0.194
C	3.95019	0.2602	0.25820	$\pm 0.0080$	0.238
D	4.25241	0.2909	-	$\pm 0.0090$	0.290

\* Error estimates are made assuming gaussian distributions of the counts.

## VII. Conclusions

The Oxygen content of the given Titanium samples were determined with the accuracies shown in Table II. Two different standards were employed for the neutron activation analysis carried out during this project. One standard, composed of Borax, was a high  $O_2$  content standard ( $\sim 72\%$   $O_2$  by weight). The other standard, one of the samples, was a lower  $O_2$  content standard ( $0.29\%$   $O_2$  by weight). The results obtained using these standards are comparable. The estimated error of these results is approximately 3%.

The accuracies attainable in the neutron activation approach for determining trace amounts of  $O_2$ , can be improved by the following considerations.

1. Increasing the neutron yields of the neutron generator,
2. Decreasing the sample transport time, i.e. minimizing the delay times,
3. Increasing the detector efficiencies by employing multiple and/or larger NaI detectors,
4. Optimizing the lower energy gamma ray cut-off, and
5. Decreasing the background counts by improving the detector assembly shielding.

The neutron activation analysis approach in assessing trace amounts of  $O_2$  appears to be quite accurate and  $O_2$  contents down to a few parts per million can be accurately obtained. The accuracies obtainable are comparable to those from chemical analysis. However, the neutron activation techniques have the advantage in that the samples are tested nondestructively and results obtained in a few minutes.

## Appendix

The muonic x-ray spectroscopic approach to the determination of the oxygen contents has not been undertaken yet, due to the inavailability of the muon production facilities. There are two facilities for the muon production available. The Los Alamos Meson Physics Facility and the TRIUMPH laboratories, Vancouver, British Columbia. The time for conducting the proposed research, on any of these systems, was not available from September 1981 until March 1982, and is not expected to be available until September 1982.

There have not been much data available on the muonic x-ray studies on pure oxygen. However, we include here, some rate estimates for the Titanium samples with oxygen contaminations.

There are data on the oxygen K lines for  $V_2O_3$  and  $V_2O_5$ . (Knight et al <sup>9</sup>) For the sake of estimating what could be expected from  $TiO$  and  $TiO_2$  samples, we make the following analogies on a somewhat speculative basis.

Let us assume the equivalences,

$TiO$  ( $Ti/O = 1$ ) equivalent to  $V_2O_3$  ( $V/O = 0.67$ )

and  $TiO_2$  ( $Ti/O = 0.5$ ) equivalent to  $V_2O_5$  ( $V/O = 0.40$ ).

Then from the data obtained by Knight et al, we have the ratios of the K lines,

$$\frac{O K_{\beta}}{O K_{\alpha}} = 0.25 \pm 0.05 \text{ for } V_2O_3$$

$$\frac{O K_{\beta}}{O K_{\alpha}} = 0.260 \pm 0.040 \text{ for } V_2O_5.$$

These indicate that there is no discernible difference for the  $K_{\beta}/K_{\alpha}$  ratios.

The same would be true for the Titanium oxides.

However, assuming that  $O K_{\beta}/O K_{\alpha} \approx 0.25$  for  $TiO$  and  $0.30$  for  $TiO_2$ , we can make some estimates on the time required for measuring each ratio with an accuracy of  $\pm 0.01$  or  $\pm 4\%$ . Based purely on the statistical requirements, this would require 15 625 counts in the  $O K_{\alpha}$  line and 3906 counts in the  $O K_{\beta}$  line. From the discussion with the group at LAMPF<sup>10</sup>, it appears that approximately 780 hours would be required to obtain 15 625 counts in the oxygen K lines.

These estimates are rather crude and are based on the assumptions made on the rates. Even if these were off by a factor of ten, it is conceivable that times as low as 150 to 200 hours would be required for each sample.

## References

- <sup>1</sup>G. Hevesey and H. Levi, Math.-Fys. Medd., 14 (5), 3 (1936),  
Institute of Theoretical Physics, University of Copenhagen.
- <sup>2</sup>R. C. Koch, Activation Analysis Handbook, Academic Press,  
New York, 1960.
- <sup>3</sup>W. S. Lyon, Jr., Ed., Guide to Activation Analysis, Van Nostrand,  
Princeton, New Jersey, 1964.
- <sup>4</sup>D. Taylor, Neutron Irradiation and Activation Analysis, George  
Newnes, London, 1964.
- <sup>5</sup>H. J. M. Bowen and D. Gibbons, Radioactivation Analysis, Oxford  
University Press, London, 1963.
- <sup>6</sup>D. DeSoete, R. Gijbels, and J. Hoste, Neutron Activation Analysis,  
Wiley, New York, in press.
- <sup>7</sup>J. M. A. Lenihan and S. J. Thomson, Eds., Activation Analysis,  
Principles and Applications, Academic Press, New York, 1965.
- <sup>8</sup>S. S. Nargolwalla and E. P. Przybylowicz, Activation Analysis with  
Neutron Generators, Chemical Analysis, a series of monographs on analytical  
chemistry and its applications, Ed. P. J. Elving and J. M. Kolthoff (Wiley,  
New York, 1973), Vol. 39.
- <sup>9</sup>Knight et al, "Chemical Effects in the Capture of Negative Muons,"  
Phys. Rev. A, Vol. 13, No. 1 (1976).
- <sup>10</sup>J. Bradbury (Private Communication).

# NEUTRON ACTIVATION ANALYSIS EXPERIMENTAL APPARATUS

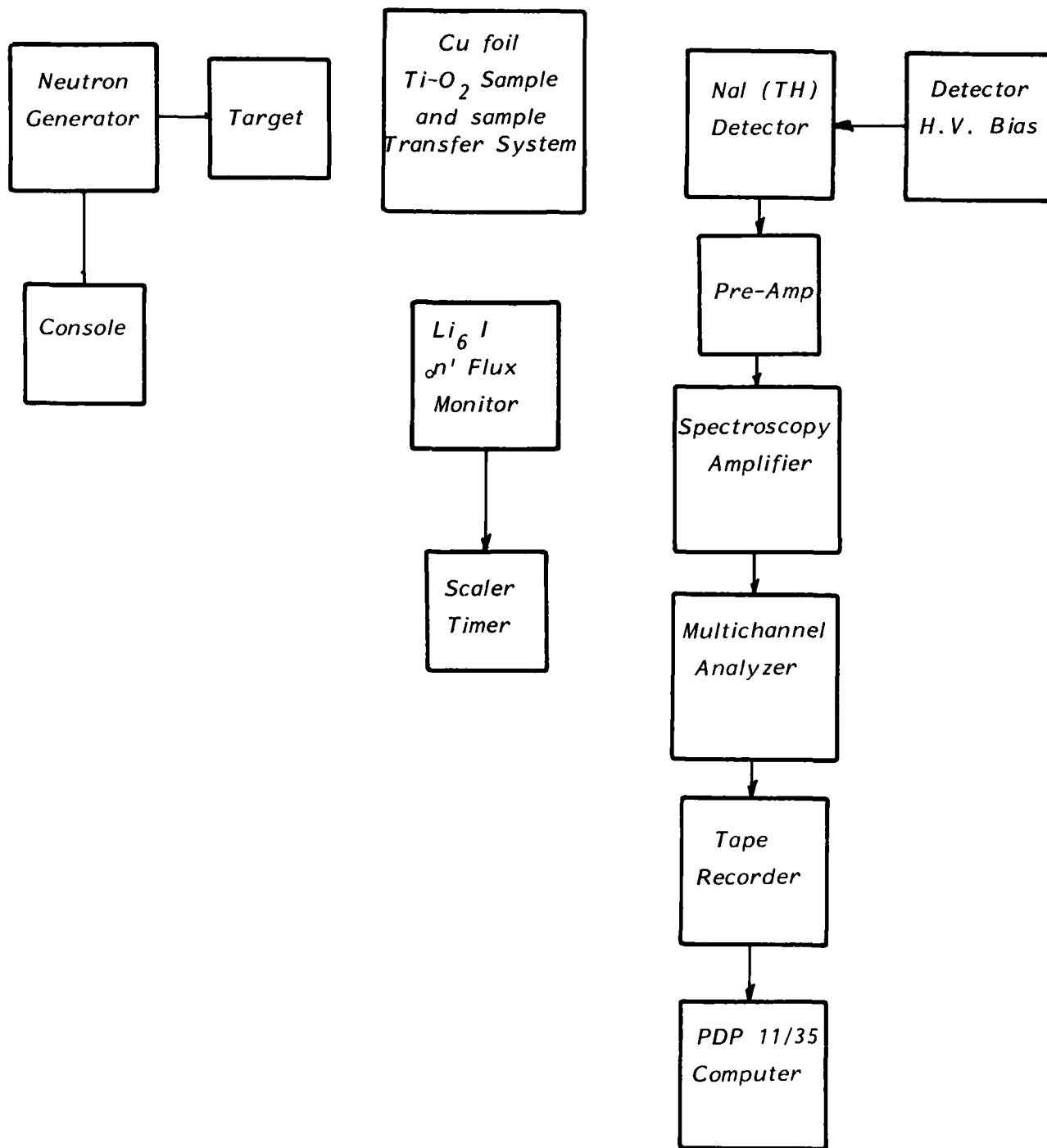


Fig. 1  
282



## SECTION 15

### NONDESTRUCTIVE EVALUATION OF TITANIUM ALLOYS: ESCA, ISS, AND SIMS EXAMINATION OF TITANIUM ALLOY SOLID SURFACES

Gheorghe D. Mateescu and Yoh-Han Pao

*Departments of Chemistry and Electrical Engineering —  
Applied Physics, Case Western Reserve University  
Cleveland, Ohio 44106*

*Oxygen first orbit*

This report will begin with the description of the basic principles and instrumentation of ESCA (Electron Spectroscopy for Chemical Analysis), ISS (Ion Scattering Spectroscopy), and SIMS (Secondary Ion Mass Spectrometry). Particular emphasis will be placed on those aspects which are of immediate relevance to the nondestructive evaluation of titanium alloys such as: the concept of chemical shift in ESCA, the relative surface probing sensitivities of ESCA, ISS, and SIMS, the depth profiling capabilities of these techniques. Preliminary results show that, even at moderate resolution, O1s photoelectron spectra of at least three types of oxygen are obtained for the five different Ti alloy samples. Sputtering by means of argon ion bombardment reveals the extreme sensitivity of titanium to oxygen: the position of the intense Ti2p photoelectron signals corresponds to an oxide which completely covers the surface of the specimen. Carbon 1s spectra served to monitor the degree of contamination. ISS-SIMS measurements provided a better insight into the O/Ti ratio on the surface and in the subsurface layers. Preliminary investigations demonstrate the feasibility of *in situ* studies of fracture surfaces. Instrumental modifications for the execution of such experiments are now in progress. Our conclusion is that, working in ultrahigh vacuum conditions, ESCA-ISS-SIMS (combined, perhaps, with conventional mass spectrometry) constitute adequate means to analyze the degree of surface and interstitial oxidation of Ti alloys.

*Oxygen*

AD-P004 135

## REPORT

Preliminary ESCA (spectra 1-14), SIMS (spectra 15-21) and ISS (spectra 22-25) measurements have been performed on titanium alloy samples. These spectra have been selected from more than 100 which were taken in different conditions to enable us to obtain a good indication about the potential of ESCA, SIMS and ISS in titanium alloy analysis. We will make brief descriptions of each, making sure to equally emphasize advantages and limitations. In the spectrum No. 1, which indicates a binding energy of 284.7 eV for the C1s electron, the curve labeled "as received" shows the high degree of contamination on the surface of the specimen. Washing with acetone and methanol removes most of this contamination which is believed to be mainly oil (highly probable contamination during machining). Spectrum No. 2 shows the opposite trend for oxygen because, after washing, the intensity of the oxygen signal increases while simultaneously shifting towards lower binding energy. This clearly demonstrates that we see now almost exclusively an oxide layer. Some contamination still persists as indicated by the arrow. Spectrum No. 3 confirms the results obtained for carbon and oxygen. The Ti2p lines are

barely seen: they become quite prominent immediately after washing (spectrum 4). So does the aluminum signal (spectrum 5). We should mention that both of the latter elements are present on the surface as oxides.

A more drastic cleaning (with emery paper) reveals a fine structure in the O1s signal. Spectrum 6, which is quite well resolved at high resolutions, i.e. lower analyzer energy: ANEN= 30V (spectrum 7) and ANEN = 20V (spectrum 8). We are probably dealing with three oxygen species belonging to different oxides, (including nonstoichiometric combinations) and residual contamination. Sputtering by Ar ion bombardment (spectrum 9) clearly reduces the surface oxygen to almost exclusively oxide oxygen, which belongs mainly to  $TiO_2$ . Even after 75 minutes sputtering (spectrum 10)  $TiO_2$  is the major component.

All the spectra described above belong to specimen A. A similar procedure was used for specimen C (spectrum 11). The dotted line curve in the middle clearly shows a difference between A and C, as revealed by the O1s spectrum. Please note that the  $TiO_2$  signal (see arrow) is smaller in C. It is interesting to observe that only 2 minutes of sputtering of A exposes aluminum metal with little oxide remaining (see arrow). The much more reactive Ti is still present in its oxide form (spectrum 13). The arrow A indicates where the metal signal should have been. Spectrum 14 shows some unusual form of carbon on the surface but the entire carbon signal disappeared after 75 minutes sputtering.

ESCA is an excellent method for obtaining detailed chemical information about the chemistry of the specimen. Recent

work done by us on super alloys indicates that ESCA used with an ultrahigh vacuum system could also yield semiquantitative results.

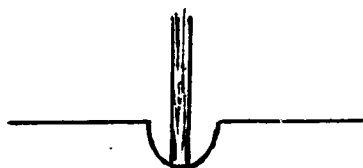
Spectra 15 through 21 are representative of our SIMS measurements. They demonstrate the great potential of this method to identify the species present on the surface, subsurface and in the bulk.

The ISS curves are shown in spectra 22-24 (the lower energy ratio peak is due to neon gas impurity). ISS is quite appropriate for the quantitative analysis of Ti alloys.

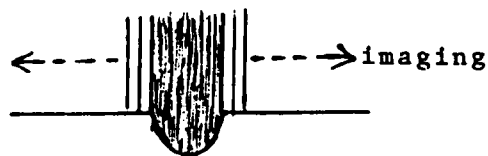
Contrary to SIMS, ISS is matrix independent and sensible only to the first monoatomic layer. It is an excellent method for depth profile analysis.

It was unfortunate that we got a leak in the cryoshroud of our ion pump system and could not work with a better vacuum than  $10^{-8}$  torr. In the meantime, the repair has been completed and we will be able to work in the  $10^{-10}$  torr range.

Table 1 shows relative SIMS intensities measured after 10 and 20 minute sputterings. As mentioned in our proposal, we did not expect quantitative SIMS results because of matrix dependence. However, these results clearly demonstrate that there is much less oxygen in the bulk, as witnessed by the large Ti/TiO ratios obtained with small ion beams. The large beam obviously touches the entire slope of the crater created by sputtering.



Sputter w. large beam  
Measure w. small beam



Sputter and measure  
with large beam

### Conclusions

There are strong indications that all the oxygen existing in the Ti alloy sample studied by us is bound in metal oxide. The oxygen content is maximum at the surface.

It is possible to obtain a quantitative analysis with ISS at  $10^{-10}$  torr. Such vacuum is now available in our laboratory.

SIMS and ESCA will be valuable complements for establishing the chemical composition of the alloys (ISS yield only elemental analysis).

The possible existence of oxygen as interstitial gas will be verified by mass spectrometry executed with samples fractured in situ. The fractures will also be analyzed by ISS and SIMS. This might bring valuable information about the nature of grain boundaries.

APPENDIX

Six Photographs pertaining to this work

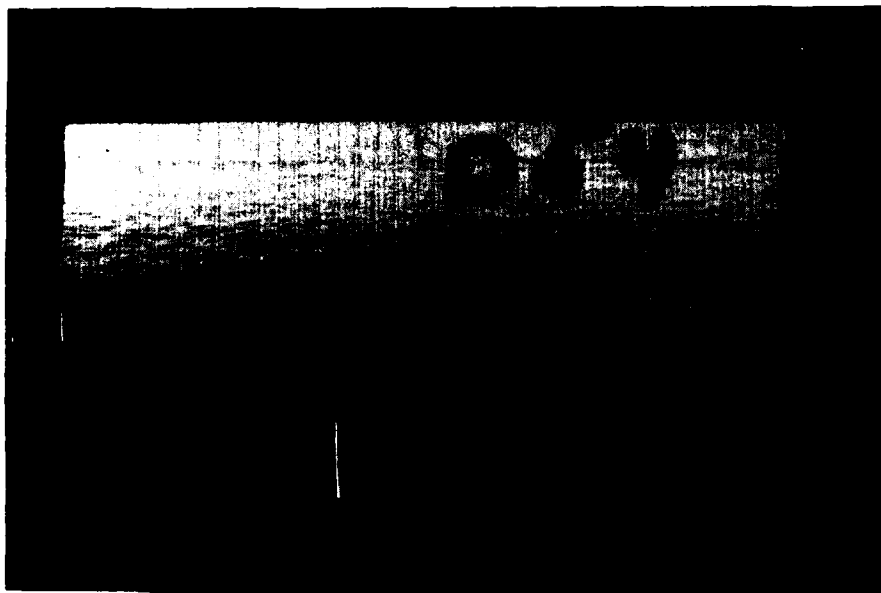


Figure 1. A -The specimen as received  
B -Machined for ESCA-ISS-SIMS  
C -Machined for fracture

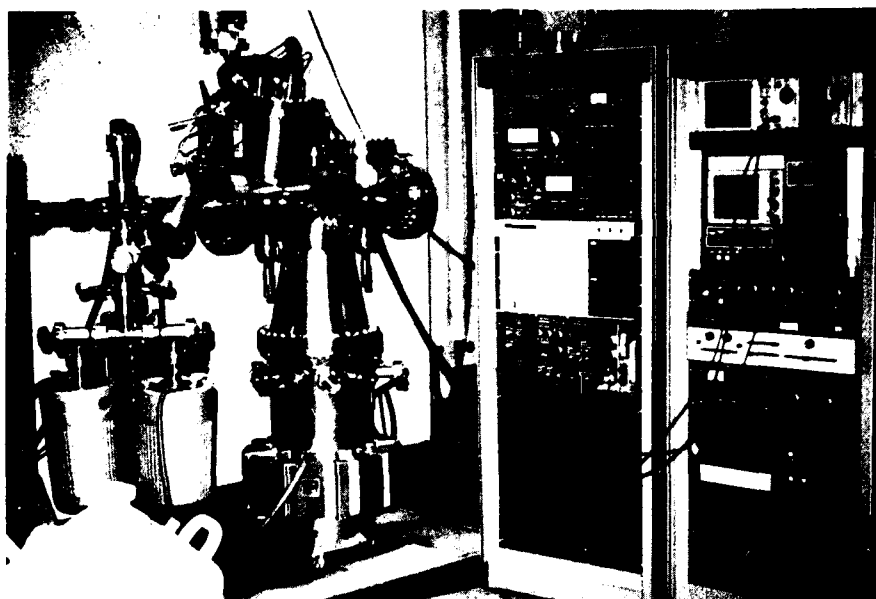


Figure 2. The ISS-SIMS system at CWRU

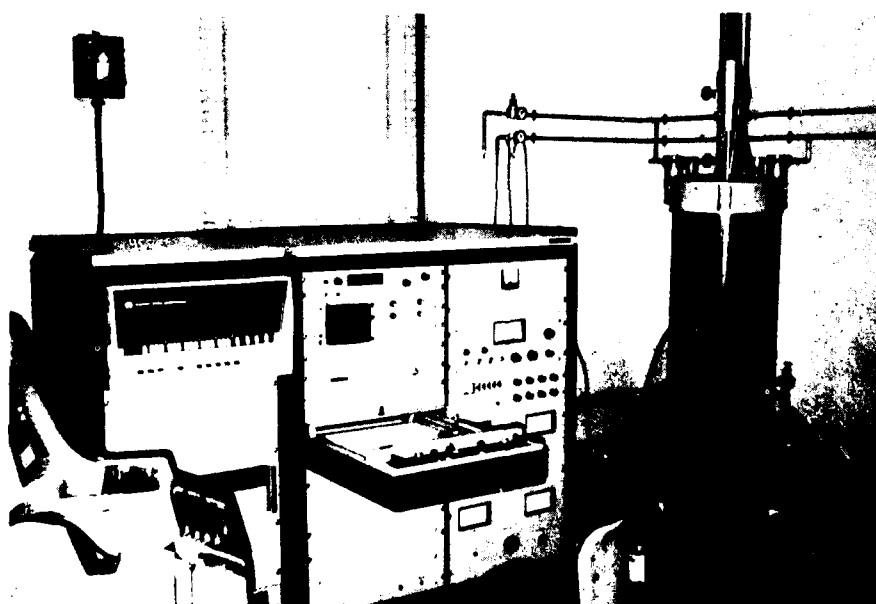


Figure 3. The ESCA system at CWRU



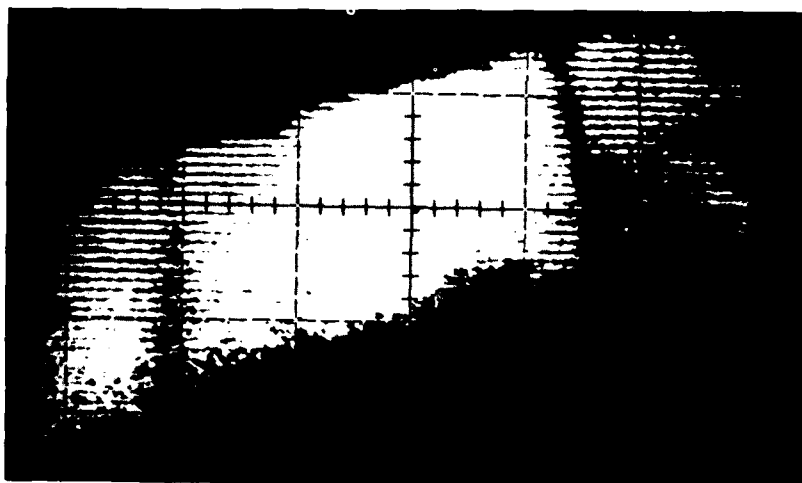


Figure 4. The Na image of A-5-4 before sputtering

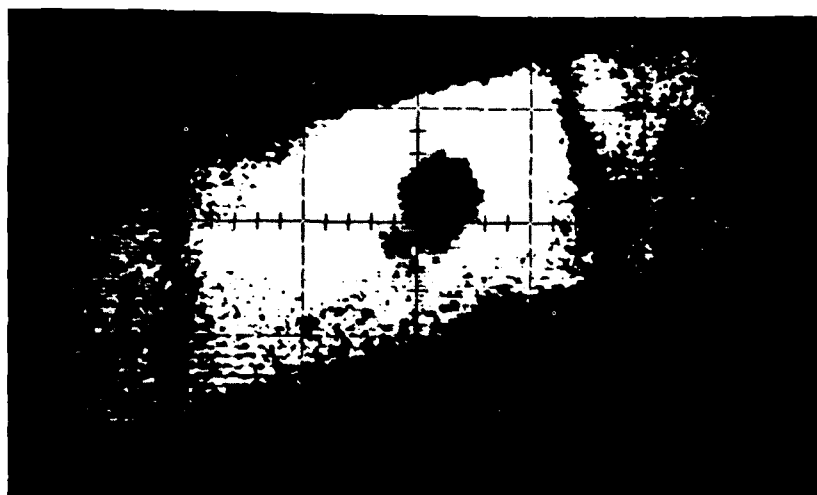
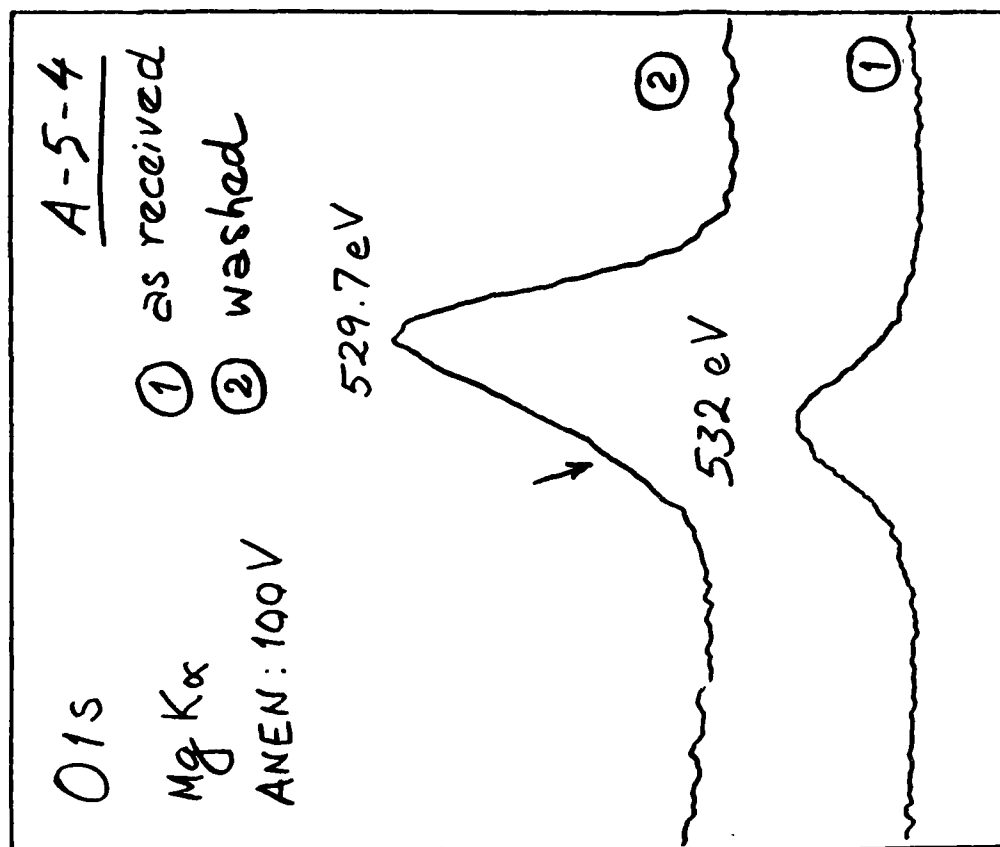
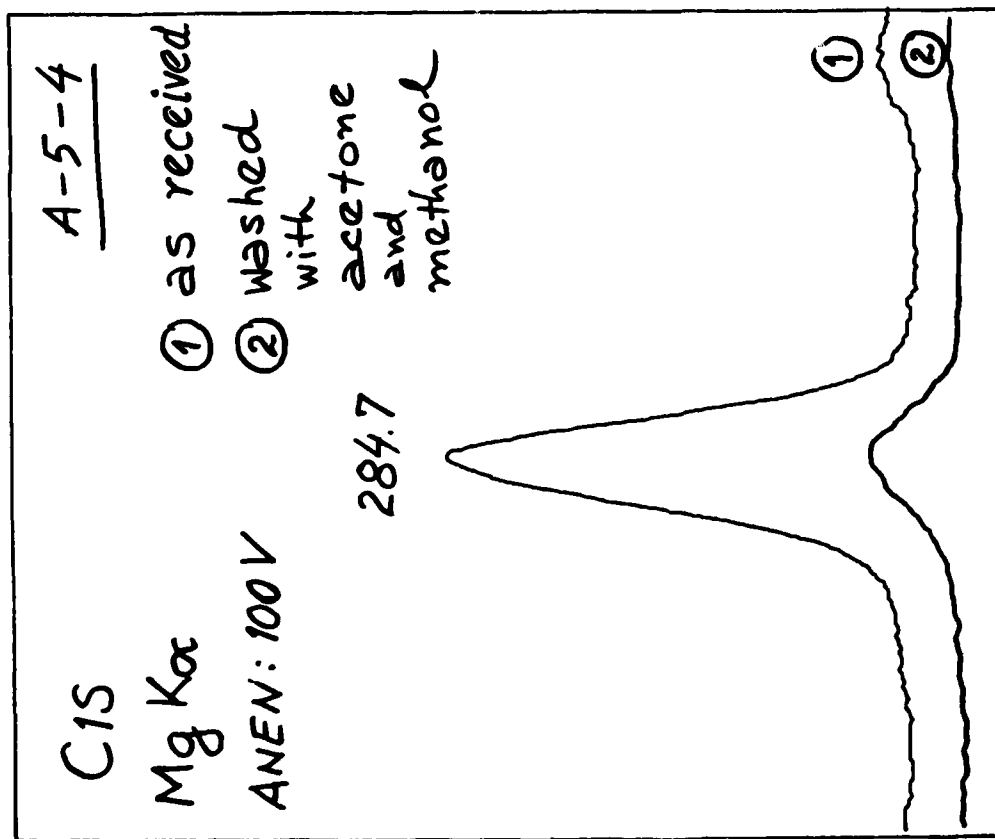


Figure 5. The Na image of A-5-4 after sputtering



Figure 6. The TiO image corresponding to Fig. 5



AD-A147 626

PROCEEDINGS OF THE WORKSHOP ON NONDESTRUCTIVE  
EVALUATION (NDE) OF TITANIUM (U) NAVAL RESEARCH LAB  
WASHINGTON DC N K BATRA ET AL. JUL 84

4/4

UNCLASSIFIED

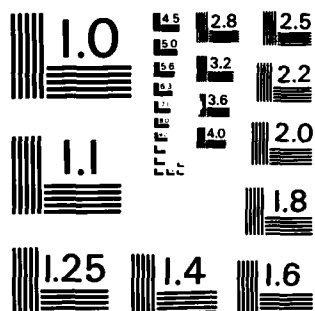
F/G 11/6

NL

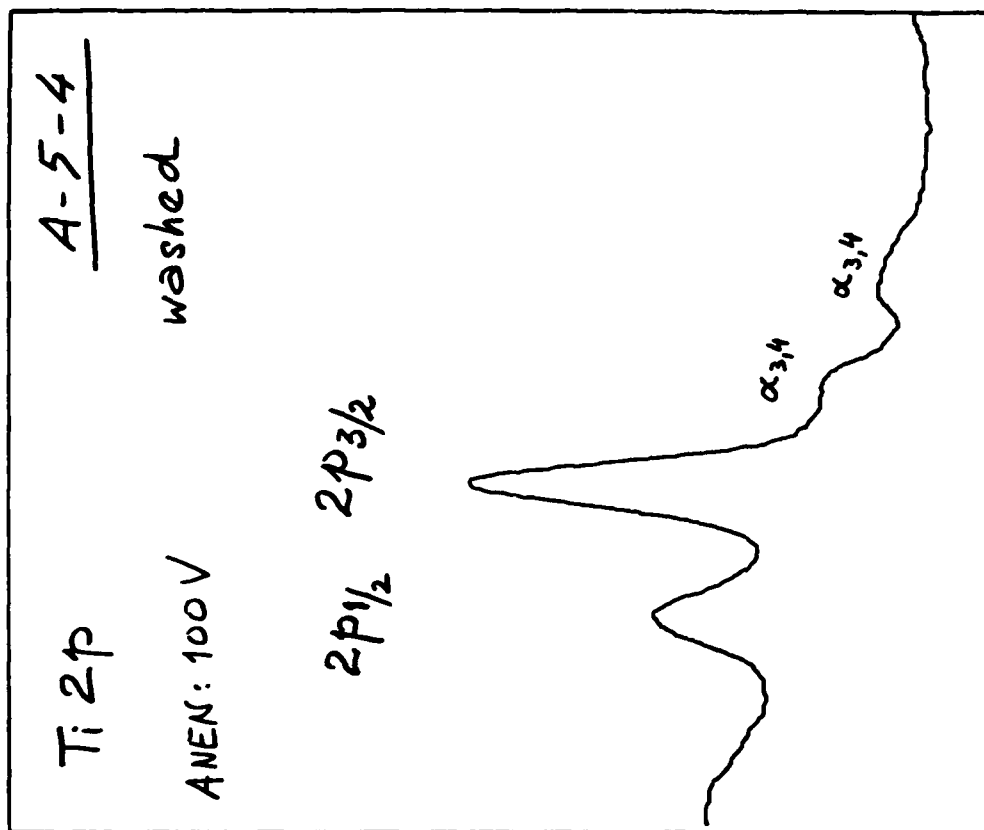
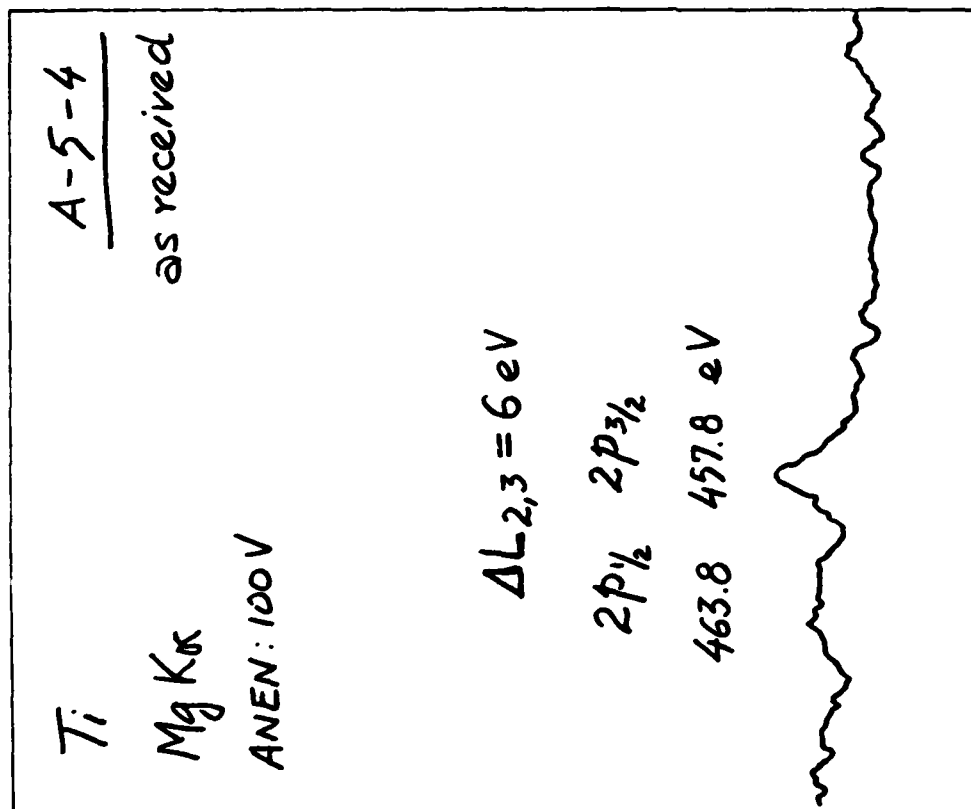
END

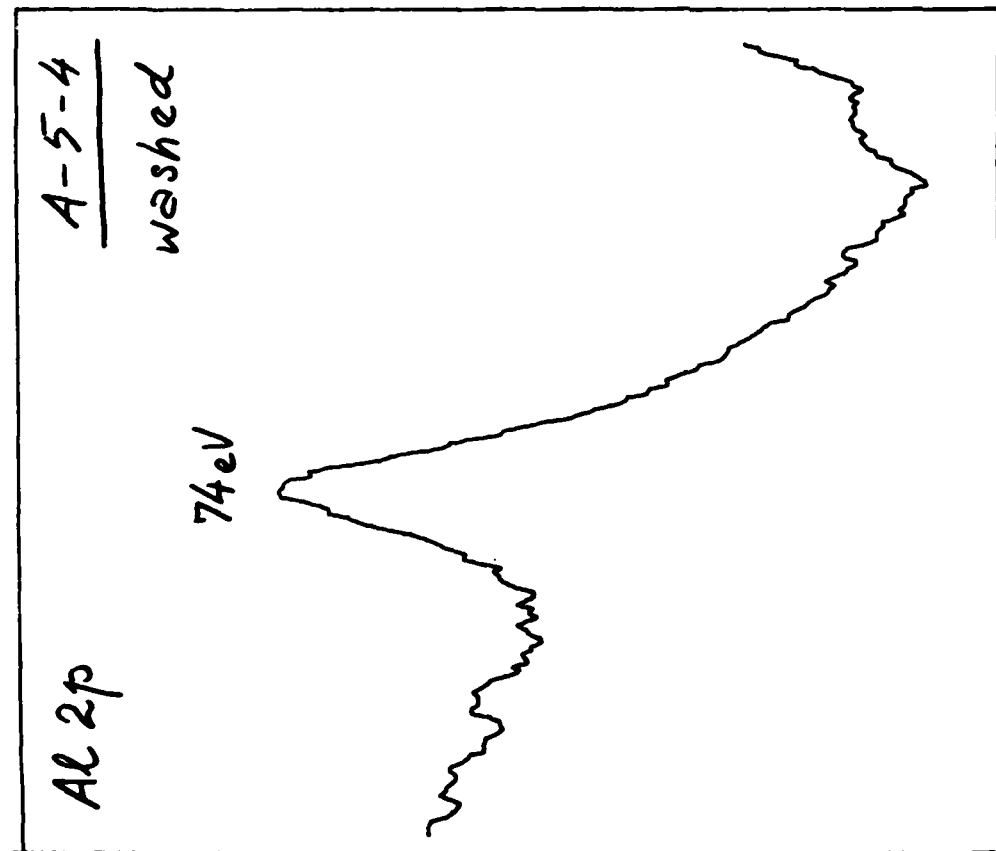
FILMED

DTIC

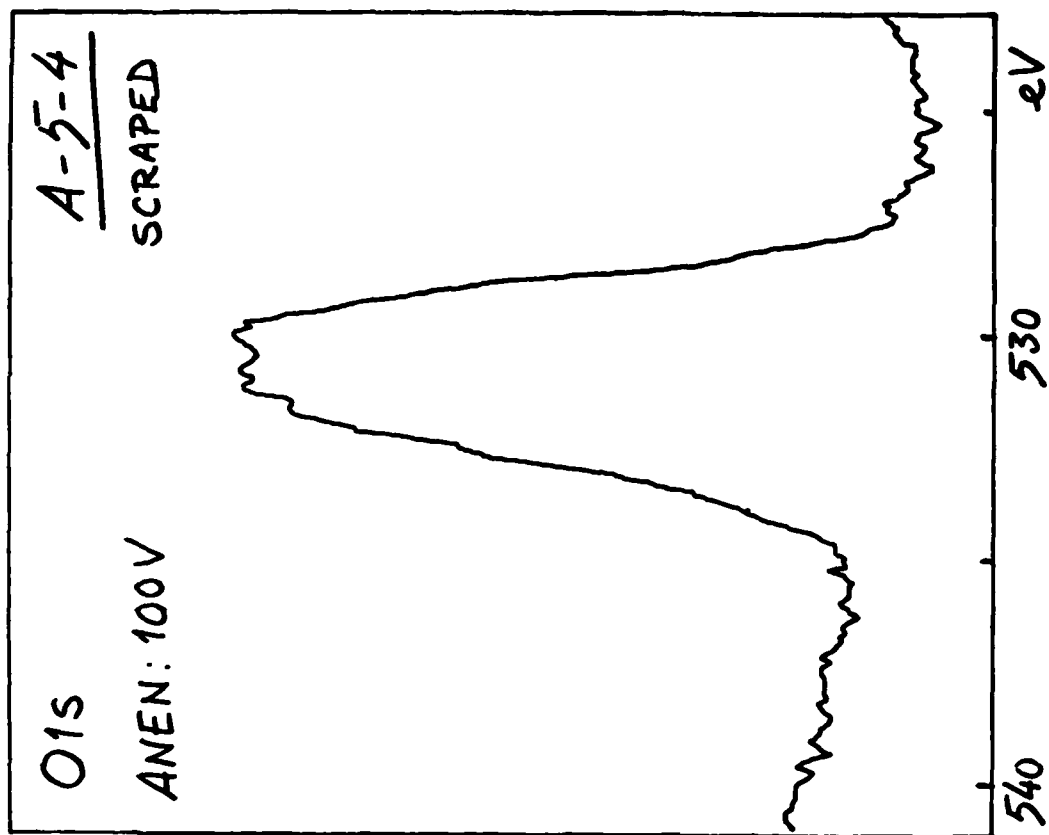


MICROCOPY RESOLUTION TEST CHART  
NATIONAL BUREAU OF STANDARDS - 1963 - A





⑤



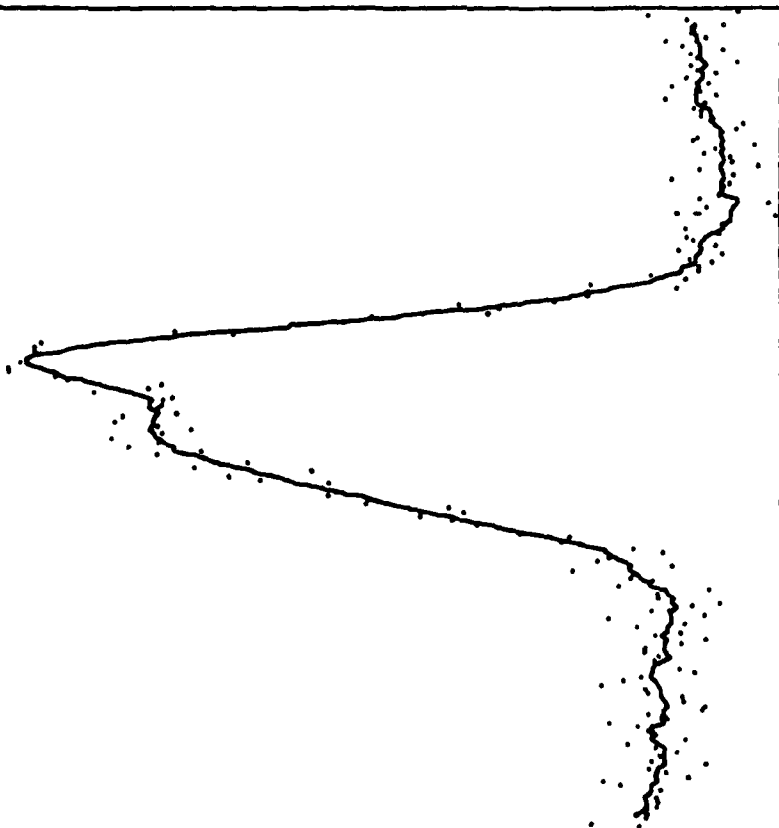
⑥

01s

A-5-4

SCRAPED

ANEN: 30V



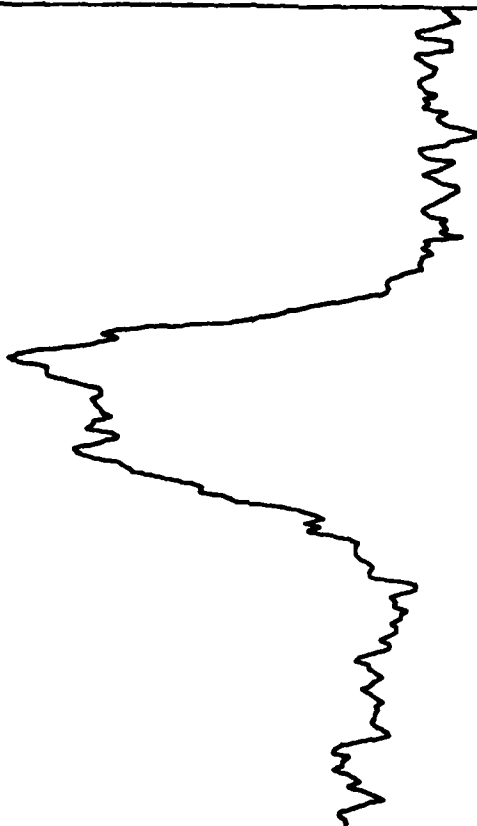
⑦

01s

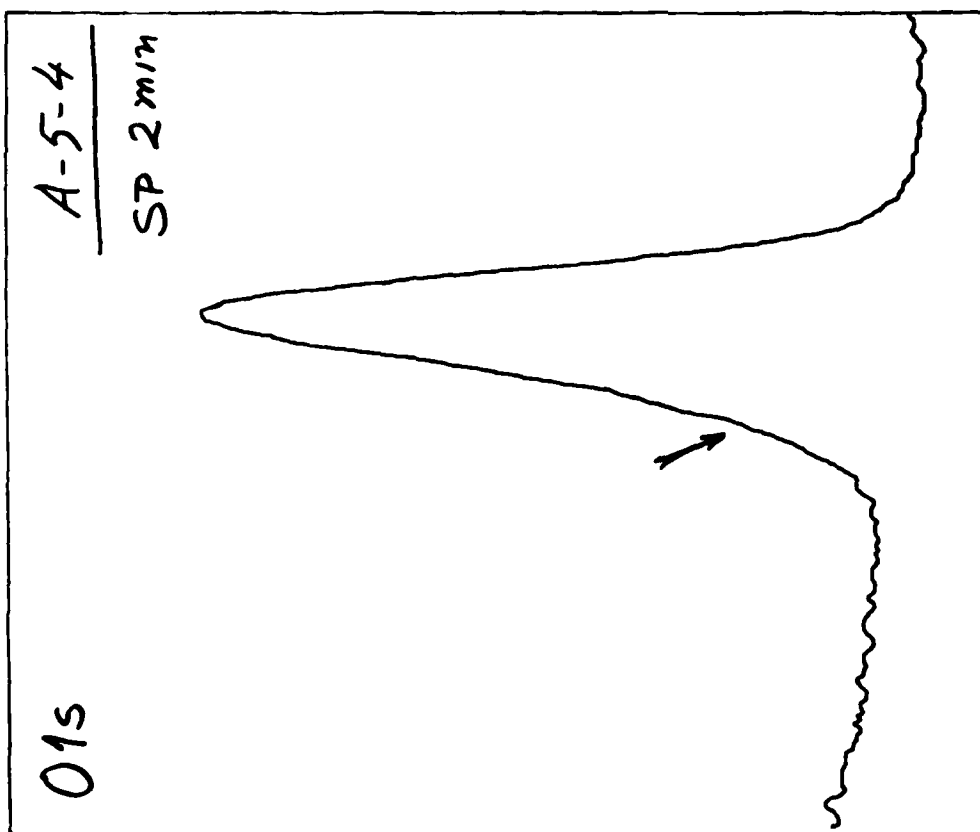
A-5-4

SCRAPED

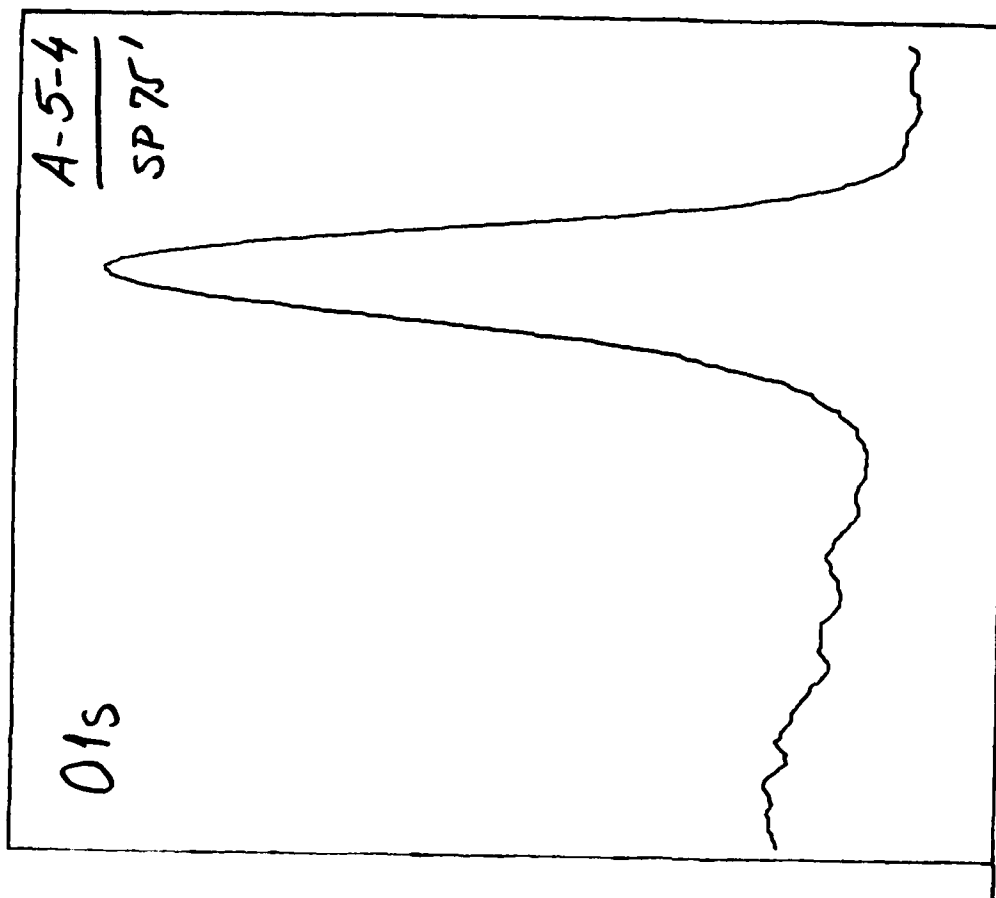
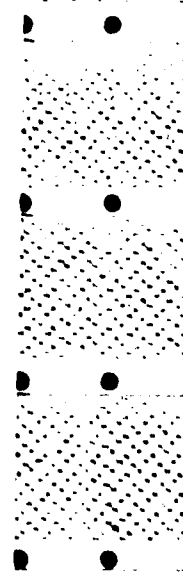
ANEN: 20V



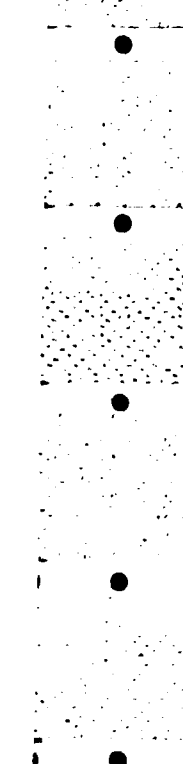
⑧



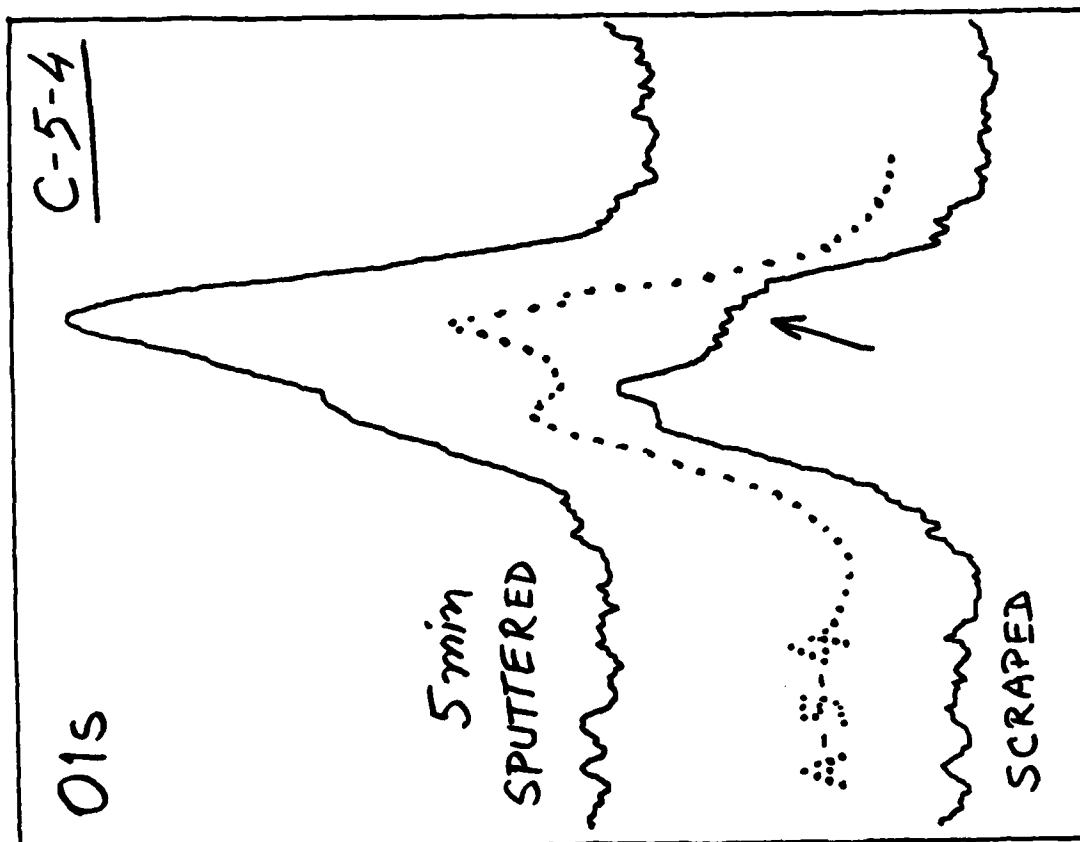
⑨



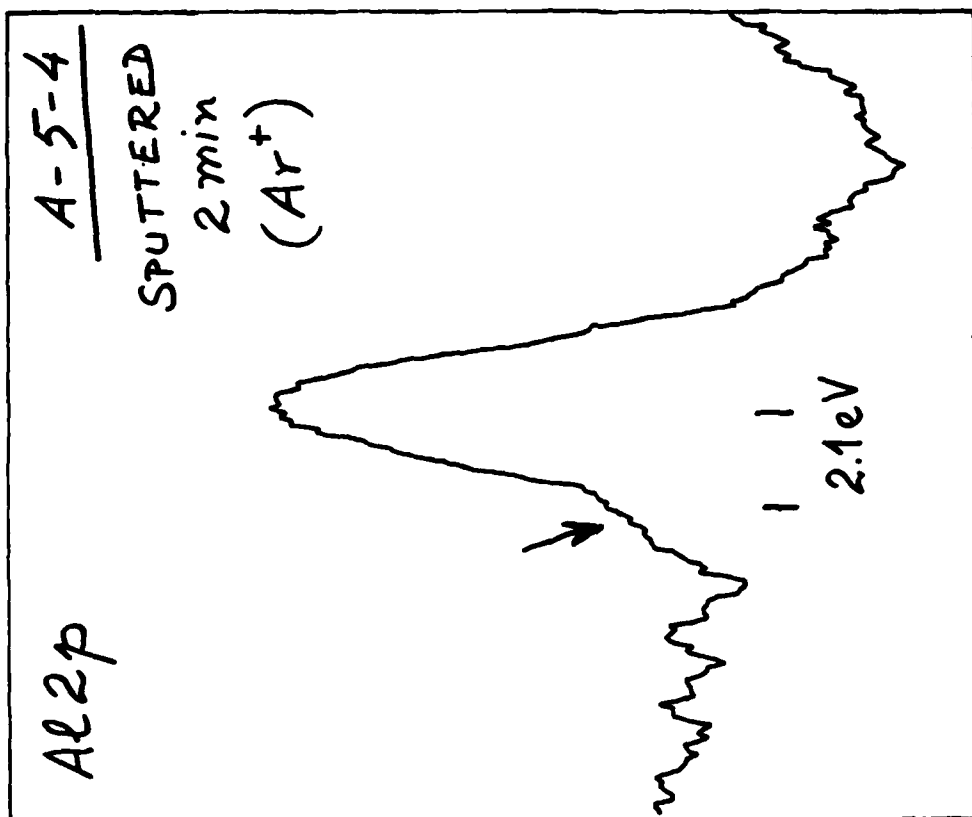
⑩







(11)



← E<sub>b</sub>

(12)

Ti 2p

A-5-4

SPUTTERED

2 min

(Ar<sup>+</sup>)

A SAME  
AFTER

75 min

A ↓ Ti<sup>0</sup>

α<sub>3,4</sub>

TiO<sub>2</sub>

← E<sub>b</sub>

(13)

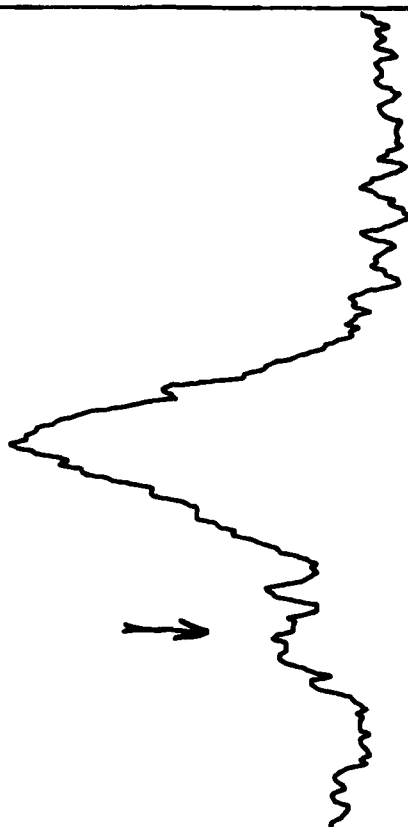
C 1s

A-5-4

SPUTTERED

2 min

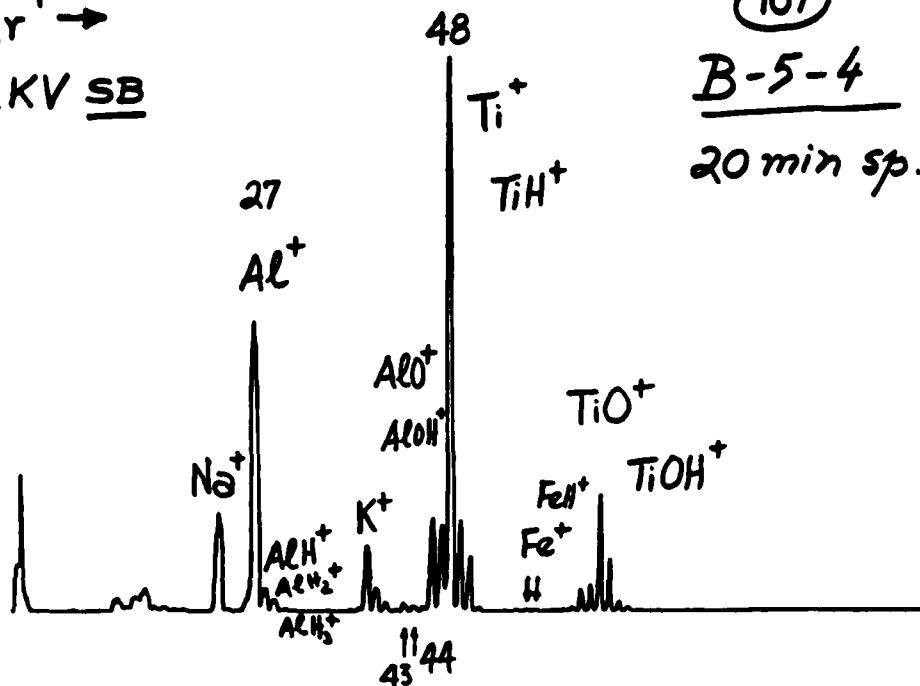
COMPLETELY  
DISAPPEARED  
AT 75' SP



← E<sub>b</sub>

(14)

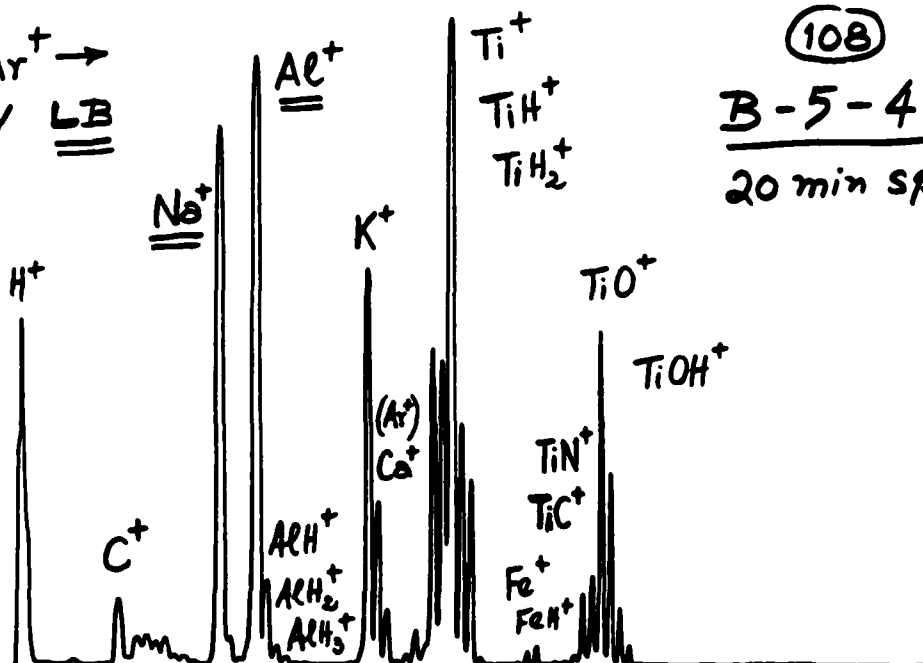
$^{40}_{18}\text{Ar}^+ \rightarrow$   
2KV SB



(107)  
B-5-4  
20 min sp.

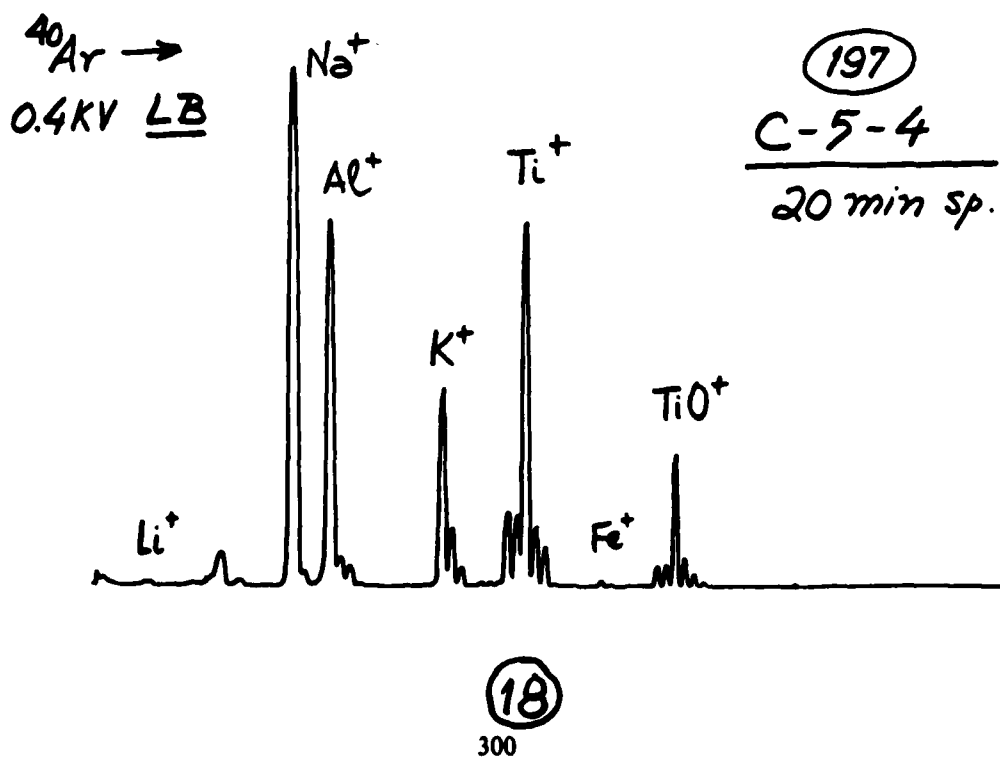
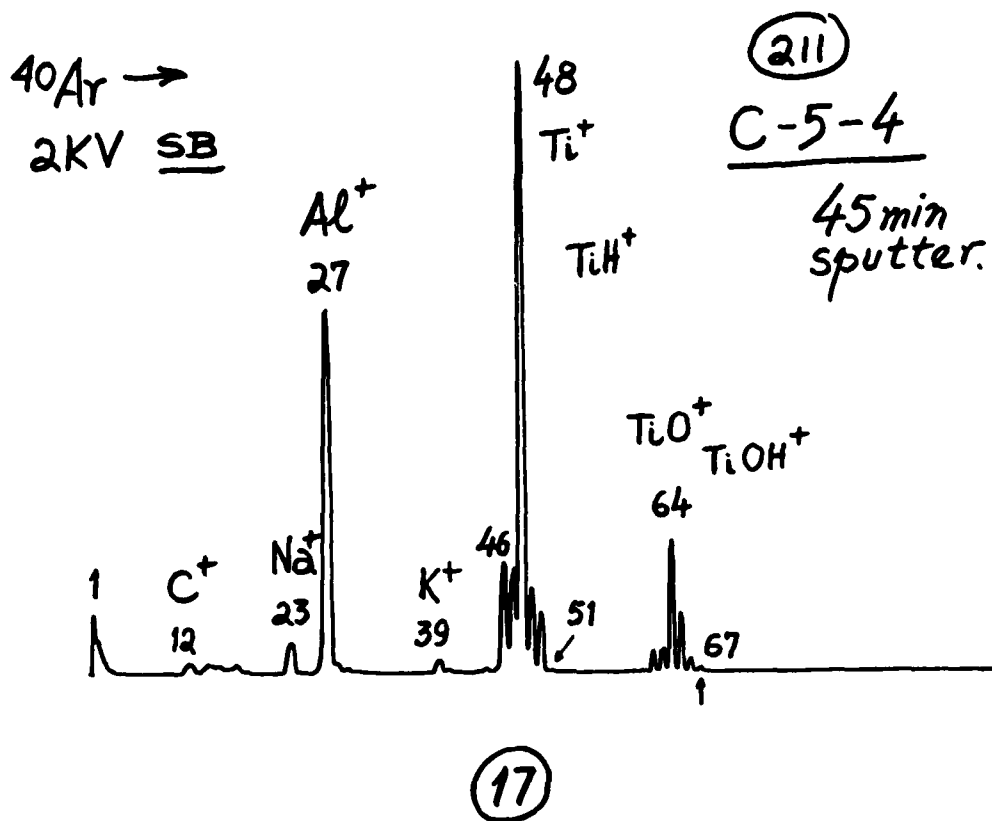
(15)

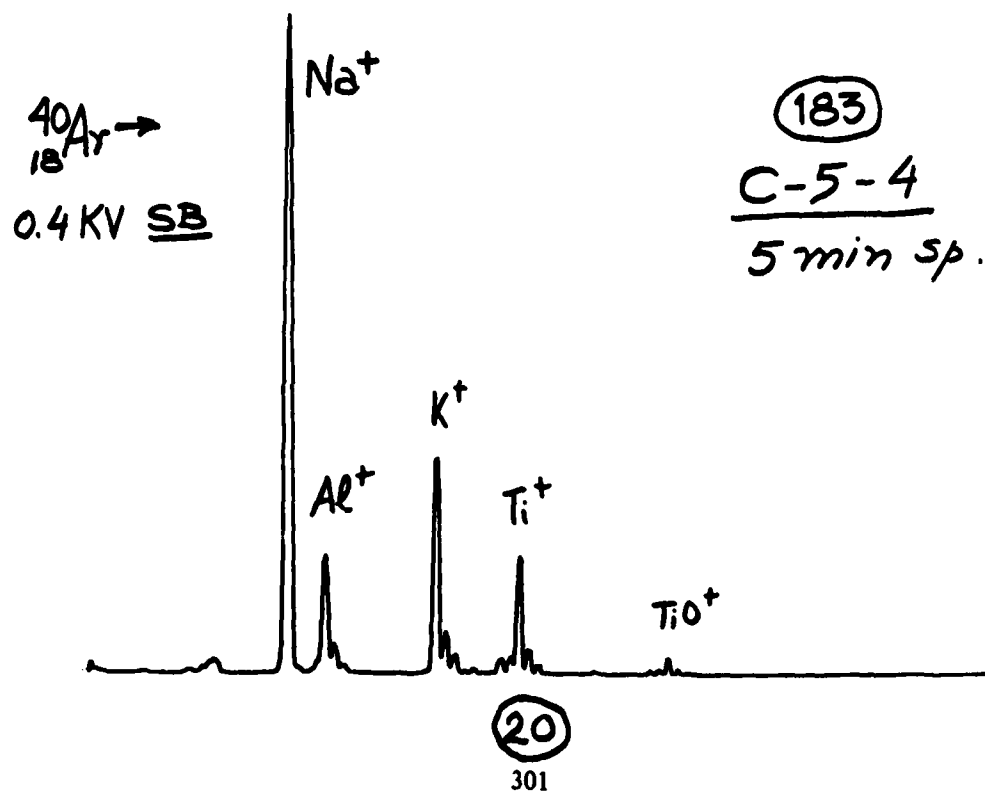
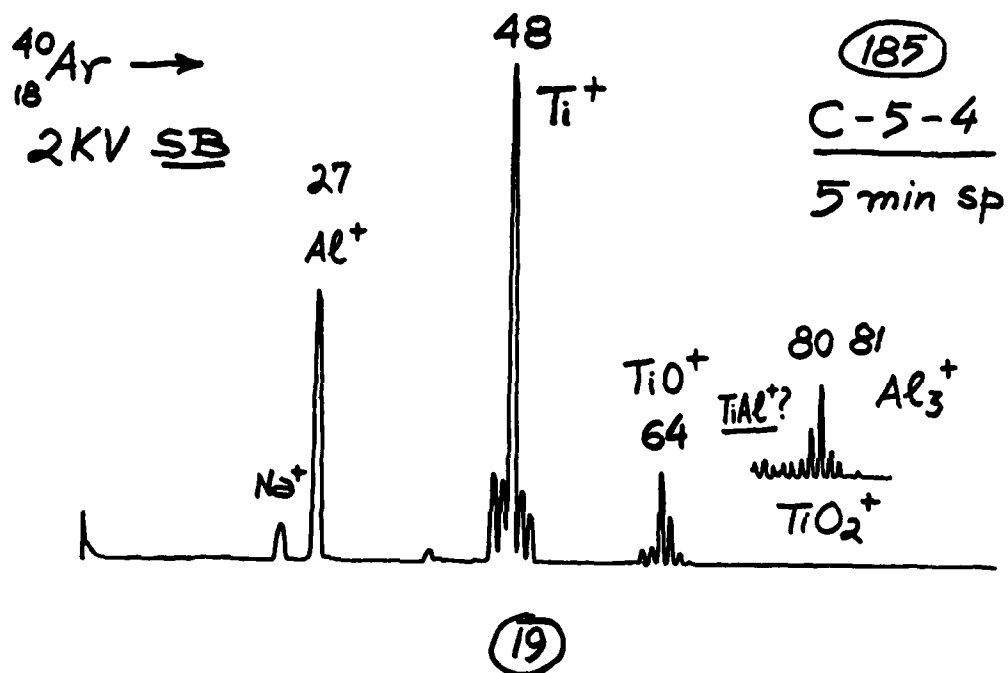
$^{40}_{18}\text{Ar}^+ \rightarrow$   
2KV LB



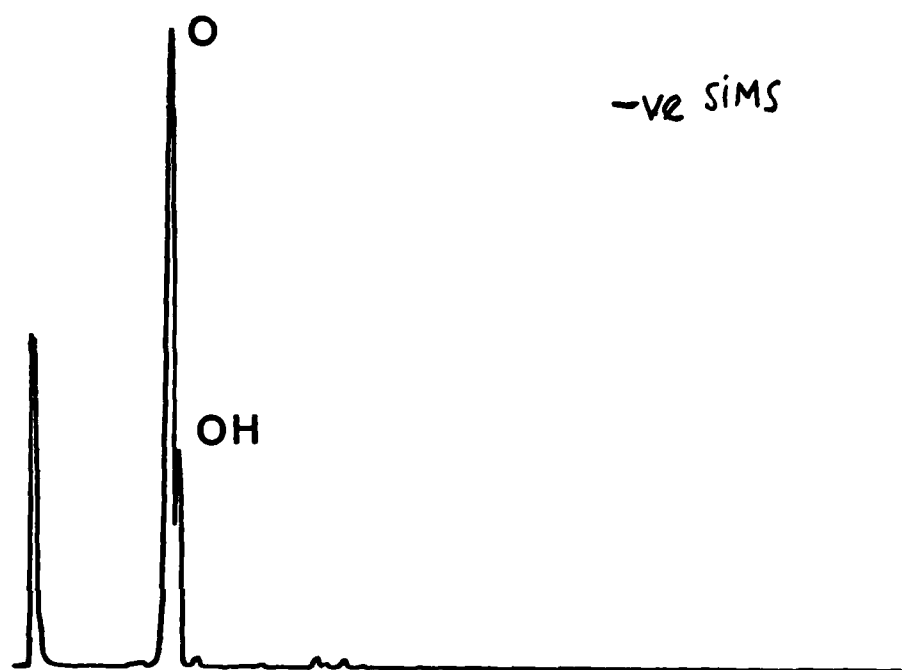
(108)  
B-5-4  
20 min sp.

(16)  
299





(21)

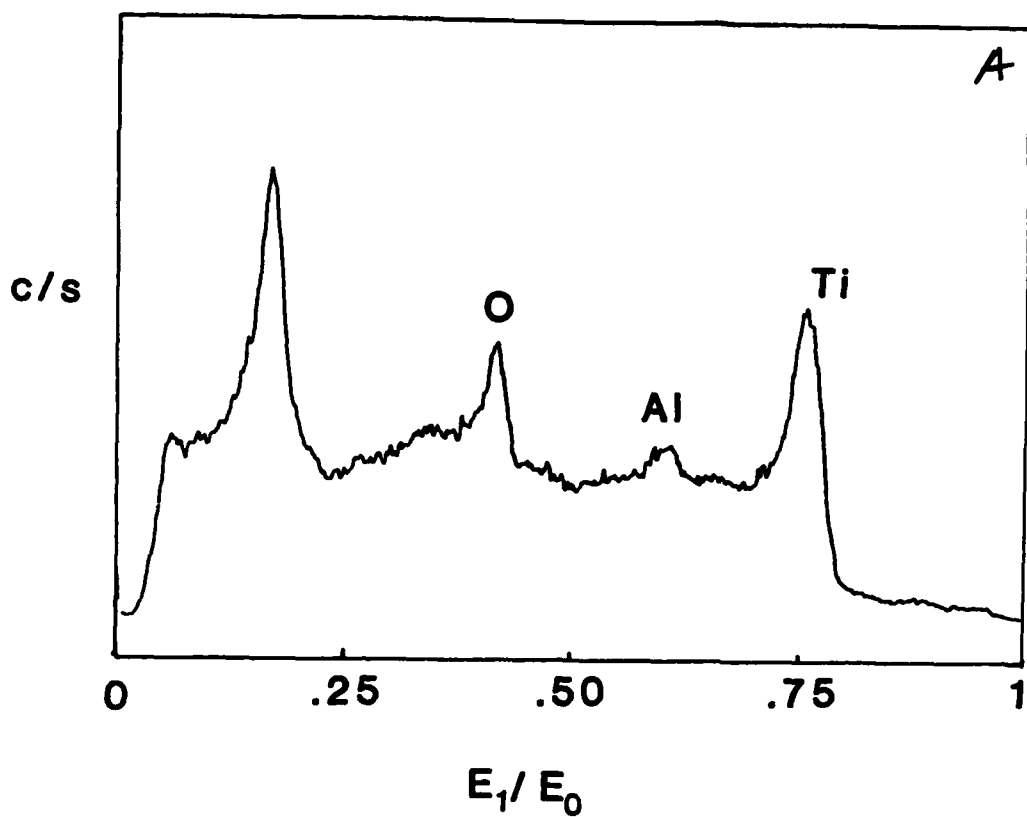


$Ti^+ / TiO^+ (cs)^*$

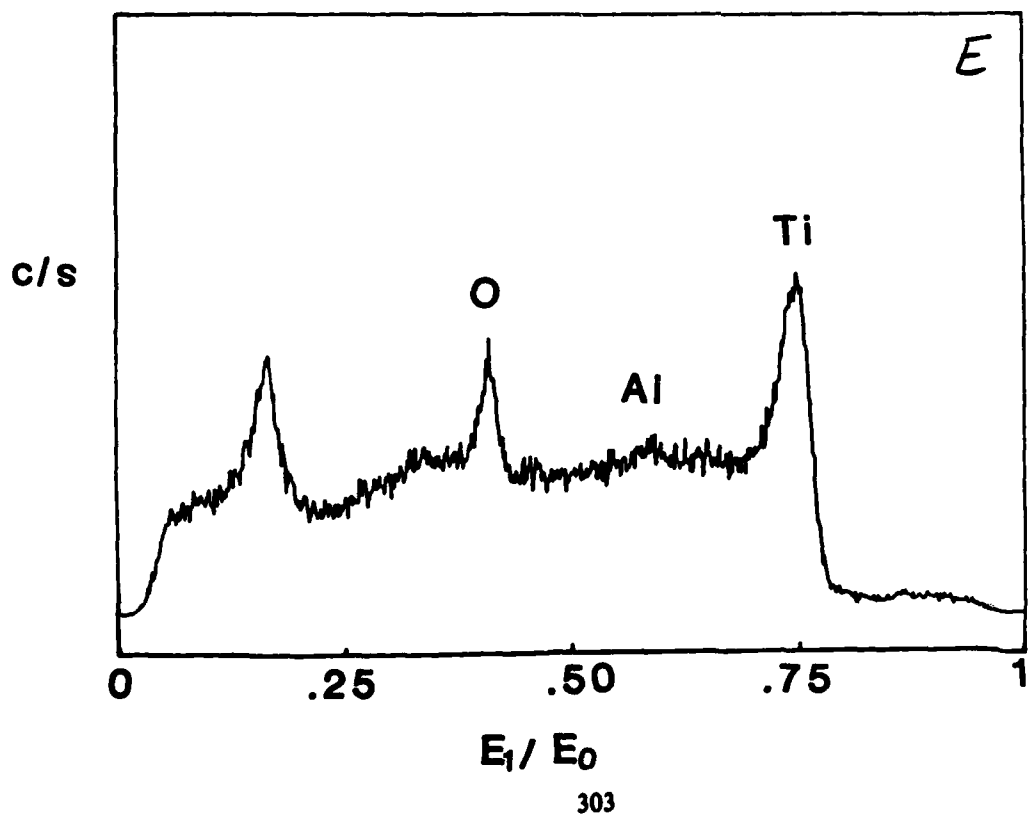
SAMPLE	10 min		20 min	
	SB <sup>xx</sup>	LB <sup>xxx</sup>	SB	LB
A	2.8	2.1	4.4	1.9
B	5.0	2.9	4.7	1.9
C	5.8	2.6	6.5	3.8
E	5.7	1.7	5.5	1.5

TABLE 1

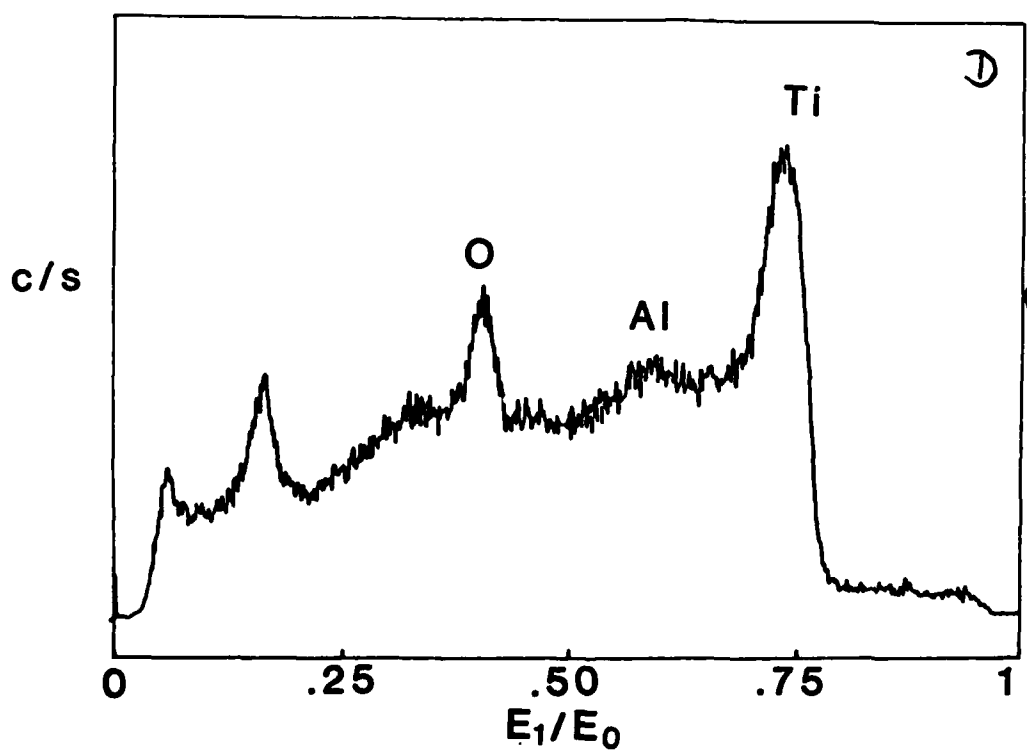
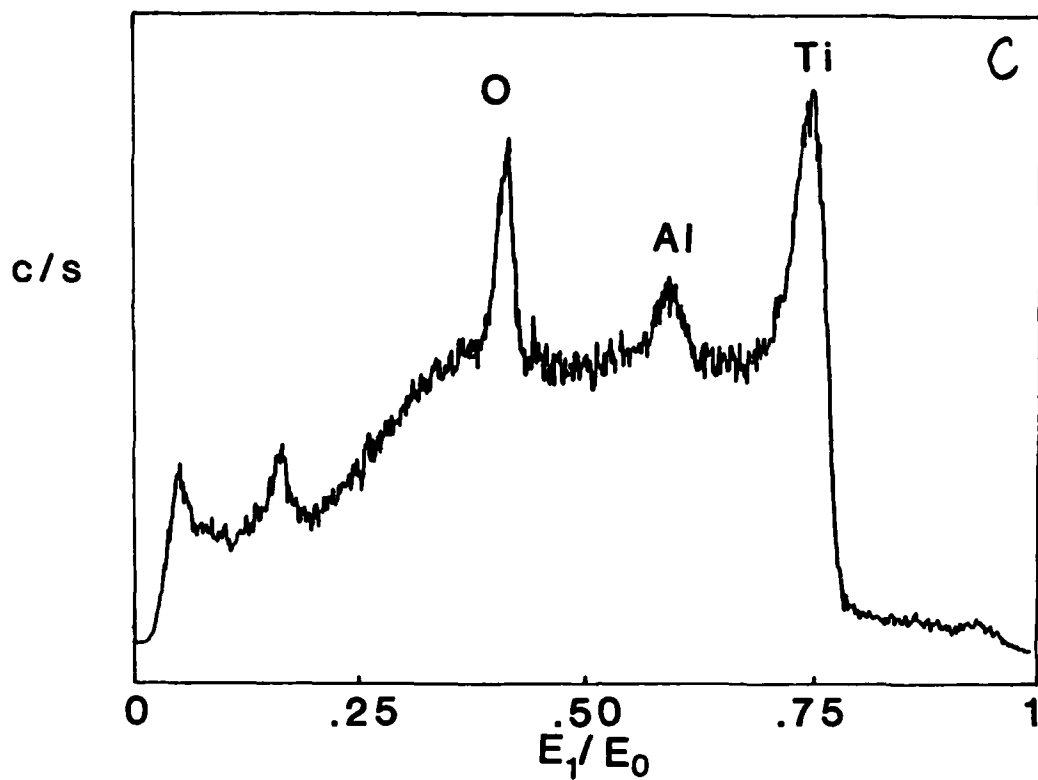
\* c/s = counts/second  
 xx SB = small beam  
 LB = large beam



(22)



(23)





PART E  
LIST OF ATTENDEES

ATTENDEES AT  
TITANIUM WORKSHOP

Sponsored By  
NRL Code 5834

2-4 Feb 1982  
Orlando, FL

ADAPTRONICS

*Tony Mucciardi*

ALLIS CHALMERS

*Darryl Miller*

*Francis Karchnak*

*P.O. Box M-101*

*York, PA 17405*

*(717) 848-1126*

CASE WESTERN RESERVE UNIVERSITY

*Gheorghe Mateescu*

*(216) 368-2589*

DARPA/DSO (MSD)

*Robert E. Green, Jr.*

*1400 Wilson Blvd*

*Arlington, VA 22209*

*(202) 694-5800*

DREXEL UNIVERSITY

College of Engineering

*Michael Fuller*

*(215) 895-2319*

EG&G IDAHO

*D.D. Keiser*

*Idaho Falls, ID*

*J.A. Seydel*

*P.O. Box 1625*

*Idaho Falls, ID*

GARD/GATX

*D.W. Prine*

*7449 N. Natchez*

*Niles, ID 80648*

*(312) 647-9000*

GENERAL DYNAMICS

Electric Boat Division

*John Stringer*

*(203) 446-7035*

*Dr. Alan Greenburg*

*(203) 446-2024*

*Michael Oravec*

GRUMMAN AEROSPACE

*James Kennedy*

JET PROPULSION LAB

*Paul Gammell*

*(213) 354-2631*

JOHNS HOPKINS UNIVERSITY

*Sandy Buzbaum*

*(301) 338-8430*

LOCKHEED OCEAN SYSTEMS

Sunnyvale, CA

*Joe Rynewicz*

LYNCHBERG RESEARCH CENTER

*Tom Powers*

*(804) 522-5038*

MASSACHUSETTS INSTITUTE OF TECHNOLOGY

*Robert Rose*

*Room 4-132*

*Cambridge, MA 02139*

*(617) 253-3230*

NAVAL RESEARCH LABORATORY

Washington, DC 20375

*Dr. Bhakta Rath*

*H.H. Chaskelis*

NAVAL RESEARCH LABORATORY

Underwater Sound Reference Detachment

P.O. Box 8337, Orlando, FL 32856

*Elmo Thomas (Code 5970)*

*(305) 859-5120*

DAVID W. TAYLOR NAVAL SHIP R&D CENTER

*Om Arora*

*Joe Cavallaro*

*Ted Dadley*

NEW YORK INSTITUTE OF TECHNOLOGY

*Dennis G. Thompson*

*800 N. Ocean Drive*

*Dania, FL 33004*

*(305) 923-0551*

OHIO STATE UNIVERSITY

*Prof. Laszlo Adler*

ORNL

*Bob McClung*

*P.O. Box X*

*Oak Ridge, TN 37830*

*(615) 574-4466*

OFFICE OF NAVAL RESEARCH

*Dr. Bruce MacDonald (Code 471)*

PURDUE UNIVERSITY

*Eric Furgason*

RMI

*John Moyers*

*(216) 652-9951*

*John Kosin*

*Don Warmuth*

*(216) 652-9951*

ROCKWELL INTERNATIONAL SCIENCE CENTER

*Lloyd Ahlberg*

*(805) 498-4545*

*Bernie Tittmann*

SCIENCE APPLICATIONS, INC.

*Adel Abusamra*

*(714) 452-9150*

SCIENTIFIC MEASUREMENT SYSTEMS, INC.

*I. Lon Morgan*

SONSCAN, INC.

*Dr. Donald Yuhas*

*(312) 766-7088*

SOUTHWEST RESEARCH INSTITUTE

*O.D. Graham*

*6220 Culebra Road*

*San Antonio, TX 78284*

*(512) 684-5111 (ext 3145)*

*George Gruber*

*(512) 684-5111 (ext 2359)*

*K. Krazywosz*

*(512) 684-5111 (ext 2884)*

SPECTRON DEVELOPMENT LABS

*Gerald Fitzpatrick*

*(206) 575-9324*

*Percy Hildebrand*

*(206) 575-9324*

SRI

*E.M. Teller*

UNITED TECHNOLOGIES RESEARCH CENTER

*R.W. Williams*

*(203) 727-7434*

*Harry Ringermacher*

*(203) 727-7213*

WAYNE STATE UNIVERSITY

*Physics Department*

*Detroit, MI 48202*

*R.L. Thomas*

*(313) 577-2720*

*L.D. Favro*

*(313) 577-2727*

**END**

**FILMED**

**1-85**

**DTIC**